

DISSERTATION

INVESTIGATIONS ON PHOTOVOLTAIC RECEIVERS IN
LINEAR CONCENTRATING SYSTEMS

AUSGEFÜHRT ZUM ZWECKE DER ERLAGUNG DES AKADEMISCHEN GRADES EINES
DOKTORS DER TECHNISCHEN WISSENSCHAFTEN UNTER DER LEITUNG VON

AO.UNIV.PROF. DIPL.-ING. DR.TECHN. KARL PONWEISER

E302

INSTITUT FÜR ENERGIETECHNIK UND THERMODYNAMIK

EINGEREICHT AN DER TECHNISCHEN UNIVERSITÄT WIEN

FAKULTÄT FÜR MASCHINENWESEN UND BETRIEBSWISSENSCHAFTEN

VON

MATTHEW J. CLARKE

E0828796

POKORNYGASSE 2B/7, 1190 WIEN

WIEN, AM MARCH 28, 2012

1. Reviewer: Name

2. Reviewer:

Day of the defense:

Signature from head of PhD committee:

Abstract

Ziel dieser Arbeit ist die Beurteilung von aktiv gekühlten, konzentrierenden Photovoltaik-Receivern in Bezug auf Netzparität und Erzeugerstrompreise unter der Annahme einer maximalen elektrischen Energieproduktion bei ungenutzter Abwärme. Das Verbesserungspotential, sowie eine detaillierte Analyse der theoretischen Grenzen dieser Verbesserungen wird untersucht. Diese Arbeit bietet einen einzigartigen Rahmen für das Verständnis und den Vergleich der Wärmeübertragungseigenschaften und der Leistungsfähigkeit von verschiedenen konzentrierenden Photovoltaik-Receiver Designs.

The purpose of this thesis is to assess whether or not an actively cooled, low concentration, concentrator photovoltaic receiver could meet either grid parity or wholesale electricity prices under the assumption that electrical energy production is maximized and heat is considered a waste load. To do so, a set of cost targets are derived for an actively-cooled concentrator photovoltaic receiver and cooler technology to meet short-term (grid parity) and long-term (wholesale) electricity price targets. The current cost of the receiver and proposed cooler are compared to these targets for three application scenarios, and necessary levels of performance and cost improvements are identified. A list of possible improvements is given, followed by a detailed analysis regarding the theoretical limits of these improvements. Taking these improvements into consideration, a final assessment of the technology is given. Perhaps most importantly, this thesis establishes a detailed and unique framework for understanding and comparing the heat transfer capabilities and ultimately performance of concentrator photovoltaic receiver designs.



The happiest excitement in life is to be convinced that one is fighting for all one is worth on behalf of some clearly seen and deeply felt good.

-Ruth Benedict

Preface

I would like to begin on a personal note. In fact, I would like to begin by highlighting the lack thereof. Unfortunate, is it not, that one's self is so often lost in the third-person narrative of scientific writing. I think we sometimes forget that the author is human, that he or she has lived or is living, is thinking, is dreaming, is hoping, is making mistakes, is unsure, but is nevertheless trying; trying to do something that he or she believes in. It is in this admission of our less than perfect selves that I hope the reader will examine the last three years of my work. I can say conclusively that I tried hard and am proud of what I could accomplish, but it was not easy. Much as I found in my brief years working in industry before my graduate studies, the technical challenges are surmountable. This is not the hard part. It is the unknown nature of the problem, the uncertainty of which solution to pursue, the unsureness of self that is of the greatest difficulty. If there is anything that I take away from this program it is this:

In these years, more important than any technical theory or learned formula, I take away the knowledge of silencing one's internal doubts and pushing forward in spite of them, knowing that what needs to be done will be done, and that what needs to be learned will be learned.

When I began this PhD program, I was asked to develop a concentrator photovoltaic receiver for an inflatable concentrator. With a background in photovoltaics from my masters studies and a background in heat transfer from my bachelor studies, I felt confident that I could achieve this. Walking into the office/laboratory for the first time, I was shocked to discover only three pieces of equipment: my left and right hand, and the spongy mass resting between my ears. In the years that followed, I managed, albeit

rather crudely at times and not without setbacks, to build a laboratory capable of characterizing concentrator photovoltaic (CPV) cells and building CPV receivers. At times, it felt as if I could have dedicated three years just to these activities. But alas, as with any PhD, I was required to make meaningful scientific/engineering contributions, which are contained in this thesis.

The somewhat unique circumstances of my PhD found me sitting next to the chief technical officer of the start-up company that partially financed my studies. This at times created much difficulty, balancing the fast-paced, result-based needs of a start-up against the back-drop of making a significant contribution to the field of concentrator photovoltaics. I appreciate his and his company's efforts to accommodate the two, at times conflicting, goals. To him, by now a good friend of mine, I owe a small apology. I wanted to take a very broad but well thought out approach to problem solving, and this certainly slowed progress in the short-term. In the long-term, it may have been worthwhile, we will have to see.

In this thesis I wanted to try and understand whether or not CPV technology, particularly linear-focus trough concentrators, could ever compete economically with grid and wholesale electricity prices. When I first began my work, I was completely shocked by the, what I thought to be quite advanced, efforts of linear concentrator designs. Several large development projects had already been carried out from the late 1990s to 2005. My first thought was a bit of a letdown, "great, I guess there is nothing for me to do but simply reverse engineer this technology." Such reverse engineering fit well with the desires of the start-up, but I was greatly concerned with regard to my PhD and the quality of such work. As I gathered the many papers and thesis surrounding past concentrator systems, I noticed a few common conclusions. The technology had been demonstrated; it worked but had much room for improvement. Most importantly, the technology was always too expensive. Myself, under constant pressure to build some type of prototype, began to fear that I was simply going to end up reverse engineering and tweaking such existing designs, only to write a thesis with

nearly the same conclusions. I found this prospect rather dismal. At this time, already several months into a PhD with a tight 3 year schedule, I considered how best to move forward. I thought to myself, these past programs had millions in funding (both in Euros and dollars), how am I, as the one engineer assigned to the development of a linear CPV receiver, supposed to contribute? What am I going to do that has not already been done before?

I started seriously questioning the idea that the existing linear CPV technologies could simply drop in place into this new concentrator and suddenly a grid parity product would leap forth. Similar past concentrators were too expensive and no matter how cheap this new concentrator might be, the optics would have to be more or less free for this technology to reach such aggressive cost targets. I slowly came to accept that the existing CPV receiver technologies needed to decrease costs and improve performance to meet grid parity. I gathered the impression that no one single design change or breakthrough could accomplish this goal, but rather that many smaller changes were needed. At length, I decided the following. First, I wanted to understand exactly how cheap a CPV receiver needed to be in order to meet grid parity and, in the long-term, wholesale electricity prices. I had never come across a detailed explanation behind the $1\$/W_{pk}$ cost target, so often touted as grid parity. I wanted to understand how one might arrive at such a number. In addition, I was unsure whether this would also be true for concentrator technologies, as the term watt peak is rather meaningless when considering the vast differences in operating principles and conditions of concentrator technologies.

With a set of cost targets established, I had guessed (correctly), that the existing technologies for CPV receivers would be too expensive and that some combination of cost and performance improvements would be necessary. I wanted to define a comprehensive list of improvements and provide the theoretical basis for the magnitudes of their respective improvements. I focused much of my efforts on cell interface and cooling design, as heat transfer is one the strengths of my department, and it seemed like an area open for contributions. I used these investigations to disprove the merits

of several cooling strategies. I summarized these results by providing a suggested ranking for the various CPV receiver designs. In the end, I determined the necessary level of improvements and defined what I believed to be possible improvements to reach the cost targets. And so, instead of drawing the conclusion of other's past work, "it's too expensive," my conclusion is rather that land-based CPV, utilizing low concentrating, linear-focus trough concentrators, with silicon solar cell technology will struggle to meet short-term (grid parity) and long-term (wholesale electricity prices) cost targets. Given what is now known, it will likely be too expensive, at least based on today's electricity and solar cell prices. This I find to be a rather powerful result, and it will certainly influence my next career considerations. I will allow, however, that CPV-T holds promise, but I envision much smaller systems, such as that under development at the Australian National University (ANU), rather than the large grid installation scale systems, originally considered in this thesis. TU-Wien is continuing forward with linear concentrators in hope of developing a floating sea-platform. As I concluded in the cost chapter, there is, from an economical stand-point, significant promise here. Needless to say, the technical challenges will be immense. But as I said before, technical hurdles are surmountable. It should be fun.

Before closing, a round of acknowledgements is in order. First, let me thank my parents for their diligent planning and savings which afforded me the luxury of, and started me on, my educational path. Thank you to my friends and family for their love, support, and understanding over the last few years. It was not easy living in a foreign country, let alone one so far away. I've missed more than my fair share of weddings and births, and you have my sincerest apologies. But, those who know me best understood that I had to take this journey. I have EUREC to thank for starting me off with a wonderful masters program, which provided me a great deal of exposure to PhD students and the interesting projects that they worked on. Sabrina, I have you to thank for bringing me to Vienna and for the many wonderful years we spent together. I've come to think of Austria as a second home, and I am sorry that your and my journey goes no further. I wish you the best of luck and know that our lives will cross paths again. To Angela, thank

you for being a spark of light during dark times in my life. As friends and colleagues, I enjoyed our time together. I hope to see you again soon.

Marta, I have many things to say to you. It is rare that I find myself in a position where another person has helped me as much as you have; I'm not used to feeling indebted to someone (not that you would allow me to feel that way). Nevertheless, thank you. Thank you for sharing your insights and experiences on both the EUCLIDES and CHAPS project and for the several months we spent working together. I have enjoyed our collaborations both during my time at ANU and since then. I hope that we find ourselves back on the same continent soon and that we have the opportunity to work together in the future. Most of all, thank you for being the caring and wonderful person that you are.

To Vernie, I owe you many thanks and more. Without your help, and the opportunity to study at ANU, I don't know where I would be. . . probably still taping cells to square pipes and setting them on fire in a concentrator. You helped make my visit to ANU a reality, opened your household, welcomed me into your family, and showed me why Australia is such a great place. Thank you for being a mentor both in and outside of the lab and for being a good friend. Both you and Marta helped me realize the main goal of my PhD: to build on the previous work of others and see whether or not this technology can carry forward. Without both your help, I would have likely produced results nearly identical (more likely worse) from the last 2 decades of work. Rather, you gave me the background and base to perform the economical and technical analysis that I present in this work. I hope you enjoy it, although. . . I think my conclusions may have killed my own career in this field. Nevertheless, I believe the ANU mini-concentrator is a great idea and wish everyone at ANU the best of luck. I hope our paths cross again soon. Best of luck to you and warm wishes to the entire family.

To my friend and fellow solar power champion, I owe you many thanks Rodrigo. Were it not for our chance encounter and your sheer persuasiveness in Loughborough, many of the chance circumstances which brought me here today would have never happened. I admire your sheer determination and

dedication, your high moral standard, and general desire to do good in this world. There is a lot of good to be doing these days, and I hope we end up joining forces, putting our heads together, and solving some of these problems. I wish you the best of luck in your PhD program. I am very proud of you my Brazilian brother.

Finally, none of this would have been possible without the support of my department. Thank you to Dr. Haider and his staff. To my supervisor, Dr. Ponweiser, thank you for your kind and patient assistance over the last few years. I have thoroughly enjoyed our extensive discussions on heat transfer. You have taught me many things and always trusted in my judgement. Thank you for giving me the opportunity to pursue the ideas and ideals that I believed and believe worth pursuing. Thank you to Dr. Summhammer; your guidance and discussions regarding photovoltaics have been very helpful. Thank you for spending time with me in the laboratory. Thank you to Heliovis AG and its two major founders, Johannes Hoeffler and Felix Tiefenbacher. I wish you both the best of luck and hope to see you again soon.

For those considering a PhD, it is a rewarding experience. But like all things in life, it is worth doing for its own sake and the personal development one derives from its efforts, much more so than any monetary reward has to offer. To my close friends and family, I send my warm wishes. Best of luck to the future; I hope to see you all soon.

Peace and much love,

Matthew

Declaration

I herewith declare that I have produced this paper without the prohibited assistance of third parties and without making use of aids other than those specified; notions taken over directly or indirectly from other sources have been identified as such. This paper has not previously been presented in identical or similar form to any other German or foreign examination board.

The thesis work was conducted from December 2008 to December 2011 under the supervision of Ao.Univ.Prof. Dipl.-Ing. Dr.techn. Karl Ponweiser at the Vienna University of Technology in Vienna, Austria.

Matthew Clarke

Contents

List of Figures	xvii
List of Tables	xxi
Glossary	xxiii
Nomenclature	xxv
1 Introduction	1
1.1 Thesis outline	1
1.2 Motivation	3
1.3 A brief history of concentrator photovoltaics	6
1.4 Classification of concentrator technologies	8
1.5 Within and beyond the current challenges	8
2 Existing Linear Concentrator Systems	15
2.1 Efforts at ANU	15
2.2 Efforts at IES	16
2.3 Commercialization efforts	19
3 Cost Targets, Estimates, and Improvements	25
3.1 Introduction	25
3.2 Total system cost targets	26
3.2.1 Maximum, theoretical, annual revenues	27
3.2.2 NPV and economic assumptions	28
3.2.3 From NPV to cost targets	30
3.3 Potential installation sites	32

CONTENTS

3.4	Nominal operating condition	32
3.5	Summary diagram and proposed cost targets	34
3.5.1	Summary diagram	34
3.5.2	Proposed total system cost targets	36
3.6	Proposed cost targets at the subsystem level	36
3.7	Cost estimates	38
3.7.1	Cost: TU-Wien CPV receiver prototype	38
3.7.2	Cost of the cooling system	40
3.7.3	Cost comparison: targets vs. estimates	41
3.8	Cost reductions and performance improvements	41
3.8.1	Water interconnectors	43
3.8.2	Cell efficiency	43
3.8.3	Alternative encapsulation	43
3.8.4	Improved thermal interface materials (TIM)	43
3.8.5	Cost reductions in the cooling system	44
3.9	Summary of improvements	47
3.10	Conclusions	49
4	Methods of Cooling CPV Receivers	51
4.1	Introduction to the cooling system	51
4.2	Methods of cooling	53
4.3	Cooling transition points: passive, active, and beyond	54
5	Design and Optimum Size of the Cooling System	61
5.1	Major components of the CPV system	61
5.2	Heat transfer within the CPV receiver	62
5.3	Back cooler	64
5.4	Nomenclature: cooling system	68
5.5	Design guidelines	71
5.6	Sizing the cooling system and comparing TIFs	75

6	Theoretical Performance of Various Thermal Interfaces	85
6.1	Designs covered and associated boundary conditions	85
6.2	Calculating the heat transfer coefficients	91
6.3	Direct immersion cooling in laminar flow	92
6.4	Direct immersion cooling in turbulent flow	95
6.5	Direct immersion cooling in pool boiling	102
6.6	Thermally conducting materials	105
6.7	Comparison of interfaces	109
6.8	Summary of thermal interfaces	113
6.9	Economically sensible operating parameters	116
6.10	Recommendations and conclusions	123
7	Preliminary Design of DI Receivers	125
7.1	Candidate fluids	125
7.2	GWP limit	127
7.3	Candidate designs	129
7.3.1	DI-CPV receivers and turbulent flow	132
7.3.2	DI-CPV receivers and pool boiling	133
7.4	Estimate of optical losses	136
7.5	Challenges and future developments	139
8	Alternative Soldering Methods	141
8.1	Introduction	141
8.2	Stencil printing	141
8.3	Pre-coated tab method	142
8.4	Experimental results	142
8.5	Conclusions	149
9	Conclusion	151
9.1	Land-based CPV	151
9.2	CPV-T	152
9.3	Sea-based CPV	153
9.4	Insights and Accomplishments	153
9.5	Future work	155

CONTENTS

A CPV Terminology from IEC-62108	159
B Equations	161
B.1 List of Equations	161
B.2 Assumptions	163
B.3 Bar-Cohen limit to passive cooling Eq. 4.2-4.3	163
B.4 Explanation of CPV cell power density Eq. 5.4-5.6	164
B.5 Optimal concentration factor for fixed HTC, Eq. 5.7	165
B.6 Power of the unit-cell Eq. 6.3-6.5	169
B.7 GWP values	170
B.8 Maximum series connected CPV receiver length	171
B.9 Performance and cost utility functions: Eq. 6.22-6.24	172
C Additional Tables and Figures	175
References	181

List of Figures

1.1	Concentrator Technologies	9
1.2	Inflatable Linear-focus Trough Concentrator	12
1.3	HELIOtube	12
2.1	ANU Two Axis Tracker	20
2.2	CHAPS	20
2.3	CHAPS at Focus	21
2.4	Chromasun	21
2.5	EUCLIDES-III	22
2.6	EUCLIDES-III at Focus	22
2.7	Skyline	23
2.8	Entech	23
3.1	Average Regional Temperatures	33
3.2	Maximum Allowed Total System Cost	35
3.3	Subsystem Relative Percent Cost SoA	37
3.4	Subsystem Relative Percent Cost BSoA	37
3.5	Cooling Cost Survey	41
3.6	Effects of Night Storage Cooling	46
4.1	Active Cooling	55
4.2	Passive Cooling	55
4.3	Heat Sink Width	57
4.4	Passive Cooling at Various X_g	59
5.1	CPV Receiver	62

LIST OF FIGURES

5.2	Optical Paths	65
5.3	Thermal Paths	65
5.4	Heat Exchanger	67
5.5	Finned Tube Back Cooler	67
5.6	TIFs	69
5.7	HTC Sums	73
5.8	Additional TIFs	74
5.9	Infinite Cooler Size	76
5.10	Optimum X_g for h_{total}	79
5.11	Approaching an Infinite HTC	81
5.12	Optimum HTC	82
6.1	TIF Conduction Passive	87
6.2	TIF Conduction Active	87
6.3	DI-CPV Receiver	89
6.4	DI-CPV Flow	90
6.5	DI-CPV Boil	90
6.6	Simplified Heat Transfer Models	92
6.7	Two Plate Laminar Flow Model	94
6.8	Optimum Fluid Velocity	98
6.9	Optimum Fluid Velocity H_2O^*	99
6.10	Maximum Installation Length of CPV Receivers	101
6.11	Pool Boiling Coolant Survey	104
6.12	Two Material Interface	106
6.13	Power Losses vs. X_g	113
6.14	Thermal Interface Technology Roadmap	115
6.15	Increasing the Back Cooler	120
6.16	Back Cooler as %TSC	121
6.17	Comparison of Designs A-G at $X_g=40$	122
7.1	Coolant Release Event	130
7.2	DI-CPV Flow	133
7.3	DI-CPV Boil	134
7.4	Light Transmission in Bubbles	137

LIST OF FIGURES

7.5	Optical Interfaces	139
8.1	Soldering Processes	143
8.2	Pre-coated Tab	144
8.3	Soldering Fixture	144
8.4	Series Resistance Measurements	145
8.5	Pre- and Post-soldering Measurement Set-ups	146
8.6	I-V Curves Pre-Post Soldering	147
8.7	Edge Shading	148
8.8	Back Side Solder Contacts	148
8.9	Front Side Solder Contacts	149
B.1	Four Square Graphs Explained	171

LIST OF FIGURES

List of Tables

2.1	CPV at IES and ANU	18
2.2	Commercialization of Linear Concentrators	19
3.1	Maximum Annual Revenues	28
3.2	Net Present Value Over Project Lifetime	29
3.3	Maximum Allowed Total System Cost	31
3.4	NOC	33
3.5	Subsystem Level Cost Targets	38
3.6	TU-Wien CPV Receiver Prototype	39
3.7	Cost Targets vs. Estimates	42
3.8	Identified Cost Reductions	42
3.9	Sea-based CPV Systems	48
3.10	Receiver Cost Reductions	48
3.11	Sea-based + Improvements	48
4.1	Active vs. Passive	53
5.1	CPV Receiver Components	63
5.2	Interface Temperatures	70
5.3	Thermal Interfaces	72
5.4	Common HTCs	75
5.5	Improving h_{total}	76
5.6	Back Cooler HTC for TIF Comparisons	83
6.1	TIF Designs	88
6.2	HTC Laminar Flow	95

LIST OF TABLES

6.3	Optimum Fluid Velocities and HTCs for H ₂ O*	100
6.4	Pool Boiling HTCs	105
6.5	Selection of TIMs	108
6.6	R _{TIM} and h _{TIM} for a Selection of TIMs	108
6.7	Parameters Used to Calculate Table 6.6	108
6.8	Summary of Conducting TIM	109
7.1	Suggested GWP Parameters	131
7.2	Dual Side vs. Back Side Cooling	131
7.3	Optical Losses at Zero Incidence	138
A.1	Terms IEC-62108	160
B.2	Assumed Parameters	163
C.1	World Wide CSP Potential in km ²	176
C.2	CSP Potential as Percent of Total km ²	177
C.3	BOM	178
C.4	BOM Total Cost Summary	179

Glossary

annual_revenue_i

A maximum theoretical revenue per square meter of collection area, assuming that the complete solar resource could be converted and sold at a stated electricity price.

capital_o

An initial one-time capital investment at the beginning of a CPV installation project used in determining the maximum allowed installed cost in €/W_{NOC}.

i

Indexing term representing project year in Eq. 3.1.

project end

End of project or project lifetime, specified in years.

r_{return}

Desired rate of return or time value of money for financing a potential project.

ANU

Australian National University

Back cooler

Heat exchanger used to exchange heat to the operating environment.

BLT

Bond Line Thickness

BOM

Bill of Materials

BOS

Balance of System

BP

British Petroleum Company

BSC

Back Side Contact solar cell

BSoA

Beyond State Of The Art

cell

Solar cell, PV or CPV

CHAPS

Combined Heat And Power Solar collector

CHP

Combined Heat and Power

Contact resistance

A resistance to heat transfer due to the contact of two surfaces.

CPV

Concentrator Photovoltaic

CPV System

All components associated with the energy conversion (“production”) and delivery of electrical energy (and thermal if CPV-T) to the end user.

CPV-T

Concentrator Photovoltaic-Thermal

CSP

Concentrator Solar Power

Cz

Czochralski process silicon

DI-CPV

Direct Immersion cooling of cells

DNI

Direct Normal Irradiation

Eff.

Efficiency, generally defined by the ratio of power produced to incoming solar irradiation.

Eq.

Equation

FZ

Float Zone silicon

grid parity

Local, regional, or national electricity prices for consumers and industry.

GWP

Global Warming Potential

H₂O*

Denotes de-ionized water

HFC

Hydrofluorocarbons

HTC

Heat Transfer Coefficient

IES

Instituto de Energia Sola

kW_{NOC}

Power rating at NOC (Section 3.4)

LGBG

Laser Grooved Buried Grid

Linear-focus trough

Parabolic or parabolic-like mirror system, focused skywards.

GLOSSARY

Long-term cost targets

Defined as whole sale electricity price, typically referenced to power production via coal.

MCT Micro-concentrator

MP Marginal Improvement in Performance

MTSC Marginal Total System Cost

NOC Nominal Operating Condition

NPV Net Present Value

O&M Operating and Maintenance

O&M_i Annual operating and maintenance cost, referenced to year “*i*”

Operating environment

The operating environment is the surrounding area in which the CPV system operates and exchanges heat via the back cooler. There is often a temperature associated with this environment which strongly influences the performance of the back cooler and ultimately the CPV system.

Optical interface

Briefly, an optical interface occurs wherever light passes through one medium into another in which the refractive index of the two materials differ, for example, air to glass.

Plate A plate is generally a flat piece of metal with width and height far exceeding its thickness. Many heat transfer examples analyze plates to illustrate or explain basic heat transfer principles and phenomena.

PV Photovoltaic

PVB Polyvinyl Butyral

Receiver body

The chassis or main body of the CPV receiver onto which CPV cells are thermally connected. In linear concentrator systems, the receiver is often extruded aluminum profile and is thus referred to as the receiver extrusion body or simply extrusion.

Short-term cost targets

Defined as grid parity within Europe.

SoA State Of The Art

STC Standard Test Conditions for establishing power output for one-sun photovoltaic cell, modules, and devices. STC conditions are: 1,000 W/m², 25°C, wind <1m/s.

Thermal interface

Generally, a thermal interface represents a physical interface or connection in which heat is transferred.

Thermal resistance

Analogous to resistance in Ohm’s law, a thermal resistance represents and impedance to the flow of heat and creates an associated ΔT across a thermal interface.

TIF Thermal Interface

TIM Thermal Interface Material

Total System Cost

All costs associated with manufacturing, producing, and delivering of electrical energy to the end user.

TSC Total System Cost

TSP Total System Performance

UPM Universidad Politecnica de Madrid

Nomenclature

Variable	Units	Description
β	-	Thermal expansion coefficient used in calculating HTC's for turbulent flow in pipes
η_e	-	Average CPV cell efficiency for a receiver or collection of receivers (case per case basis)
η_o	-	Optical efficiency of CPV system, including all optical losses from primary and secondary optics, as well as any additional optical interface
η_{stc}	-	Power efficiency under standard testing conditions
$\eta_1 \dots \eta_{11}$	-	Optical interface losses, referenced in Table 7.3
η_p	-	Pumping efficiency
γ_t	$^{\circ}\text{C}^{-1}, \text{K}^{-1}$	CPV cell power efficiency temperature coefficient
μ	$\text{Pa}\cdot\text{s}$	Kinematic viscosity
ν	m^2/s	Dynamic viscosity
ρ	kg/m^3	Density
σ	m	Root mean square roughness
τ_p	-	Transmission of p-polarized light
τ_s	-	Transmission of s-polarized light
θ	rad	Angle of incidence
θ_{cr}	rad	Critical angle
A_c	m^2	Area of the unit-cell
A_p	m^2	Aperture area, collector area (primary optics)
C_1, C_2	-	Constants used in Appendix B.5
C_o	€	Initial cost of the cooling system, i.e. back cooler
c	$\text{J}/(\text{kg K})$	Specific heat capacity
C_r	-	Initial cost of the cooling system as a percentage of total system cost for use in the economic optimum size of the cooling system, Section 6.9
d_h	m	Hydraulic diameter

continued on next page...

0. NOMENCLATURE

–continued from previous page–

Variable	Units	Description
$DNI_{(an)}$	$\text{kWh}/\text{m}^2\cdot\text{yr}$	Expected kWh available at one square meter from direct normal irradiation. By removing the unit (m^2), also represents the expected electrical production for a hypothetical CPV system rated at $1 \text{ kW}_{\text{NOC}}$
E_o	€	Initial total system cost of all components except the cooling system, $\text{TSC}-C_o$
f	-	Darcy friction factor
F_{p^*}	-	Modification factor in Eq. 6.12, accommodates deviations in applied pressure from the reference state h_o
F_{pf}	-	Parameter used by Motinski to accommodate the effects of pressure on pool boiling, see Eq. 6.15
F_q	-	Modification factor in Eq. 6.12, accommodates deviations in applied heat flux from the reference state h_o
F_w	-	Modification factor in Eq. 6.12, accommodates the combined influence of the heated wall's material properties and surface roughness
G_N	W/m^2	Direct normal irradiation, $900 \text{ W}/\text{m}^2$ at NOC
H	Pa	Micro-hardness of the softer material in a thermal interface made up of two different materials
h	$\text{W}/(\text{m}^2\text{K})$	Heat transfer coefficient, abb. HTC
h_{bc_op}	$\text{W}/(\text{m}^2\text{K})$	Heat transfer coefficient between the back cooler inlet temperature and the ambient air temperature
h_{bc}	$\text{W}/(\text{m}^2\text{K})$	Heat transfer coefficient of the back cooler
$h_{cell-wall}$	$\text{W}/(\text{m}^2\text{K})$	Heat transfer coefficient between the solar cell(s) and the receiver body's extrusion wall
h_{coh}	$\text{W}/(\text{m}^2\text{K})$	Maximum heat transfer coefficient for a finned surface (heat sink) utilizing natural convection, $320 \text{ W}/\text{m}^2\text{K}$, as given by Bar-Cohen
h_{con}	$\text{W}/(\text{m}^2\text{K})$	Heat transfer coefficient representing the thermal interface between a CPV cell and the receiver body via a series of conductive materials such as adhesives, tapes, or thermal greases, see Section 6.6
$h_{condense}$	$\text{W}/(\text{m}^2\text{K})$	Heat transfer coefficient for condensing on a pipe
h_{fl_wall}	$\text{W}/(\text{m}^2\text{K})$	Heat transfer coefficient between the surface of the receiver body's coolant wall and the coolant fluid
h_{high}	$\text{W}/(\text{m}^2\text{K})$	Upper-bound estimate of a heat transfer coefficient
h_{lam_X}	$\text{W}/(\text{m}^2\text{K})$	Heat transfer coefficient for fully developed laminar flow for a fluid denoted by X
h_{low}	$\text{W}/(\text{m}^2\text{K})$	Lower-bound estimate of a heat transfer coefficient

continued on next page...

–continued from previous page–

Variable	Units	Description
h_o	W/(m ² K)	Pool boiling heat transfer coefficients for standard reference conditions: heat flux of 20 kW/m ² , reduced pressure of $p^*=0.1$, and surface finish of $R_a=0.4\mu\text{m}$
h_{pb}	W/(m ² K)	Heat transfer coefficients for pool boiling
h_{pipe_wall}	W/(m ² K)	Heat transfer coefficient for conductive heat transfer through the pipe wall of a condenser pipe
h_{TIF}	W/(m ² K)	Total heat transfer coefficient between the solar cell(s) and the back cooler
h_{total}	W/(m ² K)	Total heat transfer coefficient
h_{total}^*	W/(m ² K)	Heat transfer coefficient resulting from the addition of h_{TIF} to h_{bc} , where h_{TIF} represents the thermal interfaces between the CPV cell and back cooler, see Eq. 6.21
h_{trb_X}	W/(m ² K)	Heat transfer coefficient for fully developed turbulent flow for a fluid denoted by X
h_n	W/(m ² K)	Heat transfer coefficient for material n , where n represents an indexing subscript
k	W/(m K)	Thermal conductivity
k_{TIM}	W/(m K)	Thermal conductivity of the TIM
k_h	W/(m K)	Harmonic mean thermal conductivity
L	m	A measurement of length. Depending on context, it may refer to cell length, receiver length, or total length of receivers connected in series.
L_{rec}	m	CPV receiver length used in Section 4.3, assumes no gaps between CPV cells such that the total length of all cells is equal to the receiver length
m	-	Mean asperity slope
M_{CO_2}	kg CO _{2eq}	Expected CO _{2eq} emissions from a coal-fired power plant over the project lifetime
M_{CPV}	kg CO _{2eq}	Expected CO _{2eq} emissions from a CPV power plant over the project lifetime
n	-	Index of heat transfer coefficient in Eq. 5.1 and 5.2, modifier of F_q in Eq. 6.13, index of successive marginal increase in Eq. 6.22 and 6.23
n_1, n_2	-	Index of refraction for material 1 and 2 respectively
Nu	-	Nusselt number
P	Pa	Pressure
P_{cr}	Pa	Critical pressure
p^*	-	Reduced pressure, P/P_{cr}

continued on next page...

0. NOMENCLATURE

–continued from previous page–

Variable	Units	Description
ΔP_p	Pa	Pressure difference
p	W/m ²	Power density, referenced to the active CPV cell area, unless otherwise specified
$p(h_{total})$	W/m ²	Power density, referenced to active CPV cell area, calculated via Eq. 5.4, assuming a HTC of h_{total}
P_{cell}	W	Power output of the unit-cell, represents power output of a solar cell minus its associated pumping losses for cooling via forced convection cooling in turbulent flow
P_{pump}	W	Pumping power necessary to overcome frictional losses in a section of the CPV receiver equivalent in length to the unit-cell's length
P_{rec}	W	Power output of a CPV receiver with a total active cell area given by $L_{rec} \cdot W_{rec}$
Q_{fl}	m ³ /s	Volumetric flow rate
Q	W	Heat
q	W/m ²	Heat flux
q_o	W/m ²	Standard heat flux for pool boiling calculations, 20kW/m ² , see Eq. 6.12 and 6.13
r	-	Rate of successive increases used for calculating TSC and reductions in T_o in Section 6.9
R_{cs}	m ² K/W	A portion of R_{cTotal} , representing the contact resistance of the asperities between the two surfaces
R_{cTIM}	m ² K/W	A portion of R_{cTotal} , representing the contact resistance between the TIM and the two joint surfaces of the thermal interface
R_{cTotal}	m ² K/W	Total thermal contact resistance between the two joint surfaces of the thermal interface
R_{rel}	-	Relative roughness of pipe wall
R_{TIM}	m ² K/W	Thermal resistance of an ideal thermal interface, assumes all gaps between the two joint faces are filled with the TIM
R_n	-	Reflectance for an angle of incidence of 0°
R_p	-	Reflectance of p-polarized light
R_s	-	Reflectance of s-polarized light
Re	-	Reynolds number
t	-	Time in years
ΔT	°C, K	Temperature difference

continued on next page...

–continued from previous page–

Variable	Units	Description
T_{amb}	°C, K	Ambient air temperature
ΔT_{amb}	°C, K	Temperature difference between an object or surface and the ambient air temperature
ΔT_{bc_op}	°C, K	Difference between the back cooler inlet temperature and the ambient air temperature
T_{cell}	°C, K	Operating temperature of the solar cell(s)
$\Delta T_{cell-bc}$	°C, K	Temperature difference between the solar cell(s) and the back cooler
$\Delta T_{cell-env}$	°C, K	Temperature difference between the solar cell(s) and the operating environment
$\Delta T_{cell-wall}$	°C, K	Temperature difference between the solar cell(s) and the receiver body’s extrusion wall
ΔT_{fl_wall}	°C, K	Temperature difference between the surface of the receiver body’s coolant wall and the coolant fluid
ΔT_n	°C, K	Temperature difference between CPV cells and T_{stc} for “n” successive reductions in cell temperature (see Eq. 6.22, Section 6.9)
T_{op}	°C, K	Operating temperature of a device
T_{plate}	°C, K	Temperature of a plate
$\Delta T_{receiver}$	°C, K	Temperature difference across the receiver
T_{stc}	°C, K	Standard temperature condition of 25°C (STC)
ΔT_{stc}	°C, K	Temperature difference from STC
$T_1 \dots T_{15}$	°C, K	See Table 5.2
ΔT_L	°C, K	Temperature difference across a length L of a CPV cell or series of receivers, depending on context.
ΔT_o	°C, K	Temperature difference between CPV cells and T_{stc}
u	m/s	Fluid velocity
V_{NOC}	liters/kW _{NOC}	Number of liters of coolant needed per 1kW _{NOC} rated of an installed CPV system
W_{rec}	m	CPV receiver width used in Section 4.3, assumes that CPV cell width is equal to the receiver width
ΔW	m	Additional width to the CPV receiver for a passive cooler, see Section 4.3
X_g	-	Geometric concentration factor
€/W _{heat}	€/W	Cost in Euros per watt of heat rejected to the operating environment, as per the manufacturer’s operating specifications
€/W _{NOC}	€/W	Cost, rated at NOC, as established in Section 3.4

0. NOMENCLATURE

1

Introduction

The purpose of this thesis is to assess whether or not an actively cooled, low concentration, concentrator photovoltaic (CPV) receiver could meet either grid parity or wholesale electricity prices under the assumption that electrical energy production is maximized and heat is considered a waste load. To do so, a set cost targets are derived for an actively cooled CPV receiver and cooler technology to meet short-term (grid parity) and long-term (wholesale electricity) price targets. The current cost of the receiver and proposed cooler are compared to these targets for three application scenarios. A list of possible improvements is derived, followed by a detailed analysis regarding the theoretical limits of these improvements. Taking these improvements into consideration, a final assessment of the technology is given. Perhaps most importantly, this thesis establishes a detailed and unique framework for understanding and comparing the heat transfer capabilities, and ultimately performance, of CPV receiver designs.

1.1 Thesis outline

This thesis is divided into nine chapters. The basic purpose of this chapter is to provide a motivation for concentrator photovoltaics, introduce a brief history of the technology, and classify various concentrator designs. In addition, current and future projects at TU-Wien, including a clarification on their interest in linear-focus trough concentrators, is outlined. These projects build upon the past efforts of other universities, which are described in Chapter 2.

1. INTRODUCTION

In Chapter 3, a cost assessment of an actively cooled CPV receiver is presented, which serves as the basis for the remainder of the cost study. A set of cost targets at both the total system and subsystem level are developed with special consideration for linear-focus trough CPV technology. To accomplish this, a nominal operating condition is proposed. A summary diagram was created, capturing a snapshot of relevant electricity prices and available solar resources, which relates the two to total system cost. The figure allows the user to quickly trace the trade-offs between cost and solar resource while also highlighting potential installation regions throughout the world. The necessary magnitudes of cost and performance improvements are highlighted by comparing the estimated costs of the CPV receiver with the derived targets. Several of such improvements are presented, including estimates on their theoretical potential for improvement. The remaining chapters provide the technical basis for these claims.

Chapter 4 describes the need for and various designs of cooling systems in CPV. Both passive and active cooling strategies are presented. Pulling from both theoretical and practical examples, a potential limit to passive cooling is proposed. The detailed discussion which follows provides numerous insights into the various cooling strategies and their relevant applications.

In Chapter 5, the major components, heat pathways, and nomenclature are defined for CPV receivers. Several design guidelines are highlighted, leaving the reader with a vivid understanding of the importance and intricacies of the cooling system. The chapter closes by deriving a quasi-optimal cooling system size (h_{bc}), which is used in the following chapters for comparing various thermal interface designs.

Chapter 6 introduces seven different linear CPV receiver designs, with each design containing a unique set of thermal interfaces between the solar cells and the back cooler. The heat transfer coefficients across these interfaces are calculated and later used to determine their respective and resulting power losses. These power losses are used to compare and rank the various designs. Taking into consideration additional known and perceived limits to the various cooling strategies, a technology road map was created, linking the various designs to increases in concentration ratio.

Chapter 7 defines several designs for direct immersion CPV receivers and discusses many of their challenges. Candidate cooling fluids are identified and a maximum global warming potential specification is derived and proposed. An estimate of the optical

losses arriving from front side boiling of the coolant is described and briefly estimated, highlighting future design challenges.

Chapter 8 introduces an alternative soldering method for CPV cells, developed in conjunction with the Australian National University (ANU). The method utilizes lead-free solders and has the potential to greatly reduce the number of cell processing and handling steps in manufacturing. Ultimately, this should provide a meaningful cost reduction.

Chapter 9 concludes the thesis by reviewing the derived cost targets and estimates, reiterating the points outlined in Chapter 3. The final technology map is again discussed and future work is outlined.

1.2 Motivation

The motivation behind concentrator photovoltaics is the same as that for traditional one-sun photovoltaics, to provide a renewable and economically competitive energy supply with a markedly reduced impact on the environment. This short and simple statement not only summarizes the motivation behind photovoltaics, but renewable energy technologies in general. Although rather motivational and morally pleasing, to be anything more than just pleasantries, such statements require a more forceful argument in today's consumer driven and, at the time of this writing, financially struggling society. The question to many, an alluringly and legitimate question, is why do we need renewable energy systems?

One might, and many do, argue the necessity, or lack thereof, of doing so. Reasons are numerous and cover a wide range of environmental, political, and social aspects. Many of these reasons, whether for or against the development of renewable energy technologies, carry with them a number of emotional sentiments. Such emotions, and the passions they drive, can be motivating. They can fire the heart into service, but they can also blind us to the true nature of a problem. Somewhere in between, we find a sensible but driven motivation. To this end, it is requested that the reader consider some of the following notions, ideas, and current bodies of research.

The last few decades have seen significant effort and study regarding the earth's climate and humankind's effects upon it. These efforts, largely organized by the Intergovernmental Panel on Climate Change (IPCC), have produced a critical mass of

1. INTRODUCTION

scientists worldwide, which have drawn the scientific conclusions that the earth's average annual temperatures are increasing, that these effects will manifest themselves in ways detrimental to human societies, and that the economic activities of humankind are driving these changes. Critics and their critiques, which when founded on a scientific basis should be welcomed, have attacked all three of these conclusions.

For the time being, critiques concerning whether increasing world temperatures constitutes itself as detrimental to human society, will be ignored. Nature will trump the ranting of the layman, and the complexity of the ecosystems that humankind currently requires for its survival are beyond even the most advanced simulation tools available. The true impacts of such temperature increases are difficult to predict. It is an uncomfortable unknown and is to be taken very seriously.

Increasing world temperatures have been scrutinized, as is to be expected and perhaps desired. The sheer magnitude of such measurements is daunting; the collection of such data and its subsequent analysis is no easy task. However, such criticisms are waning. Richard Muller, one of the leading critics to date, has concluded based on his own scientific studies that temperatures are indeed rising and finds much agreement with IPCC's 2007 conclusions [1], [2].

Muller argues for the study of the extent to which man is contributing to climate change. This question still remains, and will likely be debated for years to come. Given the cost to shift an economy from one energy system to another, some believe it is best to wait until science can better answer the question. But, this time may be unavailable. First, it takes decades to transition to new energy systems [3]. Second, evidence suggests that green house gas emissions must peak between 2010 and 2020 to avoid crossing the so called threshold between "dangerous" and "extremely dangerous" climate change [4] (information regarding these thresholds can be found in Ref. [5]). There is still an ongoing debate regarding the magnitude of such changes and their true impacts. And although it helps little to enter a state of panic, there is nevertheless reason for concern. A few excerpts from the Stern Review on the economics of climate change are particularly telling (see Ref. [6]):

Climate change threatens the basic elements of life for people around the world - access to water, food production, health, and use of land and the environment...

The risks of the worst impacts of climate change can be substantially reduced if greenhouse gas levels in the atmosphere can be stabilised between 450 and 550ppm CO₂ equivalent (CO₂e). The current level is 430ppm CO₂e today [2007], and it is rising at more than 2ppm each year. Stabilisation in this range would require emissions to be at least 25% below current levels by 2050, and perhaps much more. . .

This is a major challenge, but sustained long-term action can achieve it at costs that are low in comparison to the risks of inaction. Central estimates of the annual costs of achieving stabilisation between 500 and 550ppm CO₂e are around 1% of global GDP, if we start to take strong action now. . .

Using the results from formal economic models, the Review estimates that if we don't act, the overall costs and risks of climate change will be equivalent to losing at least 5% of global GDP each year, now and forever.

Renewable energy technologies such as photovoltaics and, as the focus of this thesis, concentrator photovoltaics have this potential to act and can play an important role in forming this new low-emission economy. This will take time and serious commitment. The question still remains, will society act? The predictions above make for great headlines and should be reason for concern, but some caution is still warranted. It would not be the first time in history that science has been manipulated to put forward the goals or political ideals of a group of individuals. The question is, what are these goals and what are these ideals? On the one hand, there are certainly large incentives for fossil fuel dependent industries and economies to manipulate or ignore the science of humankind-induced climate change, at least within the short term. On the other hand, there are those who would perhaps perpetuate the idea of climate change based on an ends-justify-the-means mentality, where the prospects of improving environmental conditions and developing a renewable and relatively inexhaustible energy supply outweigh any unfair bias or manipulation necessary to bring about such change. No matter how selfless or selfish such intentions might be, science is a quest for truth and knowledge; to manipulate it for one's own purposes, undermines its entire foundation.

In the end, climate change combines a growing and difficult scientific field with many political and economic interests. The potential is great for individuals to manipulate, influence, or altogether ignore the science of climate change. The current discussional

1. INTRODUCTION

environment can leave even the most informed and educated of individuals in a difficult position, with regard to directing economic and political actions. Nevertheless, decisions must be made. There are certainly benefits to developing renewable energy technologies outside of minimizing climate change, but it is the climate change aspect that drives the question of appropriate time frames and rates of deployment. The work derived from this thesis aims to support and accelerate these time frames. To those dedicated to similar aims, global warming may find itself listed in the pages of history books among many other apocalyptic events never to have occurred, but what of it. The opportunities to give-in, give up, or admit wrong are unlimited, but the opportunities for safeguarding the future are limited. Never be ashamed of caring too much.

In reaching for the ultimate goal of providing clean, renewable energy, concentrators compete head-on with existing fossil fuel-fired generators. Projected electricity costs from concentrator power plants are about three times the current [year 2000] cost of energy from natural gas power plants. Early concentrator plants will be twice as expensive again. There is nothing that can be done about this without government involvement, period. We need to decide as a society if environmental issues such as acid rain, global warming, and reduced health are important enough to subsidize this difference for a while. Factors of three can't be that big a deal in the broader picture.
-Richard M. Swanson[7]

1.3 A brief history of concentrator photovoltaics

An excellent review regarding the history of concentrator photovoltaics was compiled by the Instituto de Energia Solar (IES) at the Universidad Politecnica de Madrid (UPM) in the C-Rating Project [8]. In light of such work, only a brief summary of the history of concentrator photovoltaics is provided. The reader is further encouraged to consult Ref. [7] and [9] for more information.

One of the earliest reported linear concentrator systems is that of Frank Shuman, built in Meadi Egypt in 1913. The system utilized a series of parabolic concentrating mirrors to raise steam and run a small engine for pumping water. The next reported and most often cited work in concentrator technologies is the development activity following the 1973 oil crisis. In light of the first and second World Wars, 1914-18 and 1939-45

1.3 A brief history of concentrator photovoltaics

respectively, and the financial calamity of the Great Depression separating the two, this 60 year gap is perhaps understandable. Moral issues aside, a low energy density resource such as the sun did not particularly tailor itself well to the war-time efforts of developing more efficient ways of killing one's enemy. Between and throughout these wars, the sheer magnitude of technological, financial, and social change is difficult to imagine; however, it is plausible to suggest that such a time drove strategies focused on short-term survival. The oil crisis of 1973 changed all this. At a time in which environmental concerns regarding population and resources were surfacing, this sudden spike in oil prices and resulting public response sent a wave of government funding into renewable energy technologies. Serious funding for concentrator technologies began in 1976 with \$1.25M and peaked at \$6.2M in 1981 [7], approximately \$5M and \$15.5M when adjusted for year 2011. This work was largely driven by efforts at Sandia National Laboratories.

Moving into the 1980s, enthusiasm in CPV faded as energy prices declined. From the years 1975 to 1992 an estimated \$40M were invested [7]; however, no significant commercial developments were realized. CPV was envisioned as a large scale grid application, and it was believed that the prices of fossil fuels would continue to rise and that CPV would become cost competitive. As Swanson [7] states, "this did not happen." Not all was lost, cell efficiencies had been improved and flat panel one-sun photovoltaics found market share in off-grid applications [7]. With the introduction of the German feed in tariff in the late 90s, a firm market for photovoltaic panels developed. Moving into the next millennium, several factors came together to set the stage for another push in concentrator technologies. The increased demand of silicon, driven by the newly founded German market, drove prices for solar-grade silicon upwards. This put pressure on the reduction of silicon usage in module designs, for which concentrator technologies are particularly suited. In addition, cell efficiencies were dramatically increasing, moving from 30% to over 40% within the last 10 years [10]. To move beyond the relatively low system level efficiencies of the one-sun photovoltaic technologies, focus shifted towards utilizing higher efficiency concentrator cells in concentrator systems.

1.4 Classification of concentrator technologies

The various concentrator technologies can be roughly classified by three parameters: concentration factor, orientation, and type. To provide a general overview, Figure 1.1 presents various concentrator technologies according to these parameters. There are many conventions regarding concentration factor, including sometimes arbitrarily relative labels such as low, medium, and high. In this work, concentration factor will always refer to geometric concentration factor and will be represented by the term X_g . With regard to the relative levels of concentration, a convention similar to that as used by the European Photovoltaic Technology Platform was adapted, with low, medium, and high concentration ratios at 2-100, 100-300, and 300-1,000 respectively [11]. With regard to orientation, concentrator systems generally focus light either downwards or upwards with the former focusing light towards the ground and the latter towards the sky. Generally speaking, lens systems focus downwards and mirror systems focus upwards; however, light can be focused downwards by using 2 mirrors, as shown in Figure 1.1. Concerning type, concentrators generally focus in either one or two dimensions, i.e. linear and point focus systems. Except in the special case of some static concentrators ($X_g < 5$), a concentrator technology requires a minimum of D directions of tracking, where D represents the number of dimensions of concentration. This holds generally true for all lens and mirror based optic systems. However, a notable exception is the so called fluorescent planar concentrators, which utilize light-trapping techniques to concentrate both direct and diffuse light at the sides of a planar optic [12]. Most other concentrator technologies require tracking and are unable to utilize diffuse light.

1.5 Within and beyond the current challenges

In the quest for optimizing the cost to performance ratio of photovoltaics, there are two obvious factors to manipulate: cost and performance. These manifest themselves in concentrator photovoltaics as:

1. Cost: solar cells are expensive. . . use fewer of them
2. Performance: cell efficiency is limiting. . . use higher efficiency cells

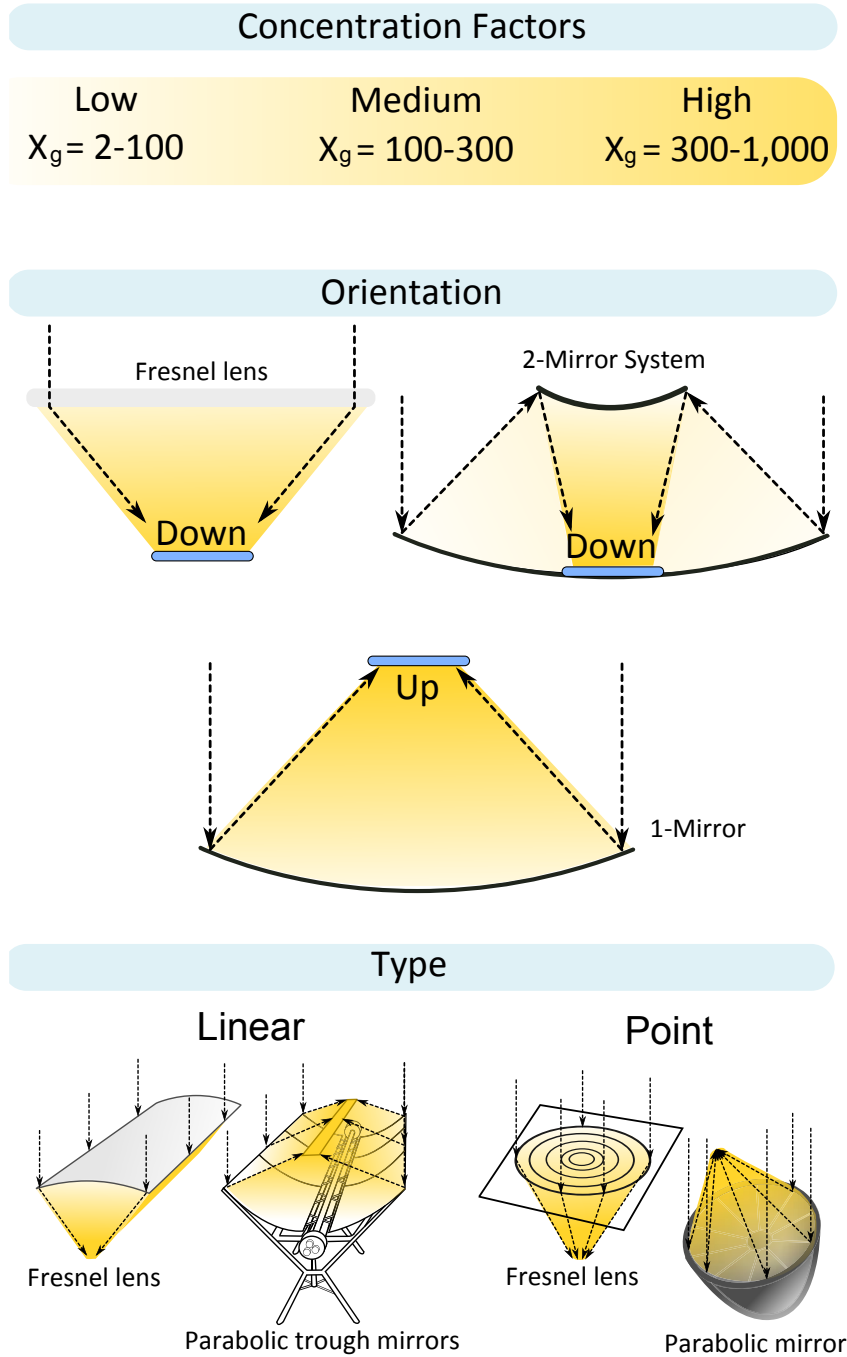


Figure 1.1: Concentrator Technologies - Classification of concentrator technologies.

1. INTRODUCTION

Within this last decade, with such high silicon prices [13], the first approach seemed promising. A number of low concentrating systems utilized modified or slightly upgraded silicon solar cells with some type of cooling system to manage cell operating temperatures [10]. However, silicon prices have decreased within the last few years [14]. In addition, alternative technologies such as thin-film photovoltaics have developed significant market share and realize similar reductions in cell material requirements without the need for tracking and additional cooling.

These developments certainly warrant reconsidering concentrator technologies, but it would be premature to dismiss the technology altogether without considering cell efficiencies. Silicon solar cell technology has nearly reached its theoretical performance limits within the laboratory [10], and efficiencies at the module level have reached 20% [15]. Additional performance improvements beyond silicon technology will require alternative cell designs such as the 30 to 40% efficient multi-junction cells [10]. Increased cell performance and its associated gains at the system level can result in cost reductions via reduced collection area e.g. fewer photovoltaic modules and reduced land usage. Unfortunately, multi-junction solar cells are much more expensive than silicon solar cells [10], and it is only at high levels of concentration where their use may be considered. Such approaches are being pursued by Soitec [16] and Amonix [17] and may prove successful, especially if the price of multi-junction cells decrease with the expected increases in production volumes.

For photovoltaic systems to reach grid parity and approach wholesale electricity prices, the cost to performance ratio is key. There are various approaches to reach these targets ranging from cheap, low efficiency materials covering large surface areas to high efficiency, expensive multi-junction cells in concentrators. There is still much debate as to which technologies will succeed in the long run; though, it is likely that there will be elements of both in the years to come. Nevertheless, there are a few factors which should be taken into consideration. Although there are efforts to integrate significant contributions of solar energy into buildings, many manufacturing and other industrial sites simply lack the physical space to operate solely on solar power. If large scale penetration is desired, then to at least some degree, utility scale integration is necessary. No matter how inexpensive a cell technology may become, large aperture areas will be necessary to capture power levels near the utility scale. Most existing technologies require substantial glass and aluminum to accomplish this. The prices of

1.5 Within and beyond the current challenges

these commodities cannot be realistically expected to decrease over time, and they make up a non-negligible portion of the total system cost.

Concentrator technologies can significantly reduce cell material requirements, and with a doubling of system efficiency, can perhaps reduce the remaining material requirement by a similar amount. However, regarding the low concentrator silicon systems of the last decade, it is difficult to imagine this technology moving forward with the prices of silicon decreasing. The efficiencies of such systems, in part due to their higher operating temperatures, do not yield higher operating efficiencies than their one-sun counterparts. One might argue that their energy yield is higher due to tracking, but such statements are unfairly biased. The yields of one-sun photovoltaic technologies also increase by utilizing tracking.

Furthermore, other than a reduction of silicon use, one must ask if there is a true savings in other materials. Although CPV receivers are typically smaller than photovoltaic modules, and utilize less glass and aluminum, this material is still needed for collection area in the concentrator itself. In other words, the material saved in the receiver is simply transferred to the optics and associated structure. Even worse, whereas a simple PVF sheet serves as a heat sink in one-sun photovoltaic modules, it is traded for an aluminum cooler in a CPV receiver. Such a cooler may utilize less surface area by utilizing highly conductive materials and by optimizing heat transfer; however, does it really make sense to trade a roll-to-roll process back sheet for an aluminum heat sink?

The purpose of this attack on low concentrator systems is not meant to dismiss the technology altogether, but rather to highlight changes in approach for a market where silicon prices are likely to remain low. It is with this idea in mind that TU-Wien began investigation into lightweight inflatable parabolic-like trough concentrators, with the hope of drastically reducing material requirements in addition to the reduction in cell material. Such concentrators use thin foils to create two pressure chambers, separated by a thin mirror foil. An example is shown in Figure 1.2.

By applying a slight over pressure to the upper chamber, the mirror foil is forced into a concave shape, which can be used to create a line focus. The shape approximates the radius of a circle better than that of a parabola, resulting in a higher positioning of the receiver. Also, the angles of incident light are typically lower as compared to the parabolic concentrating mirrors utilized in concentrator solar thermal systems.

1. INTRODUCTION

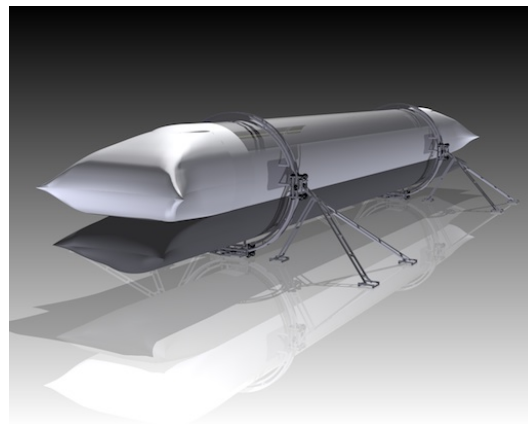
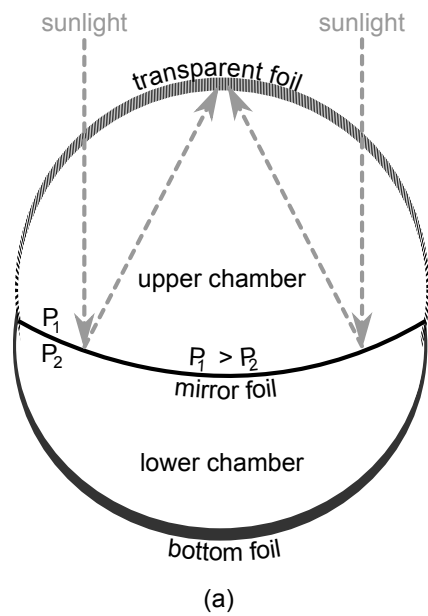


Figure 1.2: Inflatable Linear-focus Trough Concentrator - An example of an inflatable concentrator (a) basic schematic (b) artists rendition courtesy of Heliovis AG.



Figure 1.3: HELIOtube - A 40m inflatable trough concentrator in northern Austria, photo courtesy of Heliovis AG.

1.5 Within and beyond the current challenges

There are several interesting aspects to an inflatable trough concentrator which will be briefly explained. First, the design creates a continuous mirror via a roll-to-roll process and avoids shading due to gaps, typically associated with parabolic mirrors. It is hoped that this may allow for a reduction in the complexity of interconnecting and the number of bypass diodes in the CPV receiver. In addition, this should increase the overall power output of series connected CPV receivers within the concentrator. Second, inflatable concentrators aim to significantly reduce weight and material usage as the pressure chambers serve as their own internal structure. The example in Figure 1.3 illustrates this point nicely. Notice that the only supporting structure in the 40 meter prototype is a series of evenly spaced rings.

Lastly, and this brings a conclusion to background behind this thesis, it is ultimately hoped that an inflatable concentrator could be utilized on floating platforms along the seaside. Examining Europe's available land and solar resources, it becomes quickly apparent that there is a shortage of overlap between the two [18]. Some of the most promising regions of solar resource lay in and around the southern coastal regions. As an alternative to shipping concentrator solar power from Africa, it is proposed to develop concentrator systems for deployment across the southern coastal waters of Europe. Both actively and passively cooled receiver designs have been considered; however, in light of the practically infinite cooling fluid, i.e. seawater, this thesis focuses on an actively cooled receiver design. To date, the ANU Combined Heat And Power Solar (CHAPS) receiver most appropriately fits the design requirements of this project and is thus considered to be the state of the art technology in this field. As such, the cost analysis given in Chapter 3 uses the ANU CHAPS design as a baseline with a small number of modifications, further outlined in Chapter 3.

1. INTRODUCTION

2

Existing Linear Concentrator Systems

In the mid to late 90's, two universities most notably focused on developing linear-focus trough concentrator systems. They aimed to demonstrate technological feasibility and to compete with existing one-sun solar technologies. This work was carried out by the Centre for Sustainable Energy Systems of the Australian National University (ANU) and by the Instituto de Energia Solar (IES) at the Universidad Politecnica de Madrid (UPM). A brief history of their developments is given (Table 2.1), so as to describe the current state of the art of concentrator photovoltaic (CPV) receivers technology.

2.1 Efforts at ANU

In the 1990's, ANU developed a 2-axis tracking linear-focus trough system and built a 20 kW_p installation for the WA power company. See Figure 2.1. The system utilized float zone (FZ) silicon (Si) concentrator cells designed and developed at ANU for concentration ratios of 20 to 50 suns [19]. These cells achieved efficiencies of approximately 22% at 20 to 30 suns [20]. At a concentration ratio of 23 and using fin plate heat sinks, the system stabilized cell temperatures around 30 to 40°C [20] above the ambient air temperature. The system converted electrical energy at an efficiency of 13% [21] to 14.8% [20] when measured at 900 W/m², 20°C ambient temperature, and 1 m/s wind speed. From Ref. [20] and [21], it is unclear whether these efficiencies account for DC-AC conversion losses.

2. EXISTING LINEAR CONCENTRATOR SYSTEMS

ANU next attempted to transfer their 2-axis tracker technology to roof-top installations where both electricity and thermal energy could be utilized in residential homes. This program was entitled the Combined Heat And Power Solar collector (CHAPS) [22]. Shortly after beginning the program, focus shifted away from the 2-axis systems for residential homes and towards a single axis linear-focus trough design for rooftop installations. The driving factors behind this shift included concerns of wind loads induced into the rooftops of residential homes as well as the overall economics of the system [22]. Concentration factor was increased to 37 [22]. The CPV receiver incorporated the ANU concentrator cells but was adapted to use an active cooling system, so that waste heat could be utilized for residential hot water purposes. The receiver was constructed from an extruded aluminum pipe with integral internal fins for improved heat transfer. The extruded pipe included a flat section for thermally bonding the concentrator solar cells. Several thermal tapes were investigated for bonding the cells to the pipe. DC electrical efficiencies of 10-12% as well as thermal efficiencies from 54-62% were realized on smaller scale prototypes [22].

In 2006, a 40kW PV thermal system was installed for the Bruce Hall dormitory, accommodating up to 90 students [23]. See Figures 2.2 and 2.3. The system demonstrated combined electric and thermal efficiencies above 60% and included traditional boilers for supplementation when needed [23]. The possibility of commercializing such a system exists, but there is still development work needed to bring various components to market. In addition to a number of other photovoltaic projects ongoing at ANU, work on concentrator systems has shifted back to the integration of concentrator photovoltaic-thermal (CPV-T) systems onto residential roof tops. A new micro-concentrator design with a linear-focus, rotating mirror, and fixed photovoltaic thermal receiver design is currently under development [24]. See Figure 2.4

2.2 Efforts at IES

At the Instituto de Energia Solar at the Universidad Politecnica de Madrid, work on linear concentrators during the mid to late 90's was conducted under the program: European Concentrated Light-Intensity Development of Energy Sources (EUCLIDES). The EUCLIDES project developed a linear-focus trough concentrator design utilizing a unique dual row V-shaped photovoltaic receiver module [25]. In partnership with

BP solar, IES was able to develop concentrator cells with 18% efficiencies at 30 suns that could be manufactured on the BP's 1-sun Saturn cell line [25]. The EUCLIDES used these cells at a concentration factor of 33. A passive cooling system, consisting of aluminum heat sinks, limited temperatures to 35°C above ambient air temperatures under no wind conditions [26]. The size of this heat sink is estimated to be 280mm wide (transverse direction) by 140mm high with 1mm thick cooling fins [26] [27], but the exact dimensions are unclear, as several different sets of dimensions are given in the aforementioned papers. Receiver DC conversion efficiencies were reported between 14.6% (800 W/m², 20°C, wind speed unknown) and 15.1% (800 W/m², 25°C, 2m/s wind speed) [27]. One-sun receiver efficiencies at standard testing conditions (STC: 1000 W/m², 25°C, 1m/s wind speed) were 16.9% and 17.4% for the first and second generation designs [28]. The first generation system was installed in Madrid, Spain and reported year round efficiencies of 9.6% (whether DC or AC is unclear) [28].

The second generation system, 480kW_p, was installed at Tenerife on the Canary Islands, and experienced a number of module failures [29]. It was discovered that the adhesive portion of the thermal tape used in the Gen-II modules lost its adhesive properties at 100°C [29]. As such, adequate thermal contact could not be maintained which initiated a thermal failure. Alternatives were researched to replace the thermal tape. Soldering of 120mm x 120mm cells to direct bonded copper (DBC) substrates were tested, but the soldering procedure itself lead to cell temperatures of 200°C and cell warping of nearly 2mm [29]. In addition to cell warpage, the cost of DBC substrates were high and the solution was abandoned. Instead, an insulating metallic substrate (IMS) consisting of a thin dielectric material (epoxy) sandwiched between an aluminum substrate and a thin layer of copper was used. Cells of 116mm x 51mm were successfully soldered to a patterned IMS, but significant bending persisted [29]. Mention was made of the necessity of further improvements.

The solution pursued for the third generation of the EUCLIDES system glues the solar cell, using a thermally conducting epoxy, to an alumina plate. The alumina plate is then glued to an aluminum heat sink [29]. Two examples of the EUCLIDES-III system are shown in Figures 2.5 and 2.6 respectively. Since 2011, no new articles regarding the Gen-III model were found. In Ref. [25] the authors mention that BP, the licensee of the receiver technology abandoned the project.

2. EXISTING LINEAR CONCENTRATOR SYSTEMS

Table 2.1: CPV at IES and ANU - Summary of development efforts at IES and ANU.

	EUCLIDES	ANU 2-Axis Trough	ANU CHAPS
Concentration	33x	23x	37x
Optics	mirror split parabolic	mirror parabolic	mirror parabolic
Aperture			
L x W [m]	1.2 x 1.5	1.6 x 1.2	1.55 x 1.42
Area [m ²]	1.8	1.92	2.2
Cell			
Description	BP LGBG	ANU Cells	ANU Cells
Material	Cz Mono-Si	FZ Mono-Si	FZ Mono-Si
Dimensions	40mm x 116mm	40mm x 50mm	40mm x 50mm
Eff. STC	18%	22%	22%
	30 suns	20-30 suns	20-30 suns
CPV Receiver			
#/module	2	1	1
Configuration	split V	skyward	skyward
Dimensions	1.2m length	1.6m length	1.5m length
[kg/m ² aperture]	8.75	4.2	-
# Cells	10 in series	26-28 in series	28 in series
Eff. STC	16.9-17.7%	-	-
System Eff.			
Electrical	<10%	13-14.8%	10-12%
Thermal	-	-	54-62%
Location	Madrid, Spain	Rockingham, Australia	Canberra, Australia
Cooling			
Type	Passive	Passive	Active CHP
Description	Al Heat Sink	Al Heat Sink	Al pipe
ΔT_{amb}	35°C	30-40°C	65°C T_{op}
Sources	[25] [26] [27] [28] [29]	[19] [20] [21] [22] [23] [24]	[19] [20] [21] [22] [23] [24]

2.3 Commercialization efforts

Table 2.2: Commercialization of Linear Concentrators - Three commercialization efforts for linear concentrator technologies.

	ENTECH Solar Solarvolt [31]	Skyline Solar X14 [32]	Chromasun ANU MCT [30]
Concentration	20x	14x	20-30x
Optics	lens Fresnel	mirror split parabolic	mirror split Fresnel
Module			
Type	roof-top box	ground mount	roof-top box
LxWxH [m]	1.65x1.0x0.15	-	3.0x1.2x0.3
Cell			
Description	upgraded one-sun cells	upgraded one-sun cells	upgraded BSC cells
Material	Mono-Si	Mono-Si	Mono-Si
Eff. STC	18-20%	-	18%
	20 suns	-	15 suns
CPV Receiver			
#/module	6	2	10
# Cells/rec	60 series	-	30 series
Configuration	\perp lens	split V	-
Cooling			
Type	Passive	Passive	Active CHP
Description	Al plate	Al heat sink	metal pipe
T _{op}	30°C ΔT_{amb}	-	50-70°C

2.3 Commercialization efforts

Work on both the EUCLIDES project and CHAPS project have ceased. Both universities have moved on to other projects. However, elements of each technology can be seen in ongoing projects as well as some commercialization efforts. Much of the knowledge gained by ANU in the CHAPS program has been focused into their next venture with Chromasun, developing a small roof-top concentrator for CPV-T [30]. See Figure 2.4. The core elements of the EUCLIDES design, Figure 2.5, can be seen in Skyline Solar’s “Solar X14” product, Figure 2.7. A third commercialization example, by Entech Solar, is shown in Figure 2.8. Table 2.2 provides a brief summary of these three technologies.

2. EXISTING LINEAR CONCENTRATOR SYSTEMS



Figure 2.1: ANU Two Axis Tracker - Rockingham 2000 [33].

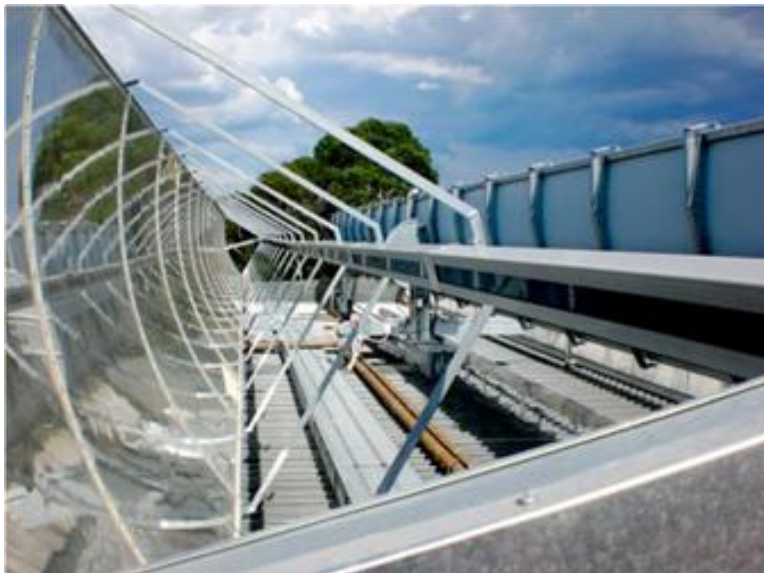


Figure 2.2: CHAPS - CHAPS at Bruce Hall 2010.



Figure 2.3: CHAPS at Focus - CHAPS in operation, 2011.



Figure 2.4: Chromasun - CPV-T micro-concentrator by ANU [34].

2. EXISTING LINEAR CONCENTRATOR SYSTEMS



Figure 2.5: EUCLIDES-III - Madrid, Spain [35].



Figure 2.6: EUCLIDES-III at Focus - Stuttgart, Germany [35].



Figure 2.7: Skyline - Skyline X14 concentrator [32].



Figure 2.8: Entech - Entech Solarvolt concentrator [31].

2. EXISTING LINEAR CONCENTRATOR SYSTEMS

3

Cost Targets, Estimates, and Improvements

3.1 Introduction

The main purpose of this chapter is to estimate the cost of the TU-Wien prototype concentrator photovoltaic (CPV) receiver design and a potential cooling system, to compare these costs to allowed targets, and to identify and characterize possible improvements. In addition, this chapter attempts to answer the following two questions:

How much should a CPV system cost?

&

Where should I install it?

To do so, cost targets are first derived at the total system level. A useful diagram is next introduced, that summarizes the total system cost (TSC) targets and presents desirable geographic locations for the installation of CPV systems throughout the world. The diagram contains a series of constant cost curves, which the user may follow along to quickly identify a minimum required solar resource and electricity price necessary to meet a desired economic rate of return. With the total system cost defined, historical data is then used to derive a set of cost targets at the subsystem level, including the CPV receiver and cooling system. Shortly thereafter, an estimate of the current CPV receiver design and cooling system is given. These costs are then compared to the derived cost targets. Lastly, several potential cost and performance improvements are identified and discussed.

3. COST TARGETS, ESTIMATES, AND IMPROVEMENTS

With regard to cost targets for CPV systems, three applications are described below, which will be referenced throughout this work. The specified total system level cost targets are valid for all three applications. At the subsystem level, cost targets are derived for land based CPV systems. These targets also apply to CPV-T and sea-based systems, but are slightly reinterpreted and discussed further in later sections.

Land-based CPV systems in which electricity production is the primary focus and excess heat is disposed to the environment via a cooling system

Concentrator Photovoltaic and Thermal Systems (CPV-T) land-based systems producing electricity and utilizing excess heat for commercial or industrial use, greatly reducing and mostly eliminating the size and cost of the cooling system

Sea-based CPV Systems where large floating platforms support CPV systems and the available sea water can be utilized for cooling, greatly reducing and mostly eliminating the size and cost of the cooling system, focus is again on electricity production

3.2 Total system cost targets

Total system cost refers to all costs associated with manufacturing, producing, and delivering of electrical energy to the end user. Targets for total system cost are derived in Sections 3.2.1-3.2.3. The methodology used to derive these targets will be briefly outlined here. A set of solar resources (direct normal) and electricity prices is used to produce a matrix of possible annual revenues for a hypothetical CPV system (see Table 3.1, Section 3.2.1). Each annual revenue entry in Table 3.1 is then appropriately discounted and summed across the project lifetime to produce a second matrix (Table 3.2, Section 3.2.2), containing total discounted revenues across the project lifetime, i.e. a net present value (NPV) for each value of the annual revenue matrix. Then, a minimum acceptance criteria of $NPV \geq 0$ is assumed for any project proposal. Next, it is assumed that the total cost of the CPV system is equal to a one time initial capital investment at the beginning of the project. Thus, the net present values in Table 3.2 represent the total cost of the proposed CPV system. These costs are then converted into cost targets, based on a power rating developed in Section 3.4. Finally, the cost targets are presented using this new power rating in Table 3.3. This matrix is used in Section

3.5.1 to produce the constant cost curves in Figure 3.2 that provide the reader with a user-friendly diagram, relating solar resource and electricity prices.

3.2.1 Maximum, theoretical, annual revenues

How much should a CPV system cost? The answer to this question depends on both geographic location and economic conditions, for which a near infinite number of possible combinations exist. In short, there is no one cost value for a CPV system but rather a range of costs. Any attempt to answer the question, how much should a CPV system cost, must therefore limit the scope of any analysis to a sensible range of parameters. Three parameters which largely affect the allowed cost of a CPV system are the average annual direct normal solar irradiation (DNI) in $\text{kWh}/(\text{m}^2\cdot\text{yr})$, electricity prices, and the nominal operating condition of the CPV system. Using the first two parameters, one can derive a range of theoretical allowed costs for a CPV system at various solar resources and electricity prices, as outlined in this section. Using the third parameter, nominal operating condition, one can adapt the range of theoretical costs to fit the expected performance of real-world systems.

A reasonable range of solar resources and electricity prices may be found in studies [18] and [36] respectively. From these sources, a series of annual revenues may be derived by multiplying the annual direct normal solar resource in kWh/m^2 by a series of electricity prices (or equivalent feed-in tariffs). Each resulting product represents the maximum theoretical revenue per square meter of collection area, assuming that the complete solar resource could be converted and sold at the stated electricity price. These annual revenues are shown in Table 3.1. This idea, complete utilization of a solar resource, assumes that 100% of the solar energy available to a direct normal surface could be converted to and sold as electrical energy to a consumer, while incurring zero losses for the entire conversion process. This is a mere mathematical assumption, necessary for the moment, so as to define an absolute upper limit for annual revenues. As neither an actual nor theoretical system could realize such conditions, it may help the reader to think of Table 3.1 as merely a list of annual revenues received for delivering a specified number of kWh at a particular electricity price. The requirements of a CPV system that is capable of delivering the specified number of kWh and the effects that this has on revenues and ultimately cost targets will be addressed in Section 3.2.3.

3. COST TARGETS, ESTIMATES, AND IMPROVEMENTS

Table 3.1: Maximum Annual Revenues - Maximum, theoretical, annual revenues in Euros for one square meter of aperture area at various solar resources (direct normal irradiation) and electricity prices, assuming complete utilization of the solar resource, but excluding O&M costs.

DNI _(an) kWh/(m ² .yr)	€/kWh								
	0.05	0.07	0.09	0.15	0.21	0.25	0.30	0.35	0.40
2000	100€	140	180	300	420	500	600	700	800
2100	105	147	189	315	441	525	630	735	840
2200	110	154	198	330	462	550	660	770	880
2300	115	161	207	345	483	575	690	805	920
2400	120	168	216	360	504	600	720	840	960
2500	125	175	225	375	525	625	750	875	1000
2600	130	182	234	390	546	650	780	910	1040
2700	135	189	243	405	567	675	810	945	1080
2800	140	196	252	420	588	700	840	980	1120
2900	145	203	261	435	609	725	870	1015	1160
3000	150	210	270	450	630	750	900	1050	1200€

3.2.2 NPV and economic assumptions

Assuming an appropriate operating and maintenance (O&M) cost, rate of return, and project lifetime, each annual revenue in Table 3.1 may be properly discounted and then summed over the project lifetime (using Eq. 3.1) to determine a net present value for each annual revenue stream. These NPVs are shown in Table 3.2, where each table entry represents the NPV for a hypothetical project proposal in which an annual revenue, cross referenced by the same row and column entry as in Table 3.1, is received throughout the project lifetime.

$$NPV = \sum_{i=year\ 1}^{project\ end} \left[\frac{annual_revenue_i - O\&M_i}{(1 + r_{return})^i} \right] - capital_o \quad (3.1)$$

To generate Table 3.2, fixed assumptions for project lifetime, rate of return, and O&M costs were adopted from Ref. [37] and are 20 years, 15%, and 10% of total system cost respectively. Reference [37] analyzes the time frame and investment required to install concentrating solar power plants in Africa, capable of providing power to Europe at prices competitive with coal based technologies. The financial assumptions made in

3.2 Total system cost targets

Table 3.2: Net Present Value Over Project Lifetime - Net present value for each annual revenue stream, cross referenced by the same row and column entry as in Table 3.1, and calculated using Eq. 3.1. Each value of NPV represents the maximum, theoretical, total revenue in Euros, discounted over the project lifetime, for one square meter of aperture area at various solar resources (direct normal irradiation) and electricity prices, assuming complete utilization of the solar resource, and including O&M costs.

DNI _(an) kWh/(m ² .yr)	€/kWh								
	0.05	0.07	0.09	0.15	0.21	0.25	0.30	0.35	0.40
2000	563€	789	1014	1690	2366	2817	3380	3943	4507
2100	592	828	1065	1775	2484	2958	3549	4141	4732
2200	620	868	1115	1859	2603	3098	3718	4338	4957
2300	648	907	1166	1944	2721	3239	3887	4535	5183
2400	676	946	1217	2028	2839	3380	4056	4732	5408
2500	704	986	1268	2113	2958	3521	4225	4929	5633
2600	732	1025	1318	2197	3076	3662	4394	5126	5859
2700	761	1065	1369	2282	3194	3803	4563	5324	6084
2800	789	1104	1420	2366	3312	3943	4732	5521	6309
2900	817	1144	1470	2451	3431	4084	4901	5718	6535
3000	845	1183	1521	2535	3549	4225	5070	5915	6760€

the study reflect currently understood and believed future performance of concentrator solar power (CSP) systems (utilizing steam turbine generators) and suggests that cost competitiveness with coal (wholesale electricity prices) is to be adopted as a long-term cost target for concentrating solar power. A CPV system could be expected to meet similar cost and performance targets. Thus, adopting the same financial assumptions seems appropriate. However, a few noteworthy exceptions were made. Whereas Ref. [37] uses a range of values for a rate of return from 5 to 15% percent, the highest value was assumed for CPV, 15%, to account for both the real and perceived increased risks associated with CPV.

Whether real or perceived, one may divide these risks between those associated with one-sun photovoltaics and those associated with CSP. With regard to one-sun photovoltaics, the moving components associated with tracking increase the number of possible failure modes. Although the non-moving components of many traditional one-sun photovoltaic installations were (and still are) particularly important for many of the early off-grid solar power applications, systems with moving parts should not

3. COST TARGETS, ESTIMATES, AND IMPROVEMENTS

be altogether shunned. One should keep in mind that tracking is also used in one-sun photovoltaic installations. The reliability of CPV tracking systems can be measured, much like any other manufactured component, and any increased risk may be assessed and included as needed. Admittedly however, if it is also assumed that many of the low concentration linear concentrator designs for CPV are still in an early development phase, then the tracking systems used by these systems may in fact incur an increased risk of failure and thus justify an increase in the rate of return, as previously stated. An argument for the existence of increased risk in CPV over CSP focuses on the receiver design itself. One might argue, based on world wide installed capacity of CSP vs. CPV, that there is more field experience for CSP absorbers than that of CPV receivers, and that this reduction in field experience carries an increased risk for CPV.

It is difficult to assess whether all these concerns warrant using the upper limit for rate of return cited in Ref. [37]. The primary reason for using this upper limit was to appease any perception that CPV carries an inherently greater risk than CSP. Further study is needed before any such claim could be made. In future studies, it may be possible and advisable to reduce the rate of return. Doing so would increase the allowed cost of a CPV system, thus making cost targets easier to meet.

Finally, it is assumed that the proposed CPV plant is financed by a one time initial capital investment. Unplanned failures or necessary replacements (inverters for example) would in fact require further investments, and these costs are unlikely to be distributed equally over the project. Nevertheless, the remaining O&M costs were distributed equally over the project lifetime and subtracted from the annual revenues ($O\&M_i$ in Eq. 3.1) to simplify the analysis.

3.2.3 From NPV to cost targets

If one were to set a minimum financial acceptance criteria for a project proposal of $NPV \geq 0$, and assuming that the project is financed by a one time initial capital investment, then the NPVs in Table 3.2 now represent the initial capital investment for each project proposal. Otherwise stated, these values represent the cost of the proposed CPV system. Furthermore, these costs represent the maximum allowed costs for a proposed CPV system in which a specified number of kWh at a particular electricity price is delivered (referenced by row and column in Table 3.1 respectively). Considering the initial assumption of complete utilization of the solar resource, a peak power rating of

3.2 Total system cost targets

Table 3.3: Maximum Allowed Total System Cost - Maximum, allowed, total system cost. ¹Cost targets in €/kW_{NOC}.

DNI _(an) kWh/(m ² .yr)	€/kWh								
	0.05	0.07	0.09	0.15	0.21	0.25	0.30	0.35	0.40
2000	563 ¹	789	1014	1690	2366	2817	3380	3943	4507
2100	592	828	1065	1775	2484	2958	3549	4141	4732
2200	620	868	1115	1859	2603	3098	3718	4338	4957
2300	648	907	1166	1944	2721	3239	3887	4535	5183
2400	676	946	1217	2028	2839	3380	4056	4732	5408
2500	704	986	1268	2113	2958	3521	4225	4929	5633
2600	732	1025	1318	2197	3076	3662	4394	5126	5859
2700	761	1065	1369	2282	3194	3803	4563	5324	6084
2800	789	1104	1420	2366	3312	3943	4732	5521	6309
2900	817	1144	1470	2451	3431	4084	4901	5718	6535
3000	845	1183	1521	2535	3549	4225	5070	5915	6760

one kilowatt (1 kW_p) per square meter would be associated with such a system, and the values of Table 3.2 could be considered as cost targets in terms of €/kW_p.

In reality, no system can achieve a lossless conversion of a solar resource into electrical energy. However, the aforementioned total system cost targets, derived under such an assumption, may still be utilized, so long as one decouples the assumption that the installed area for a 1 kW_p CPV system must equal one square meter. Effectively, this means installing more area to accommodate for the less than 100% energy conversion efficiency. Under this definition, it becomes critical to specify a set of testing conditions that define a 1 kW_p power rating. In order to use the cost targets in Table 3.2 for real CPV systems, such a system, rated at 1 kW under such testing conditions, must in fact, in its real-world application, deliver an equivalent number of kWh for its corresponding annual revenue and electricity price, as given in Table 3.1. If a limited number of geographical locations are appropriately selected, then a nominal operating condition (NOC), representative of the CPV system's average performance throughout the year, may satisfy the criteria outlined above. This approach is pursued in Section 3.4, where a NOC is proposed. Using this NOC, and assuming that the approach is reasonably appropriate, the cost targets established in Table 3.2 are suggested for linear-focus trough concentrators of low concentration. These targets are reprinted for the reader's

3. COST TARGETS, ESTIMATES, AND IMPROVEMENTS

convenience in Table 3.3 with units €/kW_{NOC} and will be used to generate a set of constant cost curves for the summary diagram in Section 3.5.

3.3 Potential installation sites

Reference [18] gives an excellent report on world solar resource relative to CSP and is used to identify possible installation locations throughout the world. The solar resource, in kWh/(m²·yr) of direct normal irradiation, is displayed across a world map, identifying areas of high solar resource. In addition, this solar resource map is overlaid with areas of available land-based CSP applications. Land deemed acceptable for solar concentrator applications was determined by considering areas with a minimum DNI of 2,000 kWh/(m²·yr) and based on the following exclusion criteria [18]:

Slope > 2,1 %, land cover like permanent or non-permanent water, forests, swamps, agricultural areas, shifting sands including a security margin of 10 km, salt pans, glaciers, settlements, airports, oil or gas fields, mines, quarries, desalination plants, protected areas and restricted areas.

The authors provide several tables, sorting the data by both solar resource and by location. As part of this thesis, these tables were adapted and modified to arrange the data in a more compact form, which could then be utilized in a convenient diagram (see Section 3.5). These modified tables are given in Appendix C for reference. Briefly, several interesting conclusions will be mentioned. A total of 26,363,055 km² of land surface were deemed acceptable for CSP [18]. Of this total, 49.1%, 23.1%, and 9.8% lies within Africa, Australia, and the Middle Eastern region respectively. Assuming traditional parabolic trough technologies with an efficiency of 12% and land use factor of 37%, the study calculates a total global potential of nearly 3,000,000 TWh/yr [18].

3.4 Nominal operating condition

A nominal operating condition, to establish an appropriate power rating, is proposed in Table 3.4. The values for irradiation and wind speed were adopted from guidelines given in IEC-62108 [38]. An average annual-operating temperature was estimated by considering three aspects: an annual average ambient air temperature, an average temperature difference between the CPV cell and the ambient air, and a consideration for

3.4 Nominal operating condition

Table 3.4: NOC - Proposed nominal operating condition.

Parameter	Irradiation	Cell Temperature	Wind Speed
Value	900 W/m ²	65°C	< 3 m/s

a temperature difference across the CPV receivers. An estimate for average ambient air temperature was derived by examining monthly average temperature data from Ref. [39] and [40]. These monthly averages are shown in Figure 3.1 for several regions of interest and range from 10°C to 35°C. As Ref. [18] identifies Northern Africa, Australia, and the Middle East regions to contain some of the earth’s most promising installation sites, in terms of solar resource and suitable land surfaces, temperatures in these regions were considered. An average yearly ambient air temperature of 30°C was selected.

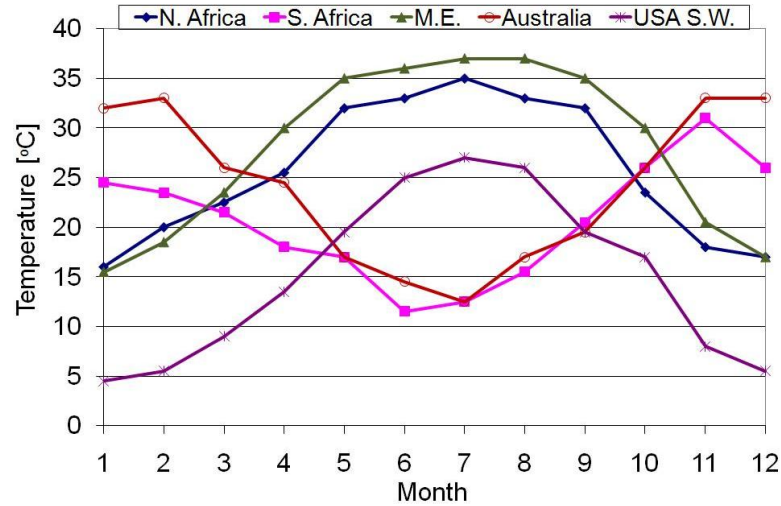


Figure 3.1: Average Regional Temperatures - Average yearly regional temperatures throughout the world.

For linear-focus trough CPV systems with geometric concentration factors between 20 and 40, average temperature differences between the CPV cells and the ambient air have been reported between 22 and 30°C [27] and 30 and 40°C [20]. Based on these reports, 30°C was selected to represent the average design target for the temperature difference between the CPV cells and the ambient air. An additional 5°C was added to the nominal operating temperature in an attempt to account for any additional decrease in the CPV system performance due to temperature differences across the receivers. By

3. COST TARGETS, ESTIMATES, AND IMPROVEMENTS

summing the three aforementioned temperature values, a nominal operating temperature of 65°C was derived.

To summarize, this section has put forth a nominal operating condition for linear-focus trough CPV systems, in light of any such existing proposal. It remains to be proven that a system rated under the proposed NOC would in fact yield, within an acceptable tolerance, the equivalent kWh necessary to generate the revenues outlined in Table 3.1. To test the validity of the proposed NOC, one must either measure or simulate the performance of a particular CPV technology for numerous locations throughout the various regions of interest and compare the annual yields in kWh. A comparison with existing data may be possible, but is outside the scope of this work.

3.5 Summary diagram and proposed cost targets

3.5.1 Summary diagram

In Sections 3.2 through 3.4, a method for calculating the maximum allowed total system cost was provided. This method was explained for a theoretical system at 100% efficiency in Section 3.2.1 and expanded to real systems with the introduction of the concept of NOC in Section 3.2.3. Finally, in Section 3.3 the distribution of solar resources throughout the world was described. In this current section, all of this information is brought together into one convenient diagram to aid the user in answering our original two questions:

How much should a CPV system cost?

&

Where should I install it?

Deriving cost targets for total system costs are difficult, as metrics normally used in traditional one-sun photovoltaics, such as €/W_p at standard testing conditions, may produce misleading results. As such, price targets are given for power ratings at the nominal operating condition (Table 3.4). The information from Sections 3.2 through 3.4, regarding solar resource, electricity prices, and location, are collected in Figure 3.2 where several constant cost curves in terms of €/W_{NOC} are displayed. These constant cost curves represent the total system cost target for a CPV system and were derived from the data available in Table 3.3. The user, knowing the total installed cost of his

3.5 Summary diagram and proposed cost targets

or her system, can search Figure 3.2 for a range of solar resources and electricity prices that satisfy this cost. In addition, the diagram highlights locations throughout the world where such solar resources are found and, with respect to resource availability, provides a rough idea for potential markets. The right-hand side of the diagram contains a list of percentages that aid the user in understanding the distribution of the available solar resource and its geographical location throughout the world. These percentages were derived from Ref. [18], where an estimate for the number of square kilometers deemed available and suitable for CSP is provided, and may be found in Appendix C.

In Figure 3.2, the ranges of annual direct normal solar resource were grouped into four categories: 2000-2199, 2200-2399, 2400-2599, and >2600 kWh/(m²·yr), and each are represented by a colored band running parallel to the x-axis. The percentage of land, deemed available and suitable for CSP, falling within these four categories is: 25, 33, 25, and 17% respectively. These values are outlined by thick black lines and are further expanded by country or geographic region. For example, 25% of the earth's land surfaces, available and suitable for CSP, experience an annual direct normal solar resource between 2,400 and 2,599 kWh/m². Of the aforementioned 25%; 42, 36, and 11% of this resource is located within Africa, Australia, and the Middle East respectively.

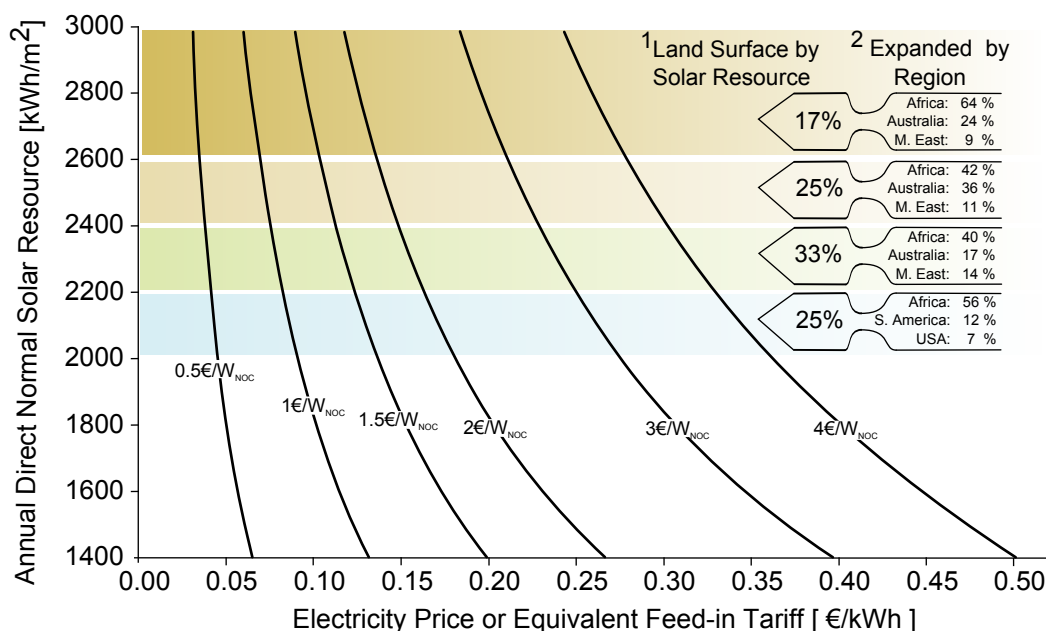


Figure 3.2: Maximum Allowed Total System Cost - Maximum allowed total system cost for various conditions and locations throughout the world.

3. COST TARGETS, ESTIMATES, AND IMPROVEMENTS

3.5.2 Proposed total system cost targets

Considering electricity prices ranging from 0.08 to 0.20 €/kWh and DNI ranging from 2,000 to 2,800 kWh/(m²·yr), short term (grid parity by 2015) and long term (wholesale electricity prices by 2030) total system cost targets are suggested at 2 and 1 €/W_{NOC} respectively, based on the cost curves in Figure 3.2. This range of electricity prices was adapted from Ref. [36], a grid parity analysis for Europe, estimating grid parity for traditional one-sun photovoltaic devices between 2012 and 2018. For CPV, the short term target date of 2015 is suggested, so as to be competitive with traditional photovoltaic technologies. Long term cost targets are placed outwards towards 2030; this is a time frame that Ref. [37] predicts that CSP could be cost competitive with electricity production via coal. As such, CPV should strive to reach these cost targets, with 2030 suggested as the long-term target.

3.6 Proposed cost targets at the subsystem level

With the total system costs defined in Section 3.5.2, the only remaining piece of information required to determine the subsystem level cost targets is the percentage of the total system cost for each subsystem. This was estimated using cost data from a similar linear-focus trough concentrator system design but updated for current prices for CPV cells. Reference [25] lists the cost of each subsystem for a linear-focus trough CPV system. These prices were updated and a new set of relative percent costs, as a percentage of a total system cost, were derived. This estimate is considered and labeled as the state of the art scenario (SoA) and is given in Figure 3.3. The balance of system (BOS) category represents all installation, transportation, and any other miscellaneous costs unaccounted for by the remaining subsystems. A second scenario, labeled beyond state of the art (BSoA), considers an additional 50% reduction to the cost of the mirrors and structure and an additional 25% reduction to the BOS. This estimate is given in Figure 3.4. The two scenarios provide a range of cost targets at the subsystem level and are provided in Table 3.5.

3.6 Proposed cost targets at the subsystem level

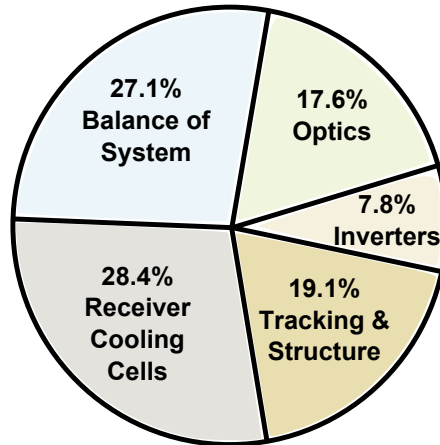


Figure 3.3: Subsystem Relative Percent Cost SoA - Subsystem relative percent cost for each subsystem with respect to total system cost. Adapted from the EUCLIDES system [25], and representative of the current state of the art (SoA).

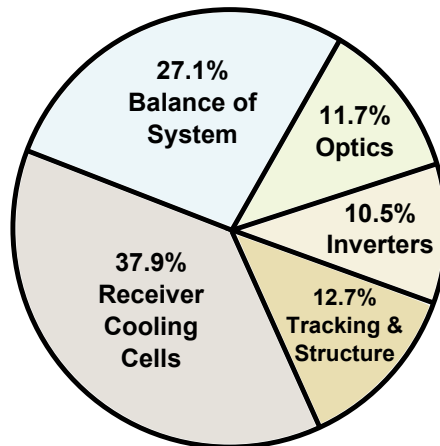


Figure 3.4: Subsystem Relative Percent Cost BSoA - Subsystem relative percent cost for each subsystem with respect to total system cost for a beyond state of the art scenario (BSoA). Based on SoA estimate (Figure 3.3), but considering an additional 50% reduction to the cost of the mirrors and structure and a 25% reduction to BOS.

3. COST TARGETS, ESTIMATES, AND IMPROVEMENTS

Table 3.5: Subsystem Level Cost Targets - Suggested cost targets at the subsystem level for SoA (Figure 3.3) and BSoA (Figure 3.4) scenarios for short term (2015, 2€/W_{NOC}) and long term (2030, 1€/W_{NOC}) goals.

Subsystem			2€/W _{NOC}		1€/W _{NOC}	
	SoA	BSoA	SoA	BSoA	SoA	BSoA
Inverters	7.8%	10.5%	0.156	0.210	0.078	0.105
Optics	17.6%	11.7%	0.352	0.234	0.176	0.117
Tracking & Structure	19.1%	12.7%	0.382	0.254	0.191	0.127
BOS	27.1%	27.1%	0.548	0.542	0.274	0.271
Receiver, Cooling, Cells	28.4%	37.9%	0.568	0.758	0.284	0.379

3.7 Cost estimates

The previous section derived and provided cost targets at the subsystem level. The remainder of this chapter will focus on cost targets with respect to the CPV receiver and its cooling system, as this thesis work focuses mainly on improvements to these two components. The BSoA scenario and associated targeted improvements to the optics and BOS are work separate from this thesis and will no longer be discussed. The remaining economic assessment, considering the three CPV applications outlined in Section 3.1, moves forward under the assumption that the BSoA targets can be met for the optics and BOS.

3.7.1 Cost: TU-Wien CPV receiver prototype

The TU-Wien CPV receiver prototype was adapted from the Australian National University Combined Heat And Power Solar (CHAPS) system. It is an actively cooled CPV receiver suitable for both CPV and CPV-T applications. At TU-Wien, alternative CPV cells, soldering methods, and thermal interfaces were utilized in the design in an attempt to reduce the cost of the CPV receiver. The basic design parameters for the TU-Wien prototype are shown in Table 3.6

The cost for such a receiver design was estimated by constructing a bill of materials (BOM). This document contains a list of all the major components that make up the assembled receiver, as well as estimates for their respective costs. For each component, a low and high price estimate is given, so as to provide a range of estimated costs. The range attempts to reflect both the uncertainty in and the variability of component

Table 3.6: TU-Wien CPV Receiver Prototype - Design parameters for the current CPV receiver design. ¹An estimate for all parasitic losses (e.g. tracking, pumping losses). ²Active length represents the total length of solar cells in the module (excludes space between cells). ³Estimated efficiency of the CPV cells at 25°C and 30 to 50 times one-sun illumination. ⁴Estimated total length of the CPV receiver, including water connectors in their tightened positions. ⁵Estimated power output of the CPV receiver operating under NOC per Table 3.4, with a 10% reduction in accordance with the estimated parasitic losses.

	Parameter	Value	Unit
System	Aperture Width	1.5	m
	Optical Efficiency	80	%
	¹ Parasitic Losses	10	%
Cell	Active Width	36	mm
	² Active Length	1.3	m
	³ Efficiency	17	%
Receiver	⁴ Length	1.4	m
	⁵ Power	180	W

cost with respect to production volumes. A condensed version of this document may be found in Table C.3 of Appendix C. Quotes were obtained for the CPV extrusion, thermal interfacing materials, CPV cells, copper tabs, solder, encapsulation material, glass cover, bypass diodes, and water connectors. Nuts, bolts, and mounting brackets, necessary to mount the CPV receiver to the concentrator optics and structure, were excluded from the CPV receiver and cooling system cost. These components are to be appropriated to the balance of system, concentrator optics, or the tracking subsystem cost targets. The wiring of the bypass diodes were excluded from the cost analysis as a matter of time savings.

With the above information compiled in the BOM, the material costs of the CPV receiver were calculated at 0.592 and 0.786 €/W_{NOC}. However, this estimate excludes manufacturing costs, which must be included. The remaining manufacturing costs for the CPV receiver are mostly assembly processes. Due to the lack of freely available data on the manufacturing costs of CPV receivers, it is assumed that the assembly costs from traditional one-sun photovoltaic panels is an appropriate target for the remaining manufacturing steps for the CPV receiver. To find such costs, Ref. [41] was consulted. The authors examine a series of technologies to assess the possibility of attaining production

3. COST TARGETS, ESTIMATES, AND IMPROVEMENTS

of a 1€ per Watt-peak (W_p) photovoltaic (PV) module. For many applications, 1€/W_p is considered grid parity [41]. Note, as of January 2012, more than one manufacturer has already reached this goal [42]. The authors provide cost data for a base-case crystalline silicon photovoltaic module in Figure 1 of page 201 of the article.

By summing the costs associated with equipment, labor, yield losses, and fixed costs and dividing this by the total cost of the PV module, one roughly estimates that the assembly costs of the PV module make up 19% of the total module cost. In the absence of any better and available data, 19% was adopted to represent the total manufacturing costs for the CPV receiver. These additional manufacturing costs come to roughly 0.139 and 0.184 €/W_{NOC}, putting the total, finished, assembled, cost of the CPV receiver between 0.731 and 0.971 €/W_{NOC}.

3.7.2 Cost of the cooling system

To estimate the cost of the cooling system, two steps are necessary. First, a survey of cooler costs in terms of watts of waste heat, €/W_{heat}, is needed. Second, a relationship between the electrical output of the CPV receiver at NOC and the thermal output of the CPV receiver must be established. Such a relationship would thus relate W_{NOC} to W_{heat}.

Figure 3.5 shows an array of various cooler costs, comparing cooler size to cost in €/W_{heat}. From this survey, cooler costs of 0.10 and 0.20€/W_{heat} were selected for the low and high cost estimates respectively. For the CPV receiver outlined in Table 3.6, an estimated maximum of 1350W of heat must be rejected. The ratio of thermal output to electrical output is approximately 6.8 (excluding parasitic losses). Thus, the cooling system is sized to 6.8 times the NOC rating of the CPV receiver. At the aforementioned estimated 0.10 and 0.20€/W_{heat} cooler costs, this places the cooler costs between 0.68 and 1.35€/W_{NOC}.

3.8 Cost reductions and performance improvements

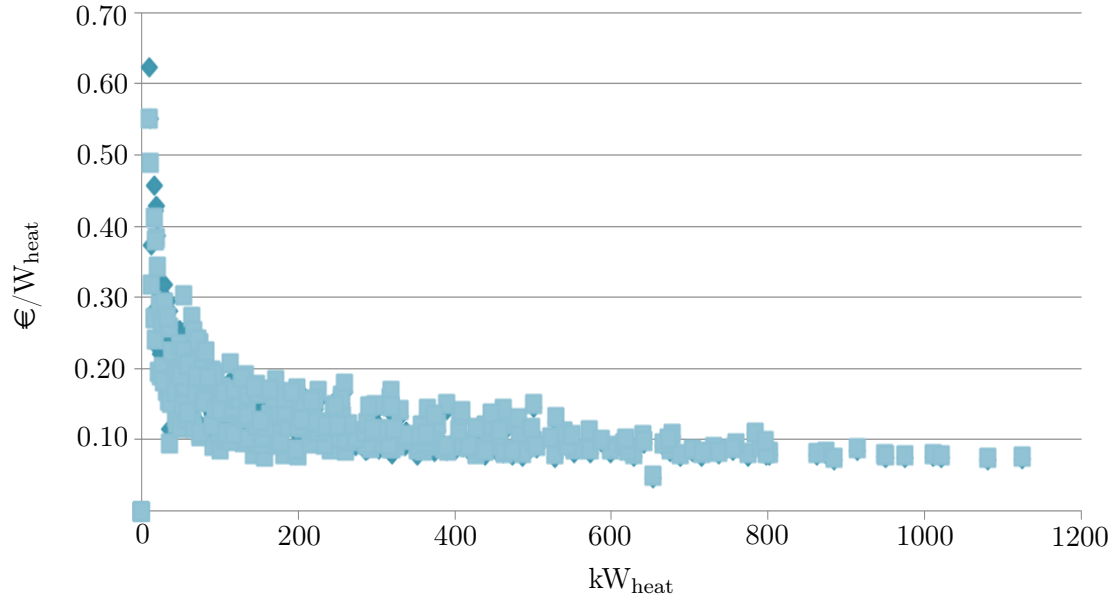


Figure 3.5: Cooling Cost Survey - Survey of various cooler sizes and their respective costs. Assembled from Ref. [43].

3.7.3 Cost comparison: targets vs. estimates

A comparison between the current estimated costs and cost targets is given in Table 3.7. The discussion which follows will be limited to the short-term targets only, as forecasting 10 to 20 years towards the long-term targets involves excessive speculative assumptions. Looking at the short-term, it is immediately apparent that both the assembled receiver and cooler cost exceed the cost targets by a factor of 2, even for the lowest cost estimates and highest target estimates. A 45 to 60% reduction in both the assembled receiver and cooler cost is required to meet short term target costs for land-based CPV (considering the low-cost estimate). Several recommended courses of action are provided in Section 3.8 to achieve these cost reductions.

3.8 Cost reductions and performance improvements

In order to reach the aforementioned cost targets, a combination of reductions in the assembled receiver and cooling costs, as well as a number of performance improvements are necessary. As such, improvements to cost and performance of the receiver and cooler are referenced to improvements in total system cost (TSC) and to total system

3. COST TARGETS, ESTIMATES, AND IMPROVEMENTS

Table 3.7: Cost Targets vs. Estimates - Comparison of TU-Wien CPV receiver prototype (Table 3.6) costs and cost targets.

Component	Cost Targets €/W _{NOC}					
	Estimated Costs €/W _{NOC}		Short-Term		Long-Term	
	Low	High	Low	High	Low	High
Assy. Receiver	0.731	0.971	0.334	0.448	0.167	0.224
Cooling	0.676	1.353	0.232	0.310	0.116	0.155
Total	1.407	2.323	0.566	0.758	0.283	0.379

Table 3.8: Identified Cost Reductions - Possible cost reductions.

New water interconnectors	2% reduction in TSC
Higher efficiency solar cells	1 to 5% increase in TSP + 2 to 10% decrease in TSC
Alternative encapsulation	2.5% reduction in TSC
Improved thermal interfaces	2 to 3% increase in TSP
Cost reduced back cooler	5 to 10% increase in TSP
Total improvements	14.5 to 32.5%

power (TSP). To do this, it is assumed that the remaining components of the CPV system meet their respective cost targets. Together, a combination of reductions in TSC and increases of TSP must sum to 25 to 30% to meet the short-term cost targets. Table 3.8 lists these improvements in increasing order of required development time. In addition to these improvements, factors such as better sourcing and larger volume discounts could provide further meaningful reductions in cost. The improvements listed, if realized, could meet the 25 to 30% target. Various development and further work is necessary, which is briefly outlined below.

3.8.1 Water interconnectors

Currently, light-weight high-precision water connections were adapted from the CHAPS design. Simpler and cheaper solutions exist, but careful material selection and corrosion properties should be considered. However, redesign of the water connectors requires relatively little development time. Development of new connectors could provide an easy and immediate cost reduction.

3.8.2 Cell efficiency

The benefit of increasing solar cell efficiency is twofold. There is the first and obvious increase in power output. Secondly, the increase in power output enables a decrease in the size of the cooling system, as less heat must be rejected. The performance and cost benefits outlined in Table 3.8 assume that the cell price remains unchanged. Although there are several designs for higher efficiency solar cells, their availability and possible increase in cost must be considered. The benefit of a 5% increase in cell efficiency by moving from 17 to 22% efficient cells would be completely lost if the price of the cells were to more than double.

3.8.3 Alternative encapsulation

Encapsulation using polyvinyl butyral (PVB) foils is a well-known process, but changes are required to the extrusion design and to the thermal interface to realize the idea. A number of trials are necessary to determine the proper dimensioning, assembly, and process steps. Also, long-term exposure testing with regard to the PVB foils and concentrated light should be further examined and tested if deemed necessary. In addition, it will be important to determine whether any cells are cracked during this encapsulation process. The 2.5% reduction in TSC is based on a material savings estimation.

3.8.4 Improved thermal interface materials (TIM)

Thermal interface materials (TIM) are a critical component of the CPV receiver. They are typically used to fix CPV cells to the body of the receiver, to conduct heat away from the cells, to maintain electrical isolation between the cells and the receiver, and to accommodate any difference in thermal expansion between the two. Numerous TIMs and methods of heat transfer are described in Chapter 6. Briefly summarized, using

3. COST TARGETS, ESTIMATES, AND IMPROVEMENTS

thermal tapes with higher thermal conductivities could increase a receiver's power output. More specifically, switching from electrically isolating to non-isolating materials may improve power output up to 2-3%. In doing so, however, electrical isolation between the cells and receiver is then lost. As such, an isolating coating on the receiver becomes necessary, for example an oxidation coating on an aluminum receiver body. This would reestablish the electrical isolation between the cells and the receiver, but not necessarily between the cells themselves. With non-isolating materials, some sort of strategy is needed to prevent the rear-side contacts of neighboring cells from creating a single electrical contact. The accidental connection of these rear-side contacts would result in a short circuit and must therefore be avoided.

Previously, with electrically isolating thermal tapes, it was possible to lay one large continuous piece of tape onto the receiver and simply drop the CPV cells into place. Although very convenient, this same type of construction would result in a short circuit when using non-isolating thermal materials. A small gap between each cell, including a corresponding gap in the thermal material, could prevent such a short circuit and may prove to be a viable solution. Any such strategy would require further development and testing. Development tests for TIMs could be carried out in parallel with the PVB foil encapsulation tests, but the thermal heat transfer capability of these new TIMs must be assessed. A method for doing so must be developed. There is no standard measurement technique particular to CPV at this time, but there are several proposals which could be relatively easily investigated.

3.8.5 Cost reductions in the cooling system

Technologies regarding heat rejection to the environment have been extensively researched and large improvements over today's industry standards may be difficult. However, there are some possibilities unique to CPV, with its lower operating temperatures and pressures (as compared to traditional steam power production methods). One idea, previously investigated in Ref. [44], utilizes thermal storage to store a portion of the heat during the day for release at night, when ambient outside temperatures are lower. Numerous combinations of passive and active cooling systems, both combined with and without storage, were considered and simulated.

One such example is shown in Figure 3.6, where the performance of two parabolic trough CPV systems were simulated. Both systems utilized equal size back coolers, but

3.8 Cost reductions and performance improvements

one system included a storage tank. Utilizing this storage tank, it was possible to shed a portion of the waste heat during the night, when ambient temperatures are lower. The power output for each system is shown in Figure 3.6, with the upper-most blue and red curves representing the night-storage and the no-storage strategies respectively. Their maximum power output is indicated by $P_{storage}$ and P_{day} in the figure. The average operating CPV cell temperature for each strategy is given by the lower-most blue and red curves, night-storage and no-storage respectively.

It is not the intention of this thesis to discuss the details behind this study. It is included here only as introduction to the concept of night time cooling. An economic analysis of the above strategy is given in Ref. [44], and a 10% increase in daily energy yield was deemed possible. The realization of such a system would require some development and testing. The next steps for such work would include identifying, procuring, and testing the system components. In addition, it may be possible to create a relatively inexpensive liquid to air heat exchanger utilizing less expensive materials, which could provide additional savings. However, this work would require a serious development commitment. The potential cost savings are at this time unknown and would require further investigation to determine.

3. COST TARGETS, ESTIMATES, AND IMPROVEMENTS

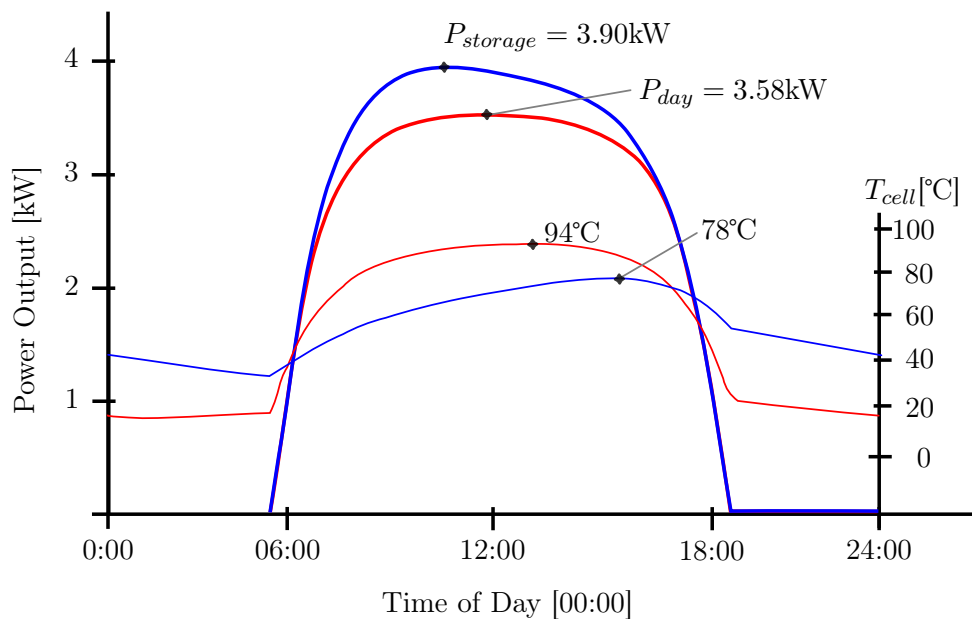


Figure 3.6: Effects of Night Storage Cooling - This figure illustrates the possible increase in power output due to night-storage cooling. The upper-most blue and red curves represent the power output for the night-storage and no-storage strategies respectively. Their respective maximum power output is indicated by $P_{storage}$ and P_{day} . The average operating CPV cell temperature for each strategy is given by the lower-most blue and red curves, night-storage and no-storage respectively. The simulation used to create this figure considered a parabolic trough of aperture dimensions 1.5 x 30m, finned tube cooler length of 22.5m, a thermal resistance between the cell and receiver of 5 W/(cm² °C), an optical efficiency of 80% and nominal cell efficiency of $\eta_{stc}=15\%$. See Ref. [44] for more details.

3.9 Summary of improvements

There are enough cost reduction and performance improving efforts which could bring the CPV receiver assembly and cooling system within their respective short-term cost targets for land-based CPV systems. An estimated 6.5% improvement could be relatively easily attained by finding new water interconnectors, using a PVB encapsulation, and implementing an improved thermal interface. The remaining improvements require more development and it is unsure whether or not these gains could be fully realized.

In conclusion, there are enough cost and performance improvements to make a land-based, low concentration, linear-focus trough, silicon solar cell CPV system feasible. However, given the development effort necessary to reach these improvements, especially with regard to cost reducing the cooling system, the realization of such systems is unlikely.

Furthermore, as it is highly probable that the CPV receiver assembly could meet its own short-term cost targets, any application in which the cooling system is to be greatly reduced or eliminated, such as in combined heat and power, holds a great deal of economic promise. Several studies exist for such applications, CPV-T, and further information can be found there. The economic viability of CPV-T would require further investigation for European markets, but the utilization of heat significantly increases the chances for success. To quickly assess the sea-based CPV application, Table 3.9 removes cooler costs from the previous estimates. In doing so, it becomes immediately apparent that the low cost estimate of the assembled receiver and cooling system fall within the short-term cost targets. The challenges of developing concentrator systems at sea are certainly significant, but the assembled receiver and cooling system targets could be met.

In addition, if the aforementioned 6.5% total system cost reductions are taken into consideration, the cost of the assembled receiver further decreases an additional 12 to 27% as outlined below in Table 3.10. By selecting 20% from this range and introducing this cost reduction, nearly the full range of the assembled receiver and cooler costs falls within the short-term low and high cost targets, as shown in Table 3.11.

3. COST TARGETS, ESTIMATES, AND IMPROVEMENTS

Table 3.9: Sea-based CPV Systems - Cost estimates for sea-based CPV systems.

Component	Estimated Costs €/W _{NOC}		Cost Targets €/W _{NOC}			
			Short-Term		Long-Term	
	Low	High	Low	High	Low	High
Assy. Receiver	0.731	0.971	0.334	0.448	0.167	0.224
Cooling	0	0	0.232	0.310	0.116	0.155
Total	0.731	0.971	0.566	0.758	0.283	0.379

Table 3.10: Receiver Cost Reductions - Performance improvements and cost reductions at the total system level (see Table 3.8) converted to cost reductions at the receiver subsystem.

New water interconnectors	7 to 10%
Alternative encapsulation	5 to 10%
Improved thermal interfaces	5 to 7%
Total improvements	12 to 27%

Table 3.11: Sea-based + Improvements - Cost estimates for sea-based CPV systems, including improvements as laid out in Table 3.10.

Component	Estimated Costs €/W _{NOC}		Cost Targets €/W _{NOC}			
			Short-Term		Long-Term	
	Low	High	Low	High	Low	High
Assy. Receiver	0.585	0.777	0.334	0.448	0.167	0.224
Cooling	0	0	0.232	0.310	0.116	0.155
Total	0.585	0.777	0.566	0.758	0.283	0.379

Lastly, in order for the low cost estimates in Table 3.11 to approach long-term targets, a 22% efficiency CPV cell at the current BOM listed price is required. Doing so would reduce the assembled receiver cost to $0.497 \text{ €/W}_{\text{NOC}}$, bringing the costs to within 25% of the long-term high cost target estimate. As originally stated, it is difficult to predict or project outwards to the 2020 to 2030 time line, but the last several scenarios demonstrate that the current short-term targets can be met and that the long-term targets could be approached for sea-based systems.

3.10 Conclusions

The current assembled receiver and cooling system costs exceed short-term cost targets. A 45 to 60% reduction in both the assembled receiver and cooler costs are necessary to make a land-based, linear-focus trough concentrator with silicon solar cell technology, economically viable (meet short-term cost targets). This roughly translates into a 25 to 30% cost reduction at the total system level, and may be accomplished by a combination of cost and performance improvements. Such improvements were identified, and fall within a range of 14.5 to 32.5%, requiring various levels of development. At least a 6.5% improvement is believed to be readily achieved. In conclusion, it is unlikely that a land-based CPV system would meet the short-term cost targets; however, there are enough potential improvements to make it feasible. Alternative applications, in which heat is utilized (CPV-T), show promise and a further cost study is warranted if this application is to be pursued in Europe. It is likely that the short-term cost targets could be met with the current receiver design. In the case of sea-based systems, short term targets can be met with the currently proposed receiver design. With additional improvements, long-term targets are approachable. Regarding the future of CPV technologies, the development process for the entire system is significantly increased for sea-based systems. The success of such a system could be very rewarding, both from an economical and geopolitical sense.

3. COST TARGETS, ESTIMATES, AND IMPROVEMENTS

4

Methods of Cooling CPV Receivers

4.1 Introduction to the cooling system

Briefly, the purpose of the cooling system is to protect the materials within a photovoltaic (PV) module or concentrator photovoltaic (CPV) receiver from exceeding maximum temperature limits and to increase the efficiency of power conversion by reducing cell operating temperatures. Avoiding a material's maximum temperature limit is particularly critical in CPV. One need only aim a magnifying glass to the sun and bring its focus to the back of one's hand to quickly gain an appreciation for the intense heat of concentrated sunlight.

To better understand the magnitude of this heat, it is helpful to examine the maximum theoretical efficiency of a photovoltaic device, as most of the non-converted energy must be rejected as heat. The theoretical maximum efficiency (power conversion) of a photovoltaic device has been calculated at 87% [45]. Multi-junction solar cells with two to five p-n junctions have theoretical efficiencies ranging from 50 to 70% [46] and represent one such attempt to approach the aforementioned theoretical maximum limit. In practice, multi-junction solar cells with two to three p-n junctions have reached efficiencies over 40% [10]. Single-junction cells, with a theoretical efficiency of 40% [46], have realized efficiencies as high as 28% [10]. Numerous cell technologies have efficiencies well below 20% [10]. Considering an efficiency range from 20 to 40% leaves 60 to 80% of the solar irradiation reaching the cell to be dissipated as heat.

The design of the PV module or CPV receiver will dictate the thermal pathway for dissipating the heat from the solar cell to the operating environment and will also greatly

4. METHODS OF COOLING CPV RECEIVERS

influence the cell's operating temperature. Generally, an increase in cell operating temperature decreases its efficiency. In designing the cooling system, one attempts to dissipate heat from the solar cell to the operating environment with the minimum increase in temperature above the operating environment.

By the nature of its design, a one-sun PV module generally serves as an adequate heat sink to the operating environment. A typical module contains a sandwich construction of glass, laminate material, and a polyvinyl fluoride back-sheet. The solar cells and other materials are typically operating above the ambient air temperature within an acceptable range to ensure adequate economic and reliable performance. Heat from the solar cells is transferred, mostly by thermal conduction, between the cell and the front and the back surfaces of the PV module. Both the front and backside transfer heat to the ambient surroundings through: a mixture of conduction through fixtures or attached structure, natural and forced convection to the ambient air, and by radiant heat transfer to the sky and surrounding objects.

In principle, the surface area necessary to dissipate heat from CPV cells is similar to the system's collector area. As such, concentrator technologies that focus light downwards (a Fresnel lens for example), may thermally bond CPV cells to a simple, highly thermal-conductive, flat plate (aluminum for example) of dimensions comparable to the collector area. In this case, the cooler design is relatively simple and straightforward.

By contrast, considerable thought and effort must be applied to the cooling system for linear-focus trough concentrators. These systems concentrate light upwards, and the space available for the cooler is limited by its potential to shade the collector area. For example, integrating large coolers into the CPV receivers would produce significant shading in both the inflatable concentrator (Figure 1.3) and the CHAPS system (Figure 2.2).

Without proper cooling, the temperature of the solar cells and surrounding materials in the receiver may reach hundreds of degrees Celsius [47]. Improper design or operation of the cooling system may result in a reduction in long-term reliability and, in extreme cases, an immediate and rapid destruction of the receiver. Depending on the design and application, a combination of material limits and economic optimal operating points will determine the proper size of the cooling system. Various cooling methods are utilized to cope with these challenges, and they will be covered in Section 4.2. Although

Table 4.1: Active vs. Passive - A comparison between active and passive cooling.

Cooling	Advantages	Disadvantages
Active	enables CPV-T	parasitic losses
	control output temperature	additional failure modes
	advanced cooling strategies	non-uniform $\Delta T_{receiver}$
Passive	fewer thermal interfaces	unlikely CPV-T application
	fewer failure modes	lacks temperature control
	uniform $\Delta T_{receiver}$	increased receiver weight

applicable to other linear concentrators, the methods discussed primarily concern linear-focus trough concentrators, where light is focused skywards.

4.2 Methods of cooling

An excellent review of the various cooling methods for CPV cells is given in Ref. [47]. The authors provide numerous examples of both passive and active cooling systems for three concentrating geometries. This is followed by an insightful section organized by heat transfer mode: passive systems (natural convection + radiant heat transfer), forced air convection, liquid single-phase forced convection, and two-phase forced convection. Finally, a summary is provided by comparing the thermal resistances for the various heat transfer modes and cooling system designs.

Although the authors of [47] identify a complete thermal network of heat transfer paths from the solar cell to the operating environment, the division between thermal interfaces is not fully stressed. Their comparisons, though helpful and insightful, contain a mixture of thermal interfaces between the CPV cell, the receiver body, and the operating environment. In this section, further clarification is given to the various thermal interfaces and an alternative organization to the methods of cooling is provided.

The various designs of cooling systems may be divided between active and passive cooling systems. Active cooling requires an energy input in order to adequately cool the CPV receiver. Forced convection cooling, in which power must be provided to fans or pumps, is one such example of an active cooling system. Passive cooling systems

4. METHODS OF COOLING CPV RECEIVERS

maintain acceptable temperatures without any such energy inputs. An extended surface heat sink, commonly found in many electronic devices, is an example of a passive cooling system. Heat is mainly dissipated by natural convection and thermal radiation.

The advantages and disadvantages of active and passive cooling are somewhat particular to the concentrator geometry and receiver design; however, some general remarks are given in Table 4.1. Examples of active and passive cooling systems (linear-focus trough concentrator) are shown in Figures 4.1 and 4.2 respectively. In principle, the active cooling system enables additional control strategies and introduces the possibility of utilizing waste heat, i.e. a concentrator photovoltaic-thermal (CPV-T) system. But, it does so at the expense of increasing the number and severity of failure modes as well as introducing parasitic losses. In addition, if a fluid is used to remove waste heat, a considerable ΔT can develop across receivers that are connected in series.

4.3 Cooling transition points: passive, active, and beyond

Establishing a practical limit for passive cooling, with respect to linear-focus trough concentrators, can be difficult. However, there is a great deal of work concerning passive cooling in electronics. Using some relatively simple assumptions, this knowledge may be applied here. For example, Bar-Cohen established a series of theoretical optimal fin spacings, thicknesses, and overall dimensions for heat sinks utilizing natural convection. His predictions yielded maximum effective heat transfer coefficients between 100 and 320 W/m²°C for aluminum fin heat sinks [48]. Bar-Cohen states, “this correlates to a 15 to 45 fold improvement over natural convection heat transfer from an unfinned surface.” It therefore may be possible to increase the heat flux 15 to 45 fold for a finned surface, in this case a passively cooled CPV receiver.

However, this would assume that the foot print of the heat sink is approximately equal in size to the length and, more importantly, the width of the CPV receiver. As evident from single point concentrators (Fresnel lens for example), it is known that concentration ratios as high as 1,000 may be achieved [47]. Confining the width of the heat sink to the width of the module, as in the example above, certainly constrains the potential limit of passive cooling in linear-focus trough CPV systems.

The question then remains, can or should the width of the heat sink be extended beyond the width of the receiver? And if so, then by how much? There is a very simple,

4.3 Cooling transition points: passive, active, and beyond

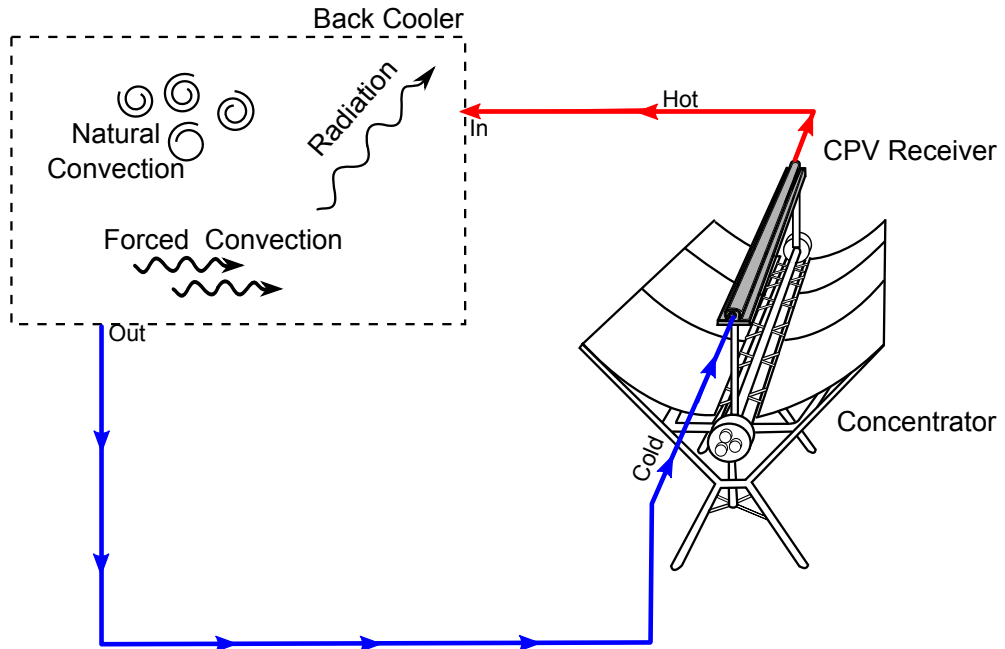


Figure 4.1: Active Cooling - A CPV receiver utilizing active cooling.

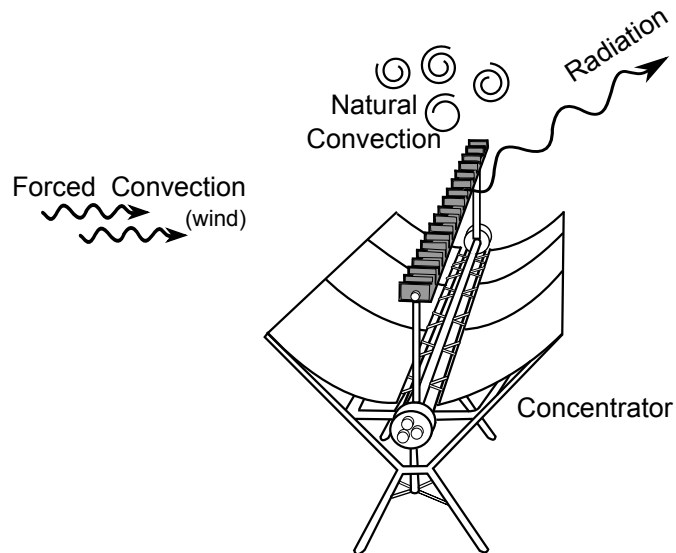


Figure 4.2: Passive Cooling - A CPV receiver utilizing passive cooling.

4. METHODS OF COOLING CPV RECEIVERS

albeit crude, way to answer this question. The increase in receiver width should be limited to a dimension such that the corresponding power loss, due to additional shading of the collector, does not exceed the expected gains in power output from improved cooling. The maximum theoretical improvement in power output, due to additional cooling, is dictated by $\Delta T_{cell-amb}$, the difference between the CPV cell operating temperature and the ambient temperature of the operating environment. By specifying a range of values for $\Delta T_{cell-amb}$, an appropriate limit to the expansion of the receiver width can thus be derived.

To begin, assume that a receiver has a theoretical power output labeled $P_{rec}(W)$, operating at a CPV cell temperature T_{cell} , a cell power efficiency temperature coefficient γ_t , a cooler width approximately equal to the cell width of W_{rec} , and length equal to the receiver length L_{rec} . Its power output may be approximated by:

$$P_{rec}(W) = L_{rec} W_{rec} G_N X_g \eta_o \eta_{stc} (1 - (T_{cell} - 25^\circ\text{C}) \gamma_t)$$

Next, assume that the width of the cooler is expanded by the value ΔW , and that the resulting temperature of the CPV cells is equal to the ambient temperature of the operating environment, T_{amb} . Please note that this is a purely theoretical description. The actual realization of such a cooler would be prohibitively difficult and would in fact only approach T_{amb} . Regardless, the additional width of the cooler, ΔW , would result in a reduction in the collector area (i.e. shading) equal to ΔW . The resulting power output, $P_{rec}(W^*)$, may be calculated as:

$$P_{rec}(W^*) = L_{rec} (W_{rec} - \Delta W) G_N X_g \eta_o \eta_{stc} (1 - (T_{amb} - 25^\circ\text{C}) \gamma_t)$$

By setting $P_{rec}(W) = P_{rec}(W^*)$ and canceling like-terms, one arrives at:

$$W_{rec} (1 - (T_{cell} - 25^\circ\text{C}) \gamma_t) = (W_{rec} - \Delta W) (1 - (T_{amb} - 25^\circ\text{C}) \gamma_t)$$

By further algebraic manipulation one may derive the parameter $\Delta W/W_{rec}$, which is the maximum increase in cooler width, referenced to the original width.

$$\frac{\Delta W}{W_{rec}} = 1 - \left[\frac{(1 - (T_{cell} - 25^\circ\text{C}) \gamma_t)}{(1 - (T_{amb} - 25^\circ\text{C}) \gamma_t)} \right] \quad (4.1)$$

Figure 4.3 plots Eq. 4.1 for a wide range of ambient operating temperatures and cell temperatures, with the later referenced to the ambient operating temperature via

4.3 Cooling transition points: passive, active, and beyond

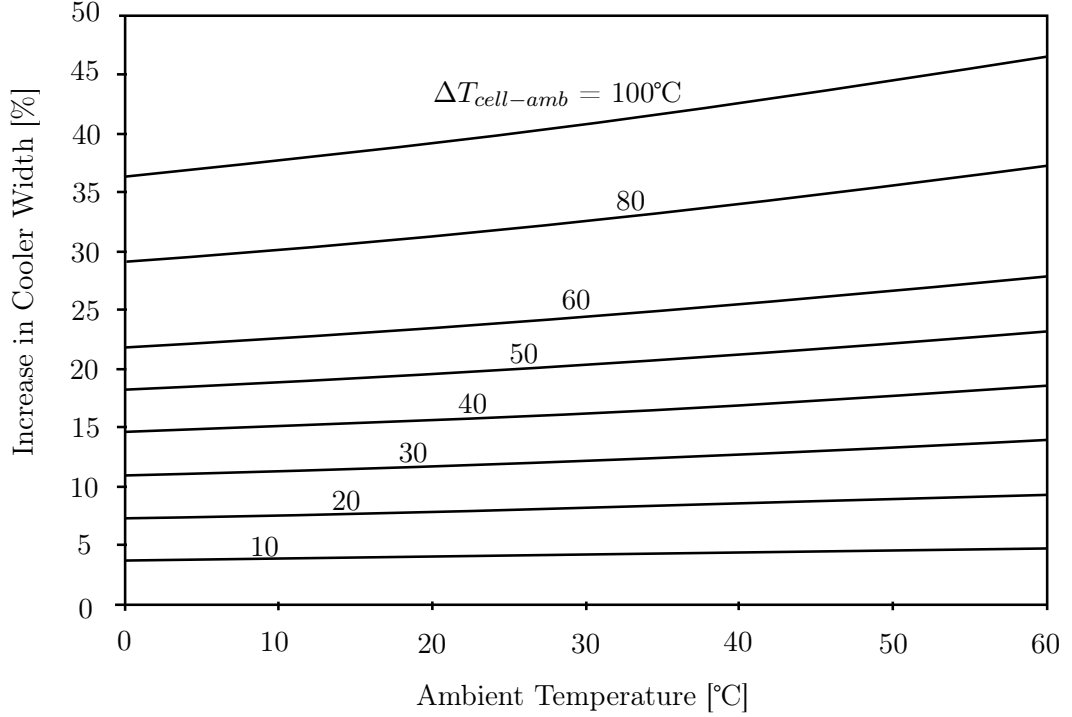


Figure 4.3: Heat Sink Width - Increasing the width of the heat sink as a percentage of its original width, W_{rec} , for various ambient operating temperatures. Each curve represents a particular delta T between the CPV cells and the operating environment, labeled $\Delta T_{cell-amb}$. The theoretical temperature of the CPV cells in this model can be approximated by adding the ambient temperature on the x-axis to the corresponding value of $\Delta T_{cell-amb}$ for each curve. The figure was calculated using $\gamma_t=0.004^\circ\text{C}^{-1}$.

the variable $\Delta T_{cell-amb}$. This figure illustrates that power reductions due to shading far outweigh any theoretical improvement in power output due to improved cooling. This is due mostly in part to the parameter γ_t , as all power improvements via improved cooling are multiplied by this parameter. Power reductions due to shading are linear with respect to ΔW and are thus much more prominent. Even at a $\Delta T_{cell-amb}=100^\circ\text{C}$, the maximum recommended increase in cooler width would fall below 50%.

4. METHODS OF COOLING CPV RECEIVERS

The analysis above illustrates that the width of the heat sink should be minimized. Therefore it may be appropriate to use the aforementioned passive cooling limits of 15 to 45, where the cooler width is assumed equal to the cell and receiver width. However, Bar-Cohen makes no mention of an operating temperature, which is important for the materials making up the CPV receiver. Using Bar-Cohen's maximum estimate of $320 \text{ W/m}^2\text{C}$, labeled h_{coh} , one can establish a relationship between the geometric concentration ratio X_g and the theoretical operating temperatures of the CPV cells.

$$X_g = \frac{h_{coh} \Delta T_{cell-amb}}{G_N \eta_o (1 - \eta_e)} \quad (4.2)$$

Assuming $T_{amb} = 30^\circ\text{C}$ (as proposed in Section 3.4) and using Eq. 4.2, a plot of geometric concentration ratio vs. cell operating temperature was created in Figure 4.4. Equation 4.2 is labeled as " W_{rec} " in the figure. Assuming a reasonable range of temperatures within the receiver of 60 to 90°C , allows for a possible limit to passive cooling between $X_g = 15$ and 30. This assumes that the width of the cooler is equal to the cell width. If width of the cooler is increased, using the values of $\Delta W/W_{rec}$ established in Eq. 4.1, then the limit to passive cooling may be slightly extended, as shown by the curve " $W_{rec} + \Delta W$." This curve was created by modifying Eq. 4.2, as follows:

$$X_g = \frac{h_{coh} \left(1 + \frac{\Delta W}{W_{rec}}\right) \Delta T_{cell-amb}}{G_N \eta_o (1 - \eta_e)} \quad (4.3)$$

Equation 4.3, and its corresponding curve " $W_{rec} + \Delta W$ " in Figure 4.4, extend the possible limit of passive cooling to $X_g = 37$. To achieve this, the heat sink must extend its width by 25%, per Eq. 4.1.

To summarize, Bar-Cohen's study of optimal heat transfer coefficients for finned surfaces was used to derive a limit for passive cooling of $X_g = 15$ to 30, considering a heat sink equal in width to the CPV cell, operating at cell temperatures between 60 and 90°C . By increasing the width of the heat sink, as per the values given by Eq. 4.1, the limit of passive cooling might be extended to $X_g = 17$ to 37. However, it should be noted that by increasing the width of the heat sink, its ability to transfer heat will be diminished. Otherwise stated, the heat sink would not be able to reach h_{coh} , the aforementioned maximum heat transfer coefficient for natural convection. The assumption was nevertheless made, in order to understand how the limit to passive cooling might be increased by extending the width of the heat sink.

4.3 Cooling transition points: passive, active, and beyond

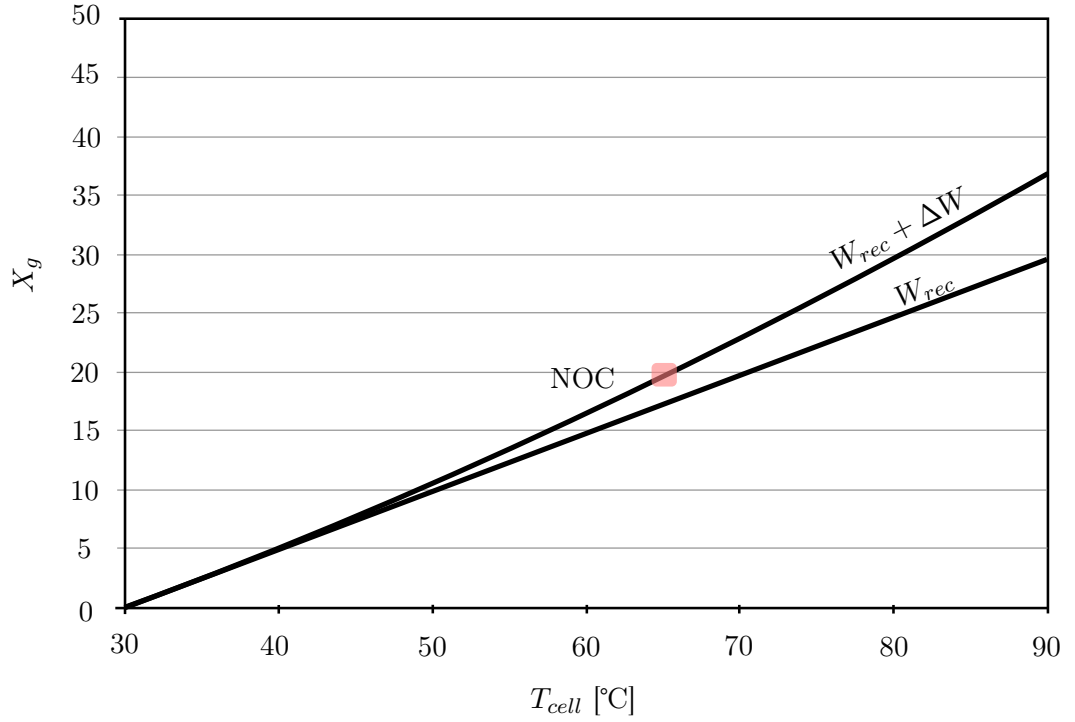


Figure 4.4: Passive Cooling at Various X_g - Recommended X_g and its various operating temperatures. Curves W_{rec} and $W_{rec} + \Delta W$ were created using Eq. 4.2 and 4.3 respectively and assume a heat sink width equal to W_{rec} and $W_{rec} + \Delta W$ respectively. The following parameters were assumed: $G_N=900$ W/m², $\eta_o= 0.80$, $\eta_e= 0.10$, $\gamma_t=0.004^\circ\text{C}^{-1}$, and $T_{amb}= 30^\circ\text{C}$. The value NOC represents the nominal operating condition established in Section 3.4 and is provided as a reference point.

4. METHODS OF COOLING CPV RECEIVERS

The above analysis assumes that natural convection is the primary mode of heat transfer. With any presence of a meaningful wind velocity, heat transfer coefficients may increase in actual operation. However, there will be operating conditions under maximum heat load and zero wind, so it is likely a good idea to design for a no-wind case, or to at least keep this in mind. It is therefore reasonable to use natural convection as the limiting factor to establish the practical limit of passive cooling for linear-focus trough CPV systems.

In actual practice, reaching such high cooling values may prove difficult. It should be noted that heat sinks become increasingly heavier and more complex as the concentration ratio increases. This can seriously affect the design and construction of the concentrator system. Reference [47] explains that heat sinks for linear-focus trough concentrators, in which light is focused upwards and shading of the concentrator is a concern, become “intricate and therefore very expensive for concentration values above 20 suns.” However, the Universidad Politecnica de Madrid (UPM) managed to develop a passively cooled parabolic trough concentrator at $X_g=40$ [35]. Their EUCLIDES concentrator utilizes a split mirror (2 mirrors form a parabolic trough with a gap in the middle), so as to avoid shading from the heat sinks.

In light of the theoretical limits established in this section and available data for existing linear-focus trough CPV systems, a limit of passive cooling is suggested at $X_g=15$ to 30, for systems in which shading via the CPV receiver is a concern. Based on the extending the width of the receiver’s heat sink and based on the experience of the EUCLIDES concentrator, it may be possible to consider concentration ratios approaching $X_g=40$.

An upper limit for active cooling for linear CPV receivers is unknown and difficult to specify, as many design parameters would affect such a limit. Nevertheless, one need only look to the power electronic industry to gain an understanding into the known limits of thermally interfacing small substrate materials, especially silicon. Reference [49] specifies a year 2016 target for achieving heat fluxes up to 0.93 W/cm^2 , with a maximum temperature limit of $125 \text{ }^\circ\text{C}$. This roughly correlates to geometric concentration factors in the previous analysis of $X_g > 80$. In both Ref. [47] and [49] mention is made of utilizing forced convection liquid cooling and pool boiling. It is therefore proposed that above $X_g=80$ that these technologies be considered (Designs F and G as described in Section 6.1). This concentration will be named the next-generation transition point.

5

Design and Optimum Size of the Cooling System

As previously explained, the operating temperature of the solar cell ultimately limits the performance of the concentrator photovoltaic (CPV) system. To better understand the operating temperatures of the solar cell, one must examine the thermal paths in which heat is transferred from the solar cell to the operating environment. In order to facilitate this understanding, the active cooling case in Figure 4.1 (Chp. 4) is referenced, and the major components of both the CPV system and receiver are identified.

5.1 Major components of the CPV system

The concentrator, receiver, and back cooler are three major components of a CPV system and primary functions are:

Concentrator:	collect incoming solar irradiation and focus it onto the receiver
Receiver:	accept incoming concentrated solar irradiation, convert solar irradiation to electricity, provide a mechanical structure and thermal interface to deliver heat to the working fluid
Back Cooler:	accept heat from the working fluid to transfer to the operating environment

5. DESIGN AND OPTIMUM SIZE OF THE COOLING SYSTEM

The primary components of a CPV receiver are shown in Figure 5.1 and are listed in Table 5.1 for an actively cooled receiver. This receiver has been rotated 180° from its normal operating position, as shown in Figure 4.1 (Chp. 4), for ease of clarification.

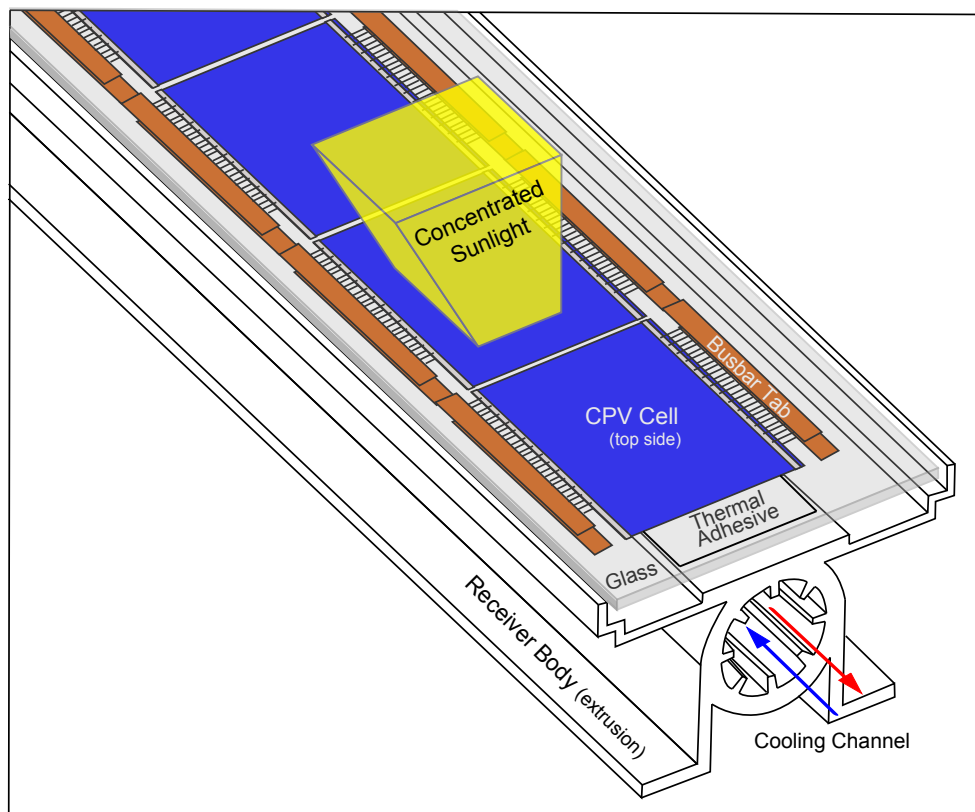


Figure 5.1: CPV Receiver - Actively cooled receiver design utilizing a thermal adhesive.

5.2 Heat transfer within the CPV receiver

At the receiver, concentrated sunlight passes through several optical interfaces until finally reaching the solar cells. At each optical interface, a portion of the light is transmitted, reflected, and absorbed. With regard to the CPV receiver, reflected and absorbed light are considered losses, as they reduce the available power for conversion

Table 5.1: CPV Receiver Components - Major components and function.

Glass:

- protect CPV cells and improve optical interface
- reduce area of encapsulant exposed to moisture
- provide surface for ease of handling and cleaning

CPV Cell:

- accept incoming concentrated light
- convert light to electrical power
- direct electrical power to bus bars

Thermal Adhesive:

- position and fix solar cells to extrusion
- conduct heat to extrusion
- maintain electrical isolation
- accommodate thermal expansion

Extrusion:

- provides basic structure of receiver
- incorporate cooling channel (active cooling)
- integrate and support heat sink (passive cooling)

Encapsulant:

- protect electrical components from environment
- mount glass to extrusion
- maintain electrical isolation
- optical interface between glass and CPV cells

5. DESIGN AND OPTIMUM SIZE OF THE COOLING SYSTEM

to electrical or thermal power. These losses exist at each optical interface, but are typically summed together to represent a total optical loss. Figure 5.2 illustrates the major optical pathways and associated losses for an actively cooled receiver design. Total losses are summed, beginning at the receiver's glass front surface and ending at the solar cell. For the CPV system, these losses extend further, including the primary optics and any secondary optics (assuming that the secondary optics are not already integrated into or serve as the receiver's front surface).

A portion of the light reaching the solar cell will be converted to electrical power. The vast remainder will become heat and must be dissipated by the cooling system. Heat will conduct between the solar cell and its surrounding materials, as illustrated in Figure 5.3. The magnitude and direction of each heat conduction is dependent on the temperature gradients between the various materials within the CPV receiver. Most of the heat is transferred through the receiver body to the coolant channel. By flowing a working fluid through the coolant channel, heat is delivered from the receiver to the back cooler, where it is finally dissipated to the operating environment. During operation, as the temperature of the receiver and coolant piping increase, heat will be transferred to the operating environment by a mixture of natural convection, forced convection (wind), and thermal radiation from the receiver's surfaces to the surroundings. Such heat transfer may be desirable, when considering heat a waste load, but may be deemed losses, as in the case of a concentrator photovoltaic-thermal (CPV-T) system.

5.3 Back cooler

Back cooling is a term generally associated with active cooling cycles in which a heat exchanger reduces the temperature of an incoming working fluid by transferring heat to the operating environment. The temperature of the fluid leaving the back cooler is thus reduced and is returned to cool the device for which the cooling system exists. The working fluid is heated and returned via a pump to the back cooler to start the cycle over again. The various heat exchangers used in back cooling may be wet or dry coolers, open or closed systems respectively. The former utilize evaporative cooling to increase cooling performance and the latter cycles a fluid in a closed loop so as to avoid release into the environment. As much of the world's desirable land for CPV

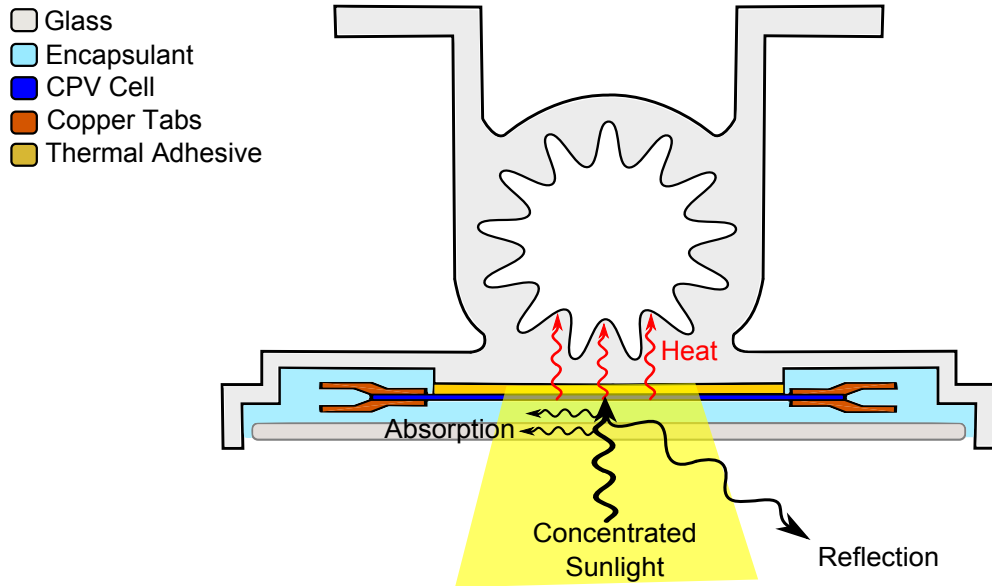


Figure 5.2: Optical Paths - Actively cooled CPV receiver under illumination.

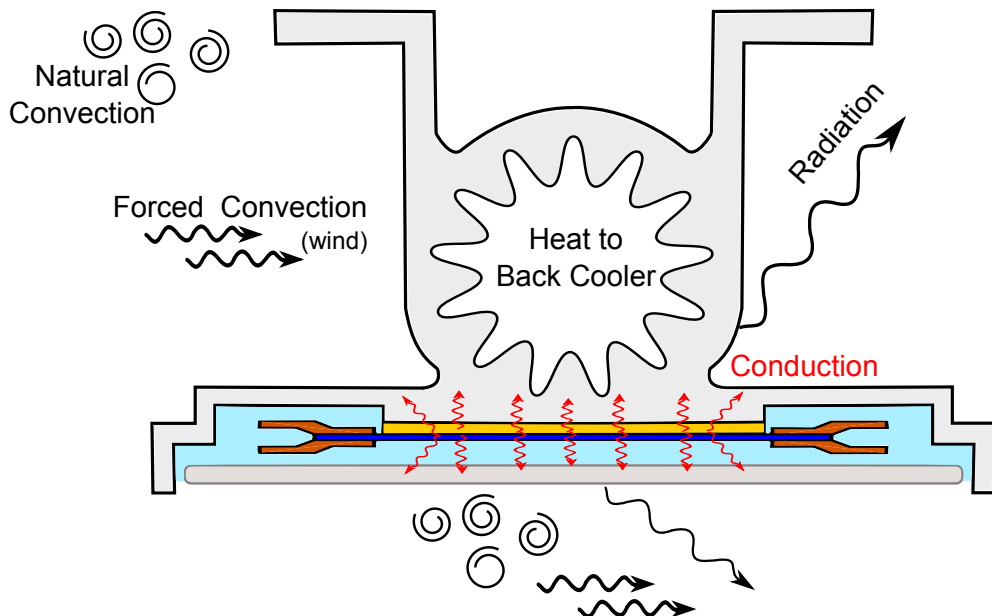


Figure 5.3: Thermal Paths - Heat transfer in an actively cooled receiver.

5. DESIGN AND OPTIMUM SIZE OF THE COOLING SYSTEM

installations, with respect to availability and a large annual direct normal irradiation, lie within desert climates [18], it is advisable to consider closed systems in which water is conserved.

With regard to CPV, the definitions of back cooling and back cooler are slightly broadened so as to include both active and passive cooling cases. In this text, back cooling is considered the primary means of shedding waste heat to the operating environment, and the back cooler is defined as the primary device responsible for this task. Thus, the back cooler serves as the final thermal interface, transferring heat originating from the CPV receiver to the operating environment. Generally, the back cooler is an air cooled heat exchanger. In the case of a passive cooling system, the back cooler is integrated into the receiver body and consists of a series of extended surface fins, a type of heat sink. Thus, heat transfer to the operating environment takes place directly at the receiver. In an actively cooled system, heat transfer to the operating environment is primarily accomplished away from the receiver body. The back cooler is generally separate and positioned away from the receiver such as shown in Figure 5.4. This design utilizes one or more fans to force air over a series of densely arranged finned-tubes. High heat transfer rates relative to installation footprints are achievable with this arrangement. Alternatively, it is possible to utilize passive cooling elements away from the receiver body, such as the finned-tubes in Figure 5.5. But as a pump is required to transfer heat away from the receiver, Figure 5.5 is thus still considered an active cooling case. Comparing the forced convection air cooler of Figure 5.4 and the passive elements of Figure 5.5, the former benefits from a reduced installation footprint and reduction in material requirements. However, additional power is necessary to power the cooling fans and such parasitic losses must be considered.

Regardless of the cooling elements utilized in the back cooler, separating the back cooler from the receiver body and employing a working fluid increases the selection of back cooler designs and can significantly reduce the size and weight of the receiver. This is especially important when considering inflatable concentrator systems. The actual location of the back cooler within the CPV system can vary, depending on the design of the concentrator. For some linear-focus trough installations, there may be space available underneath the concentrator itself. For other designs, such as the inflatable linear concentrator (Figure 1.3), no such space exists, and cooling elements must be placed away or next to the concentrator.

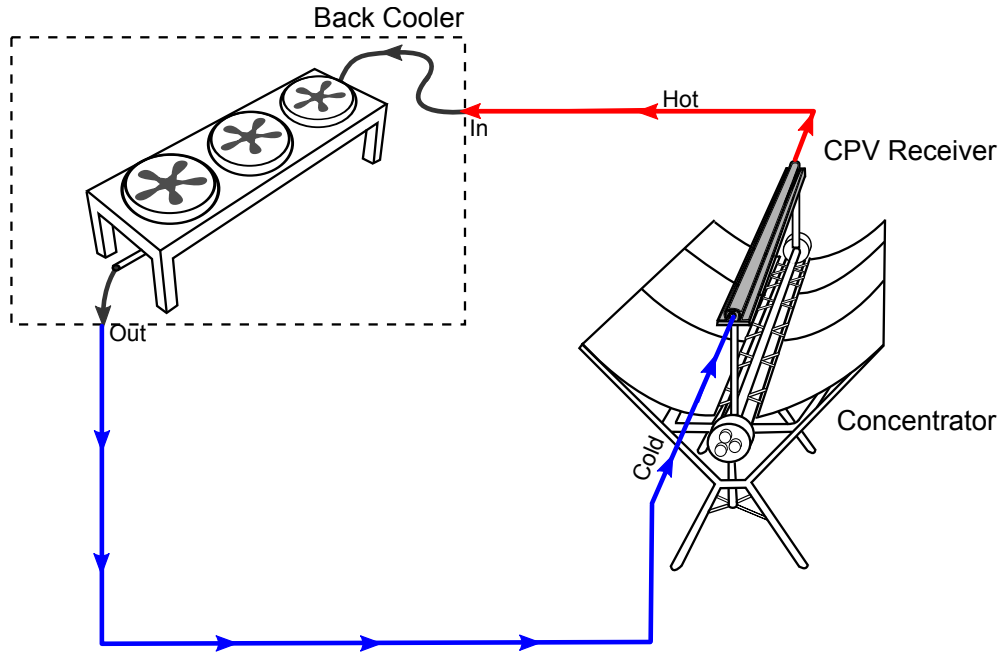


Figure 5.4: Heat Exchanger - A liquid-to-air heat exchanger utilizing forced convection serves as the back cooler.

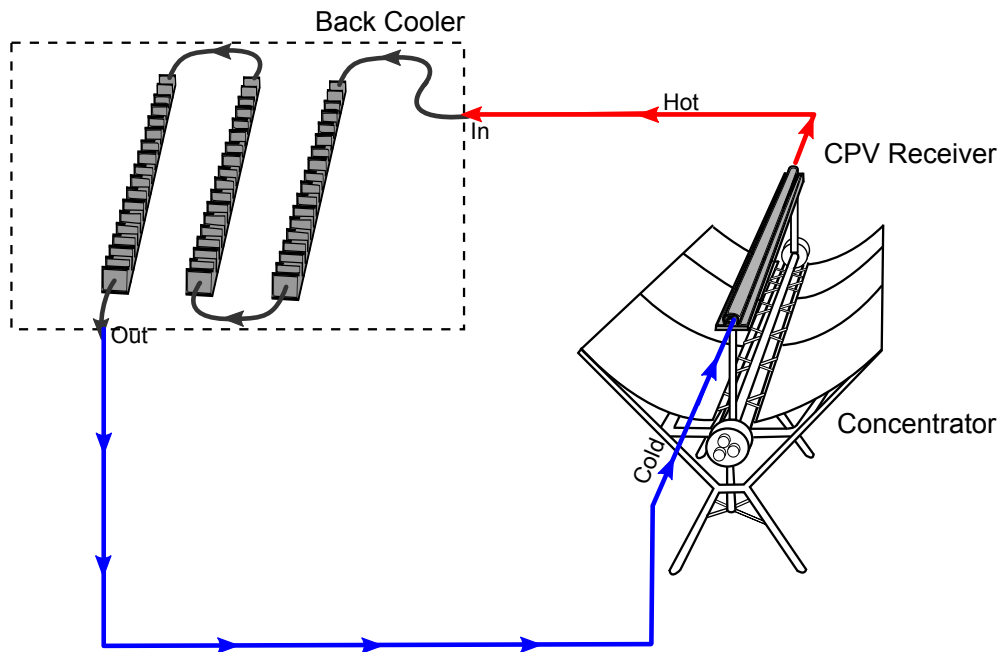


Figure 5.5: Finned Tube Back Cooler - Passive cooling utilized in the back cooler.

5.4 Nomenclature: cooling system

Section 5.5 and Chapter 6 will cover the design and theoretical performance of numerous thermal interfaces in the CPV receiver and cooling system. Before visiting these sections, a common nomenclature for the various thermal interfaces, temperature differences (ΔT), and heat transfer coefficients (HTC) must be established. Figure 5.6 identifies 15 important thermal interfaces (TIFs) and temperatures within the CPV system, and Table 5.2 provides a corresponding naming convention, to be used throughout this text. The definitions in Table 5.2 will be briefly expanded here.

Beginning with item 1 of Figure 5.6, the bulk temperature of the working fluid within the receiver represents the average temperature of the working fluid far from the coolant channel's wall surface, for one particular location along the receiver's length. The temperature is defined so as to differentiate it from item 2*, the temperature of the working fluid near the wall surface. The temperature of the actual wall surface, part of the receiver body, is labeled item 2. Items 3 through 7 represent temperatures at various thermal interfaces, representing in most cases the physical contact of two different materials. In principle, there is a thermal resistance between the two surfaces, known as a contact resistance. Each surface has its own temperature and there is a finite temperature difference between the two. For the purpose of the forthcoming analysis, the two-surface interfaces in items 3 through 7 are considered isothermal, that is, the front side of one material meeting the back side of a second material are considered equal in temperature unless otherwise specified. Any significant temperature difference resulting from the contact resistance is divided between the two surfaces on a case by case basis. This will simplify some of the forth coming analysis in Chapter 6. Starting at the coolant channel surface and moving downwards to the front glass surface (as shown in Figure 5.6), the interface temperatures are named in column three of Table 5.2 using the following convention: T subscript [name of back side surface *dash* name of front side surface]. Items 8 though 13 relate to the back cooler. The bulk temperature of the back cooler for item 8 is analogous to the bulk temperature established in item 1. Items 9-11 essentially describe the operating environment to which the back cooler exchanges heat. Items 12 through 15 can be understood from Figure 5.6.

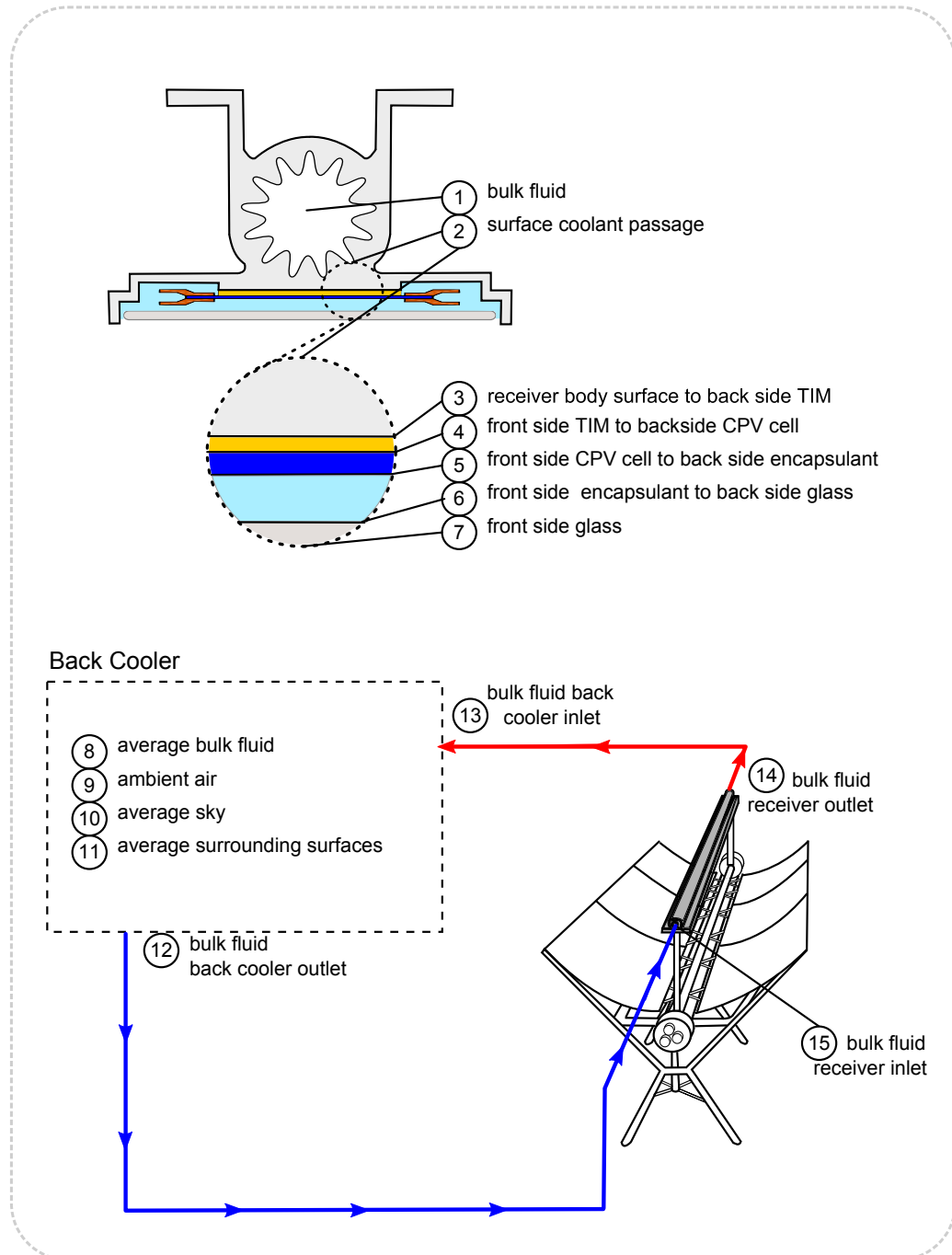


Figure 5.6: TIFs - Heat transfer surfaces, interfaces, and associated temperatures.

5. DESIGN AND OPTIMUM SIZE OF THE COOLING SYSTEM

Table 5.2: Interface Temperatures - Nomenclature for temperatures in Figure 5.6.

$T_{fig\ 5.6}$	$T_{equivalent}$	T_{name}	Description
T_1	T_{bk_fluid}	-	bulk fluid
T_2	T_{scp}	-	wall surface, coolant passage
T_2^*	T_{fl_wall}	-	fluid at coolant passage surface
T_3	$T_{fsREC},$ T_{bsTIM}	$T_{rec-TIM}$	receiver body surface \Leftrightarrow bs TIM
T_4	$T_{fsTIM},$ T_{bsCell}	$T_{TIM-cell}$	fs TIM \Leftrightarrow bs CPV cell
T_5	$T_{fsCell},$ T_{bsEcp}	$T_{cell-ecp}$	fs CPV cell \Leftrightarrow bs encapsulant
T_6	$T_{fsEcp},$ $T_{bsGlass}$	$T_{ecp-glass}$	fs encapsulant \Leftrightarrow bs glass
T_7	$T_{fsGlass}$	-	glass outer surface
T_8	T_{bc_avg}	-	back cooler average bulk fluid
T_9	T_{amb_air}	-	ambient air
T_{10}	T_{sky_avg}	-	average sky
T_{11}	T_{ss_avg}	-	average surrounding surfaces
T_{12}	T_{bc_out}	-	bulk fluid back cooler outlet
T_{13}	T_{bc_in}	-	bulk fluid back cooler inlet
T_{14}	T_{rec_out}	-	bulk fluid receiver outlet
T_{15}	T_{rec_in}	-	bulk fluid receiver inlet
		fs	front surface
		bs	back surface

In addition, the term T_{cell} will frequently occur in this text, and is defined as an average temperature for the CPV cell. Due to the cell material's relatively high thermal conductivity and mere few hundred micron thickness, the temperature of the front and back side of the CPV cell are considered equal, unless explicitly stated otherwise. As the front side of the thermal interface and back side of the CPV cell (T_4) are considered isothermal, the temperature of the top side of the thermal interface, including any contact resistance, thus becomes the average cell temperature T_{cell} . Any ΔT associated with the contact resistance between the back side of the CPV cell and the front side of the thermal interface, is added to the thermally interfacing material. At higher concentration ratios where a noticeable temperature difference occurs, for example a few degrees Celsius, a temperature difference across the cell is calculated and corresponding front and back side temperatures are defined.

Moving forward, there are several temperature differences and associated heat transfer coefficients referenced throughout this text. They will be briefly covered now and are conveniently collected in Table 5.3. The heat transfer coefficient h_{TIF} represents the summation of all thermal interfaces from the CPV cell just up to the back cooler. In the case of the actively cooled receiver design, this corresponds to the bulk fluid. Before reaching the bulk fluid, however, heat must conduct through the coolant channel surface. The associated temperature difference is particular to each location within the receiver and the distance to the coolant channel wall surface. The temperature difference between the coolant channel wall surface and the working fluid nearest this surface is defined as ΔT_{fl_wall} and is strongly influenced by the properties and flow pattern of the working fluid. Lastly, in order to establish a framework for comparing the performance of various back cooler technologies, a temperature difference between the back cooler and operating environment, ΔT_{bc_op} is defined. In keeping with standard ENV1048, ΔT_{bc_op} is defined as the difference between the back cooler inlet temperature and the ambient air temperature.

5.5 Design guidelines

Generally, a thermal interface represents a physical contact or connection in which heat is transferred from one surface to another. It may be easier to associate such a "contact" with the surfaces of two solid materials, but a thermal interface also includes

5. DESIGN AND OPTIMUM SIZE OF THE COOLING SYSTEM

Table 5.3: Thermal Interfaces - Nomenclature for frequently referenced TIFs.

ΔT_{name}	$\Delta T_{equivalent}$	HTC	Description
$\Delta T_{cell-bc}$	$T_4 - T_1$	h_{TIF}	TIF_{total} between cell & back cooler
ΔT_{ext_wall}	$T_3 - T_2$	h_{ext_wall}	through extrusion wall
ΔT_{fl_wall}	$T_2 - T_{fl_wall}$	h_{fl_wall}	wall & fluid, surface-cooling channel
ΔT_{bc_op}	$T_{13} - T_9$	h_{bc_op}	back cooling operating parameters

heat transfer from solid to fluids (liquids and gases). For example, heat transfer between the back cooler and the ambient air or between the inner wall of a pipe and the working fluid can be considered thermal interfaces. In all CPV systems, heat is transferred from the CPV receiver through a series of thermal interfaces until finally reaching the operating environment. A heat transfer coefficient and ΔT may be associated with each thermal interface. In addition, heat transfer coefficients and ΔT s may be added together across the interfaces. Heat transfer coefficients (W/m^2K) are added as follows: For thermal interfaces connected in series:

$$h_{total} = \left[\frac{1}{\frac{1}{h_1} + \frac{1}{h_2} + \dots + \frac{1}{h_n}} \right] \quad (5.1)$$

and for thermal interfaces connected in parallel:

$$h_{total} = h_1 + h_2 + \dots + h_n \quad (5.2)$$

Series connections can be understood by imagining a stack of various materials in which heat must conduct through one material before arriving to the next. Parallel connections can be thought of as placing materials side by side, thus enabling two pathways for heat to flow. Figure 5.7 provides an example of each. Due to the stack-like construction of many CPV receivers, most thermal interfaces connecting the CPV cell to the receiver body are series connections. As such, and as evident from Eq. 5.1, the first design guideline for CPV cooling systems is derived:

The total number of thermal interfaces should be minimized, while increasing the heat transfer of the necessary and remaining few.

In principle, each additional thermal interface added between two components will roughly halve the total heat transfer coefficient, assuming that $h_1 = h_2$. This concept may be further expanded to the remaining cooling components, namely the back cooler.

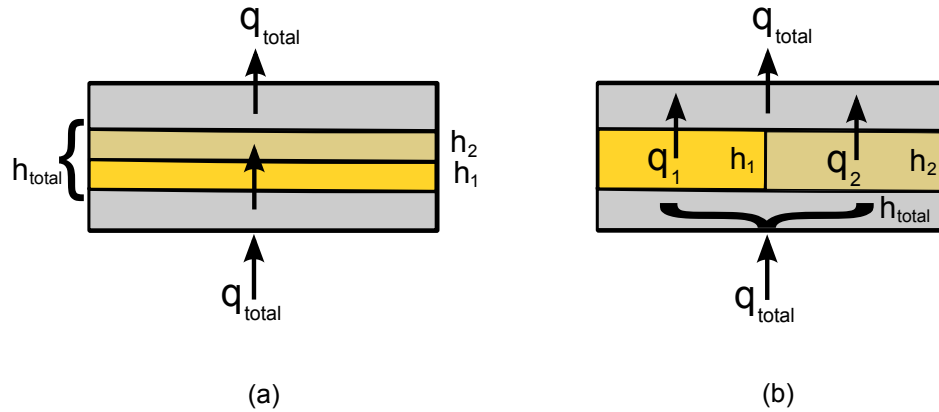


Figure 5.7: HTC Sums - Two thermal materials connected in a) series and b) parallel.

It must be stressed that despite many efforts, several thermal interfaces will still exist between the CPV cell and the operating environment. As such, a second important design guideline from Eq. 5.1 is derived:

The ultimate performance of the cooling system will be limited by the worst performing (smallest HTC) thermal interface between the CPV cell and the operating environment.

Figure 5.8 emphasizes this point by comparing the total heat transfer coefficient resulting from the series connection of h_1 and h_2 to that of h_1 alone. Notice that the value of h_2 must increase by a factor of 10 in order for h_{total} to approach within 10% of h_1 . From this example, a third design guideline is given:

It is critical to identify the relative magnitudes of each thermal interface's HTC so as to identify areas for improvement as well as to understand the likely impact of such improvements.

To this end, Table 5.4 provides a brief overview of some common heat transfer modes and corresponding heat transfer coefficients found in the CPV receiver and cooling system. From this table, one may draw several conclusions regarding the behavior and performance of the cooling system, namely concerning the back cooler. The back cooler designs introduced thus far (see Figures 4.2, 5.4, and 5.5) largely rely on either natural

5. DESIGN AND OPTIMUM SIZE OF THE COOLING SYSTEM

or forced air convection to exchange heat to the operating environment. As such, the back cooler not only requires relatively large surface areas to provide adequate cooling capacity, especially in the case of passive cooling, but ultimately serves as the limiting factor to the cooling system's performance. It is worth mentioning that radiant heat transfer, excluded from Table 5.4, can become a significant contribution to the overall heat transfer, especially for single point concentrators where heat flux is high. However, in the case of low concentration linear-focus trough concentrators, with operating temperatures typically below 100°C, heat transfer via thermal radiation is less significant.

Regardless of the heat transfer mode, the back cooler designs introduced thus far can transfer significant quantities of heat by utilizing large surface areas. Other thermal interfaces, especially within the CPV receiver, can begin to limit the total system performance if improperly designed. The problem of back cooling is one common to many power systems, and its development can be much further dated than that of the development of thermal interfaces within the CPV receiver. Therefore, particular attention will be given to the thermal interfaces within the CPV receiver. Several designs are identified and theoretical performance calculated in Chapter 6.

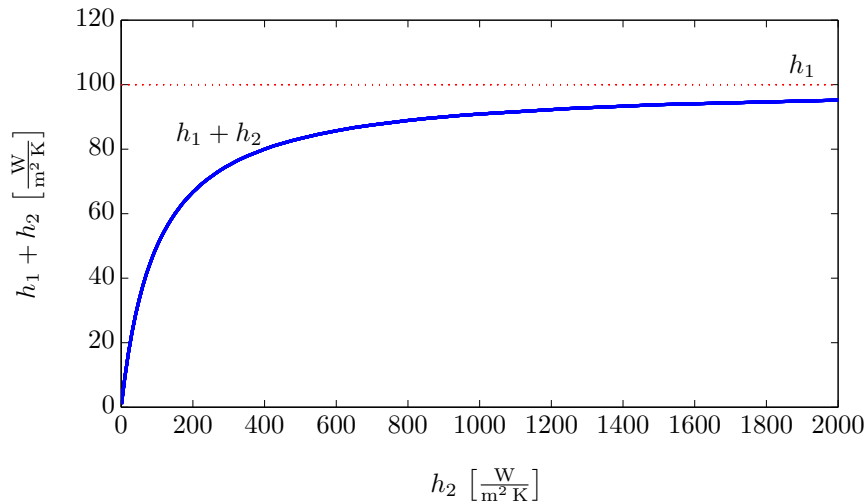


Figure 5.8: Additional TIFs - The effect of one additional series-connected thermal interface to the total heat transfer coefficient, represented above by the value $h_1 + h_2$, is calculated using Eq. 5.1 $\frac{1}{\frac{1}{h_1} + \frac{1}{h_2}}$ and produces the blue curve above. The red dotted line represents the heat transfer coefficient of h_1 , prior to the addition of h_2 .

5.6 Sizing the cooling system and comparing TIFs

Table 5.4: Common HTCs - Some common heat transfer coefficients.

Heat Transfer	Medium	HTC [$\frac{W}{m^2 K}$]	Ref.
Natural convection	air	5 - 20	[50]
Forced convection	air	5 - 40	[50]
Natural convection	water	200 - 1,000	[50]
Forced convection	water	1,500 - 20,000	[50]
Conduction	Al [2-4mm]	40,000 - 60,000	Sec. 6.6
Conduction	thermal adhesives	2,900 - 21,700	Sec. 6.6

5.6 Sizing the cooling system and comparing TIFs

Before comparing the design and theoretical performance of various thermal interfaces within the CPV receiver, it is necessary to establish some boundary conditions or a base-case to provide a fair comparison between thermal interface designs. To illustrate this need, an example is provided. Table 5.5 presents a simplification in which the cooling system is represented by two heat transfer coefficients, h_{bc} and $h_{cell-bc}$. Here, h_{bc} represents the total heat transfer coefficient between the back cooler and the operating environment. For an actively cooled system, it is equivalent to h_{bc_op} (see Table 5.3). For a passively cooled system, h_{bc} would represent the heat transfer coefficient of the heat sink to the operating environment. $h_{cell-bc}$ is equivalent to h_{TIF} as explained in Table 5.3. The total heat transfer coefficient, h_{total} , for the two-HTC model in Table 5.5 is calculated for a doubling of $h_{cell-bc}$, and the corresponding percent improvement in h_{total} for each successive doubling is given in row “Relative Improvement.” When the value of $h_{cell-bc}$ is significantly larger than h_{bc} , successive increases in $h_{cell-bc}$ provide a relatively small improvement in h_{total} . With regard to the CPV receiver, large improvements in the cell to receiver interface may provide little overall benefit, if the thermal interfaces in the receiver already far outperform the back cooler. This brief example further reiterates design guideline 3 from Section 5.5, and provides the basis for the remainder of this section, namely, to establish a set of fair boundary conditions for use in comparing thermal interface designs within the CPV receiver.

5. DESIGN AND OPTIMUM SIZE OF THE COOLING SYSTEM

Table 5.5: Improving h_{total} - Relative improvement of h_{total} for a doubling of $h_{cell-bc}$.

	HTC [W/m ² K]			
h_{bc}	100	100	100	100
$h_{cell-bc}$	100	200	400	800
h_{total}	50	67	80	89
Relative Improvement	-	33%	20%	11%

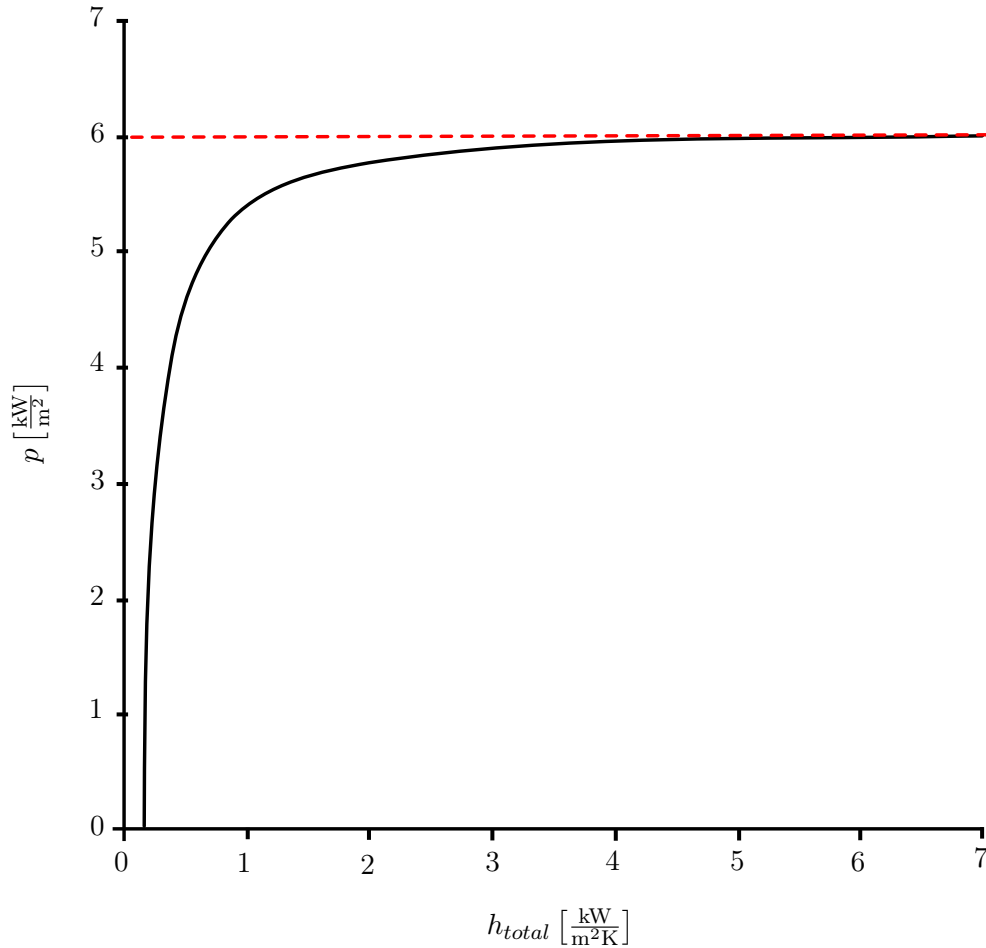


Figure 5.9: Infinite Cooler Size - Improvement in power output (power density) by increasing the HTC of the cooling system.

5.6 Sizing the cooling system and comparing TIFs

Having explained the importance of understanding the values of h_{bc} and $h_{cell-bc}$, the question still remains: what value of h_{bc} should be used to compare the various designs of TIFs between the receiver and back cooler? A proposal is made here. First, an optimal value for h_{total} is investigated for the concentration value of interest. Next, it is assumed that h_{bc} is equal to this optimal value of h_{total} . Then for each receiver design, and corresponding set of TIFs making up $h_{cell-bc}$, the additional $h_{cell-bc}$ will be added to h_{bc} , and a new h_{total} , named h_{total}^* , is calculated. The additional thermal interfaces, and associated $h_{cell-bc}$, for each receiver design will yield a value of h_{total}^* which is less than the established optimal h_{total} . The resulting power loss associated with each design may be described by the following percentage:

$$\text{Power Loss} = \left[\frac{p(h_{total}) - p(h_{total}^*)}{p(h_{total})} \right] 100 \quad (5.3)$$

where $p(h_{total})$ and $p(h_{total}^*)$ will be calculated using Eq. 5.4. This percentage power loss, with respect to $p(h_{total})$, will serve as the basis for comparing various receiver designs and their associated TIFs in Section 6.7.

With a basis for comparing thermal interfaces described, an optimal h_{total} must be derived. An obvious choice might be power output. Unfortunately, there is no optimal value of h_{total} with respect to a maximum power output. Figure 5.9 illustrates this point, where the power output (power density with respect to cell area) for a CPV receiver is shown at a particular geometric concentration factor (X_g) for an increasing value of h_{total} . Every increase in h_{total} offers an increase in power density; however, each successive increase brings with it a diminishing return. The design engineer could select any number of points along the curve, but there is no optimal power density with respect to h_{total} . As h_{total} approaches infinity, the ΔT between the CPV cells and the operating environment approaches a fixed value, at which point a maximum power density is approached. Approaching such a point would require an excessively large cooling system and would be prohibitively expensive. In practice, the design target for h_{total} lies away from this maximum value of power density.

The idea of using power output alone for determining an optimal value of h_{total} has been eliminated. Thus, an alternative idea is needed. It can be shown that an optimal geometric concentration factor X_g exists for a given value of h_{total} . And although this h_{total} is not an optimal value with respect to power output, it will be shown to be a practical alternative and will be adopted for h_{bc} in the thermal interface comparison

5. DESIGN AND OPTIMUM SIZE OF THE COOLING SYSTEM

in Section 6.7. But before doing so, an optimal value of X_g for a given h_{total} must be mathematically described. To aid in this derivation, the following example is provided.

Imagine that the size of the cooling system is fixed, and that it operates under a reasonable set of operating conditions in which one could assume that h_{total} remains relatively constant. The design engineer could then adjust the incoming solar irradiation, via concentration, to produce a range of power outputs particular to one CPV cell technology. Increasing the concentration (holding cell dimensions constant and increasing aperture area) would increase the incoming solar irradiation reaching the CPV cell. Both power output and temperature would increase. Although power output is increasing, the efficiency of the cell will begin to decrease due to its rise in temperature. Eventually, the cell temperature will become high enough and its efficiency low enough that further increases in concentration will reduce the total power output. Finally, temperatures can reach levels so high and efficiencies so low, that for all practical purposes power output is theoretically zero (assuming the cell has not already failed from thermal overload). Thus for this one fixed value of h_{total} , there will exist a concentration factor at which power output is maximized, i.e. an optimal concentration factor for a given initial value of h_{total} . This behavior is illustrated in Figure 5.10 for three values of h_{total} and is mathematically described by Eq. 5.4 - 5.6. See Appendix B.4 for derivations. It is important to note, that these equations, along with the phenomena described above, merely model the CPV cell's behavior. Its actual performance depends on numerous design factors (target concentration ratio, doping levels, series resistance, front side grid shading, etc...), and may vary from the ideal case as described above.

$$p = G_N X_g \eta_o \eta_e \quad (5.4)$$

$$\eta_e = \eta_{stc}(1 - \Delta T_{stc} \gamma_t) \quad (5.5)$$

$$\Delta T_{stc} = \frac{G_N X_g \eta_o (1 - \eta_e)}{h_{total}} \quad (5.6)$$

Examining Figure 5.10, three optimal values of X_g are found, one for each value of h_{total} . These solutions are found by taking the partial derivative of Eq. 5.4 with respect to X_g , setting $\partial p / \partial X_g = 0$, and solving for X_g as shown in Eq. 5.7. See Appendix B.5 for its derivation.

$$X_g = \frac{h_{total} - h_{total} \sqrt{1 - \eta_{stc}}}{G_N \eta_o \eta_{stc} \gamma_t} \quad (5.7)$$

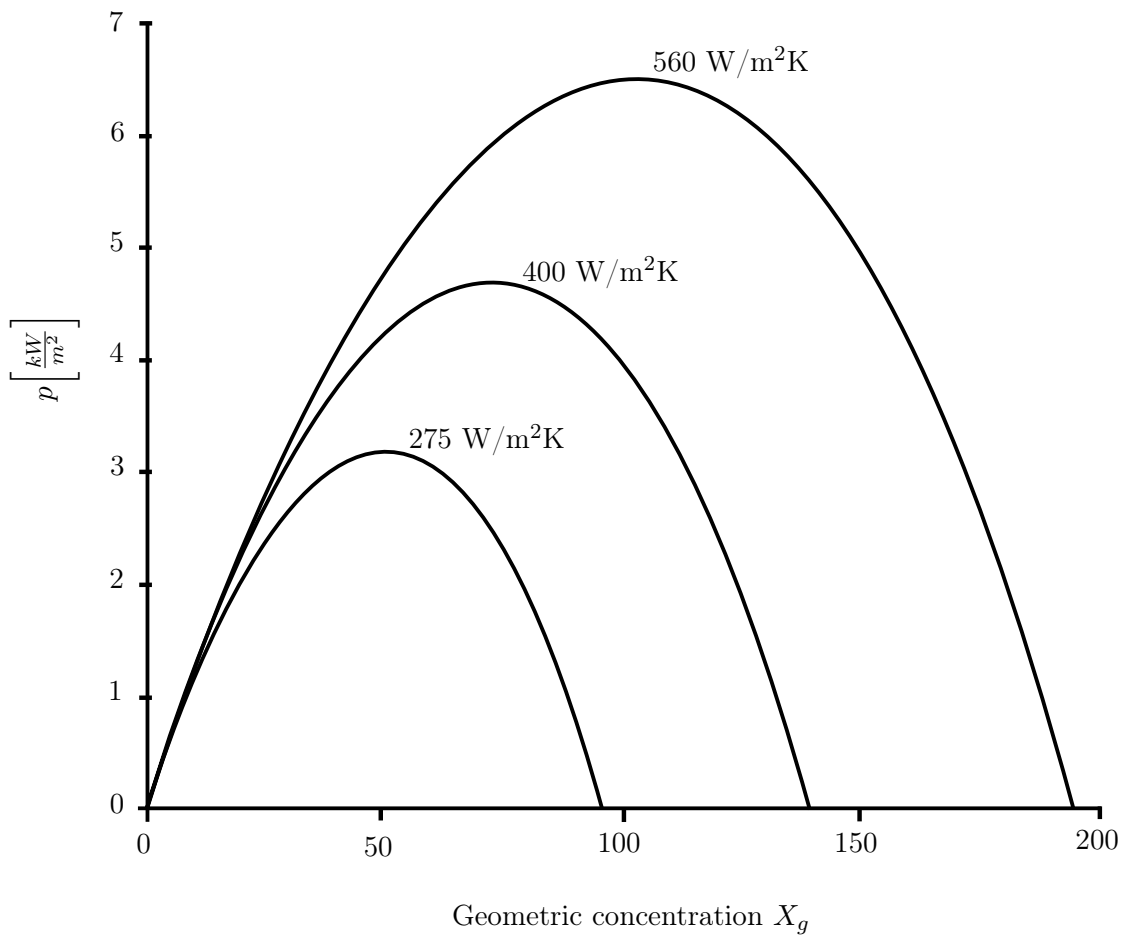


Figure 5.10: Optimum X_g for h_{total} - Power output (power density with respect to cell area) against increasing concentration for various values of h_{total} .

5. DESIGN AND OPTIMUM SIZE OF THE COOLING SYSTEM

An optimal X_g for a given value of h_{total} is derived by finding the maximum power output as X_g is increased. As X_g is typically known or stated, it is convenient to rewrite Eq. 5.7 in terms of this parameter to aid in finding h_{total} , the proposed optimum h_{bc} for comparing TIFs. See Eq. 5.8.

$$h_{bc} = h_{total} = G_N \eta_o \gamma_t X_g (1 + \sqrt{1 - \eta_{stc}}) \quad (5.8)$$

It is tempting to assume that if X_g from Eq. 5.7 is the optimal concentration ratio for a given h_{total} and that this optimal resulted in maximizing power output, then the reverse may also be true. Meaning that, this h_{total} , by rearranging Eq. 5.7 to solve for an optimal h_{total} for a given X_g (Eq. 5.8), maximizes power output. However tempting, such conclusions are nevertheless wrong, for reasons outlined earlier in this section. Namely, there is no maximum power output given by h_{total} . To reiterate this important point, let us briefly visit Figures 5.10 and 5.11. From Figure 5.10, it is clear that $X_g = 50$ is the optimum concentration ratio for $h_{total} = 275 \text{ W/m}^2\text{K}$; however, if the three values of h_{total} from Figure 5.10 are plotted against power density vs. h_{total} for $X_g = 50$, then one finds that significant improvements in power density are still possible (see Figure 5.11). However, these gains can only be realized if the increase in power output outweighs the cost of increasing the size of the back cooler. Lacking a proper economic analysis, there is no way to know if these gains can be realized. If one were to select points 400 or 560 $\text{W/m}^2\text{K}$ from Figure 5.11, then one would quickly moves away from the optimum h_{total} , as illustrated in Figure 5.12. Notice that the new operating points lie to the left of the peak of each curve, and that power output increases by moving to $X_g = 75$ and 100 for an h_{total} of 400 and 560 $\text{W/m}^2\text{K}$ respectively. For the time being, and in light of the discussions above, h_{bc} (Eq. 5.8) will serve as a practical optimum cooler size. These values are conveniently provided in Table 5.6 and form a basis for comparing the various thermal interface designs in Chapter 6. At the end of Chapter 6, with the comparison of each design completed, a brief economic analysis addresses further possible performance improvements by examining increases to the cooler size above the values of h_{bc} .

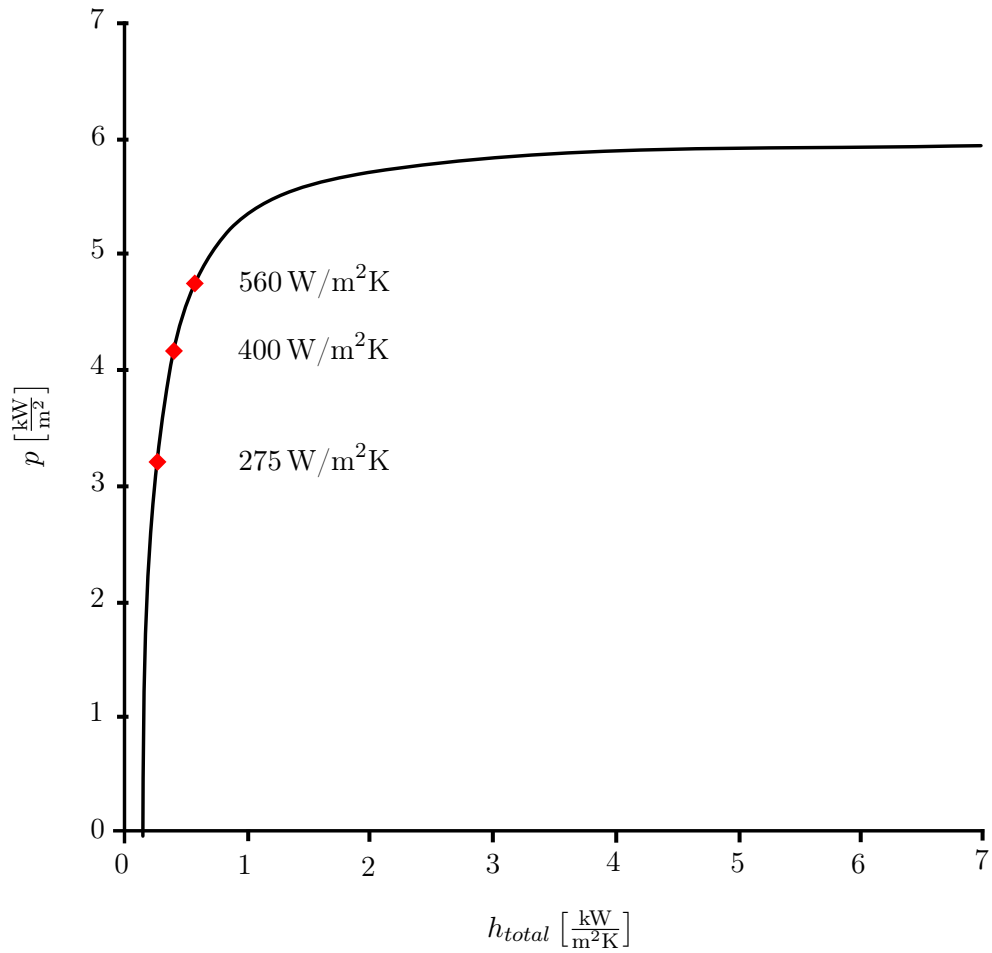


Figure 5.11: Approaching an Infinite HTC - Demonstration of increased power output (power density with respect to cell area) for $X_g=50$ by increasing h_{total} beyond its initial value, $275 \text{ W/m}^2\text{K}$, as calculated in Eq. 5.7. Points correspond to those in Figure 5.12.

5. DESIGN AND OPTIMUM SIZE OF THE COOLING SYSTEM

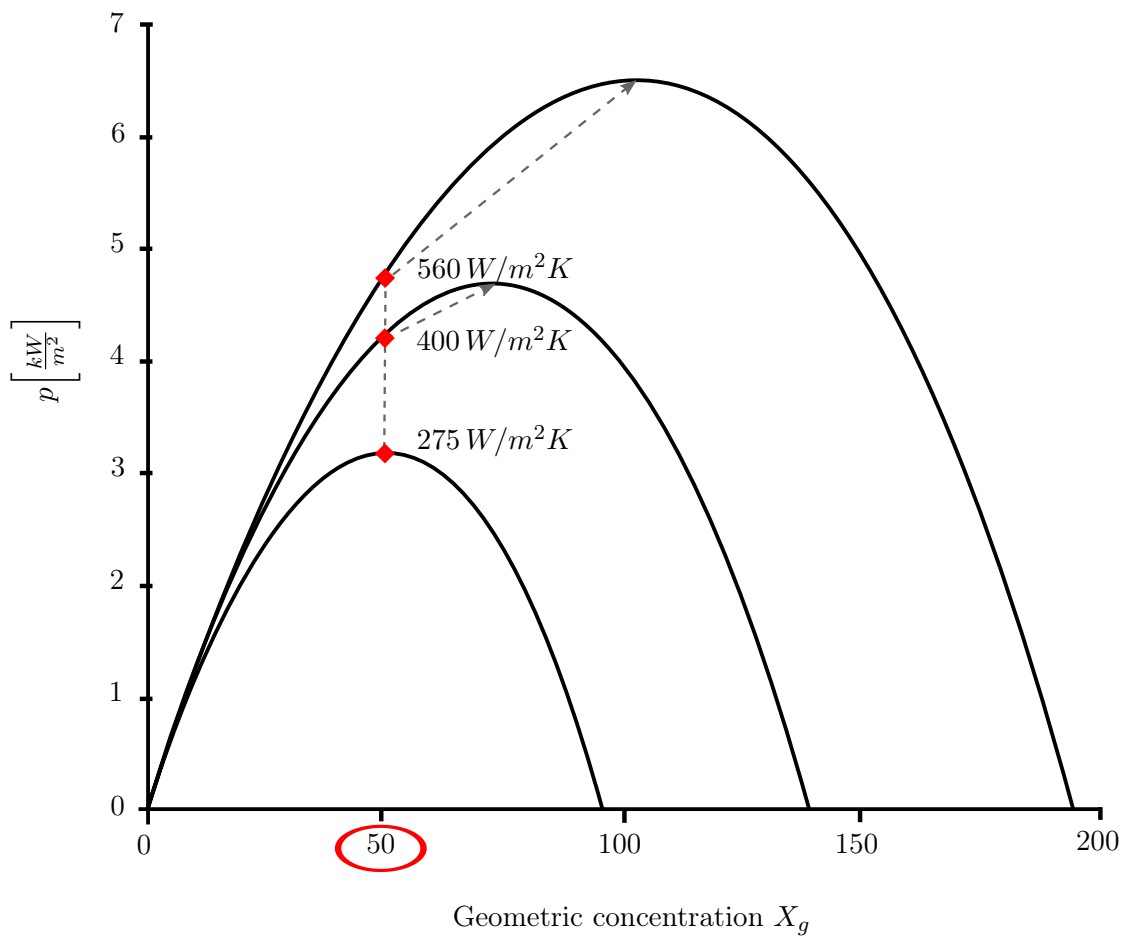


Figure 5.12: Optimum HTC - Sub-optimal performance, power density compared against concentration factor X_g , by increasing h_{total} .

5.6 Sizing the cooling system and comparing TIFs

Table 5.6: Back Cooler HTC for TIF Comparisons - Selected values of h_{bc} as given by Eq. 5.8 for a silicon CPV cell with $\eta_{stc} = 0.17$ and $\gamma_t = 0.004$.

X_g	$h_{bc} \left[\frac{\text{W}}{\text{m}^2 \text{K}} \right]$
1	5.5
5	28
10	55
20	110
30	165
40	220
50	275
60	330
70	385
80	440
90	495
100	550

To summarize, it was first shown that h_{total} cannot be optimized with respect to power output, as illustrated by Figure 5.9. However, an optimal X_g for a given h_{total} was derived in Eq. 5.7, and is conveniently illustrated in Figure 5.10. Rearranging this equation, h_{total} was stated in terms of X_g to give Eq. 5.8. Next, it was further clarified and illustrated in Figure 5.11, that the h_{total} of Eq. 5.8 is not an optimum h_{total} with respect to power output. Lacking the proper economic analysis to justify further increases to the size of the cooling system, a practical optimum of h_{total} was established using Eq. 5.8. These values were chosen to represent the size of the back cooler, h_{bc} , utilized in the forthcoming comparison of TIF designs in CPV receivers (Section 6.7). Table 5.6 conveniently lists h_{bc} for each X_g .

5. DESIGN AND OPTIMUM SIZE OF THE COOLING SYSTEM

6

Theoretical Performance of Various Thermal Interfaces

Having established a practical “optimal” value of h_{bc} , the various receiver designs, and associated thermal interfaces (TIFs), are compared by calculating the various TIFs between the concentrator (CPV) cell and the back cooler. Before doing so, a brief introduction to various receiver designs, particular to linear-focus trough concentrating systems, is presented. Following this, the remaining sections provide the detailed calculations for each design and a comparison of their relative performances.

6.1 Designs covered and associated boundary conditions

In principle, this chapter covers two main approaches to the cooling of CPV cells: receiver designs which utilize thermally conductive materials and those which utilize the direct immersion of the CPV cell in a cooling fluid (DI-CPV). Designs utilizing conductive materials, conduct heat to the receiver body where it is either dissipated via a heat sink (passive cooling) or is sent to the back cooler via a cooling fluid (active cooling). The cooling of CPV cells by direct immersion in a cooling fluid is one possible alternative that may potentially improve both heat transfer rates and power efficiency. This chapter estimates the theoretical performance of both approaches by comparing their effects on both h_{total} and power output. Several receiver designs utilizing thermally conductive materials and several utilizing direct immersion cooling are considered. The various receiver designs and their associated thermal interfaces are summarized in Table 6.1,

6. THEORETICAL PERFORMANCE OF VARIOUS THERMAL INTERFACES

labeled A through G. The column “Main description” lists thermal interfaces common between each design and the column “Variations” highlights any major differences. In column “ h_{TIF} ,” the names of the associated heat transfer coefficients (HTC) are listed, which are to be summed, and include all thermal interfaces necessary to deliver heat from the CPV cell to the back cooler.

Each design is briefly described here and the assumptions used for calculating their respective heat transfer coefficients are given in Section 6.2. Designs A and B represent passively cooled receivers, which utilize a heat sink for the back cooler, and use a thermal adhesive between the cell and the receiver body. It is assumed that the heat sink is integrated into the receiver body, both made from aluminum, and that the heat transfer associated by the combination of the heat sink-receiver body is accounted for by h_{bc} . Thus, no h_{ext_wall} term is included. Figure 6.1 provides an example. Design-A utilizes thermal adhesives which are electrically isolating whereas Design-B uses non-isolating thermal adhesives. Design-B must take special care to apply the adhesive with some space between cells and utilize an isolation coating on the receiver, so as to avoid creating a single back contact for the CPV cells. Thus, an additional oxidation coating and its effect is included in h_{TIF_B} . Designs C and D utilize an aluminum receiver body that is similar to Designs A and B, but a cooling channel is integrated into the center of the receiver, as shown in Figure 6.2. Thus, two additional heat transfer coefficients are considered, h_{fl_wall} and h_{ext_wall} , representing an additional heat transfer coefficient at the coolant surface wall and through the extrusion wall respectively. As in Designs A and B, Designs C and D utilize electrically isolating and non-isolating thermal adhesives respectively. The heat transfer coefficients h_{TIF_A} through h_{TIF_D} include the heat transfer across the thermal conductive materials, i.e. the thermal adhesives, isolation coatings (if needed) and any thermal contact resistances. These conduction based heat transfer coefficients are labeled h_{con} and are calculated in Section 6.6.

Designs E and F consider the direct immersion of CPV cells in a cooling fluid under laminar and turbulent flow respectively. Their associated heat transfer coefficients are labeled h_{lam} and h_{trb} respectively. An example of such a receiver design is shown in Figure 6.3, with an associated 2-D cross Section in Figure 6.4. In principle, a CPV cell is mounted to a narrow glass tube, through which coolant flows. After removing excess heat from the CPV cell, the fluid is transferred to the back cooler for heat exchange

6.1 Designs covered and associated boundary conditions

to the environment. Several cooling fluids are investigated, but only the back side (single side) cooling case will be considered (see explanation in Chapter 7). Finally, a brief analysis is given considering heat transfer via pool boiling and condensing, labeled Design-G. For the analysis, the same receiver body from Designs E and F is assumed, but an additional condenser must be utilized and its associated heat transfer coefficients are considered in h_{TIFG} . Again, only the back side (single side) case is considered (see explanation in Chapter 7.)

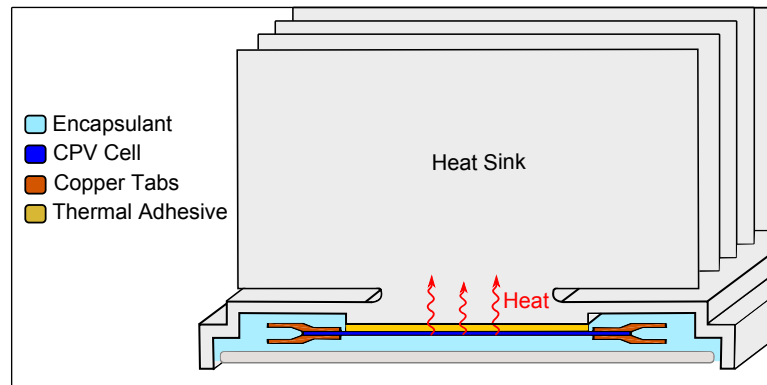


Figure 6.1: TIF Conduction Passive - Passive cooling CPV receiver utilizing a thermal conductive adhesive and heat sink: Designs A and B.

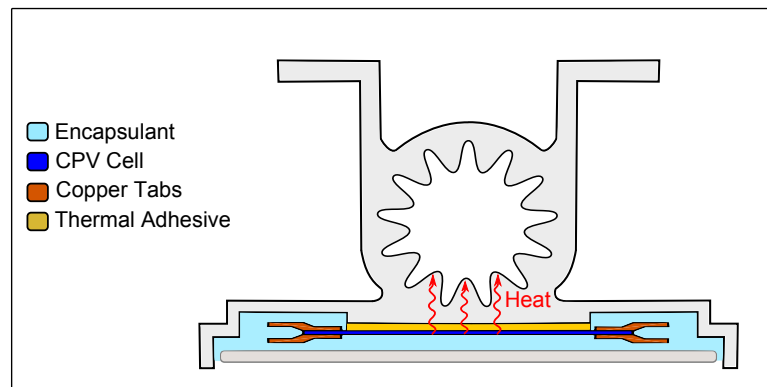


Figure 6.2: TIF Conduction Active - Actively cooled CPV receiver utilizing a thermal conductive adhesive: Designs C and D.

6. THEORETICAL PERFORMANCE OF VARIOUS THERMAL INTERFACES

Table 6.1: TIF Designs - List of TIF designs and associated HTC. ¹The parameter h_{pipe_wall} represents a HTC for conductive heat transfer through the pipe wall of a condenser pipe.

Main Description	Ref.	Variations	h_{TIF}	Fig.
passive cooler (heat sink) Al extrusion body thermal adhesive	A B	thermal adhesive (dielectric) oxide layer thermal adhesive (non-isolating)	h_{con}	6.1
back cooler (active) H ₂ O*-coolant channel Al extrusion body thermal adhesive	C D	thermal adhesive (dielectric) oxide layer thermal adhesive (non-isolating)	h_{fl_wall} h_{ext_wall} h_{con}	6.2
back cooler (active) fluid flow back side	E F	laminar flow turbulent flow	h_{lam} h_{trb}	6.4
back cooler (active) condensing boiling back side	G	-	h_{fl_wall} ¹ h_{pipe_wall} $h_{condensing}$ h_{pb}	6.5

6.1 Designs covered and associated boundary conditions

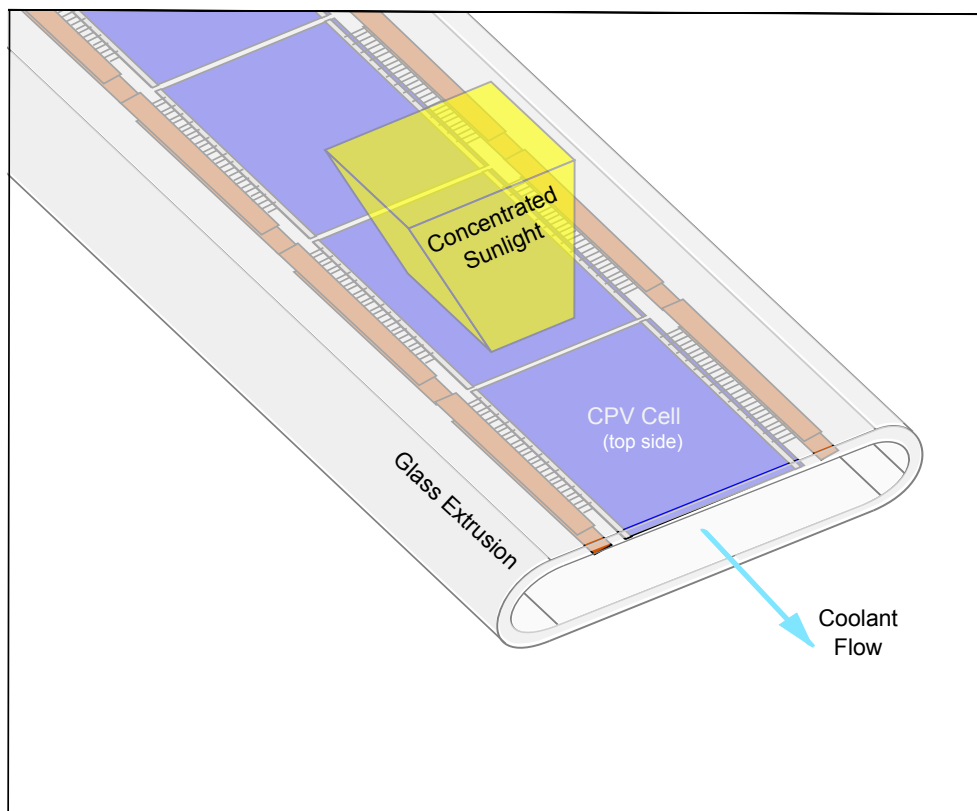


Figure 6.3: DI-CPV Receiver - Actively cooled receiver design with direct immersion of the CPV cell in a heat transfer fluid: receiver body for Designs E, F, and G.

6. THEORETICAL PERFORMANCE OF VARIOUS THERMAL INTERFACES

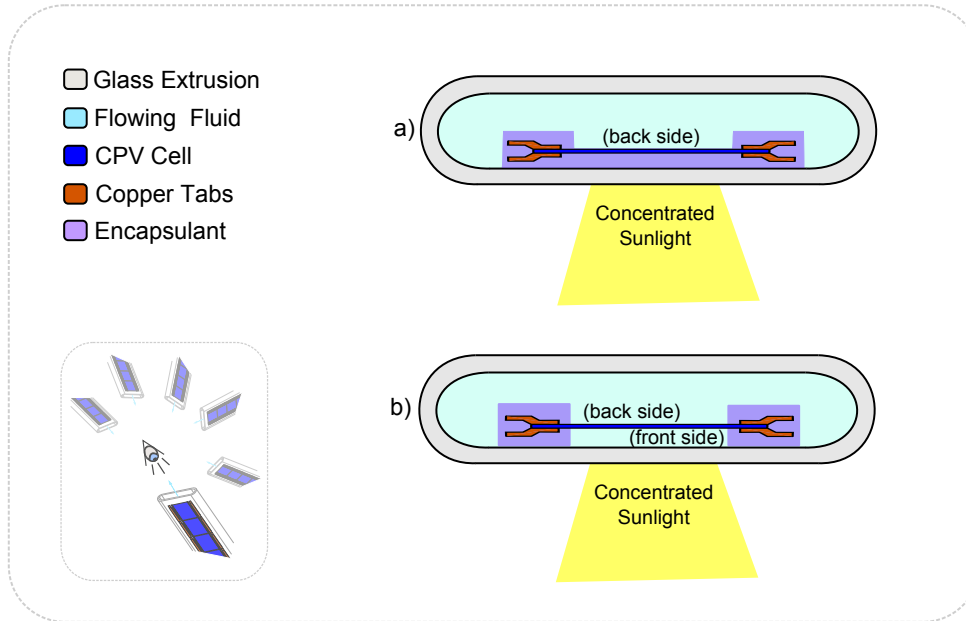


Figure 6.4: DI-CPV Flow - Cross section of Fig. 6.3: Receiver body for Design E & F.

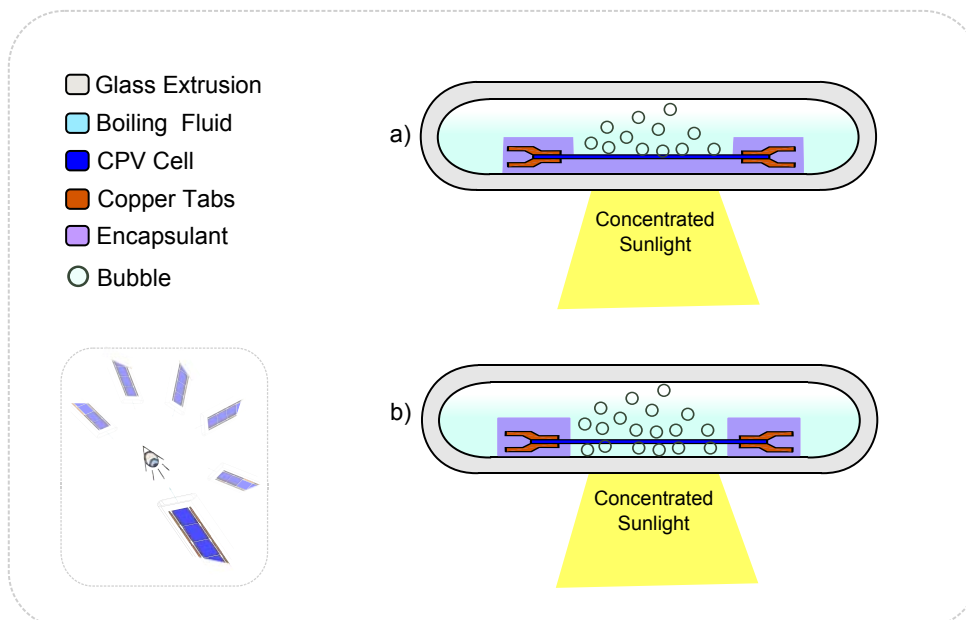


Figure 6.5: DI-CPV Boil - Cross section of Fig. 6.3: Receiver, pool boiling Design-G.

6.2 Calculating the heat transfer coefficients

Considering the number of thermally conductive materials, heat transfer fluids, receiver geometries, and combinations thereof, the task of generalizing a set of heat transfer coefficients to account for the various thermal interfaces within each receiver design appears implausible. However, by an appropriate survey of both thermally conductive materials and plausible heat transfer fluids and by narrowing the scope of the analysis to several representative geometries, some general but powerful conclusions can be drawn. A survey of available thermally conductive materials, necessary to calculate h_{TIFA} through h_{TIFD} , is given in Section 6.6, including a “Best in Class” list. Chapter 7 identifies three candidate fluids for Designs E and F: de-ionized water (denoted as H_2O^*), silicon oil (Si-Oil), and hydrofluorocarbon fluids (HFC). These same three fluids are considered for pool boiling, Design-G, but heat transfer coefficients from many other fluids are also included. Further details are given in Section 6.5.

To facilitate the calculation of the various heat transfer coefficients, the complex receiver geometries were reduced to four simplified models. Figure 6.6 illustrates. All models ignore heat transfer from the receiver body to the operating environment. In model-b, the complex gear-like shape of the extrusion body’s coolant passage (see Figure 6.2) is reduced to a 4mm thick pipe wall, spanning the width of the CPV cell. Model-c is similar to model-b, but lacks a thermal adhesive or receiver body wall. For both models b-c, heat is transferred to the flowing coolant which is then sent to the back cooler. Any heat transfer from the piping between the receiver and the back cooler is assumed to be incorporated in the optimized h_{bc} from Section 5.6. Model-d illustrates a potential design utilizing pool boiling. A cooling fluid is boiled in the receiver body and travels upwards where it condenses on a condensing tube. A second cooling fluid flowing through the condenser tube transfers heat to the back cooler.

Designs C-G utilize a flowing fluid to transfer heat from the CPV cell to the back cooler. Their heat transfer coefficients will be dependent on the velocity or flow rate of the cooling fluid. If one wishes to make a fair comparison between each design, then an appropriate fluid velocity must be utilized to establish values for h_{fl_wall} (in Designs C, D, and G) and to calculate h_{lam} and h_{trb} for Designs E and F respectively. There is an associated parasitic loss for pumping this fluid through the receiver which must be considered. In Section 6.4 an optimal range of fluid velocities and associated heat

6. THEORETICAL PERFORMANCE OF VARIOUS THERMAL INTERFACES

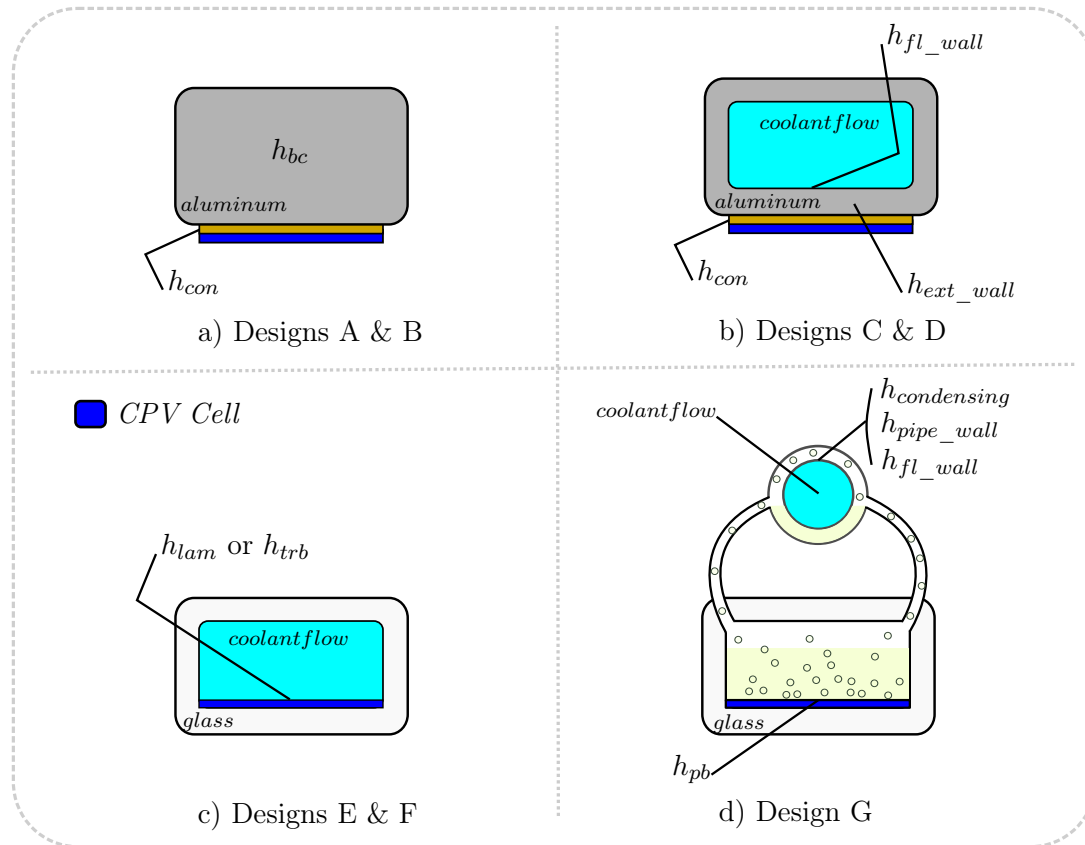


Figure 6.6: Simplified Heat Transfer Models - Equivalent heat transfer models for receiver Designs A-G.

transfer coefficients is established for h_{trb} , the back side direct immersion cooling case. In order to differentiate between the various fluids, the notation h_{trb_X} will be adopted, where X refers to the fluid under consideration. The heat transfer coefficients calculated for h_{trb_X} , will consider model-c as a simple pipe with an appropriate hydraulic diameter. As such, the optimal fluid velocities and associated heat transfer coefficients determined in Design-F are utilized for h_{fl_wall} for Designs C, D, and G. A special case is given for laminar flow, Design-E, in Section 6.3.

6.3 Direct immersion cooling in laminar flow

In laminar flow, heat transfer coefficients vary along the length of a pipe as both the velocity and temperature profile develop. Higher heat transfer coefficients are exhibited

near the inlet of the pipe. As one continues further downstream of the fluid entry point, the laminar flow eventually becomes fully developed (both the velocity and temperature profiles develop), and the heat transfer coefficient reaches a minimum value. When considering the limits of cooling by laminar flow, it is important to understand where this minimum value occurs. The so called hydrodynamic entry length, the length required to fully develop the velocity profile, is dependent on both fluid and geometric properties. To better understand this length and its relation to CPV, the velocity profile is discussed further. For a pipe carrying a fluid near the transition Reynolds number (2100), the hydrodynamic entry length can extend beyond 100 diameters [51]. Considering pipe diameters (or equivalent hydraulic diameter of the receiver's cooling path) in the range of 20 to 50 mm would set this length at 2 to 5 meters. Although there are numerous applications below this point, in the application of linear-focus trough CPV systems spanning tens of meters, this length is likely met. In such a long chain of CPV receivers, this minimum heat transfer coefficient is reached and it is advisable to consider this value when discussing the performance limits of cooling by laminar flow.

To determine this limit, the receiver design in diagram-(a) Figure 6.4 is used to establish appropriate boundary conditions and represents the back side cooling case. Under the assumption that the design engineer attempts to minimize the necessary volume of a potentially expensive cooling fluid by minimizing the size of the receiver, the width of the receiver would likely be considerably larger than its internal height. Under such geometric conditions, heat transfer at the sides of the receiver becomes less significant. Calculating the HTCs inside the receiver can be simplified by omitting the slight heat transfer at the receiver's side walls. Thus, the receiver geometry was approximated by two parallel plates, with the CPV cell fixed to the bottom plate. See Figure 6.7 for an illustration. HTCs between two parallel plates, separated by a fluid in laminar flow, may be calculated by finding the appropriate Nusselt number and solving for h_{lam} . From Ref. [51], the Nusselt number may be calculated as:

$$Nu = \frac{h_{lam} d_h}{k} = \begin{cases} 7.541 & \text{fixed } T_{plate} \\ 8.235 & \text{fixed } q_1, q_2 \\ 5.385 & \text{fixed } q_1, q_2 = 0 \end{cases} \quad (6.1)$$

As heat is mainly absorbed from the CPV cell on the bottom side of the receiver, the assumption $q_1, q_2 = 0$ is selected, representing one constant heat flux plate and

6. THEORETICAL PERFORMANCE OF VARIOUS THERMAL INTERFACES

one adiabatic plate. Thus, a Nu of 5.385 is considered for all fluids. Considering the relative magnitude of heat fluxes between the top and bottom portions of the receiver, the assumption seems appropriate. Rearranging Eq. 6.1 the HTC may be calculated as:

$$h_{lam} = 5.385 \frac{k}{d_h} \quad (6.2)$$

With the hydraulic defined as: twice the distance “b” between two parallel plates, the analysis becomes independent of the width of the receiver design. Furthermore, if one assumes a practical minimum value for b, then the geometry for a direct immersion cooling CPV receiver utilizing laminar flow heat transfer is more or less fixed. Thus the associated heat transfer coefficients, and cooling capability by utilizing this method, are defined for the majority of geometric designs. Only fluid selection, fluid thermal conductivity, alters the heat transfer coefficients. Considering a minimum hydraulic diameter of $2b = 2 \times 10 \text{mm} = 20 \text{mm}$, the heat transfer coefficients for a fully developed hydrodynamic laminar flow across the backside of a CPV cell is estimated for the three candidate fluids using Eq. 6.1 and are provided in Table 6.2:

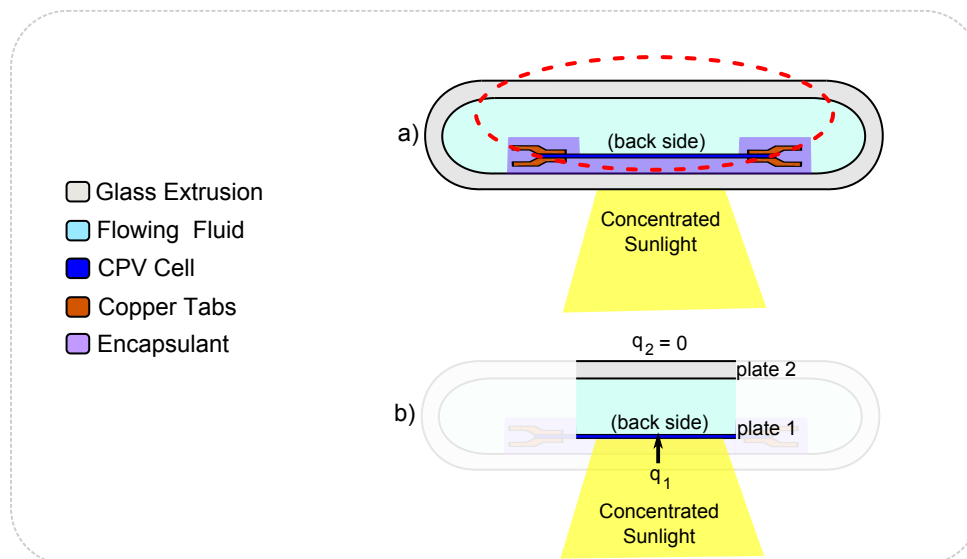


Figure 6.7: Two Plate Laminar Flow Model - Simplification of receiver body geometry from Figure 6.4 for laminar flow HTC calculations in Eq. 6.1 and 6.2.

Table 6.2: HTC Laminar - Heat transfer coefficients for candidate fluids, $Re = 2100$.

Fluid	Thermal Conductivity $[\frac{W}{mK}]$	h_{TIFE} $[\frac{W}{m^2K}]$
Distilled Water	0.58	156
Silicon-Oil	0.15	40
Hydrofluorocarbon Solvents	0.07	19

6.4 Direct immersion cooling in turbulent flow

It is desired to provide a general range of heat transfer coefficients for the cooling of CPV cells that are directly immersed in a cooling fluid in turbulent flow. To do so, numerous cooling fluids as well as geometries must be considered. The possible combinations are exceedingly large and the scope must be limited. As such, three hydraulic diameters: 10mm, 25mm, and 50mm were chosen to represent a range of possible linear CPV receiver designs. An optimization of CPV cell power output to fluid velocity was conducted using these three diameters. Furthermore, only geometric concentration ratios from 1 to 100 were considered.

It is advantageous to optimize the fluid velocity independent of the receiver and total installation length so as to generalize the heat transfer coefficients for the numerous receiver designs and installation sizes. This would be possible, as the pumping losses within the receiver and power output of the CPV cell scale linearly with the length; however, the increase in ΔT across the receiver complicates the matter. To keep the analysis independent of length, the optimum fluid velocity is determined considering a single CPV cell, here named “unit-cell.” In addition, a range of fluid velocities is calculated that produce a power output within 1% of the maximum power, so as to accommodate various system lengths. Further explanation, regarding system length, can be found in Figure 6.10 and in the coming paragraphs.

To determine an appropriate range of fluid velocities, Eq. 5.4 is modified based on the unit-cell concept, resulting in Eq. 6.3. The power output of the unit-cell is represented by P_{cell} and is calculated by subtracting any pumping losses (generated by frictional losses at the walls of receiver body’s coolant passage) from the electrical output of the

6. THEORETICAL PERFORMANCE OF VARIOUS THERMAL INTERFACES

unit-cell, the second and first terms of Eq. 6.3 respectively. Furthermore, the electrical efficiency of the cell, η_e , is calculated utilizing h_{trb_X} rather than h_{total} as shown in Eq. 6.5. Effectively, this removes the back cooler, h_{bc} , from the analysis and assumes that h_{trb_X} is solely responsible for heat transfer to the environment. Although this is a physically unrealistic condition, doing so allows the analysis to strictly focus on the decrease in $\Delta T_{cell-fluid}$ as compared to the increase in pumping losses for an increasing fluid velocity. Further explanation regarding Eq. 6.3-6.5 can be found in Appendix B.6.

$$P_{cell} = G_N X_g A_c \eta_o \eta_e - \frac{\Delta P_p Q_{fl}}{\eta_p} \quad (6.3)$$

$$= [G_N X_g A_c \eta_o \eta_e] - \frac{1}{\eta_p} \left[0.125 \pi \rho f L d_h u^3 \right]$$

$$f = \left[-2 \log_{10} \left(\frac{R_{rel}}{3.7} + \frac{5.74}{Re^{0.9}} \right) \right]^{-2} \quad (6.4)$$

$$\eta_e = \frac{\eta_{stc} G_N X_g \eta_o \gamma_t - \eta_{stc} h_{trb_X}}{\eta_{stc} G_N X_g \eta_o \gamma_t - h_{trb_X}} \quad (6.5)$$

For the fluid velocity optimization, a 40 by 50mm CPV cell, operating under parameters given in Table B.2 of Appendix B.2, is considered the unit-cell. Fluid dynamic properties are calculated at 25°C, but the temperature of the CPV cell and its associated η_e is allowed to change with respect to h_{trb_X} , as the fluid velocity is varied. Although η_e varies with flow rate, and although this would effectively change the heat load on the cell, the reduction in heat to the cell due to η_e was fixed at 10% to simplify the analysis. The heat transfer coefficient h_{trb_X} may be approximated by considering turbulent flow in a pipe, as described on page 150, Subsection 2.1.2 of Ref. [52]. This method is summarized in this thesis by Eq. 6.6-6.10, where an appropriate Nusselt number is found for a particular hydraulic diameter, d_h , and is subsequently used to solve for h_{trb_X} . The parameter C_L is a modifying term to account for entrance velocity. It may be approximated by a value of one, as assumed in this analysis, once pipe length significantly exceeds diameter ($L > 20d_h$, see Figure 1.3.5-8 of Ref. [52]).

$$h_{trb_X} = \frac{Nu \ k}{d_h} \quad (6.6)$$

$$Nu = \frac{\beta(Re - 1000)Pr}{1 + 12.7\beta^{0.5}(Pr^{0.667} - 1)} C_L \quad (6.7)$$

$$\beta = \frac{1}{(5.15 \log(Re) - 4.64)^2} \quad (6.8)$$

$$Re = \frac{u \ d_h}{\nu} \quad (6.9)$$

$$d_h = \frac{2(\text{width} \cdot \text{height})}{\text{width} + \text{height}} \quad (6.10)$$

Figure 6.8 gives an example of the unit-cell, fluid velocity, optimization for $X_g=40$. The three candidate fluids clearly exhibit a maximum power and optimum fluid velocity. In Figure 6.9, the optimum velocities and corresponding heat transfer coefficients (h_{trb_H2O}) for de-ionized water are plotted for $d_h=10, 25,$ and 50mm . The three curves cover an area that is highlighted in green and is labeled “maximum power.” Their corresponding heat transfer coefficients are given in the upper portion of the figure. The red and blue regions represent the lower and upper bound fluid velocities to maintain power output within 1% of its maximum value. These velocities are conveniently condensed into Table 6.3 and will be used in Section 6.7.

Figure 6.10 illustrates the need for establishing this range of fluid velocities. The figure gives the maximum length (L) of a series-connected cooling system for the three candidate fluids for a given geometric concentration ratio and maximum desired temperature difference (ΔT_L) across the CPV receivers (start of first to end of last). Starting with the concentration ratio in the upper left portion of the diagram, one moves rightward, across the diagram to the desired maximum temperature difference. From this temperature curve, one moves downwards to the lower left portion of the figure, intersecting the appropriate cooling fluid for the design in question. From here, one moves rightward, across the diagram and shifts across 8 constant velocity curves. At the desired fluid velocity, one traces downward to the x-axis to determine the allowed installation length. If this length is too small or too large, one may shift across the various velocity curves until one arrives at the desired length of CPV receivers.

6. THEORETICAL PERFORMANCE OF VARIOUS THERMAL INTERFACES

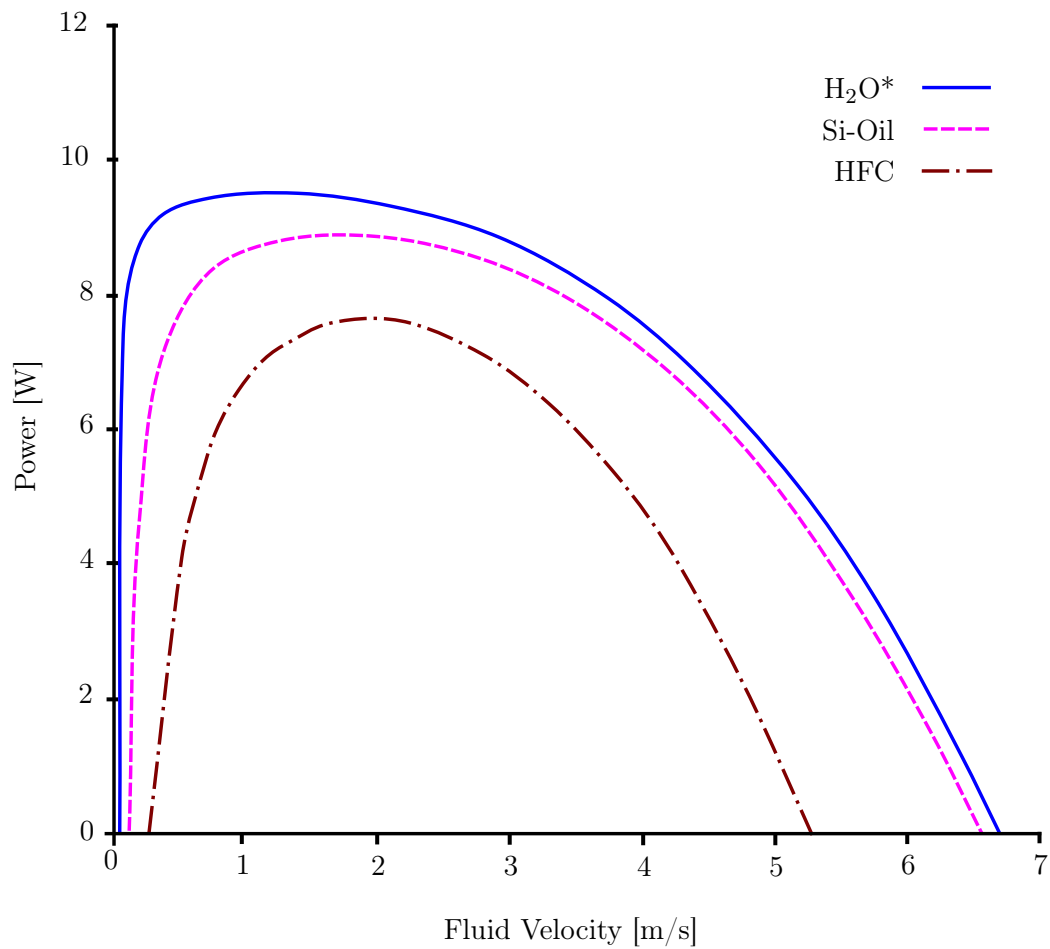


Figure 6.8: Optimum Fluid Velocity - Power output for the unit-cell concept under assumptions listed in Table B.2. A pipe diameter of 25 mm is considered.

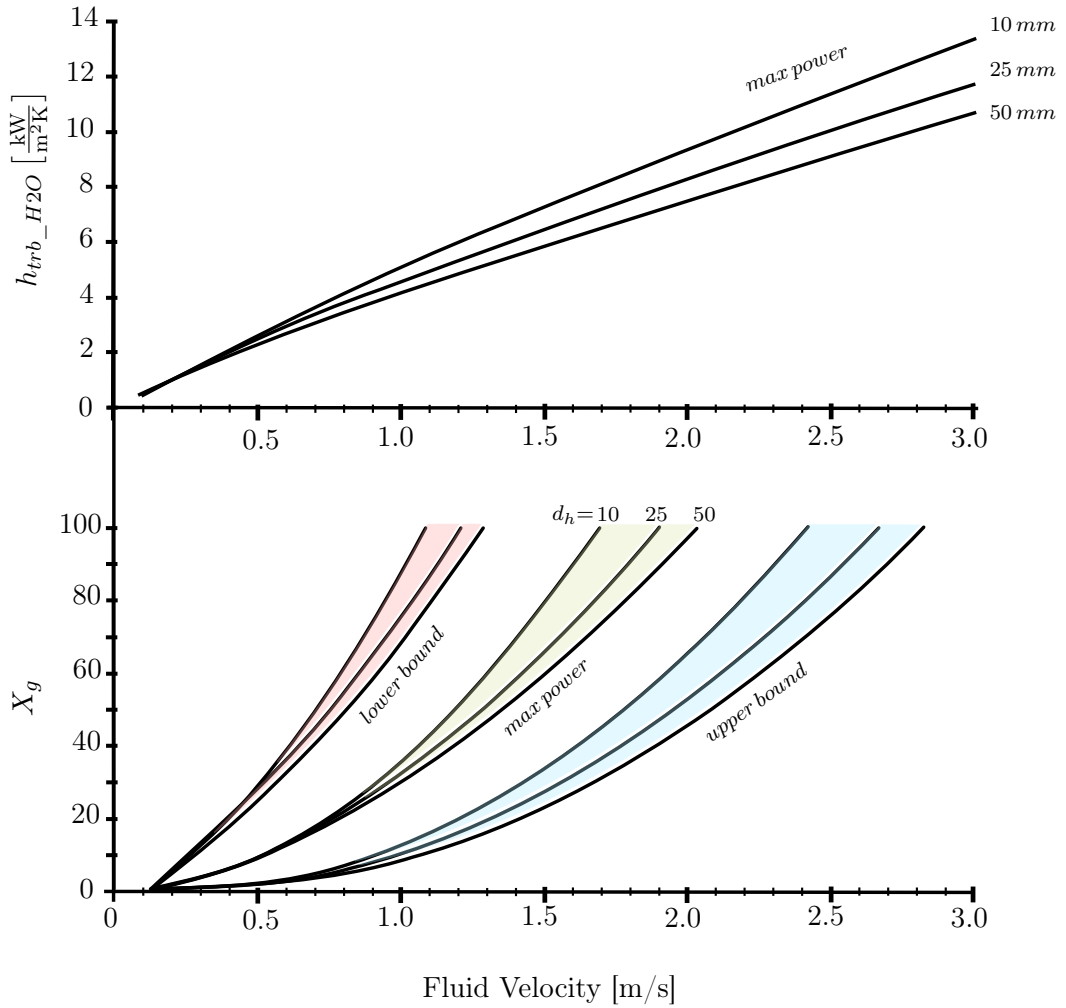


Figure 6.9: Optimum Fluid Velocity H₂O* - Optimum fluid velocities and HTCs for de-ionized water at three hydraulic diameters: 10, 25, and 50mm under assumptions listed in B.2.

6. THEORETICAL PERFORMANCE OF VARIOUS THERMAL INTERFACES

Table 6.3: Optimum Fluid Velocities and HTCs for H₂O* - Optimum fluid velocities and heat transfer coefficients for de-ionized water. Averaged values of three hydraulic diameters 10, 25, and 50mm.

X_g	Velocity [m/s]			h_{trb_H2O} [W/m ² K]		
	opt	low	high	opt	low	high
1	0.2	0.1	0.4	1,030	410	2,030
5	0.4	0.2	0.8	2,000	860	3,650
10	0.5	0.3	1.0	2,470	1,460	4,620
20	0.8	0.4	1.4	3,620	1,880	5,990
30	1.0	0.5	1.7	4,450	2,490	6,880
40	1.1	0.6	1.9	5,010	2,930	7,740
50	1.3	0.7	2.1	5,760	3,430	8,590
60	1.4	0.8	2.2	6,150	3,770	9,000
70	1.5	0.9	2.4	6,650	4,160	9,830
80	1.7	0.9	2.6	7,150	4,520	10,220
90	1.8	1.0	2.7	7,520	4,870	10,640
100	1.9	1.1	2.8	7,890	5,210	11,040

Figure 6.10 was produced using Eq. 6.11 (see derivation in Appendix B.8) and considers a hydraulic diameter of 25mm and $\eta_e = 10\%$. The remaining system level assumptions are laid out in Table B.2 of Appendix B.2.

$$L = \frac{\Delta T_L (\rho \pi d_h c) u}{4 G_N X_g \eta_o (1 - \eta_e)} \quad (6.11)$$

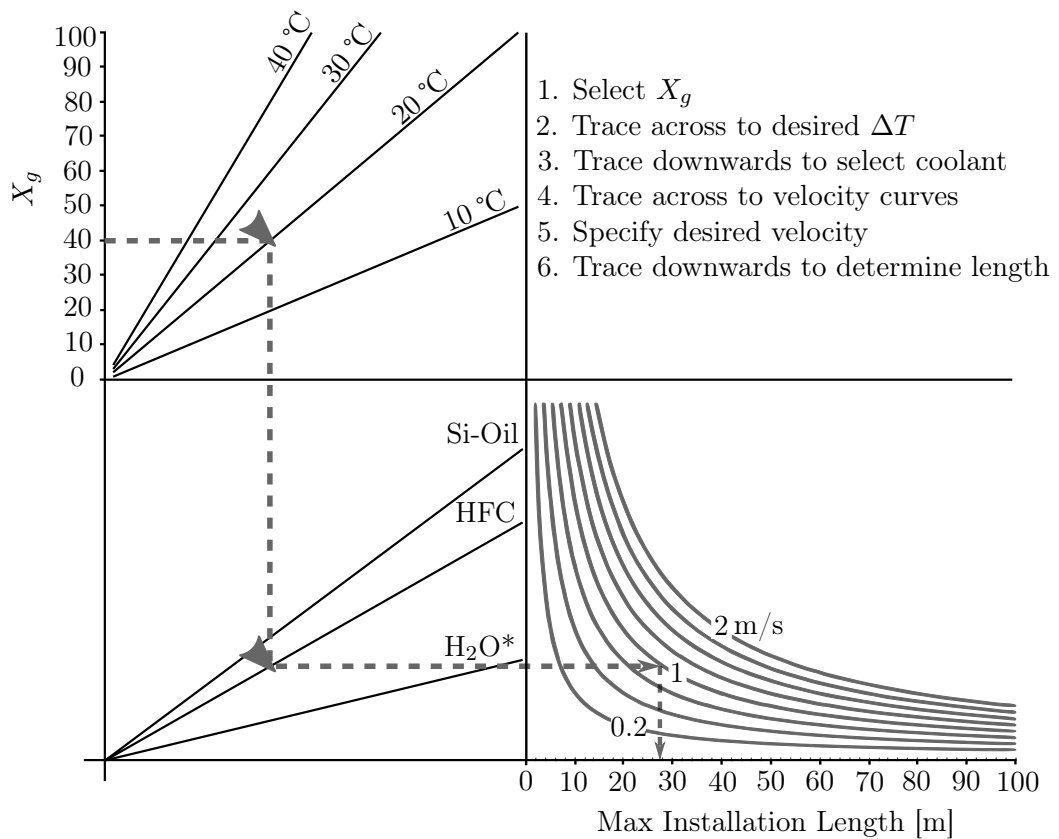


Figure 6.10: Maximum Installation Length of CPV Receivers - Maximum installation length of CPV receivers for a series connected cooling system for three candidate fluids. The figure considers a hydraulic diameter of 25mm and an additional reduction in the thermal input of 10%, to represent a minimum electrical operating efficiency of the system. The remaining system level assumptions are laid out in Table B.2 of Appendix B.2. For further information regarding the creation of this graph see Appendix B.8.

6. THEORETICAL PERFORMANCE OF VARIOUS THERMAL INTERFACES

6.5 Direct immersion cooling in pool boiling

This section provides estimates for the HTCs for both pool boiling on flat surfaces and condensation on pipes so as to provide the necessary HTCs to determine h_{TIFG} for Design-G in Figure 6.6(d). The calculation of heat transfer for pool boiling is especially difficult. The 2010 edition of the VDI Heat Atlas summarizes the scientific and engineering standing with regard to pool boiling and prediction thereof [53]:

Despite the large number of treatises that have appeared on the subject in the literature... no coherent theory yet exists that would allow heat transfer coefficients during nucleate boiling to be predicted from first principles to the accuracy required in engineering. Thus, in the light of the current state of the art, only empirical or semi empirical correlations can be applied in practice.

Nevertheless, the source provides heat transfer coefficients for over 50 fluids at a standard reference state: heat flux of 20 kW/m², reduced pressure of $p^* = 0.1$, and surface finish of $R_a = 0.4\mu\text{m}$. The heat transfer coefficients for the standard reference conditions, h_o , can be adapted for other conditions by the following formula [53]:

$$h_{pb} = h_o F_q F_{p^*} F_w \quad (6.12)$$

Essentially, h_o is modified by three terms, F_q , F_{p^*} , and F_w . The modification factors F_q and F_{p^*} accommodate deviations from the reference state for the applied heat flux and reduced pressure respectively. F_w represents the combined influence of the heated wall's material properties and surface roughness. An appropriate design pressure is unknown at this point in time and, in fact, would be specified by the would be designer. Thus, F_{p^*} is left at its reference condition for the pool boiling HTC calculations. With regard to F_w , it is the least well understood parameter of Eq. 6.12, and there is accordingly, "limited experimental evidence available at present"[53]. Lacking additional experimental evidence, it was thought to be unwise to deviate from the reference state. Thus, F_w was left at its reference state.

In Section 6.4, optimal fluid velocities and heat transfer coefficients were reported as a function of geometric concentration ratio. To continue with this methodology, the range of HTCs for pool boiling is also specified in terms of the geometric concentration

6.5 Direct immersion cooling in pool boiling

ratio. The incoming heat flux to the solar cell will vary with geometric concentration ratio, and as h_{pb} varies with incoming heat flux, the parameter F_q of Eq. 6.12 must be considered, as described by Eq. 6.13 and 6.14 [53].

$$F_q = (q/q_o)^n \quad (6.13)$$

$$n = 0.95 - 0.3(p^*)^{0.3} \quad (6.14)$$

From the uppermost diagram of Figure 11, located on page 766 of Ref. [53], a range of refrigerants, alcohols, and other fluids provide standard state HTC's between 3,000 and 6,000 W/m²K. These two standard state HTC's are selected as an upper and lower bound for the coolant survey. Using Eq. 6.12 - 6.14, these bounds were modified for increasing heat flux for geometric concentration ratios between 10 and 100. The resulting range of HTC's is illustrated in Figure 6.11 and is provided in a convenient table form in Table 6.4. In addition to this cooling survey, HTC's were calculated for the three candidate fluids and added to Figure 6.11. Methods outlined by Mostinski, Cooper, and Gorenflo were considered from Ref. [54], but ultimately methods by Mostinski were used. The method selected was based on the availability of various fluid and heat transfer properties for each fluid. The general lack of existence or reluctance of manufacturers to provide fluid and heat transfer properties of various HFC fluids, made the use of Mostinski's methods necessary, where fewer such parameters are required. His method is outlined below:

$$h_{pb} = 0.00417 q^{0.7} P_{cr}^{0.69} F_{pf} \quad (6.15)$$

$$F_{pf} = 1.8 (p^*)^{0.17} 4 (p^*)^{1.2} 10 (p^*)^{10} \quad (6.16)$$

In addition to the pool boiling calculations, it is necessary to provide an estimate for the condensing tubes contained in Design-G. As a simple approximation, the values in Table 6.4, are used for $h_{condensing}$. A quick look at Table 9-4 in Ref. [55] shows HTC's ranging from 680 to 24,000 W/m²K for seven heat transfer fluids. This falls just outside the range of HTC's used for pool boiling and by adapting the pool boiling HTC's in Table 6.4, a quick and conservative estimate for $h_{condensing}$ is found. With this assumption, it is now possible to calculate the total heat transfer coefficient for Design-G. This is carried out in Section 6.7.

6. THEORETICAL PERFORMANCE OF VARIOUS THERMAL INTERFACES

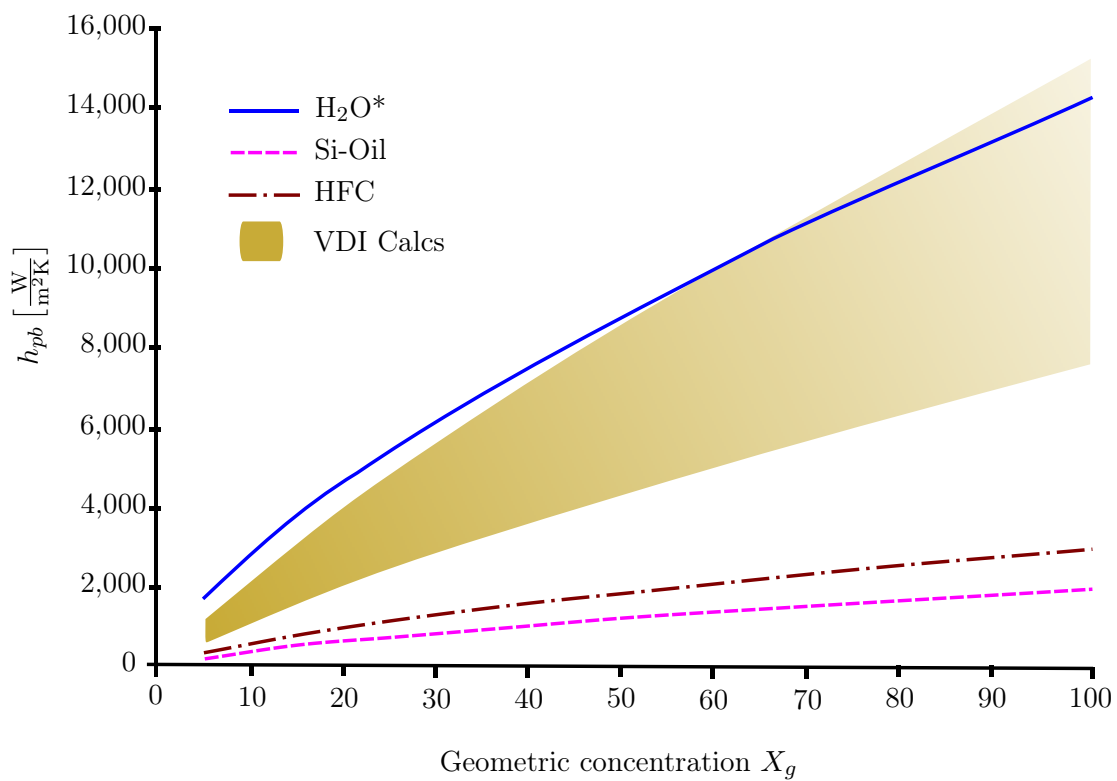


Figure 6.11: Pool Boiling Coolant Survey - HTC vs. X_g assuming parameters as laid out in Table B.2 of Appendix B.2 and including a 10% reduction to q , assumed for a minimum electrical output.

Table 6.4: Pool Boiling HTC

X_g	h_{low}	h_{high}
[-]	[W/m ² K]	
5	700	1,400
10	1,218	2,436
20	2,121	4,241
30	2,933	5,865
40	3,691	7,382
50	4,412	8,824
60	5,105	10,210
65	5,442	10,884
70	5,774	11,549
80	6,425	12,850
90	7,060	14,119
100	7,680	15,361

6.6 Thermally conducting materials

Thermally conductive materials can be sandwiched between the CPV cells and the receiver extrusion body to improve heat transfer. Materials with a high thermal conductivity are generally well suited for such applications. Such materials are typically applied in thin layers between the CPV cell and the extrusion and are commonly produced in the forms of tapes, glues, pastes, or greases. However, there are additional factors to take into consideration regarding the performance of such thermal interfaces.

Consider two materials forced together under pressure to form a simple thermal interface, as shown in Figure 6.12(a). At the microscopic level, there is relatively little contact between the two surfaces, indicated by the small red stars in the figure. This area can be as little as 1-2% of the total contact area between the two surfaces [56]. This provides relatively little area to transfer heat, as the remaining air gap is a poor heat transfer medium. An ideal thermal interface would fill this gap with a highly conductive material. In reality, such materials may not necessarily fill this gap entirely, as shown in Figure 6.12(b). The depth of penetration depends on the ability of thermal interface material (TIM) to wet the two bonding surfaces and depends on the pressure applied to the joint. Nevertheless, Figure 6.12(a) can be used to calculate a best performance

6. THEORETICAL PERFORMANCE OF VARIOUS THERMAL INTERFACES

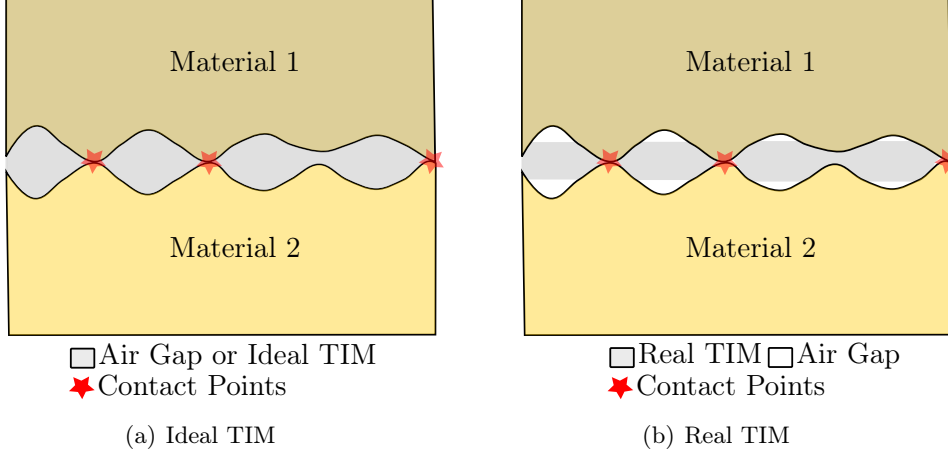


Figure 6.12: Two Material Interface - Thermal interface between two materials.

estimate of the thermal interface. The method utilized in Ref. [56], which calculates performance via a thermal resistance, will be used to estimate the performance of several candidate materials. Afterwards, these values will be converted into their appropriate HTCs for the sake of comparison with the other proposed interface designs.

$$R_{TIM} = \frac{BLT}{k_{TIM}} + R_{cTotal} \quad (6.17)$$

$$R_{cTotal} = \frac{R_{cTIM}R_{cs}}{R_{cTIM} + R_{cs}} \quad (6.18)$$

$$R_{cTIM} = \frac{1.53\sigma}{k_{TIM}} \left(\frac{H}{P} \right)^{0.097} \quad (6.19)$$

$$R_{cs} = \frac{0.8\sigma}{m k_h} \left(\frac{H}{P} \right)^{0.95} \quad (6.20)$$

The thermal resistance of the ideal case shown in Figure 6.12(a) may be calculated according to Ref. [56] by Eq. 6.17 - 6.20. R_{TIM} represents the total thermal resistance between materials 1 and 2 for an ideal interface. R_{TIM} is the sum of the bulk thermal resistance of the TIM and the total contact resistance, i.e. the first and second term in Eq. 6.17 respectively. BLT stands for bond line thickness. It is the assumed thickness of the TIM, and is represented by a gray band in Figure 6.12(b). The total contact

6.6 Thermally conducting materials

resistance, R_{cTotal} , is the sum of the contact resistance between the TIM and the two joint surfaces of the thermal interface and the contact resistance of the asperities between the two joint surfaces of the thermal interface, terms R_{cTIM} and R_{cs} respectively. The term H represents the microhardness of the weaker of the two materials, and P is the pressure between the materials. The root mean square roughness for materials 1 and 2 is given by $\sigma = (\sigma_1^2 + \sigma_2^2)^{0.5}$ and the mean asperity slope is $m = (m_1^2 + m_2^2)^{0.5}$. The term k_h is the harmonic mean thermal conductivity and is calculated by $k_h = 2k_1k_2/(k_1+k_2)$.

To provide a general overview of the heat transfer capabilities of thermally conductive materials, for use in thermally interfacing the CPV cells to the receiver body, over 100 materials were investigated. The theoretical thermal resistance of 50 of these materials were calculated according to Eq. 6.17 - 6.20. The various materials and associated designs may be summarized by the following categories:

- Thermally conducting, electrically isolating tapes
- Thermally conducting, electrically isolating gel-pads
- Thermally conducting, electrically isolating adhesives (glues)
- Thermally conducting, electrically conducting adhesives (glues)

For the last category, application of the electrically conductive adhesive requires additional care, so as to avoid any short-circuiting of the solar cells. A special application pattern is required such that each solar cell acts as a sort of island, i.e. the TIM from one cell does not connect between adjacent cells. In addition, an isolating oxidation coating is required on the receiver body.

A selection of TIMs, representative of the 50 calculated samples, is summarized in Table 6.5. Various properties are listed for each material. Calculations for the thermal resistance and associated heat transfer coefficient for each of these materials is given in Table 6.6. For these calculations, the following properties were adapted from Ref. [56] and are collected in Table 6.7. The calculations in Table 6.6 are further summarized in Table 6.8, so as to provide a range of HTC's that are to be used in Section 6.7 for h_{TIFA} , h_{TIFB} , h_{TIFC} , and h_{TIFD} . To conclude, the survey of highly conductive TIM estimates best performances between 2,900 and 13,100 W/m²K for most of the isolating materials and between 8,400 and 75,900 W/m²K for electrically conducting materials.

6. THEORETICAL PERFORMANCE OF VARIOUS THERMAL INTERFACES

Table 6.5: Selection of TIMs - Chm = Chomerics, AIT = AIT, B = Bergquist, Mb = Masterbond, Ao = Aremco, LocT = Loctite, DC = Dow Corning

Company	Chm	AIT	B	Mb	AIT	Ao	LocT	DC
Product	T-404	CB7208-A	Sil-Pad 2000	EP 36AN	ME 7159	556	QMI 5030	TC 5600
Type	tape	tape	pad	glue	glue	glue	glue	grease
Isolating	yes	yes	yes	yes	yes	no	no	yes
$k \left[\frac{W}{m K} \right]$	0.4	3.6	3.5	3.6	11.4	2.2	25	7.1
Thick[mm]	0.127	0.152	0.254	0.254	0.254	0.254	0.254	0.254

Table 6.6: R_{TIM} and h_{TIM} for a Selection of TIMs - Calculations for the thermal resistance and heat transfer coefficients corresponding to the TIM in Table 6.5 ($P=10$ psi).

Units	[°C cm ² /W]						[W/m ² K]
Product	R_{AlOx}	R_{cs}	R_{cTIM}	R_{cTotal}	BLT/k_{TIM}	R_{TIM}	h_{con}
T-404	-	8.38	0.30	0.290	3.18	3.46	2,900
CB7208-A	-	8.38	0.033	0.033	0.42	0.46	22,000
Sil-Pad 2000	-	8.38	0.040	0.040	0.73	0.77	13,100
EP36AN	-	8.38	0.033	0.033	0.71	0.74	13,500
ME7159	-	8.38	0.011	0.010	0.22	0.23	42,900
556 Series	0.0254	8.38	0.008	0.008	1.16	1.19	8,400
QMI 5030	0.0254	8.38	0.005	0.005	0.10	0.13	75,900
TC-5600	0.0254	8.38	0.017	0.017	0.36	0.40	25,000

Table 6.7: Parameters Used to Calculate Table 6.6 - k evaluated at approximately 300K. ¹Assumed values. ² m calculated using $m = 0.076(\sigma)^{0.5}$ as recommended in [56].

Name	Material 1 Aluminum	Material 2 Silicon	Units	Respective Sources
k	209	148	$\frac{W}{m K}$	[57],[58]
H	686.5	5100	MPa	[57],[59]
σ	3.2	0.1	μm	note 1
m	0.136	0.024	-	note 2

Table 6.8: Summary of Conducting TIM - A summary of Table 6.6 providing a range of thermal resistances and heat transfer coefficient for each TIM category.

Summary	R_{TIM} [°C cm ² /W]	h_{con} [W/m ² K]
Thermal Tapes (isolating)	0.46 - 3.46	2,900 - 22,000
Thermal Pads (isolating)	0.77 - 1.74	5,700 - 13,100
Thermal Adhesives	0.23 - 0.74	13,500 - 42,900
Therm-elec Adhesives	0.13 - 1.19	8,400 - 75,900

6.7 Comparison of interfaces

The simplified models in Figure 6.6 and their respective descriptions of h_{TIF} in Table 6.1, only provide a general description of the heat transfer coefficients in each design. This ambiguity was deliberate, as it was necessary to outline several concepts and calculate various heat transfer coefficients before providing an exact solution for each h_{TIF} . At this point, the HTC's associated with the various thermal interfaces for Designs A-G have been defined and calculated and will be assembled here.

Design-A: $h_{TIFA} = h_{con}$

A value of $h_{con} = 10,000$ W/m²K is adapted from Table 6.8 of Section 6.6 as an approximate, representative, mean value, for electrically isolating thermal tapes.

Design-B: $h_{TIFB} = h_{con}$

A value of $h_{con} = 50,000$ W/m²K is adapted from Table 6.8 of Section 6.6 as an approximate, representative, mean value, for electrically conducting thermal adhesives. This value also includes an aluminum oxide coating for the receiver extrusion.

Design-C: $h_{TIFC} = h_{con} + h_{ext_wall} + h_{trb_H2O}(X_g)$

A value of $h_{con} = 10,000$ W/m²K is adapted from Table 6.8 of Section 6.6 as an approximate, representative, mean value, for electrically isolating thermal tapes. $h_{ext_wall} = 59,250$ W/m²K, considering a 4mm thick extrusion wall of aluminum with an assumed thermal conductivity of $237 \frac{W}{mK}$. The values for $h_{trb_H2O}(X_g)$ are taken from Table 6.3 of Section 6.4.

6. THEORETICAL PERFORMANCE OF VARIOUS THERMAL INTERFACES

Design-D: $h_{TIF_D} = h_{con} + h_{ext_wall} + h_{trb_H2O}(X_g)$

Same HTCs as Design-C except that a value of $h_{con} = 50,000 \text{ W/m}^2\text{K}$ is adapted from Table 6.8 of Section 6.6 as an approximate, representative, mean value, for electrically conducting thermal adhesives. This value also includes an aluminum oxide coating for the receiver extrusion.

Design-E: $h_{TIF_E} = h_{lam_X}$

The heat transfer coefficient h_{lam_X} may be found in Table 6.2 of Section 6.3 for each respective fluid denoted by “_X.”

Design-F: $h_{TIF_F} = h_{trb_X}(X_g)$

The method for calculating the heat transfer coefficient $h_{trb_X}(X_g)$ may be found in Section 6.4. Values of $h_{trb_H2O}(X_g)$ can be found in Table 6.3 of this same section. The values in the column labeled “optimum” are used. Values of $h_{trb_X}(X_g)$ for the other two candidate fluids, although calculated for the sake of comparison, were omitted from any listing in this text.

Design-G: $h_{TIF_G} = h_{pb} + h_{condense} + h_{pipe_wall} + h_{trb_H2O}(X_g)$

The range of values for h_{pb} can be found in Table 6.4 of Section 6.5. These same values are also used as an approximation of $h_{condense}$, as explained in Section 6.5. The parameter h_{pipe_wall} , where $h_{pipe_wall} = 267,000 \text{ W/m}^2\text{K}$, represents the heat conduction through the condenser pipe. The condenser pipe is made of copper with an assumed 1.5mm thickness and thermal conductivity of $401 \frac{\text{W}}{\text{m K}}$. The values for $h_{trb_H2O}(X_g)$ are taken from Table 6.3 of Section 6.4.

The performance of each design, and their associated thermal interfaces, will be compared utilizing the parameter h_{bc} (introduced in Section 5.6) as follows. Utilizing Eq. 5.4, the theoretical power output of a hypothetical CPV receiver is calculated under the assumption that h_{total} from Eq. 5.6 is equal to h_{bc} , with values of h_{bc} for each X_g provided in Table 5.6. This results in a series of calculated power outputs for a given h_{bc} and its corresponding geometric concentration factor X_g . Now, for each design, the total heat transfer coefficient from the CPV cell to the back cooler will be added to h_{bc} , resulting in a new h_{total} , denoted h_{total}^* :

$$h_{total}^* = \frac{1}{\frac{1}{h_{bc}} + \frac{1}{h_{TIF}}} \quad (6.21)$$

Here, h_{TIF} represents the total heat transfer coefficient from the CPV cell to the back cooler for Designs A-G as previously outlined. The addition of h_{TIF} will increase the operating temperature of the CPV cells. In doing so, there is an associated decrease in power output. The decrease in power output vs. geometric concentration ratio for each design is shown in Figure 6.13, illustrating the relative performance of the various designs.

Several interesting conclusions may be drawn from Figure 6.13. If one were to rank the overall performance of each design, then Designs A and B, CPV cells directly interfaced with a heat sink (passive cooling), demonstrate the best theoretical performance. For actively cooled systems, the state of the art technology, ANU's CHAPS (represented by Design-C), sits somewhere in the middle of this ranking. As initially believed, there are meaningful performance improvements by considering electrically conducting materials, which typically have a higher thermal conductivity than their electrically isolating counterparts. These improvements are clearly illustrated by comparing Designs A and B, for passively cooled systems, and Designs C and D, for actively cooled systems. However, please note that introducing electrical conducting thermal materials will require design changes to the CPV receiver. Namely, an additional isolation coating and special application of the thermal adhesive become necessary (as discussed in Section 3.8.4).

Designs C, D, and F(H₂O*) all utilize forced convection cooling, de-ionized water in turbulent flow, to transfer heat away from the CPV cells. Design-F(H₂O*) benefits from one less thermal interface, as the CPV cells are directly immersed in the cooling fluid. It should thus come as no surprise that it outperforms Designs C and D. Interestingly enough however, Design-D comes very close to the same performance as Design-F(H₂O*). This can be attributed to the relatively high thermal conductivities of the thermal adhesives considered in Design-D. Furthermore, improvements available in moving from Design-D to Design-F(H₂O*) are much smaller than those between C and D. Otherwise stated, larger relative improvements in power output for actively cooled receivers are predicted for continued research on higher performing thermal materials rather than moving to a new technology altogether (direct immersion cooling using de-ionized water).

If one does consider direct immersion cooling of CPV cells via forced convection, then it is important to realize that this design is only practical in the turbulent flow regime. Heat transfer via forced convection is a mass transfer process and is therefor

6. THEORETICAL PERFORMANCE OF VARIOUS THERMAL INTERFACES

highly dependent on fluid velocity. The fluid velocities associated with fully developed laminar flow are simply too low to adequately remove heat from the CPV cells. Even at geometric concentration ratios as low as $X_g=5$, losses are over 15% for de-ionized water in laminar flow, as Design-E(H_2O^*) shows in Figure 6.13. Si-Oil and HFC fluids in laminar flow were omitted from the figure for the sake of clarity. For reference, their losses are significantly higher, as calculated cell temperatures exceed $200^\circ C$ for $X_g=5$.

For turbulent flow (Design-F), it was already mentioned that de-ionized water offers some performance improvements with regard to heat transfer. Si-Oil and HFC were included in Figure 6.13, but the performances of these two fluids are significantly worse than de-ionized water. This may be attributed to the much lower thermal conductivity of both fluids with respect to water. The higher density of HFC fluids increases pumping losses, thus lowering its performance with respect to Si-Oil.

The last remaining direct immersion cooling design, Design-G, utilizes pool boiling. Although the heat transfer coefficients for boiling are large and outperform many of the other TIFs, Design-G nevertheless contains the greatest number of TIFs. Altogether, each TIF and its associated HTC, reduce the overall heat transfer coefficient, so much so, that the design is surprisingly outperformed by the state-of-the-art active cooling design (Design-C). There are several practical considerations for realizing Design-G, which will be covered in greater detail in Chapter 7.

The above observations more or less support the first design guideline from Section 5.5, i.e. reduce the total number of thermal interfaces. This guideline is perhaps best demonstrated when comparing designs that directly interface CPV cells to a heat sink (A and B) with designs utilizing a flowing coolant channel (C and D), with the first pair having fewer thermal interfaces than the latter pair. However, it is perhaps surprising that Designs A and B should outperform the direct immersion cooling for de-ionized water (Design-F(H_2O^*)) as all three contain more or less only one major thermal interface, and considering that HTCs for water in forced convection can be very large. This is one of the most interesting results of the study and was yielded by the efforts made in Section 6.4, where optimal fluid velocities and associated pumping losses were taken into consideration. If pumping losses are ignored, then the performance of Design-F approaches Design-A for fluid velocities (assuming H_2O^*) above 2 and 3 m/s for hydraulic diameters between 10 and 50mm respectively. This may be verified by examining the heat transfer coefficients in Figure 6.9, and selecting a fluid velocity which yields a HTC

greater 10,000 W/m²K (assumed value of the thermal interface in Design-A). Meeting the performance of Design-B (50,000 W/m²K) may prove difficult, as these theoretically calculated values are extremely high. Experiments are necessary to determine whether or not such values could be practically realized for both Design-F and Design-B.

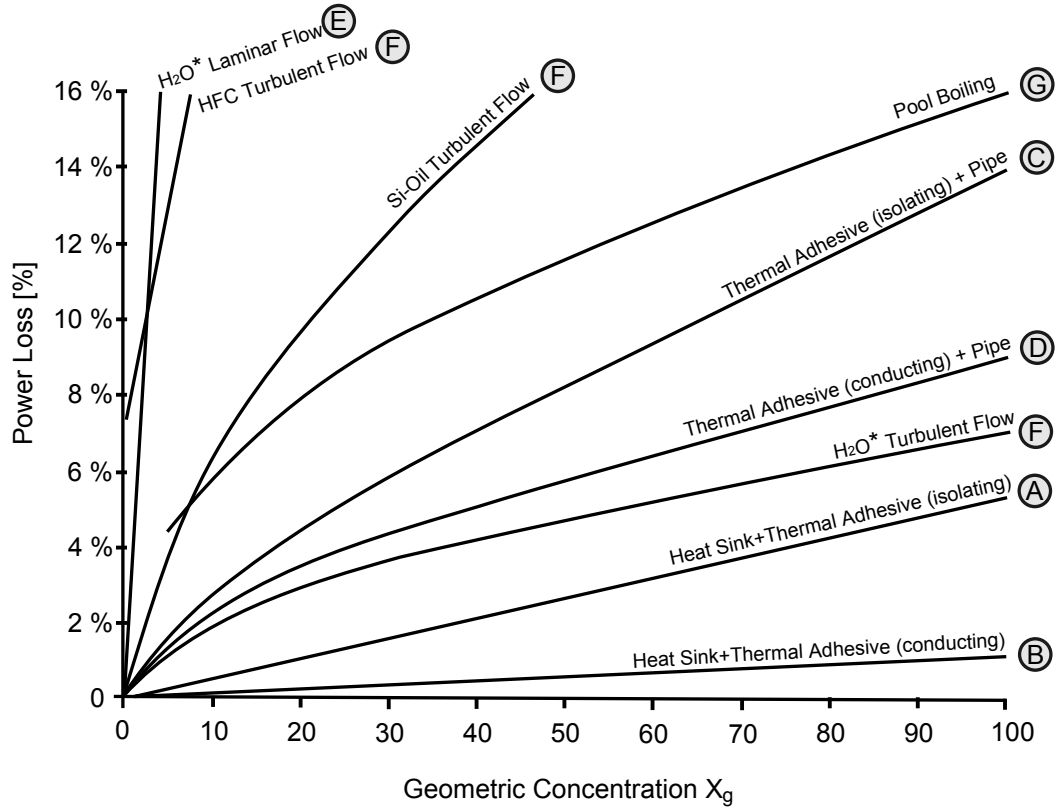


Figure 6.13: Power Losses vs. X_g - Percent induced power loss vs. geometric concentration ratio for the additional thermal interfaces associated with Designs A-G. Power loss = $[p(h_{total}) - p(h_{total}^*)]/p(h_{total}) * 100$. Chart assumes parameters as laid out in Table B.2 of Appendix B.2 and includes a 10% reduction to q , assumed for a minimum electrical output.

6.8 Summary of thermal interfaces

In the previous section, Figure 6.13, and the discussion that followed, provided a general ranking of TIF designs. However, only the thermal effects on power output were considered. In this section, a final recommendation is proposed, taking into consideration additional factors which affect both the performance and practical realization of the

6. THEORETICAL PERFORMANCE OF VARIOUS THERMAL INTERFACES

various designs. For instance, not every design can realize the full range of concentration ratios presented in Section 6.7. For linear-focus trough systems, there are practical limits with respect to passive cooling. Additionally, there are some material limits to consider.

Considering the thermal performance of Designs A-G, and their subsequent and respective effects on power output, the following final ranking is given in Figure 6.14. It is recommended that linear-focus trough CPV systems utilize passive cooling elements, Designs A and B, for concentration ratios below the passive/active transition point ($X_g=40$). Above this point, it is recommended to utilize a coolant channel in the receiver body, flowing a coolant in turbulent flow, and interfacing the CPV cells to the receiver body via thermal adhesives, Designs C and D. Designs A-D may all benefit from the utilization of electrically conductive thermal adhesives, typically yielding higher thermal conductivities and thus better HTCs, but some changes to the receiver design become necessary (see Section 3.8.4). Namely, both a special isolating coating and application of the thermal adhesive. Although the direct immersion cooling of CPV cells via de-ionized water, Design-F, theoretically outperforms Designs C and D, more research is needed before this design can be recommended over Designs C and D. However, this thesis has helped define the possible improvements in power output, via improved heat transfer, for such a design and may serve as a possible support for motivating future work on Design-F. In addition, Design-F may become necessary when exceeding the capability of existing thermal material technologies, perhaps near $X_g=80$. Pool boiling, Design-G, may also serve as a solution beyond $X_g=80$, however, its predicted performance is worse than that of Design-F. This is due in part to the large number of thermal interfaces contained in Design-G. Design-E, laminar flow, and also Design-F using Si-Oil or HFC are not recommended, based on their considerably higher losses, as evident in Figures 6.13 and 6.14.

In addition, it is also worth considering that only the single side cooling cases were calculated. In principle, the heat transfer coefficients at the cell to liquid interface may approximately double, considering that twice the surface area is available for heat transfer. Again, this could also affect the final ranking, but the spectral transmission of the fluid must be considered. Further optical losses may exceed any potential benefit. Although the absorption of frequencies outside the use of the CPV cell, would avoid “non-usable” light from reaching and potentially heating the cell, it must be remembered

that the fluid will absorb this energy and a portion of it will transfer to the cell in the form of heat. Again, the potential benefit may be eliminated.

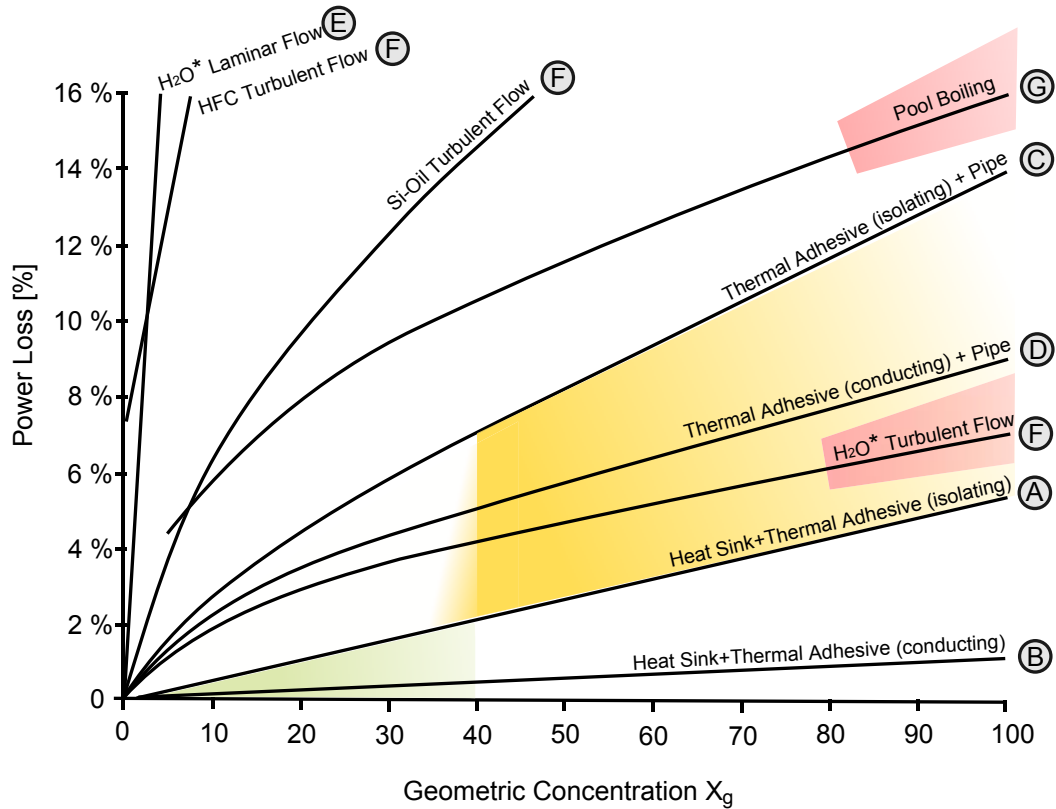


Figure 6.14: Thermal Interface Technology Roadmap - Final recommendations for cooling strategies overlaid with corresponding power loss data from Figure 6.13.

It is important to note that the cooling strategies implemented for Designs E, F, and G only consider the heat transfer aspects of the fluid. These same fluids exhibit other effects on solar cells in operation, some beneficial and some detrimental. For example, the differing cooling strategies of Designs A-G change the optical interface between the cell and concentrating optics, therefore affecting both optical efficiency and power output. There are also so called “fluid-effects,” for example, polar fluids exhibiting a positive influence on solar cell performance [60]. The magnitude of these optical and fluid effects may be larger than the predicted improvements in thermal performance. For example, Figure 6.14 communicates that the absolute performance improvement between each design is typically on the order of a few percent and perhaps upwards of 12% at its extreme (Designs B and G). Comparatively speaking, the optical per-

6. THEORETICAL PERFORMANCE OF VARIOUS THERMAL INTERFACES

formance, as to be discussed in Section 7.4, may vary by several percent between the various receiver designs. The magnitude of the so called fluid-effects, for example polar fluids, may be even higher. Both in spite of and in part due to the lack of available information on fluid-effects and given the magnitudes of the expected thermal performance improvements between Designs A-G, it recommended that the liquid immersion of solar cells be considered and investigated from the point of view of the fluid-effects. Simply stated, the effects of improved thermal design may be outweighed by changes in optical interfaces or by the fluid-effects. As much less is understood about these fluid-effects, they should be the primary reason, assuming they exhibit positive cost or performance improvements, for moving to such a design.

6.9 Economically sensible operating parameters

Before closing this chapter, special attention is given to the passive/active transition point, as the TU-Wien prototype CPV receiver operates very close to this point. It is intended here to illustrate that the actively cooled designs may still yield an economic optimal solution, as their use may be required as one surpasses the passive/active transition point. To illustrate their economic feasibility, one must understand that the additional power loss associated with h_{TIF} may be mitigated by increasing the size of the back cooler over the original h_{bc} . Recall from Section 5.6 that the method for determining the optimal cooler size (h_{bc}) was purely performance based. If the economic cost of increasing the back cooler size is outweighed by an improvement in its electrical performance, then an active cooling design may still indeed be an economically viable option. This relationship may be mathematically described by examining the marginal increase in performance (MP) and marginal increase in total system cost (MTSC), as described in Eq. 6.22 and 6.23 respectively (see derivation in Appendix B.9).

$$MP = \frac{\eta_e(n+1) - \eta_e(n)}{\eta_e(n)} = \left[\frac{1 - \Delta T_o(1-r)^{(n+1)}\gamma_t}{1 - \Delta T_o(1-r)^{(n)}\gamma_t} \right] - 1 \quad (6.22)$$

6.9 Economically sensible operating parameters

$$MTSC = \frac{TSC(n+1) - TSC(n)}{TSC(n)} = \left[\frac{E_o + C_o(1+r)^{(n+1)}}{E_o + C_o(1+r)^{(n)}} \right] - 1 \quad (6.23)$$

$$= \left[\frac{1 + \frac{C_r}{1-C_r}(1+r)^{(n+1)}}{1 + \frac{C_r}{1-C_r}(1+r)^{(n)}} \right] - 1 \quad (6.24)$$

Both equations examine the change in total system performance and total system cost by considering subsequent 1% increases in the size of the back cooler (h_{bc}), represented by a rate of increase “ r .” For the sake of simplicity, it is assumed that the cost of the back cooler scales linearly with an increase in h_{bc} , which implies that the ΔT between the CPV cells and the operating environment also scales linearly with cost. Although this assumption is somewhat inaccurate, it has the overwhelming benefit that the same rate “ r ” used to determine improvements in performance may also be used for calculating increases in total system cost. Thus “ r ” is shared between Eq. 6.22 and 6.23. The parameter ΔT_o is the initial ΔT above 25°C for the CPV cells, as derived from the optimal h_{bc} (see Table 5.6 for h_{bc}). Considering the same performance parameters assumed in Table 5.6, ΔT_o is approximately equal to 120°C. This initial ΔT is important, as it defines the ratio between increases in h_{bc} and improvements in the operating temperature of the CPV cells. The total system cost consists of two parameters, “ C_o ” and “ E_o ,” representing the initial cost of the back cooler and the remaining components (everything else) respectively. The cost of the back cooler is increased by 1% for each successive computation of “ n ,” while E_o remains constant. To further generalize Eq. 6.23, “ C_o ” and “ E_o ” are replaced with the parameter C_r , where $C_r = C_o/(C_o + E_o)$, representing the initial cost of the back cooler as a fraction of total system cost.

Using Eq. 6.22 and 6.24, Figure 6.15 was produced. The figure contains a marginal improvement in performance curve, labeled thus and given by Eq. 6.22. There are also three marginal total system cost curves, calculated using Eq. 6.24, with values of $C_r = 5\%$, 10% , and 20% of total system cost (TSC). The three curves are provided as it is unknown whether a back cooler yielding a HTC equal to h_{bc} (operating at 120°C above STC), would represent 5, 10, or 20% of TSC. However, given that the systems described in Chapter 2 operated below 100°C and considering that the cooling costs made up approximately 10% of the total system cost, it is assumed here in this analysis that a

6. THEORETICAL PERFORMANCE OF VARIOUS THERMAL INTERFACES

value of $C_r= 10\%$ TSC is an appropriate starting point for establishing recommended cooler size and operating parameters. This analysis aims to justify an increase in cooler size over the theoretical optimum size (h_{bc}), as the resulting cell temperatures are much higher than those seen in the systems outlined in Chapter 2. In addition, a number of the materials within the receiver design (encapsulant and TIMs) are unable to handle such high temperatures over prolonged periods of time.

What is important to take away from Figure 6.15, are the intersections between the marginal improvement curve and each of the three TSC curves. These intersections, and the corresponding percentages along the x-axis, indicate the point at which further increases in cooler size (h_{bc}) and its accompanying performance improvement would be outweighed by increases in the total system cost. These points are indicated by red dots in the figure. Two important conclusions can be made here. First, recall in Section 5.6 that the method for determining the optimal cooler size (h_{bc}) was purely performance based. Mention was made that it may not necessarily be the optimum economical size. With the assumption that h_{bc} initially represents 10% of the total system cost, Figure 6.15 shows that further increases of h_{bc} , between 100 and 250%, may in fact improve system performance. Thus, an additional increase of 100 to 250% of the values listed in Table 5.6 may yield an economically optimum solution for a CPV system. Second, the figure identifies a suggested range of operating temperatures for the CPV cells, namely between 59 and 87°C. For ease of convention, a temperature range of 60 to 90°C is recommended.

At this point, a suggested range of back cooler sizes and operating temperatures have been derived, based on an assumed $C_r= 10\%$ TSC. In addition to these values, it is helpful to understand the final %TSC of the cooling system at the economical optimum points, as identified in Figure 6.15. This information is contained in Figure 6.16, where the cooler cost as a percent of TSC is plotted against increasing cooler size with respect to h_{bc} . The same initial %TSC curves (C_r) from Figure 6.15 are adopted here and the optimum operating points are again highlighted in red. From Figure 6.16, an appropriate range of final cooler costs, as measured in %TSC, can be determined. Using the 10% TSC curve as previously assumed, the economically sensible cost of the back cooler is anywhere between 10 and a maximum of 25% of the total system cost.

In Section 4.3, the two cooling transition points, $X_g= 40$ and 80, were established. In this section, the technologies necessary to achieve these higher concentration ratios

6.9 Economically sensible operating parameters

were outlined in the technology road map Figure 6.14. In addition, it was established that increases in the back cooler (h_{bc}) ranging from 100 to 250% may still allow for economically viable solutions. If the actively cooled designs are to have any chance of economic viability, then their necessary increase in h_{bc} to overcome their respective h_{TIF} must fall within or below this range. Thus, Designs A-G were examined at the two transition points. Their respective increases in h_{bc} for $X_g=40$ and 80 are shown in Figure 6.17. It should be immediately apparent that the necessary increases to h_{bc} fall below this range. Thus, in the case where passive cooling is no longer possible, a transition to active cooling may still yield an economically viable system. If necessary, a transition to the next generation designs is also economically feasible.

6. THEORETICAL PERFORMANCE OF VARIOUS THERMAL INTERFACES

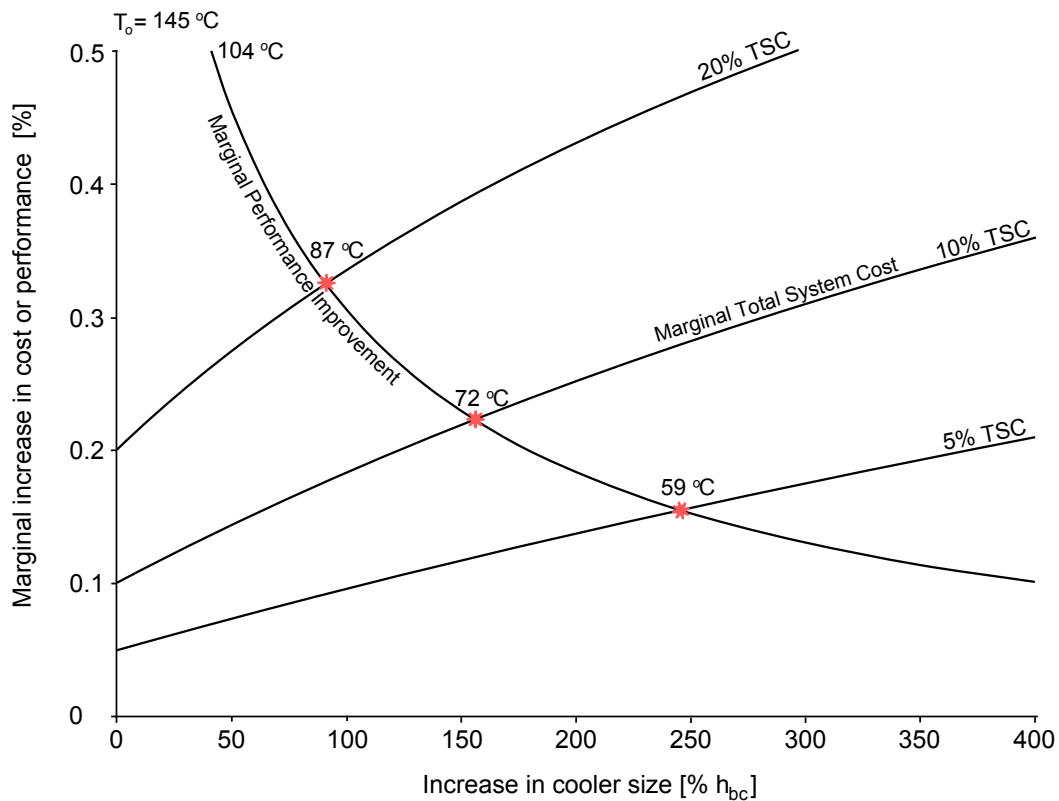


Figure 6.15: Increasing the Back Cooler - Comparison of the marginal increase in total system performance and corresponding marginal increase in total system cost (TSC) for an increase in the size of the back cooler. The curves TSC 5%, 10%, and 20% represent an initial back cooler cost of 5%, 10%, and 20% of the total system cost respectively. For this analysis, a cell temperature coefficient of $\gamma_t = 0.004^\circ\text{C}^{-1}$ is assumed. Key intersections of marginal performance improvement and marginal total system cost curves are labeled in red with corresponding average cell temperatures. These values serve as references for Figure 6.16, where the relationship between the increase in cooler size and cooler size as a function of percent total system cost is illustrated.

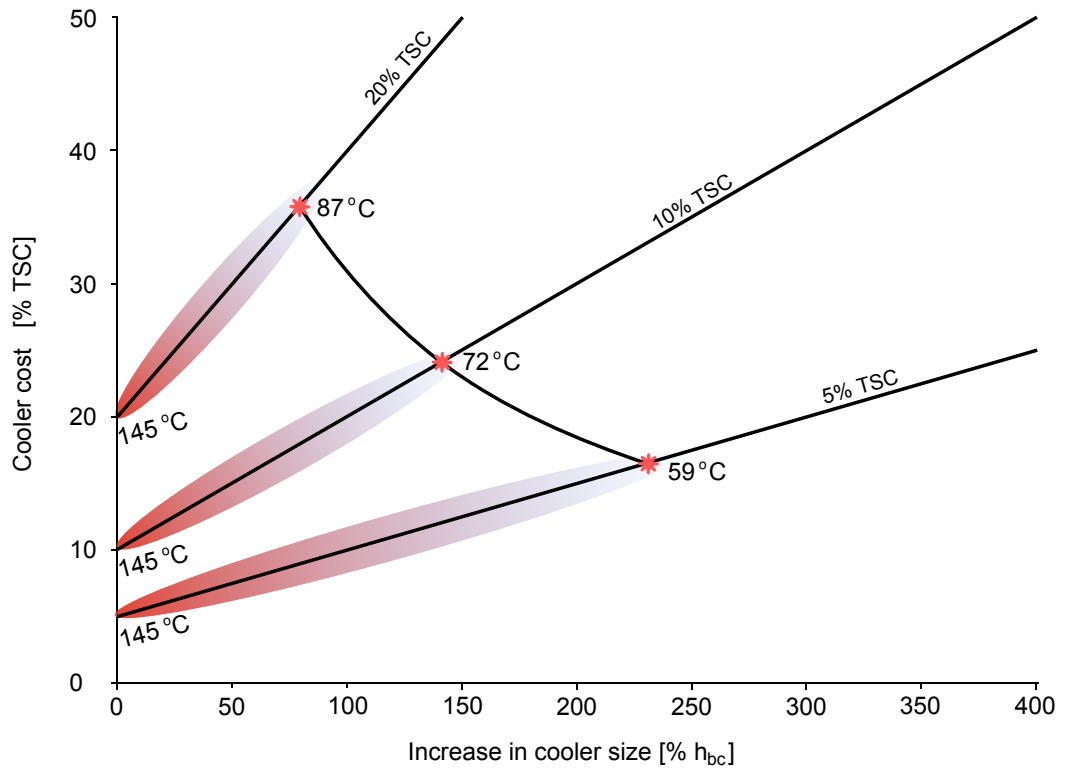


Figure 6.16: Back Cooler as %TSC - Examination of the maximum allowed cost of the back cooler as a percentage of total system cost (TSC) with respect to an initial TSC of 5%, 10%, and 20%. The figure is derived from the same analysis used in 6.15. Points highlighted in red, representing the optimal increase in cooler size from Figure 6.15, provide the optimal values of the back cooler cost in terms of its percentage of total system cost. Temperatures represent the average cell temperature.

6. THEORETICAL PERFORMANCE OF VARIOUS THERMAL INTERFACES

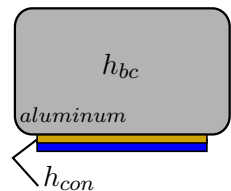
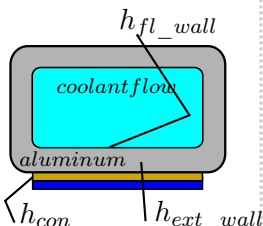
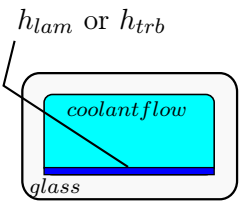
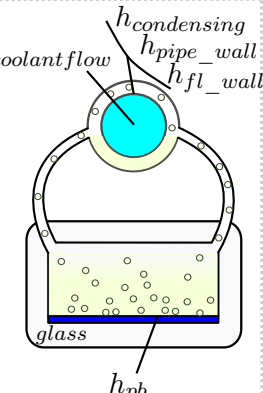
Design	Description	% h_{bc}	40X	80X
	(A) Passive Cooler (Heat Sink) + Thermal Tape (isolating)		2.3%	4.5%
	(B) Passive Cooler (Heat Sink) + Al Oxide Layer + Thermal Tape (conducting)		0.5%	0.8%
	(C) Back cooler (active) + H ₂ O* through Al pipe + Thermal Tape (isolating)		7.2%	13%
	(D) Back cooler (active) + H ₂ O* through Al pipe + Al Oxide Layer + Thermal Tape (conducting)		5.3%	8.4%
	(E) Back cooler (active) + Direct cell immersion Laminar flow	H ₂ O* Si-Oil HFC	-	-
	(F) Back cooler (active) + Direct cell immersion Turbulent flow	H ₂ O* Si-Oil HFC	4.5% 15% 51%	6.5% 26% 94%
	(G) Back cooler (active) + H ₂ O* through Cu pipe + Condensing on Cu pipe + Pool boiling back side	H ₂ O* Si-Oil HFC	11% 41% 27%	16% 58% 37%

Figure 6.17: Overcoming h_{TIF} for Designs A-G - Necessary increase in h_{bc} to overcome the effects of h_{TIF} at $X_g = 40$ and 80 .

6.10 Recommendations and conclusions

This chapter has outlined seven different Designs, A-G, for thermally interfacing CPV cells to the receiver and subsequent back cooler. A technological road map (Figure 6.14) was developed, illustrating the relationships between increasing concentration X_g and power losses for the seven technologies. A range of back cooler sizes, operating temperatures, and maximum relative percent cost of the cooling system were theoretically derived. To briefly summarize, the economically optimum size of the back cooler may lie anywhere between 2 and 3.5 times the values of h_{bc} (as established in Table 5.6), operating at cell temperatures between roughly 60 and 90°C, and making up anywhere between 10 and 25% of the total system cost. These targets consider linear-focus trough concentrators operating up to $X_g=100$.

Mention has also been made regarding possible changes to the final ranking, by including dual side cooling and including non-thermal effects of the cooling fluids. The final recommendation of this chapter is to consider using conventional, highly conductive, thermal adhesives for as large of values of X_g as possible. A 2-3% improvement in power output, as first introduced in Section 3.8.4, is believed to be readily available. This was determined by comparing the power losses in Figure 6.13 of Designs C and D near $X_g=40$. Further work should better establish an upper concentration limit of the various thermally conductive materials (tapes, glues, etc. . .) in CPV applications.

If such design limits are reached, the direct immersion cooling designs perhaps offer a solution. However, given the added complexity and unknown factors regarding the fluid to cell interface, it may be best to avoid moving to such designs unless absolutely necessary. Significant development work is to be expected and further research is necessary. The possible improvements via improved cooling were calculated in this thesis, typically on the order of a few percent, and may be outweighed by the so called fluid-effects, which require more study. It is hoped to combine the results of Figure 6.14 with additional optical and fluid-effect data, as it becomes available, to improve the final ranking given in this chapter.

6. THEORETICAL PERFORMANCE OF VARIOUS THERMAL INTERFACES

7

Preliminary Design of DI Receivers

The origins of cooling by direct immersion of solar cells in fluids may be well warranted and well intentioned, but as already shown in Chapter 6 and further elaborated in this chapter, the true benefits of and difficulty in realizing such a design are perhaps not what they first seem. This chapter discusses some of the initial design approaches and considerations for realizing a direct immersion cooling CPV receiver (DI-CPV) for linear concentrators.

7.1 Candidate fluids

The first and perhaps most obvious question regarding a DI-CPV receiver is, “which fluid should I use for cooling the CPV cells?” An ideal candidate fluid for DI-CPV would possess some, if not all, of the following properties.

Dielectric - Fluids should be dielectric to prevent shunt currents and to electrically isolate the various components of the CPV receiver.

Transparent - It is not necessarily required that a fluid be transparent; however, it may be highly desirable, as it would enable dual side cooling, i.e. front and back side cooling. If the fluid is non-transparent, or is too highly absorbing of wavelengths in a region of overlap of the solar cell’s high absorption and high quantum efficiency, then significant losses to power output may result. As such, receiver designs utilizing non-transparent fluids are best suited to back side cooling.

7. PRELIMINARY DESIGN OF DI RECEIVERS

Proper Operating Temperatures - Minimum and maximum operating temperatures of fluids are application based. However, it should be noted that thermal cycling standards according to IEC-62108 require cycle temperatures as low as -40°C , and it should be at least considered for a minimum operating temperature [38]. With regard to an upper temperature limit, this will depend on the temperature limits of the surrounding components of the CPV receiver. For systems utilizing pool boiling, the design point for an upper temperature limit is no trivial matter, and is rather an interesting optimization. The fluid's boiling point must, for thermodynamic reasons, be higher than the temperature of the operating environment. However, if this target boiling point is too high, the receiver may exhibit lower efficiencies when operating in colder environments, as the receiver must warm to boiling before the cooling system is truly fully functioning.

Chemically Inert - The solar cells within the CPV receiver may be expected to last 20 to 25 years. As such, it is important that the fluid has no adverse effects on critical design or performance functions of the receiver over time. The receiver, its internal components, and the cooling fluid maintain physical contact in an environment which is highly illuminated by UV radiation. This highly energized, test tube like condition has the potential for adverse chemical reactions. It is critical that these reactions are understood. Ideally, the fluid itself would be stable across the 20 to 25 year lifetime. If the fluid must be replaced, then the receiver must be designed to facilitate this and economics must allow for it.

Economical - Considerable quantities of the cooling fluid are likely necessary. As such, it is important that the cost of the fluid is relatively low.

Environmentally Appropriate - In surveying possible cooling fluids, there are numerous choices to consider. Unfortunately, there are many fluids which present potential environmental and safety problems for use in a DI-CPV receiver. It is desirable that such fluids contain the following properties:

- noncarcinogenic
- nonmutagenic
- non-ozone depleting

- low global warming potential (GWP)
- recyclable
- noncombustible or high flash point

When selecting the cooling fluid and considering the design of the CPV receiver, one should plan for leaks. One should NOT fool themselves into believing that he or she will be the first to design a “leak-proof” design. Leaks will happen over the course of a product’s life-time, and it is critical that the environmental impact of such an event is as insignificant as possible. In addition, a design operating under high temperatures and high pressures has an innate ability to explode. Consideration for such risks must be taken seriously and appropriate safety measures must be implemented into the design of the system.

A survey of 50 various cooling fluids produced three likely candidates, meeting the above standards: deionized water, silicon oils, and various hydrofluorocarbon fluids. All three fluids are more or less dielectric and have a reasonable range of operating temperatures. In addition, they are transparent and thus leave open the possibility of front side (dual-side) cooling. Two of the three fluids, de-ionized water and silicon oil, are inexpensive and their respective environmental effects are rather benign when compared to refrigerant coolants.

7.2 GWP limit

Some of the fluids considered thus far contain rather high GWPs. As of this writing, there is no established guideline for a maximum allowed GWP for a DI-CPV receiver. This section lays forth the logic and ground work for establishing such a limit and also proposes such a limit.

First and foremost, a few assumptions are necessary. Over the lifetime of a CPV project, there is an expected savings in green house gases, often equated in terms of CO₂ equivalencies (CO₂_{eq}). For the sake of argument, assume that a hypothetical CPV installation suffers a complete loss of coolant within the first half of the project lifetime. Further assume that the system is repaired and refilled with coolant. The system then continues to run for the latter half of its intended lifetime. The GWP value of the coolant in question should fall below a value that, given the remaining half

7. PRELIMINARY DESIGN OF DI RECEIVERS

of a product's expected lifetime, the CO₂ equivalent released from the total coolant loss event does not exceed the original expected savings of CO_{2eq}. Thus, in the case of a complete coolant loss, the actual CO_{2eq} release to the environment would be no worse than the CO_{2eq} emissions of a coal power plant. This concept is illustrated in Figure 7.1 and may be mathematically described as follows:

$$(M_{CO_2} - M_{CPV}) \cdot DNI_{(an)} \cdot t = V_{NOC} \cdot \rho \cdot GWP \quad (7.1)$$

The left hand side of the equation represents the additionally expected kg CO₂ emissions from a coal-fired power plant over a CPV system, with M_{CO_2} and M_{CPV} representing emissions in kg equivalent of CO₂/kWh for a coal-fired power plant and the CPV plant respectively. $DNI_{(an)}$ represents the expected annual kWh production for the hypothetical CPV system, and “ t ” represents the project lifetime in years. The right hand portion of the equation represents the total kg CO₂ equivalent of the coolant fluid necessary for a 1kW_{NOC} system. GWP is the global warming potential of the fluid, and V_{NOC} represents the number of kilograms of coolant needed per 1kW_{NOC} of CPV installed. Equation 7.1 may be rearranged to solve for the allowed GWP as follows.

$$GWP = \frac{(M_{CO_2} - M_{CPV}) \cdot DNI_{(an)} \cdot t}{V_{NOC} \cdot \rho} \quad (7.2)$$

The analysis above is a worse-case scenario and is intended to provide an upper limit on GWP values. It assumes that the CO_{2eq} emissions of the CPV system, following a complete coolant loss, would match those of a typical coal-fired power plant. Using Eq. 7.2 and properties from Table 7.1 an upper limit on GWP values is established at 4,000 and 2,000 kg CO_{2eq} for the passive/active transition point ($X_g=40$) and the next generation ($X_g=80$) respectively. See calculation in Appendix B.7. These values serve as an initial upper-limit during this developmental stage of research, as photovoltaic systems are aiming to reduce CO_{2eq} emissions rather than simply match coal-fired power plant emissions.

Looking ahead to further developments and eventual commercial applications, allowed GWP values should be significantly reduced. In Eq. 7.2, the allowed GWP values are calculated based on the entire project lifetime, variable “ t .” As a next step, the time frame “ t ” could be reduced to a value similar to the energy payback times of conventional one-sun photovoltaic modules (1 to 3 years [61]). Otherwise stated, rather than

allowing a full coolant leak to release emissions equivalent to the expected savings over the entire project, the release would be limited to 1 to 3 years worth of planned emission savings. Calculated at 3 years, allowed GWP decrease to 600 and 300 CO_{2eq} for $X_g=40$ and $X_g=80$ respectively. At 1 year, allowed GWP drops to 200 and 100 CO_{2eq} for $X_g=40$ and $X_g=80$ respectively. These values form a potential developmental road map, but it must be clarified that the reference to payback times, and their subsequent use to calculate more aggressive allowed GWP values, is only a qualitative argument and has nothing to do with the actual payback time for the CPV system. That is to say, one might foresee another making such an argument in light of the fact that no one has yet calculated an updated payback time for a CPV system utilizing such a cooling fluid. Eventually, such payback times must be calculated, and they should approach values similar to other photovoltaic technologies. When making these calculations, the cooling fluid's resulting CO_{2eq} emissions from the manufacturing process must be added to the payback time. In addition, it may be advisable to include some account or contribution for leaked coolant. Assuming a complete coolant loss is perhaps unnecessarily extreme. Some reasonable quantitative arguments, based on potential leak rates and modes of failure, might produce a more practical and reasonable safety factor. Future study is needed.

7.3 Candidate designs

There are two basic designs for direct immersion cooling, those which transfer heat from both the front and back side of the solar cell and those which transfer heat from only the back side of the solar cell. The two designs will be called dual side and back side cooling respectively. There are advantages and challenges to each approach which are summarized in Table 7.2.

Briefly, dual side cooling suspends a series of CPV cells in a cooling fluid, where the cooling fluid functions both as an optical interface (front side of cell) and as the primary heat transfer mechanism. Fewer fluids are available to meet both functions, but such a design may also eliminate the need for an encapsulant or significantly reduce its size and significance. However, something is needed to suspend the cells in the fluid. Encapsulating from the side edges of the cell up to the bus bars may be adequate, or perhaps a special fixture, with integrated electrical contacts, could be used.

7. PRELIMINARY DESIGN OF DI RECEIVERS

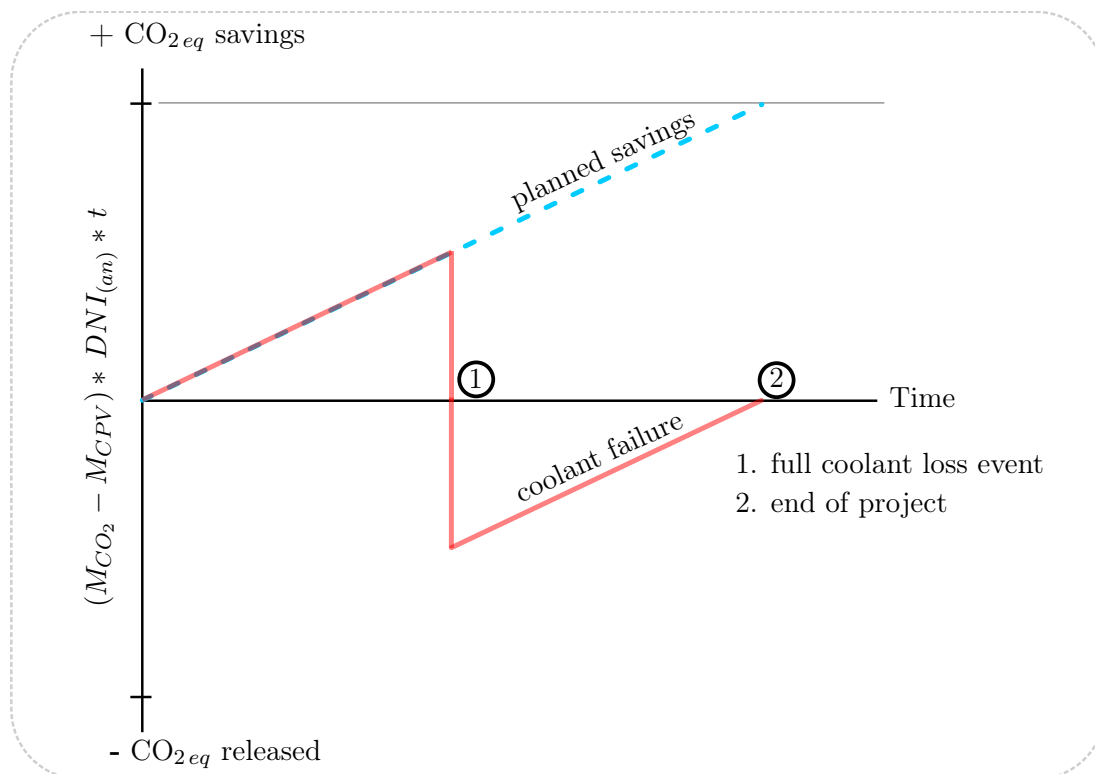


Figure 7.1: Coolant Release Event - Expected savings in CO_{2eq} for a CPV plant as compared to a typical coal-fired power plant over the project lifetime. The dashed blue curve, labeled planned savings, indicates the planned savings in CO_{2eq} for a CPV installation. The solid red curve represents a complete loss of coolant failure. The GWP value of the coolant should be low enough such that the CPV system could recover to the zero point (x-axis) in which CO_{2eq} emissions of the CPV plant would then be equal to that of a coal-fired power plant.

Table 7.1: Suggested GWP Parameters - Parameters used to propose a maximum allowed GWP for DI-CPV receivers at $X_g=40$ and 80 (apertures width > 1.5 meters). ¹Reference [62]. ²Reference [62], average of 0.053 and 0.250 kg CO₂ eq. ³Minimum required DNI for CPV according to Ref. [18]. ⁴Estimate is based on a minimum extruded chamber for the CPV cells requiring 1 liter of coolant per meter length and capable of an estimated power output of 130 W/m and 260 W/m at $X_g=40$ and $X_g=80$ respectively. ⁵Density of a commercially available, but proprietary, hydrofluorocarbon (HFC) fluid.

Parameter	Value	Units	Notes
M_{CO_2}	0.975	$\frac{\text{kg CO}_2 \text{ eq}}{\text{kWh}}$	1
M_{CPV}	0.150	$\frac{\text{kg CO}_2 \text{ eq}}{\text{kWh}}$	2
$DNI_{(an)}$	2,000	$\frac{\text{kWh}}{\text{kW}_{\text{NOC}} \cdot \text{yr}}$	3
$V_{\text{NOC}}(X_g)=40$	10.8	$\frac{\text{liters}}{\text{kW}_{\text{NOC}}}$	4
$V_{\text{NOC}}(X_g)=80$	5.4	$\frac{\text{liters}}{\text{kW}_{\text{NOC}}}$	4
ρ	1.6	$\frac{\text{kg}}{\text{liter}}$	5
t	20	years	-

Table 7.2: Dual Side vs. Back Side Cooling - A comparison of the advantages and challenges of dual side and back side cooling.

Design	Advantages	Challenges
Dual Side	<ul style="list-style-type: none"> • doubles heat transfer surfaces • eliminates encapsulation • cell replacement possible 	<ul style="list-style-type: none"> • fewer fluid candidates • requires mounting method
Back Side	<ul style="list-style-type: none"> • non-transparent fluids • utilize encapsulant for mounting 	<ul style="list-style-type: none"> • one sided heat transfer • requires an encapsulant • cell replacement is difficult

7. PRELIMINARY DESIGN OF DI RECEIVERS

Back side cooling, as the name implies, cools the CPV cells only on the back side of the cell and thus requires some way, for example via encapsulation, of preventing coolant from reaching the front side of the solar cell. In doing so, the optical and heat transfer functions may be decoupled and the designer has additional cooling fluids to choose from. As a note, the significance of realizing such a one-sided encapsulation should not be underestimated, especially considering the mere few hundred micron thickness of most CPV cells. Again however, a type of partial encapsulation, leaving the back side of the cell open to the coolant, may suffice. It is inadvisable to completely encapsulate the back side, as most polymers have relatively low thermal conductivities. This additional thermal barrier may significantly contribute to temperature rise within the cell, likely on the order of magnitude and similar in size to the thermal tapes discussed in Section 6.6. However, if the CPV cells could be encapsulated by a thin layer of a relatively high thermally conductive material, such a design could benefit over the more traditional tape and pipe Designs C and D, as shown in Figure 6.6-(b).

Having described many of the advantages, challenges, and basic concepts behind each design, the obvious question remains: “Dual side or back side?” Unfortunately, further work is needed to fully answer this question. But interestingly enough, its answer depends on the mode of heat transfer utilized in the DI-CPV receiver design, which will be further discussed in the next section. This discussion will focus on designs moving beyond passive and into active and next generation cooling, direct immersion turbulent flow and pool boiling, Designs F and G respectively.

7.3.1 DI-CPV receivers and turbulent flow

If one considers dual side cooling in turbulent flow, one immediate concern should come to mind; namely, turbulent flow on both the front and back side of the solar cell will exert forces and place stress on the CPV cell. Such transient forces may be rather unpredictable and difficult to model. The resulting concern is the cracking of cells during operation. Such phenomena can be studied and perhaps an assuring solution found, but such work is outside the scope of this thesis. This brings the discussion to a second challenge of dual side cooling. There is a fundamental trade-off between optical losses and fluid pumping losses with regard to the distance between the front side of the solar cell and the receiver’s front glass surface. From an optics stand point, the distance between the front side of the CPV cells and the glass should be minimized (as shown

in Figure 7.2-(b)) so as to minimize the depth of fluid between the two. Increasing this fluid depth increases absorption of the incoming light within the fluid itself [60], thus reducing the amount of light reaching the CPV cells and ultimately reducing power output. However, it would be beneficial to the fluid flow and resulting heat transfer if the cells were centered within the receiver glass extrusion (resulting in an increased fluid depth). Thus a trade-off exists. Back side cooling presents fewer challenges in this regard, as the cells may be mounted via an encapsulation to the front glass surface and fluid depth becomes essentially zero. The fluid is instead replaced by some sort of encapsulant material, as shown in Figure 7.2-(a). In addition, concern over stress induced cracking may be lessened, as the typically elastic nature of the encapsulant may help to more evenly distribute any forces on the solar cell.

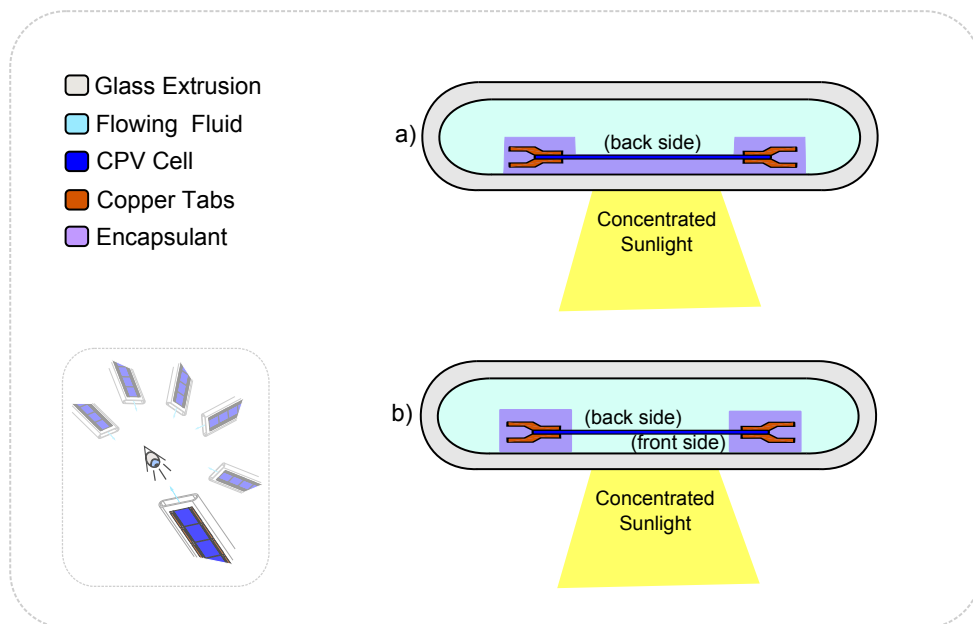


Figure 7.2: DI-CPV Flow - Cross section of Fig. 6.3: Receiver body for Design E & F.

7.3.2 DI-CPV receivers and pool boiling

In the case of pool boiling, the challenges are somewhat different. With the absence of turbulent flow, the previous concerns regarding stress induced cell cracking may be somewhat ignored. However, special attention must be given to the dual side boiling case shown in Figure 7.3-(b). The design must enable the escape and prevent the formation

7. PRELIMINARY DESIGN OF DI RECEIVERS

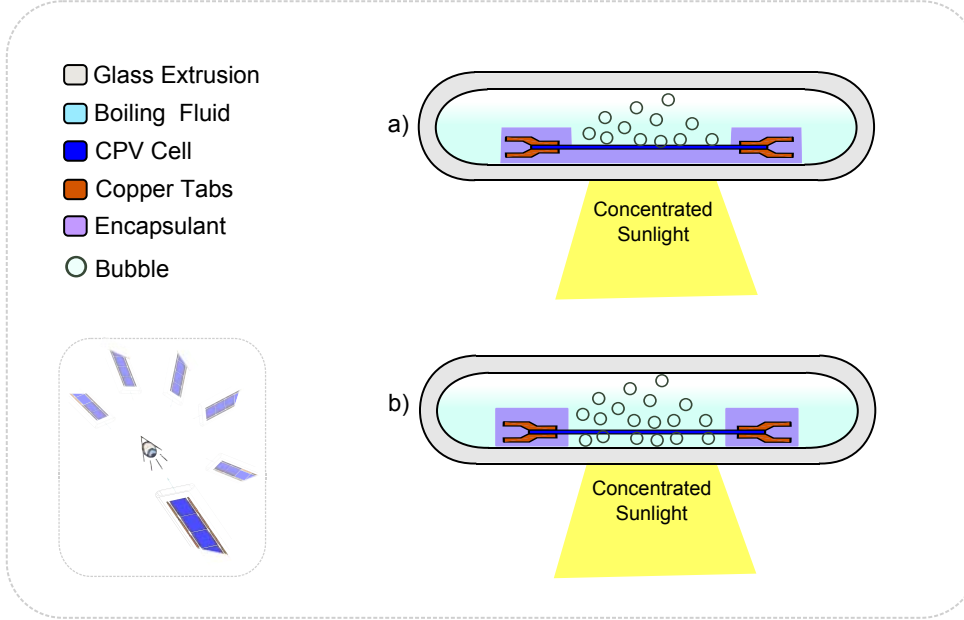


Figure 7.3: DI-CPV Boil - Cross section of Fig. 6.3: Receiver, pool boiling Design-G.

of large vapor pockets of coolant. Such vapor pockets are not only extremely detrimental to the local heat transfer coefficients, but will also change the optical interface at the cell's front surface. The difference between the index of refraction for the liquid and vapor phase of the cooling fluid will reflect portions of the incoming concentrated light. A significant difference in the size and location of vapor pockets, labeled as "bubbles" in Figure 7.3-(b), may act as a form of optical shading. This shading effect could be similar to that seen in one-sun photovoltaics, including its associated losses.

To better understand the transmission of light through the cooling fluid, a simple example is given in Figure 7.4 for de-ionized water. Light is shown entering the bottom of a steam bubble. A graph is provided showing the transmission through the liquid to vapor interface. With an estimated index of refraction of 1.33 and 1.004 for the liquid (<100°C) and vapor phase respectively (according to Ref. [63] for a wavelength=600nm), light emitted through the liquid water must exhibit an entrance angle below the critical angle θ_{cr} :

$$\theta_{cr} = \arcsin\left(\frac{n_2}{n_1}\right) = \arcsin\left(\frac{1.004}{1.33}\right) = 0.855 \text{ rad} \approx 49^\circ \quad (7.3)$$

Thus, light entering the bottom surface of the steam bubble must have an entrance angle below 49 degrees, otherwise the light will be reflected at the bubble's surface. This is illustrated in the figure by the approximate +/- 49° beam of light shown entering the bottom of the steam bubble. Overlaid, is a transmission curve for s-polarized and p-polarized light, labeled τ_s and τ_p respectively. Similarly at the top of the steam bubble, transmission curves are provided for this vapor to liquid interface. With the values of n_1 and n_2 now reversed, there is no critical angle. Rather, there is a wide range of exit angles and associated transmission coefficients. The transmission curves τ_s and τ_p are calculated assuming that all non-reflected light is transmitted and may be calculated by $1 - R_s$ and $1 - R_p$ (see Eq. 7.4 and 7.5). The reflectance R_s and R_p can be found by combining Snell's law with the Fresnel equations (see page 44 of Ref. [64]). This implies that no light is absorbed in the optical medium itself, which is a simplification of the actual case.

$$\tau_s = 1 - R_s = 1 - \left[\frac{\cos \theta - \sqrt{n^2 - \sin^2 \theta}}{\cos \theta + \sqrt{n^2 - \sin^2 \theta}} \right]^2 \quad (7.4)$$

$$\tau_p = 1 - R_p = 1 - \left[\frac{-n^2 \cos \theta + \sqrt{n^2 - \sin^2 \theta}}{n^2 \cos \theta + \sqrt{n^2 - \sin^2 \theta}} \right]^2 \quad (7.5)$$

$$n = n_2/n_1$$

This rather simple example illustrates one very important point: at a liquid to vapor phase interface, the critical angle leads to a total internal reflection and can limit the light reaching the CPV cell. Such phenomena might exhibit a type of shading and result in an associated power loss. Estimating such losses is quite difficult. The simple example in Figure 7.4 considers only a single exit and entrance point, and completely ignores the modification of the light's pathway within the bubble itself. In reality, the bubble's surface is curved and there are many possible points of entrance and exit. In addition, light which is internally reflected by the liquid to vapor phase may further be reflected by the glass to liquid interface. To better understand the effects of such bubbles on the systems optics, a ray tracing simulation is necessary, considering the complete optical path from the primary optics through to the cell itself. Of particular difficulty, is the defining of a standard bubble size and bubble density for an accurate

7. PRELIMINARY DESIGN OF DI RECEIVERS

running and comparison of various simulation trials. Such work is outside the scope of this thesis. Lacking such an analysis, one can however, still gain an appreciation for the optical losses by simply considering the reflectance at the liquid-vapor and vapor-liquid interfaces at zero angle of incidence. Focusing on either R_s or R_p , in Eq. 7.4 and 7.5 respectively, and by setting $\theta=0$, one arrives at the reflected losses:

$$R_n = \left(\frac{n_1 - n_2}{n_1 + n_2} \right)^2 \quad (7.6)$$

For de-ionized water, this reflection amounts to roughly 2% of the incoming light. As light passing through such a bubble must enter and exit, and thus travels through 2 optical interfaces, these losses approximately double to 4%. Considering that solar cells are available for purchase with power matching in the range of +/-0.5%, the significance of such optical losses becomes suddenly apparent. However, it should be remembered that matching losses due to the optical interference of bubbles would depend on the differences between bubble size and location for each cell. If this is relatively uniform from cell to cell, then power matching losses may become less significant. Nevertheless, an additional optical loss exists.

7.4 Estimate of optical losses

The optical pathways leading up to the CPV cell are shown in Figure 7.5 for Designs A-G. Their corresponding optical losses are crudely estimated by considering each optical interface separately and simply summing their reflective losses for zero angle of incidence, Eq. 7.6. Both refraction and absorption in the material itself are ignored to simplify the analysis. These results are presented in Table 7.3. The estimated losses for Designs A-D, and E and F are similar, slightly over 4%, which can be attributed mostly to the air-glass interface. Optical losses for Design-G are nearly double. This can be attributed mostly to optical losses in the vapor bubbles. However, it should be noted that a value of 1 was assigned to the vapor phase of all three candidate cooling fluids. For de-ionized water, this is reasonable, but may not hold true for the other two fluids. In the absence of available data, a value of 1 was assigned.

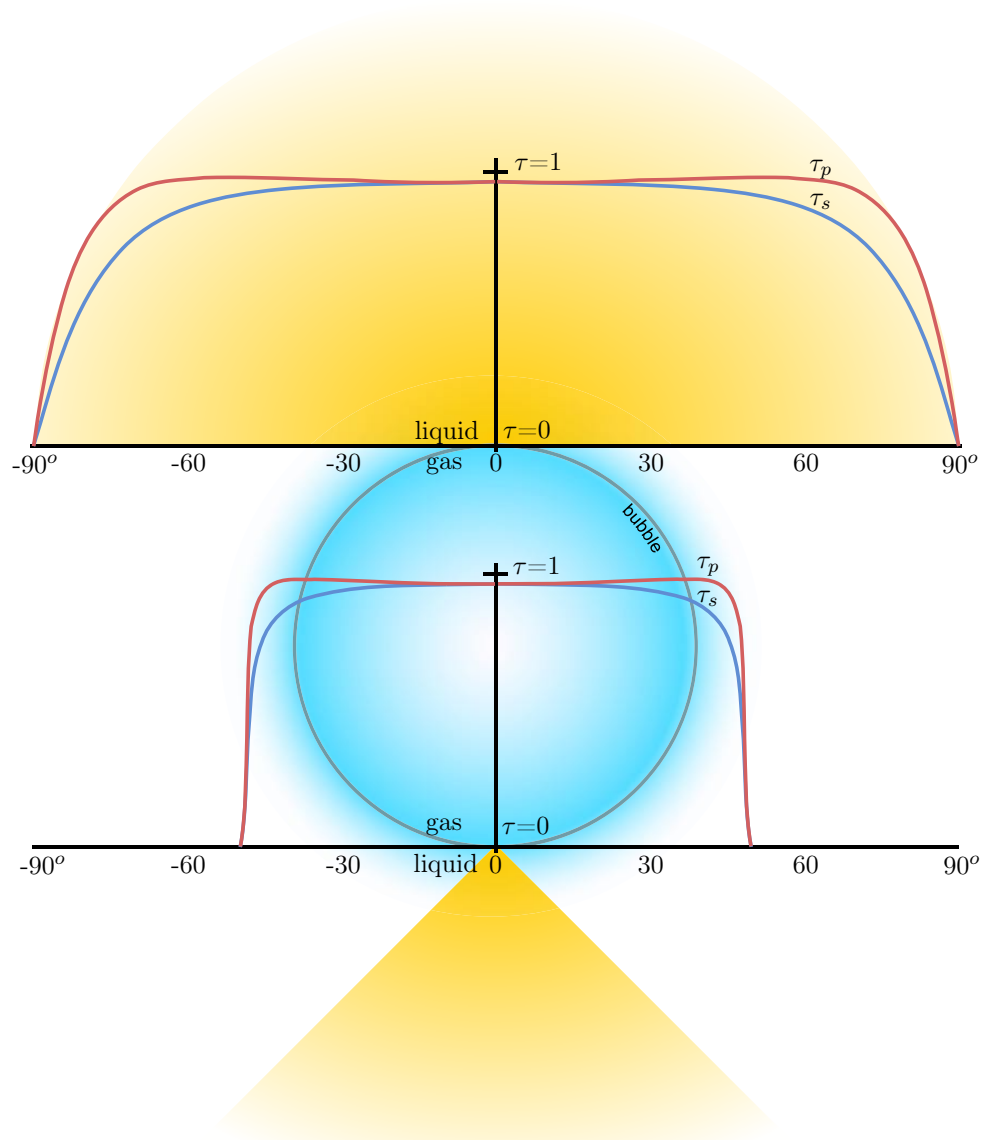


Figure 7.4: Light Transmission in Bubbles - Transmission of light entering and leaving a steam bubble in de-ionized water for s-polarized (τ_s) and p-polarized (τ_p) light, Eq. 7.4 and 7.5 respectively.

7. PRELIMINARY DESIGN OF DI RECEIVERS

Table 7.3: Optical Losses at Zero Incidence - Optical losses for Designs A-G, considering each optical interface separately and simply summing their reflective losses for zero angle of incidence, Eq. 7.6.

Optical loss	mat1	mat2	n_1	n_2	Loss %
η_1	air	- glass	1.0	1.5	4.0
η_2	glass	- silicone	1.5	1.4	0.1
η_3	glass	- water	1.5	1.33	0.4
η_4	glass	- Si-oil	1.5	1.4	0.1
η_5	glass	- HFC	1.5	1.3	0.5
η_6	water	- vapor	1.33	1.0	2.0
η_7	Si-oil	- vapor	1.4	1.0	2.8
η_8	HFC	- vapor	1.3	1.0	1.7
η_9	vapor	- water	1.0	1.33	2.0
η_{10}	vapor	- Si-oil	1.0	1.4	2.8
η_{11}	vapor	- HFC	1.0	1.3	1.7

Design	Fluid	Total Losses	Loss %
A,B,C,D	-	$\eta_1 + \eta_2$	4.1
E,F	water	$\eta_1 + \eta_3$	4.4
	Si-oil	$\eta_1 + \eta_4$	4.1
	HFC	$\eta_1 + \eta_5$	4.5
G	water	$\eta_1 + \eta_3 + \eta_6 + \eta_9$	8.4
	Si-oil	$\eta_1 + \eta_4 + \eta_7 + \eta_{10}$	9.7
	HFC	$\eta_1 + \eta_5 + \eta_8 + \eta_{11}$	7.9

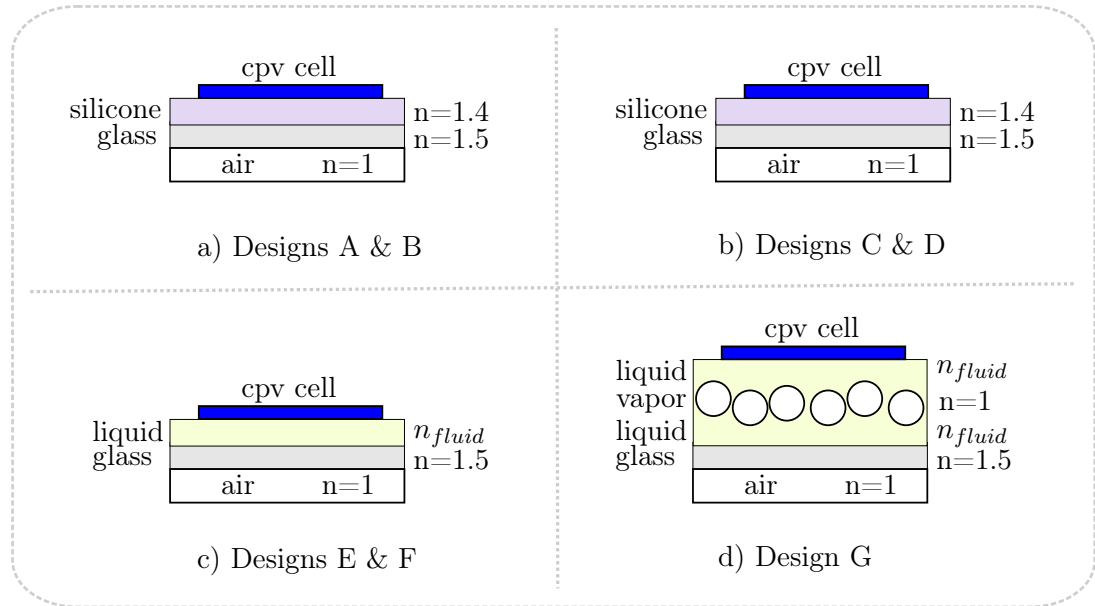


Figure 7.5: Optical Interfaces - Optical interfaces for Designs A-G.

7.5 Challenges and future developments

To give a final assessment of DI-CPV cooling, one must consider all aspects of its cost and performance. This chapter has outlined some of the design challenges present for a DI-CPV receiver. Candidate fluids were identified, and the basic properties of such fluids explained. In Chapter 6, the heat transfer capabilities of DI-CPV receivers were outlined, and it was established that such a technology may become necessary when considering designs beyond the capabilities of thermal adhesives. In addition, it was shown that the technology could be economical, with regard to necessary increases in the size of the back cooler.

Even given its design and development challenges, a DI-CPV receiver could prove worthwhile, as it would eliminate both the thermal adhesive and encapsulation, two of the most expensive portions of the bill of materials (BOM, Table C.3). However, the practical realization of such a design has proved somewhat difficult. In this thesis, investigations into candidate fluids and compatible encapsulates ran into major problems. Many of the fluids that were found to have an acceptable cost and heat transfer properties were organic fluids. Such fluids tend to react poorly with polymers, and thus it was difficult to find an inexpensive encapsulating agent. Also, many of these

7. PRELIMINARY DESIGN OF DI RECEIVERS

organic fluids are flammable, proposing other practical safety issues. The HFC fluids have reasonable heat transfer capabilities and are more or less chemically inert, but are extremely expensive. Estimates from manufacturers were obtained in the range of 40 to 60 €/liter. In comparison to the existing BOM, this cost is relatively high. To summarize: it is difficult to find both an inexpensive cooling fluid and inexpensive encapsulant. Typically a cheap cooling fluid required an expensive encapsulant and vice versa.

Without further study, it is difficult to stem away from the final ranking of receiver designs provided in Section 6.8, even though the study largely focuses on the cooling aspects of the various designs. Given the amount of work necessary to redesign and realize the DI-CPV receiver, it is inadvisable to recommend doing so, unless a design reaches a material limit with regard to the thermal adhesives. Any future studies regarding DI-CPV should focus on the fluid to cell interactions, the so called fluid-effects.

8

Alternative Soldering Methods

8.1 Introduction

Both the higher current density and the close proximity of bus bars to the side edges of concentrator photovoltaic (CPV) cells present additional challenges with respect to the soldering and interconnection of such cells. Previously at the Universidad Politecnica de Madrid and the Australian National University, the front and back side of a cell were directly stencil-printed with a leaded solder-paste and fitted with small copper tabs for electrical contacts [22], [35]. In this chapter, a new and novel method for soldering CPV cells was investigated and successfully demonstrated, eliminating both stencil-printing and the use of lead. Copper tabs were pre-coated with small amounts of lead-free solder in a solder-bath dipping process and soldered to the CPV cell in a vapor phase soldering machine.

8.2 Stencil printing

Figure 8.1(a) illustrates the key steps to the solder-paste stencil printing method for soldering CPV cells. Small pads of solder-paste are applied to the front and back side of the CPV cell via a stencil. Afterwards, the cell and four copper tabs are placed in a special fixture so as to properly align the small copper fingers of each tab to the printed solder paste. Finally, the assembly is placed in a vapor phase soldering machine to reflow the solder and complete the solder joints. The stencils used in the aforementioned solder-paste processes require frequent cleaning. If clogged, cells become incompletely

8. ALTERNATIVE SOLDERING METHODS

stenciled with solder-paste. Reprocessing involves removing the cell for cleaning, further increasing handling and the risk of breakage or loss.

8.3 Pre-coated tab method

The key steps of the pre-coated tab method are summarized in Figure 8.1(b). Tabs are first rotated through a liquid flux in both the counter and clockwise directions. Under a nitrogen blanket, the tabs are next rotated through a solder-bath, leaving the copper tabs coated with a conical finger of solder.

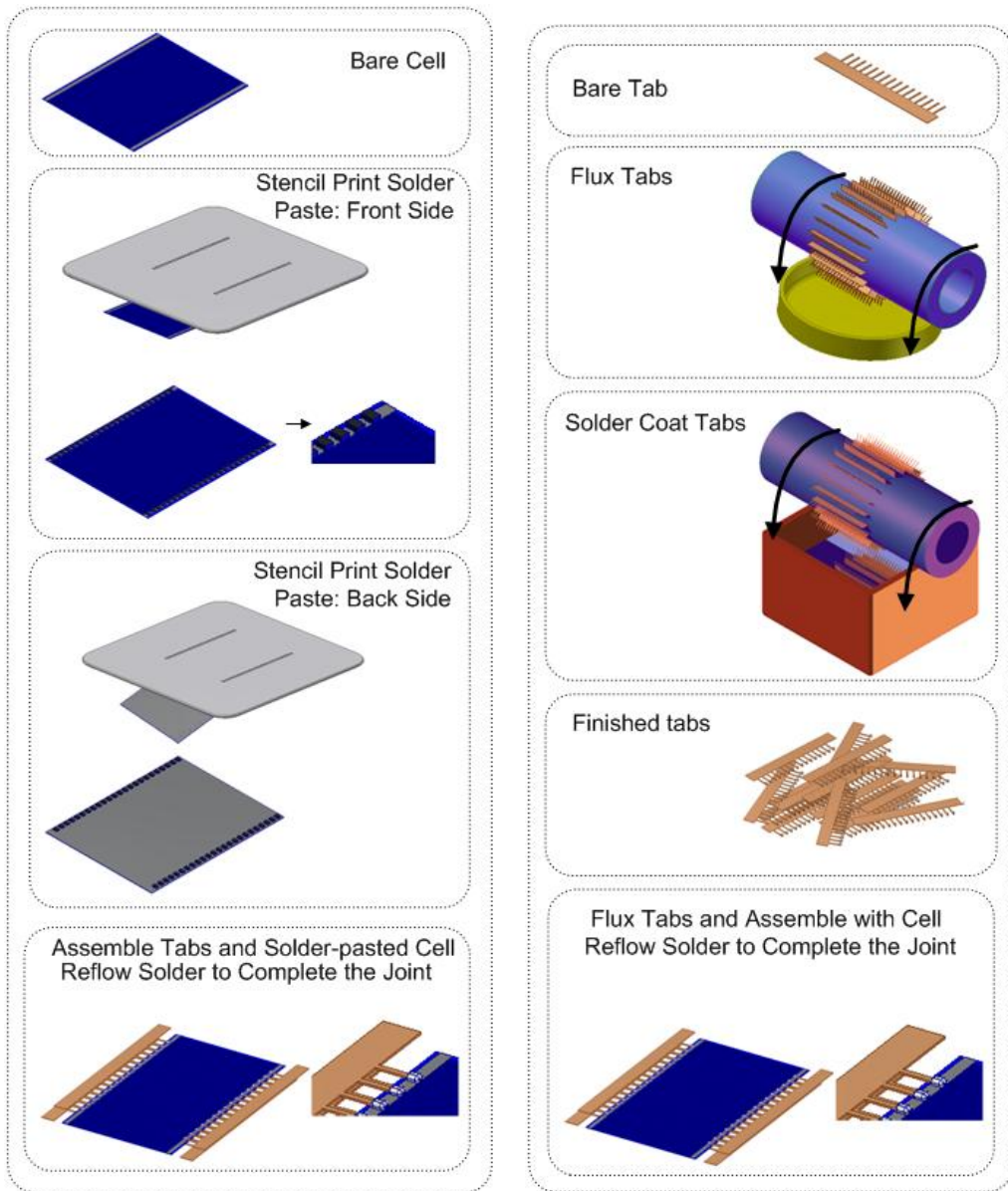
A small machine was designed that is capable of rotating numerous copper tabs through a solder-bath at a controlled height and depth of penetration. Several hundred tabs were produced by this method using SAC-305 lead-free solder ($\text{Sn}_{96.5}\text{Ag}_{3.0}\text{Cu}_{0.5}$). Various processing temperatures and process cycles were investigated. A typical example of the pre-coated solder tab is shown in Figure 8.2.

Using a special fixture, Figure 8.3(a), pre-coated tabs were set in place around a CPV cell and coated with a liquid flux around the joint area. The fixture carefully aligns the pre-coated tabs over the cell's bus bars as shown in Figure 8.3(b). The entire assembly then undergoes a controlled heating cycle in a vapor phase soldering machine, under an oxygen-free environment, to complete the solder joints.

The pre-coated tab method provides significant savings in time, waste, and ultimately cost by eliminating stenciling and its associated cleaning. Pre-coated tabs can also be inspected and conveniently stored for use at a later time. To the best of the author's knowledge, this unique method is one of the first to utilize a lead-free solder in a linear-focus CPV receiver.

8.4 Experimental results

Several mono-crystalline CPV cells were soldered using the pre-coated tab method. An initial assessment as to the quality of the solder joint's electrical properties was determined by comparing I-V curves and cell series-resistance before and after the pre-coated tab soldering process. The pre-soldering measurements were taken using a special fixture (see Figure 8.5-a) containing a set of spring loaded copper fingers that press into the bus bars of the CPV cell. For the post-soldering measurements, an appropriate



(a) Stencil Print Method

(b) Pre-coated Tab Method

Figure 8.1: Soldering Processes - Comparison of soldering methods.

8. ALTERNATIVE SOLDERING METHODS

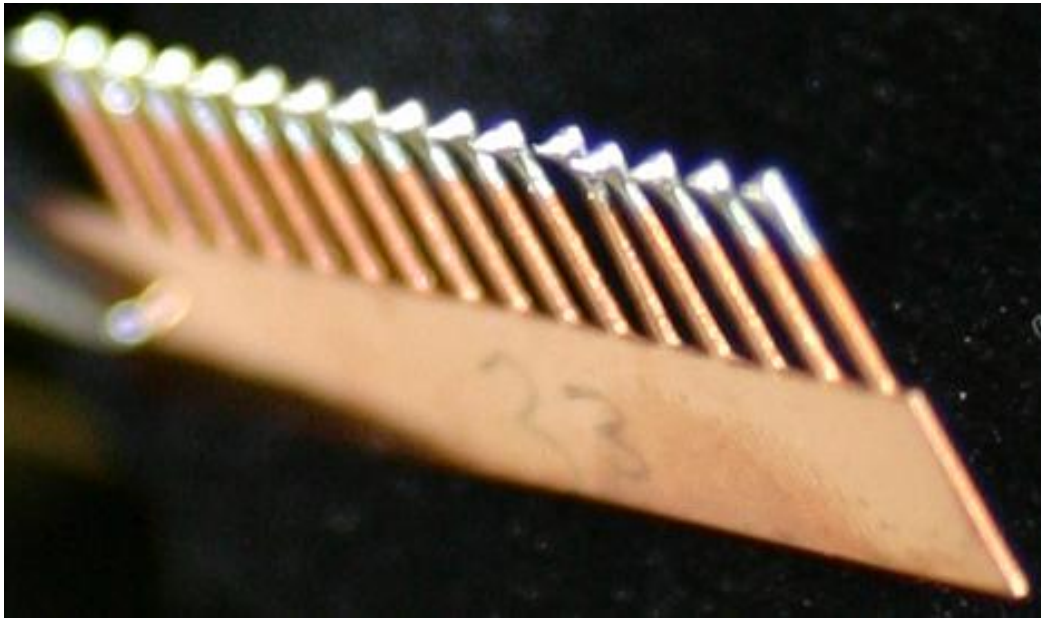
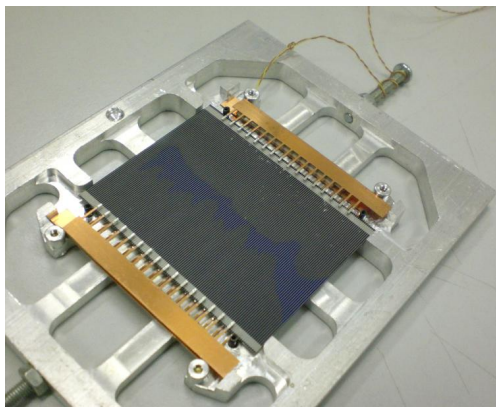
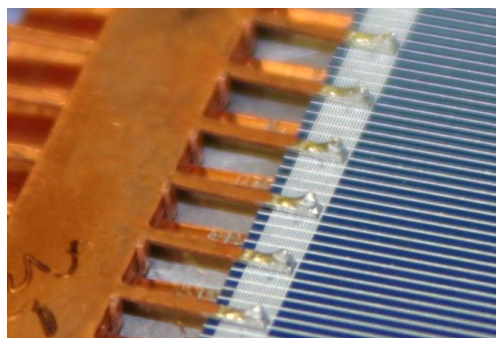


Figure 8.2: Pre-coated Tab - Typical example of a finish pre-coated tab.



(a)



(b)

Figure 8.3: Soldering Fixture - (a) CPV cell assembled to pre-coated tabs, ready for soldering. (b) close up, alignment of the pre-coated tab fingers and the cell bus bar.

four point probe was utilized in place of the fixture (see Figure 8.5-b). Care was taken to keep the wiring of each sample identical, so as to avoid introducing any changes. Post-soldering measurements showed a reduction in total series resistance of the CPV cell, with its now soldered copper tabs. The measurements are shown in Figure 8.4 and are comparable to data from previous solder-paste methods [35]. The magnitude of each reduction is rather meaningless, as the improvements in series resistance are made in comparison to the measurement fixture. Rather than quantify or qualify any potential performance improvements, the purpose of the measurement was to identify any malfunctions or major problems in the soldering process. The improvement in series resistance likely results from the difference in contact areas in the two measurement set-ups. Although there are significantly more electrical contact fingers in the pre-soldering measurements (Figure 8.5-a), the point-contact made by each finger is extremely small, approximately the size of a sharpened pencil tip. The finished solder contacts in Figure 8.5-b are significantly larger, with each contact yielding a foot print of approximately 0.5 x 1.5mm.

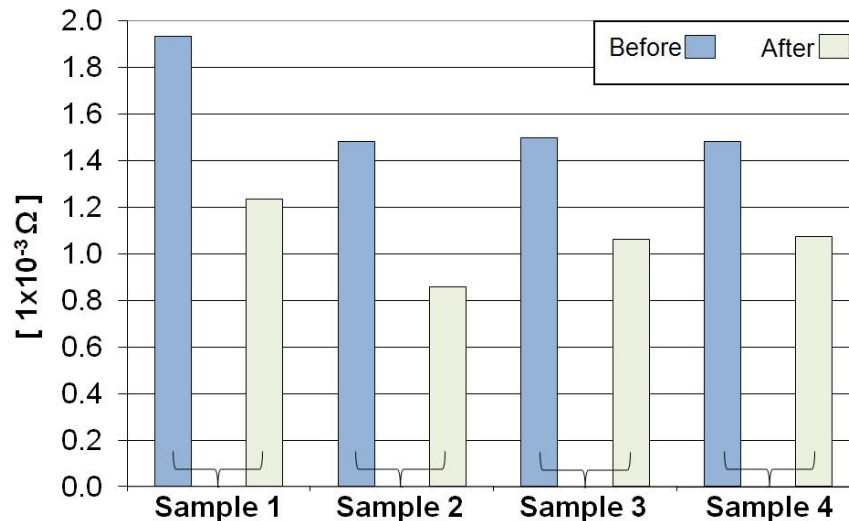


Figure 8.4: Series Resistance Measurements - Before and after soldering measurements for series resistance, four samples.

A typical example of pre- and post-soldering I-V curves is shown in Figure 8.6 for sample #4 at multiple concentration ratios (referenced to multiples of 1000 W/m²). The pre- and post-soldering curves exhibit similar behavior. However, a slight increase

8. ALTERNATIVE SOLDERING METHODS

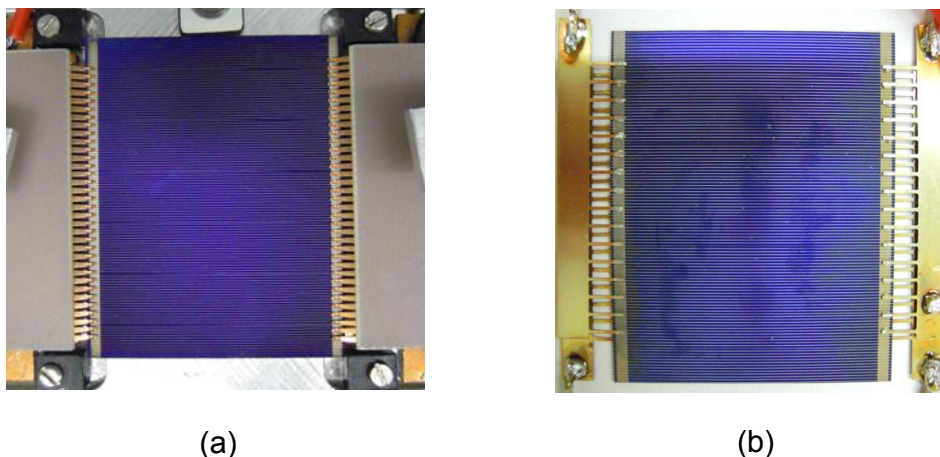


Figure 8.5: Pre- and Post-soldering Measurement Set-ups - (a) CPV cell, pre-soldering, ready for an I-V curve measurement. (b) CPV cell, post-soldering, ready for an I-V curve measurement. Notice that the pre-soldering measurement-fixture (a) shades the cell edge more than (b).

in short circuit current is noticeable. This is likely due to a small increase in the active area in the post-soldering measurement set-up. From Figure 8.5, notice that the fixture for pre-soldering measurements, (a), shades the CPV cell more than the post-soldering case (b). There are a total of 69 top-side contact points for (a), “fingers,” which shade the CPV cell, whereas (b) has only 32 fingers. Although this shading primarily occurs over the bus-bars, where it is assumed that no electric current is generated, there is a small 0.5mm edge, capable of generating current, which is shaded by the fingers. See Figure 8.7 for an illustration. A 1.46% increase in active area was estimated for the post-soldering measurements set-up over the pre-soldering measurements. This result agrees reasonable well with the 1.54% to 1.72% increase in short circuit current seen for the four samples.

The remaining increase in short circuit current may have resulted from a slight increase in temperature between the two set-ups. The slight decrease in open circuit voltage, as seen in Figure 8.6, supports this hypothesis. Although both set-ups used a temperature control system, the pre-soldering measurement fixture (a) was easier to interface with the existing mounting hardware. This fixture enabled the use of a vacuum pump to hold the cell in place. Measurements taken post-soldering were unable to utilize the vacuum pump. As such, the quality of the thermal contact between the cell and

the cooling block may have been reduced and could have resulted in a slightly higher temperature in the post-soldering measurements. However, as the I-V curve tracer used for these measurements is a flash-tester, the actual heating from a single measurements is rather small.

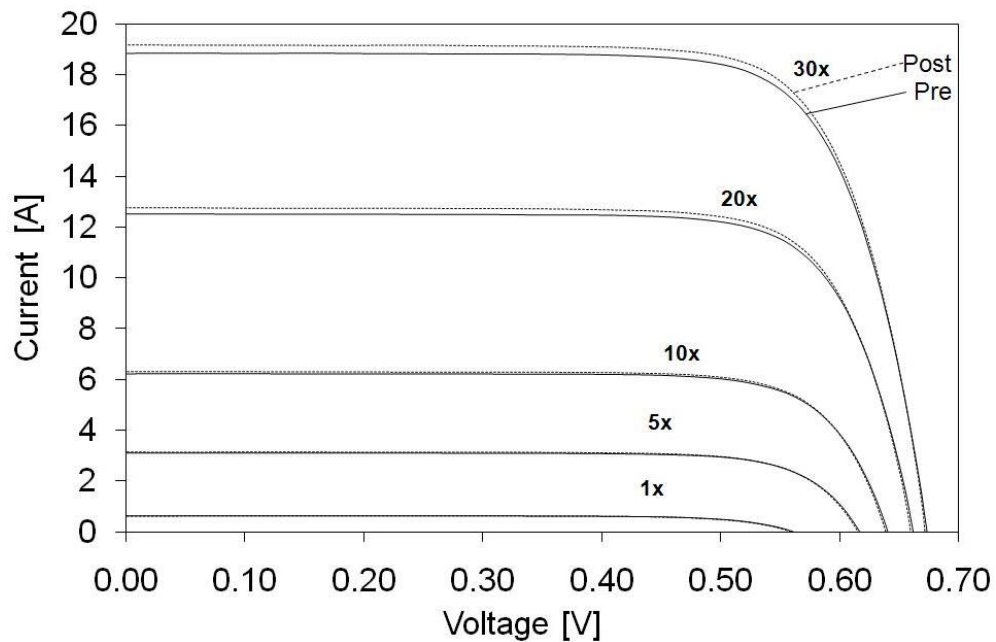


Figure 8.6: I-V Curves Pre-Post Soldering - I-V curves, before and after soldering for the pre-coated tab method.

The front and rear solder contacts were examined microscopically to visually assess joint quality. Rear-side contacts appear smooth and well rounded, see Figure 8.8. Subsequent pull tests indicate a full wetting of the surface. Contact to the front side bus bars proved more difficult. Following vertical pull tests, the uniquely etched surface, making up the bus bar, left matching patterns between the copper tab and cell. Figure 8.9 illustrates. Future samples will utilize a “fuller” bus bar, with increased contact surface area. Two of the four samples were selected for thermal cycle testing per IEC-62108, using a maximum cycle temperature of 85°C. Over 500 cycles were accumulated and the samples indicated power degradation within the pass criteria limits [65]. Visual inspection yielded no cracks or joint failures.

8. ALTERNATIVE SOLDERING METHODS

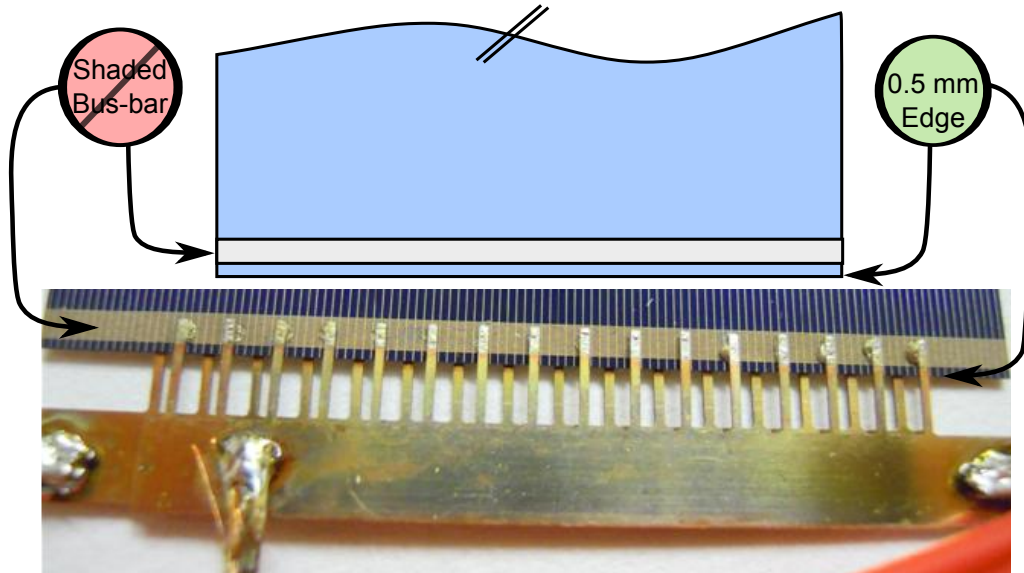
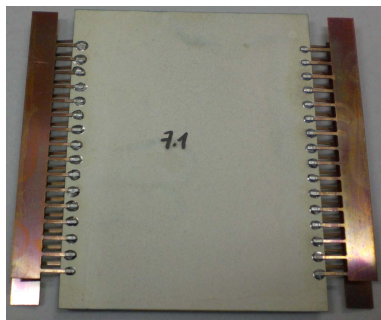
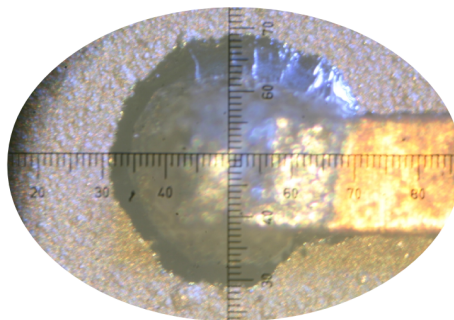


Figure 8.7: Edge Shading - Shading of the 0.5mm thick edge by the copper contacts.



(a)



(b)

Figure 8.8: Back Side Solder Contacts - (a) Back side contacts after soldering with pre-coated tab method. (b) Back side contact under 10x magnification.

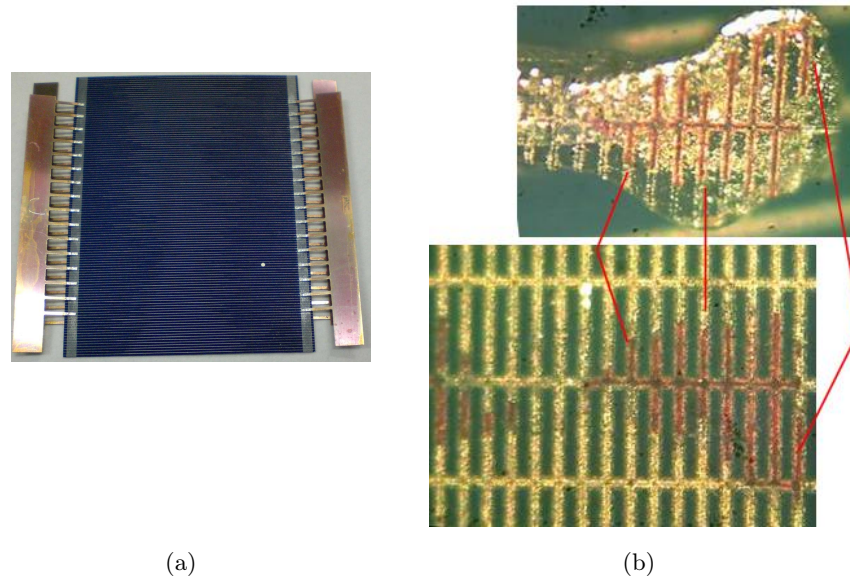


Figure 8.9: Front Side Solder Contacts - (a) Front side contacts after soldering with pre-coated tab method. (b) Results of solder pull off test under 10x magnification.

8.5 Conclusions

A new and novel approach to soldering CPV cells utilizing a lead-free solder process was successfully demonstrated. The pre-coated tab method may provide significant savings in time, materials, and ultimately cost by eliminating stenciling and its associated cleaning. Pre-coated tabs can also be inspected and conveniently stored for use at a later time. The I-V curves and series resistance measurements, before and after soldering, indicate acceptable performance. In addition, thermal cycle testing (per IEC-62108) of the initial samples has indicated power degradation within the pass criteria limits. Further reliability testing is necessary to characterize and confirm the long-term mechanical and electrical stability of this new soldering method.

8. ALTERNATIVE SOLDERING METHODS

9

Conclusion

The purpose of this thesis was to assess whether or not an actively cooled, low concentration, concentrator photovoltaic (CPV) receiver could meet either grid parity or wholesale electricity prices under the assumption that electrical energy production is maximized and heat is considered a waste load. To do so, a set cost targets were derived for an actively cooled CPV receiver and cooler technology to meet short-term (grid parity) and long-term (wholesale) electricity price targets. The current cost of the receiver and proposed cooler were compared to these targets for three application scenarios. A list of possible improvements were derived, followed by a detailed analysis regarding the theoretical limits of these improvements. After deriving cost targets, determining current cost, and developing several unique methods to calculate and compare the various CPV receiver designs, several conclusions regarding the three CPV applications can be drawn.

9.1 Land-based CPV

Land-based CPV utilizing low concentrating, linear-focus trough concentrators with silicon solar cell technology will struggle to meet short term (grid parity) and long term (wholesale electricity prices) cost targets. Possible cost and performance improvements demonstrate that it is theoretically possible to meet short term targets, but significant design challenges and development remain, especially with reducing the cost of the cooling system.

9. CONCLUSION

The believed likelihood of the two largest improvements: higher cell efficiency and a cost reduced back cooler is relatively low. Higher cell efficiencies while still maintaining low cost is difficult in the sense of manufacturing volumes. Additionally, such improvements may carry into the traditional one-sun photovoltaic market and quickly erase any advantage to CPV. The back cooler technology, briefly discussed in Section 3.8.5, requires the design and development of relatively large and inexpensive liquid to air heat exchangers utilizing plastic membranes. Such a concept is novel, and there is a high likelihood of failure.

Most importantly, the study could not identify enough improvements to meet long-term targets. In light of the evidence collected in this thesis and considering that existing one-sun technologies are already meeting the short-term cost targets [42], it is concluded that land-based CPV systems utilizing low concentrating, linear-focus trough concentrators with silicon solar cell technology will not find a marketplace. Otherwise stated, other technologies will overshadow or replace it. Granted, there are many assumptions made throughout this thesis, and a more positive outlook is possible by changes to these assumptions (as will be discussed in Section 9.5). However, even if long-term cost targets could be met, the question still remains:

What advantage does a land-based CPV system (utilizing low concentrating, linear-focus trough concentrators with silicon solar cell technology) have over traditional one-sun technologies?

Claims of higher operating efficiencies belong only to the point concentrating systems like those of Concentrix and Amonix. In practice, linear-focus trough CPV systems utilizing silicon cells have not exhibited higher efficiencies than the record holding one-sun technologies. Even in areas of extremely high solar irradiation, where perhaps a CPV system could yield lower costs and higher performance over traditional one-sun photovoltaic technologies, it still seems more likely that CSP, with the ability to store heat and generate electricity at night, will take this market segment.

9.2 CPV-T

CPV-T, in which the cooling system may be drastically reduced in size and cost, shows promise, as it can meet short term cost targets and even approach long term cost targets.

However, with respect to grid scale integration, CPV-T seems an unlikely candidate. The problem of “point of generation vs. point of use” and the ratio of thermal to electrical energy production, which can prevent the large scale use of combined heat and power for traditional fossil fuel power plants, correspondingly apply to CPV-T. If such systems are to be installed near the point of use, space must be available, and space is not always available. There are also civil works to consider. In the Combined Heat And Power Solar (CHAPS) program, the roof of the installation site had to be specially reinforced to accommodate the weight of the concentrators. For new buildings, such considerations are possible, but this can be a problem for existing buildings.

There is of course sense in designing and developing concentrator systems for building integration or roof-top applications. Generation and point of use are practically coupled and may produce meaningful contributions of heat and electricity to the home or small business. In large distributed quantities, a significant contribution to the grid may be possible. To do this, smaller roof-top friendly designs like ANU’s micro-concentrator show promise.

9.3 Sea-based CPV

Similarly, sea-based CPV can drastically reduce the size and cost of the cooling system. As such, it too can meet short term cost targets and even approach long term cost targets. For installations in Europe, where available land is a concern, the sea-based CPV systems may provide a utility scale solution. However, there are significant technical challenges to overcome. Drawing from oil platform technologies, it is hoped to create lightweight structures comparable in performance. The feasibility of such concepts remains to be demonstrated.

9.4 Insights and Accomplishments

Having summarized the cost targets and future outlook for low concentrating, linear-focus trough concentrators with silicon solar cell technology, this section will cover some of the important technological insights gained during this work. Many of the improvements investigated in this thesis have focused on thermally interfacing the CPV cells to the receiver. The reason for this is that many of the other components within

9. CONCLUSION

state of the art CPV receivers are similar to or adapted from one-sun solar technologies. Already, a great deal of research has been conducted in these areas. However, the thermal interface, and the design challenges that it imposes, is unique to the CPV receiver. At the beginning of this thesis, there were many unanswered questions with regard to how best to design such an interface. There seemed to be much to learn, much to optimize, and much more information to share with others.

One of the first questions was, “what is the limit of passive cooling for CPV receivers in linear-focus trough concentrators?” Here of course, shading is considered an issue. This thesis derived a geometric concentration limit, based on Bar-Cohen’s work with natural convection heat sinks, in the range of $X_g=15-30$. By extending the width of the heat sink an additional 25%, as calculated using Eq. 4.1, this limit might be extended to $X_g=37$.

Next, seven different CPV receiver designs were introduced and the performance of each design was assessed. The most interesting result from this study was the relatively small performance improvements predicted via direct immersion cooling of CPV cells. These improvements were predicted to be only a few percent. It was noted that the magnitude of such improvements could be easily matched by changes in the optical interface and perhaps outweighed by any fluid to cell interactions. Thus, the decision to utilize direct immersion cooling should be based on some unique positive impact of the cooling fluid itself, rather than its heat transfer capabilities. These heat transfer capabilities were established in this thesis, which is an important first step for this new technology. It has shown that future research should focus on better understanding the fluid to cell interactions.

To compare each of the seven designs, a unique method was necessary, and was derived as part of this thesis. Previous works have analyzed various heat transfer coefficients and cooling methods in CPV receivers [47]; however, these comparisons did not always include all components of the cooling system. For example, passive cooling technologies generally included a back cooler in their heat transfer coefficient, whereas active cooling technologies did not. By excluding the heat transfer coefficient of the back cooler, performance improvements via active cooling may have been exaggerated. The difficulty in making a fair comparison between passive and actively cooled designs lies in establishing a common and appropriate heat transfer coefficient for the back cooler. This challenge was overcome in this thesis by deriving an optimal size of back

cooling, expressed as a heat transfer coefficient, for a particular concentration ratio. By referencing all designs, and possible improvements thereof, to this common back cooler size, it was possible to make a fair comparisons between each design. To the best of the author's knowledge, this methodology is unique to this thesis. It is possible that it will become the new standard for future comparisons of thermal interfaces in CPV receivers.

To the best of the author's knowledge, this thesis is the first to derive a set of optimal fluid velocities, taking pumping losses into consideration, for direct immersion cooling. The optimal velocities were calculated for a range of fluid velocities, yielding within 1% power output of the optimum velocity. In doing so, one can then accommodate various lengths of CPV systems (number of CPV receivers connected in series). The relationship between the total system length and its various design parameters: concentration ratio, allowed system ΔT , and choice of coolant, is given in Figure 6.10. This graph, when used in conjunction with Table 6.3, allows the user to quickly understand the affect of fluid velocity on power output and system length. This is a unique tool, not previously presented, and greatly aids in quickly assessing design changes to a CPV system.

In general, this thesis serves as an excellent introduction and in depth analysis to various cooling strategies for CPV receivers, with a particular focus on linear-focus trough systems. Numerous receiver designs are discussed, and their performances relative to one another are described in Sections 6.7-6.8. Many of these results were derived by examining various design changes and their corresponding effects on performance. In Section 6.9, the discussion is opened up to economical considerations, where expanding the size of the back cooler is proposed. In this analysis, an increase to the back cooler, from its established value in Eq. 5.8, by 2 and 3.5 times is suggested. Such an increase would result in cell temperatures between 60 and 90°C, and would put the cost of the cooling system anywhere between 10 and 25% of the total system cost. Until more data, regarding the operating and cost of linear-focus trough CPV systems, becomes publicly available, these parameters may serve as useful guidelines for future CPV designs.

9.5 Future work

As previously stated, the goal of this thesis was to determine whether or not a low concentrating, linear-focus trough concentrator, utilizing silicon cells could meet grid

9. CONCLUSION

parity and whole-sale electricity prices in the foreseeable future. Answering such a question required the consideration of a wide scope of economic, engineering, and scientific subjects. As such, many assumptions were necessary. Due to the sheer breadth of this thesis, there are many areas where the underlying assumptions could be (and perhaps should be) reexamined and challenged.

As explained in Chapter 3, it remains to be proven that a system rated under the proposed NOC would in fact yield, within an acceptable tolerance, the equivalent kWh necessary to generate the revenues outlined in Table 3.1. To test the validity of the proposed NOC, one should either measure or simulate the performance of a particular CPV technology for numerous locations throughout the various regions of interest and compare the annual yields in kWh. If a reasonable correlation is found, then the NOC power rating and correlation to annual DNI may be appropriate. Otherwise, an economic model based on annual energy yield is necessary. However, in defense of the W_{NOC} rating proposed in this thesis, such calculations are used in initial economic studies for traditional one-sun photovoltaic technologies, utilizing the watt peak rating at standard testing conditions.

In future economic studies, the rate of return, O&M costs, and project lifetime might be reconsidered. More specifically, the 15% rate of return is rather high and reducing it would somewhat relax the total system cost targets. Further study into the O&M requirements and costs, either by testing or acquiring industry data, could be used to improve the accuracy of this parameter.

There are numerous assumptions in Chapters 5 and 6 which might be reconsidered. Modifying the CPV cell's temperature coefficient, γ_t , will change the optimum back cooler size vs. concentration ratio from Table 5.6. This will also change the power losses from the various interface designs given in Figure 6.13. Changing γ_t will also affect the optimum fluid velocities calculated in Section 6.4. Equation 6.6 should be incorporated into a more comprehensive computer coded simulation, in which γ_t , pipe roughness, pump efficiency, optical efficiency, and electrical efficiency could be quickly changed and solutions found for fluid velocities within 1% of the maximum power. These parameters were selected with the intention of representing a wide range of possible CPV receiver designs for silicon concentrator cells, but such a simulation would provide a convenient method for investigating alternative technologies. In addition, the fixed value of electrical operating efficiency assumed in this thesis could be solved for iteratively.

As a matter of simplification the fluid properties used in Eq. 6.6 were assessed at 25°C, even though the cell temperatures and corresponding power output were allowed to change with fluid velocities. Thus, losses due to fluid pumping are decoupled from operating temperatures whereas cell performance is coupled. This is a simplification, but is rather harmless. The difference in pumping losses for water at 10°C and 90°C is negligible in comparison to the effect on cell power output through γ_t . Nevertheless, for certain cooling fluids, it may be desirable to couple fluid properties with cell operating temperatures. This could also be incorporated into an improved simulation model.

In Section 6.6, the method used to calculate heat transfer coefficients for thermally conductive materials considers an ideal thermal interface, such as that shown in Figure 6.12 (a). Although the heat transfer coefficients calculated in this section fall within reported values [49], they should be experimentally validated for the materials identified in Table 6.6. The heat transfer coefficients may be significantly reduced based on the contact resistances. This would increase the potential improvements available to the direct immersion cooling strategies. Future work should examine the limit of thermal adhesives with respect to concentration ratio, especially considering the thermal expansion between the various materials making up the thermal interface.

If the direct immersion cooling strategies outlined in Chapter 7 are to be realized, more detailed study of the optical, electrical, and long-term effects of the candidate fluid on CPV cells is necessary. Furthermore, additional cooling fluids should be considered. Of particular importance, the shading effect discussed in 7.3.1 should be tested to determine its magnitude.

For future TU-Wien projects, an actively cooled CPV receiver should be fabricated and installed in the inflatable concentrator, in order to progress design work at the total system level. There are many known, but likely many more unknown, problems with such an installation, and it should be started as soon as possible. A modified version of ANU's CHAPS receiver is recommended for this purpose. The design challenges are significant, but so are the rewards. Good luck.

9. CONCLUSION

Appendix A

CPV Terminology from IEC-62108

Summary of CPV terminology per IEC-62108. See Ref. [38].

- concentrator -

term associated with photovoltaic devices that use concentrated sunlight

- concentrator cell -

basic photovoltaic device that is used under the illumination of concentrated sunlight

- concentrator optics -

optical device that performs one or more of the following functions from its input to output: increasing the light intensity, filtering the spectrum, modifying light intensity distribution, or changing light direction. Typically, it is a lens or a mirror. A primary optics receives unconcentrated sunlight directly from the sun. A secondary optics receives concentrated or modified sunlight from another optical device, such as primary optics or another secondary optics.

- concentrator receiver -

group of one or more concentrator cells and secondary optics (if present) that accepts concentrated sunlight and incorporates the means for thermal and electric energy transfer. A receiver could be made of several sub-receivers. The sub-receiver is a physically standalone, smaller portion of the full-size receiver.

- concentrator module -

group of receivers, optics, and other related components, such as interconnection

A. CPV TERMINOLOGY FROM IEC-62108

and mounting, that accepts unconcentrated sunlight. All of the above components are usually prefabricated as one unit, and the focus point is not field adjustable. A module could be made of several sub-modules. The sub-module is a physically stand-alone, smaller portion of the full-size module.

- concentrator assembly -

group of receivers, optics, and other related components, such as interconnection and mounting, that accepts unconcentrated sunlight. All of the above components would usually be shipped separately and need some field installation, and the focus point is field adjustable. An assembly could be made of several sub-assemblies. The sub-assembly is a physically stand-alone, smaller portion of the full-size assembly.

Table A.1: Terms IEC-62108 - Summary of terms used in CPV, reproduced from IEC-62108. See Ref. [38].

	Primary optics	<p>CPV Module: prefabricated and the focus point is not field adjustable, similar to most Fresnel lens systems.</p> <p>CPV Assembly: needs some field installation and the focus point is field adjustable, similar to most reflective systems.</p>
Secondary optics	CPV Receiver	
CPV cells		
Electric energy transfer means		
Thermal energy transfer means		
	Interconnection	
	Mounting	

Appendix B

Equations

B.1 List of Equations

Equation	Page	Description
3.1	28	Modification of Eq. 6.4 on page 32 of Ref. [66]. In Eq. 3.1 of this thesis, an additional term for a yearly operating and maintenance cost is included ($O\&M_i$).
4.1	56	This equation is derived in Section 4.3. It is derived from a series of equations that are nearly identical to Eq. 5.4-5.6. See Eq. 5.4-5.6 for further details.
4.2	58	See Appendix B.3.
4.3	58	See Appendix B.3.
5.1, 5.2	72	Refer to pages 46-49 of Ref. [67], Chapter 3, Section 3.2, entitled “Heat circuit analysis and terminology,” for an explanation of adding thermal interfaces. The source uses an analogy to Ohm’s law to describe the addition of thermal resistances in series and parallel. Equations 3.1-3.7 on page 48 of Ref. [67] provide an example, and Eq. 3.8 and 3.9 extend this method to heat transfer coefficients.
5.3	77	Generic equation derived in this thesis to describe the percent change in power output of a CPV cell due to the addition of a thermal interface.

continued on next page...

B. EQUATIONS

–continued from previous page–

Equation	Page	Description
5.4-5.6	78	See explanation in Appendix B.4
5.7	78	See explanation in Appendix B.5.
5.8	80	Rearrangement of Eq. 5.7 to solve for h_{bc} .
6.1	93	Adapted from Eq. 7.63 on page 373 of Ref. [51]. See all of Chapter 6 of Ref. [51] for an introduction to the laminar flow regime.
6.2	94	Rearrangement of Eq. 6.1 to solve for h_{lam} .
6.3-6.5	96	See Appendix B.6.
6.6-6.10	97	HTCs for turbulent flow in a pipe, as described on page 150 of Ref. [52]. Eq. 6.6 relates h_{trb_x} to the Nusselt number. Eq. 6.7 calculates the Nusselt number. Eq. 6.8 and 6.9 calculate the thermal expansion coefficient and Reynolds number, respectively. Eq. 6.10 gives the hydraulic diameter of a square pipe.
6.11	100	See Appendix B.8.
6.12	102	HTCs for pool boiling using methods described by VDI. See Eq. 5 on page 761 of Ref. [53]
6.13, 6.14	103	Modification parameters for non-standard states in Eq. 6.12. See Eq. 6 and 6a on pages 761-762 of Ref. [53], respectively.
6.15, 6.16	103	HTCs for pool boiling using methods derived by Mostinski. See Eq. 9.2b and 9.4 on pages 388-389 of Ref. [68].
6.17-6.20	106	See Ref. [56] for a detailed explanation regarding the calculation of thermal resistance for thermally conducting materials.
6.21	110	Modification of Eq. 5.1 in this thesis (addition of two series connected thermal interfaces) to fit the terminology used in Section 6.7.
6.22-6.24	116	See Appendix B.9.
7.1, 7.2	128	GWP targets for potential cooling fluids. Derived and proposed as part of this thesis work. See Section 7.2.
7.3	134	See Eq. 1.4 on page 52 of Ref. [69].
7.4 - 7.5	135	See pages 43-44 of Ref. [64].
7.6	136	See Eq. 2.61 on page 44 of Ref. [64].

B.2 Assumptions

Table B.2: Assumed Parameters - Parameters used for various optimizations.

<i>Parameter</i>	Value	Unit
G_N	900	$\frac{W}{m^2}$
η_{stc}	0.17	-
γ_t	0.004	$^{\circ}C^{-1}$
η_o	0.80	-
R_{rel}	0.001	-
η_p	0.5	-

B.3 Bar-Cohen limit to passive cooling Eq. 4.2-4.3

Equation 4.2:

$$X_g = \frac{h_{coh} \Delta T_{cell-amb}}{G_N \eta_o (1 - \eta_e)}$$

Equation 4.2 can be broken down into two main terms, namely, the numerator and the denominator of the equation. The numerator represents the maximum heat flux that can be transferred, assuming the maximum HTC for natural convection, h_{coh} , at a temperature difference given by $\Delta T_{cell-amb}$. The denominator essentially defines the heat flux for $X_g=1$, assuming a direct normal irradiation value given by G_N and an optical and electrical efficiency of η_o and η_e respectively. Dividing the maximum heat flux by the heat flux at $X_g=1$, gives the concentration ratio X_g for passive cooling.

Equation 4.3:

$$X_g = \frac{h_{coh} \left(1 + \frac{\Delta W}{W_{rec}}\right) \Delta T_{cell-amb}}{G_N \eta_o (1 - \eta_e)}$$

To derive Eq. 4.3, Eq. 4.2 is multiplied by the parameter $1 + \Delta W/W_{rec}$. This additional term represents the increase in cooler area that is available to transfer heat at h_{coh} . The values for $\Delta W/W_{rec}$ are derived from Eq. 4.1. This equation assumes that an increase in area of the cooler would not have any detrimental effects with regard to h_{coh} . In practice this is not true, as the fin efficiency of the cooler would decrease. However, this analysis is intended only to describe possible extensions to the passive cooling limit, rather than to calculate them exactly.

B. EQUATIONS

B.4 Explanation of CPV cell power density Eq. 5.4-5.6

Equation 5.4:

$$p = G_N X_g \eta_o \eta_e$$

The power output of a CPV cell, in terms of power density, is described by Eq. 5.4. Power density is a measure of CPV cell power output divided by the cell's active area. Active area is considered the design's target area. It is the area of the cell intended for illumination. Active area can be calculated by multiplying the length of the CPV cell (along the axis of the linear concentrator, i.e. parallel to the CPV cell's bus-bars) by the width of the CPV cell (distance between the bus-bars).

Equation 5.4 may be derived by multiplying the incoming direct normal solar irradiation, G_N , in W/m² by the geometric concentration factor, X_g , by the efficiency of the CPV cell η_e (see Eq. 5.5). An additional parameter, η_o , represents an average optical efficiency of the entire CPV system. This factor is included as a simplification of all optical losses in the CPV system. An optical loss is defined as a unintentional loss of light that could be used in the CPV system. For example, such losses might include the less than perfect reflection and transmission in the optics.

Equation 5.5:

$$\eta_e = \eta_{stc}(1 - \Delta T_{stc} \gamma_t)$$

Equation 5.5 represents the operating efficiency of the CPV cell. It was adopted from Eq. 7.36 on page 223 of Ref. [70]. The efficiency of the CPV cell under one-sun photovoltaic standard test conditions, η_{stc} , is modified by the parameter $(1 - \Delta T_{stc} \gamma_t)$ to account for the operating temperature of the CPV cell. Here, ΔT_{stc} represents the operating temperature of the CPV cell above or below the standard test condition, 25°C, and is calculated using Eq. 5.6. The parameter γ_t represents the CPV cell's power efficiency temperature coefficient and approximates the corresponding decrease in cell efficiency for a 1°C increase in operating temperature above 25°C.

Equation 5.6:

$$\Delta T_{stc} = \frac{G_N X_g \eta_o (1 - \eta_e)}{h_{total}}$$

Equation 5.6 is an expression of Eq. 3.8 on page 48 of Ref. [67]. Equation 3.8, a common expression for heat transfer problems, reads $q = h\Delta T$, where q , h , and ΔT

B.5 Optimal concentration factor for fixed HTC, Eq. 5.7

represent heat flux (W/m^2), a heat transfer coefficient ($\text{W}/\text{m}^2\text{K}$), and a temperature difference (K or $^{\circ}\text{C}$) respectively. It may be rearrange to solve for ΔT as $\Delta T = q/h$. Equation 5.6 takes this same form with $G_N X_g \eta_o (1 - \eta_e)$ representing q and h_{total} representing h . The heat reaching the CPV cell is calculated by considering the energy reaching the cell, $G_N X_g$, and subtracting any optical losses as well as electrical energy conversion. The parameter η_o represents the optical efficiency of the system. It has the same value as used in Eq. 5.4, which is somewhat of a simplification, as some optical losses may in fact heat the CPV cells. The parameter $(1 - \eta_e)$ subtracts the electrical energy converted by the CPV cell, leaving the remaining energy as a heat load.

B.5 Optimal concentration factor for fixed HTC, Eq. 5.7

Beginning with Eq. 5.5, insert ΔT_{stc} from Eq. 5.6.

$$\begin{aligned} \eta_e &= \eta_{stc} (1 - \Delta T_{stc} \gamma_t) \\ \Delta T_{stc} &= \frac{G_N X_g \eta_o (1 - \eta_e)}{h_{total}} \\ &= \eta_{stc} \left[1 - \left(\frac{G_N X_g \eta_o (1 - \eta_e)}{h_{total}} \right) \gamma_t \right] \\ &= \eta_{stc} - \eta_{stc} \frac{G_N X_g \eta_o \gamma_t}{h_{total}} (1 - \eta_e) \end{aligned}$$

$$\eta_e h_{total} = \eta_{stc} h_{total} - \eta_{stc} G_N X_g \eta_o \gamma_t (1 - \eta_e)$$

$$\eta_e h_{total} = \eta_{stc} h_{total} - \eta_{stc} G_N X_g \eta_o \gamma_t + \eta_e (\eta_{stc} G_N X_g \eta_o \gamma_t)$$

$$0 = \eta_{stc} h_{total} - \eta_{stc} G_N X_g \eta_o \gamma_t + \eta_e (\eta_{stc} G_N X_g \eta_o \gamma_t) - \eta_e h_{total}$$

B. EQUATIONS

$$\eta_{stc} G_N X_g \eta_o \gamma_t - \eta_{stc} h_{total} = \eta_e (\eta_{stc} G_N X_g \eta_o \gamma_t) - \eta_e h_{total}$$

$$\eta_{stc} G_N X_g \eta_o \gamma_t - \eta_{stc} h_{total} = \eta_e (\eta_{stc} G_N X_g \eta_o \gamma_t - h_{total})$$

$$\eta_e = \frac{\eta_{stc} G_N X_g \eta_o \gamma_t - \eta_{stc} h_{total}}{\eta_{stc} G_N X_g \eta_o \gamma_t - h_{total}} \quad (\text{B.1})$$

Insert the newly derived expression for η_e into Eq. 5.4, so as to remove parameters ΔT_{stc} and η_e .

$$p = G_N X_g \eta_o \eta_e$$

$$p = G_N X_g \eta_o \frac{\eta_{stc} G_N X_g \eta_o \gamma_t - \eta_{stc} h_{total}}{\eta_{stc} G_N X_g \eta_o \gamma_t - h_{total}}$$

Introduce and insert constants C_1 and C_2 into the expression above, so as to improve the aesthetics and aid the reader in forth coming derivation.

$$C_1 = G_N \eta_o \quad C_2 = G_N \eta_o \eta_{stc} \gamma_t$$

$$p = C_1 X_g \left(\frac{C_2 X_g - \eta_{stc} h_{total}}{C_2 X_g - h_{total}} \right)$$

Take the partial derivative of power density, p , with respect to geometric concentration ratio, X_g :

B.5 Optimal concentration factor for fixed HTC, Eq. 5.7

$$\begin{aligned}
\frac{\partial p}{\partial X_g} &= C_1 X_g \frac{\partial}{\partial X_g} \left(\frac{C_2 X_g - \eta_{stc} h_{total}}{C_2 X_g - h_{total}} \right) + \left(\frac{C_2 X_g - \eta_{stc} h_{total}}{C_2 X_g - h_{total}} \right) \frac{\partial}{\partial X_g} (C_1 X_g) \\
&= C_1 X_g \left(\frac{(C_2 X_g - h_{total})(C_2) - (C_2 X_g - \eta_{stc} h_{total})(C_2)}{(C_2 X_g - h_{total})^2} \right) \\
&\quad + C_1 \left(\frac{C_2 X_g - \eta_{stc} h_{total}}{C_2 X_g - h_{total}} \right) \\
&= C_1 X_g \left(\frac{-C_2 h_{total} + C_2 \eta_{stc} h_{total}}{(C_2 X_g - h_{total})^2} \right) + C_1 \left(\frac{C_2 X_g - \eta_{stc} h_{total}}{C_2 X_g - h_{total}} \right) \\
&= C_1 \left(\frac{-C_2 h_{total} X_g + C_2 \eta_{stc} h_{total} X_g}{(C_2 X_g - h_{total})^2} \right) \\
&\quad + C_1 \left(\frac{(C_2 X_g - \eta_{stc} h_{total})(C_2 X_g - h_{total})}{(C_2 X_g - h_{total})^2} \right) \\
\frac{\partial p}{\partial X_g} &= \frac{C_1 [C_2^2 X_g^2 - 2 C_2 h_{total} X_g + \eta_{stc} h_{total}^2]}{(C_2 X_g - h_{total})^2}
\end{aligned}$$

Set $\partial p/\partial X_g=0$ and solve for X_g using the quadratic formula

$$\frac{\partial p}{\partial X_g} = 0 = C_2^2 X_g^2 - 2 C_2 h_{total} X_g + \eta_{stc} h_{total}^2$$

$$X_g = \frac{-b/2 \pm \sqrt{(b/2)^2 - ac}}{a}$$

$$a = C_2^2$$

$$b = -2 C_2 h_{total}$$

$$c = \eta_{stc} h_{total}^2$$

B. EQUATIONS

$$\begin{aligned}
 X_g &= \frac{C_2 h_{total} \pm \sqrt{(-C_2 h_{total})^2 - C_2^2 \eta_{stc} h_{total}^2}}{C_2^2} \\
 &= \frac{C_2 h_{total} \pm \sqrt{(-C_2 h_{total})^2 - \eta_{stc} (C_2 h_{total})^2}}{C_2^2} \\
 &= \frac{C_2 h_{total} \pm C_2 h_{total} \sqrt{1 - \eta_{stc}}}{C_2^2} = \frac{h_{total} \pm h_{total} \sqrt{1 - \eta_{stc}}}{C_2}
 \end{aligned}$$

Substitute back in constant C_2 to arrive at:

$$X_g = \frac{h_{total} \pm h_{total} \sqrt{1 - \eta_{stc}}}{G_N \eta_o \eta_{stc} \gamma t}$$

Only one of the two solutions yields a physically meaningful result. The other is removed, and one arrives at Eq. 5.7:

Equation 5.7:

$$X_g = \frac{h_{total} - h_{total} \sqrt{1 - \eta_{stc}}}{G_N \eta_o \eta_{stc} \gamma t}$$

B.6 Power of the unit-cell Eq. 6.3-6.5

Equation 6.3:

$$P_{cell} = G_N X_g A_c \eta_o \eta_e - \frac{\Delta P_p Q_{fl}}{\eta_p}$$

Equation 6.3 represents the power output of the unit-cell, taking into consideration its corresponding pumping losses. It may be derived by multiplying power density, given by Eq. 5.4, by an active area, and subtracting its pumping losses, P_{pump} . The active area is defined by the unit-cell and represented by A_c .

The pumping losses, P_{pump} , represent the power needed to overcome the frictional losses arising from the fluid flowing through a section of receiver (cooling channel in Designs C and D or the receiver itself in Designs E and F), considering a length equal to the unit-cell. The frictional losses create a pressure drop that must be compensated by the pump. The pressure drop, ΔP_p , may be calculated by,

$$\Delta P_p = \frac{2\rho f L u^2}{d_h}$$

where “ ρ ” represents density, “ f ” represents the Darcy friction factor (see Eq. 6.4), “ L ” represents pipe length (unit-cell length), “ u ” represents fluid velocity, and “ d_h ” represents hydraulic diameter of the pipe. This formula can be found in many introductory fluid dynamic textbooks and is presented in numerous forms. For this thesis, the formula was adapted from Eq. 2.12 on page 36 of Ref. [71]. The power necessary to overcome the pressure loss may be calculated by,

$$P_{pump} = \frac{\Delta P_p Q_{fl}}{\eta_p}$$

where “ Q_{fl} ” represents the volumetric flow rate of the fluid and “ η_p ” represents the operating efficiency of the pump. The formula was adapted from Eq. 8.1 on page 240 of Ref. [72]. It is assumed that $\eta_p=0.5$ (see page 255 of Ref. [72] for an explanation).

B. EQUATIONS

Equation 6.4:

$$f = \left[-2 \log_{10} \left(\frac{R_{rel}}{3.7} + \frac{5.74}{Re^{0.9}} \right) \right]^{-2}$$

The friction factor, Eq. 6.4, is calculated from the Swamee and Jain explicit approximation of the Colebrook equation. See Ref. [73] for further details.

Equation 6.5:

$$\eta_e = \frac{\eta_{stc} G_N \eta_o X_g \gamma_t - \eta_{stc} h_{trb_X}}{\eta_{stc} G_N X_g \eta_o \gamma_t - h_{trb_X}}$$

Equation 6.5 is derived by the insertion of ΔT_{stc} from Eq. 5.6 into Eq. 5.5. See Eq. B.1 in Appendix B.5 for its derivation. However, please note that the term h_{total} was replaced by h_{trb_X} . For an explanation behind this change in nomenclature, please refer back to the last paragraph of Section 6.2.

B.7 GWP values

The calculations for recommended GWP values, as described in Section 7.2, are given here. Please note that L =liters and m =meters.

$$GWP = \frac{(M_{CO_2} - M_{CPV}) \cdot DNI_{(an)} \cdot t}{V_{NOC} \cdot \rho}$$

$$V_{NOC}(X_g = 40) = \frac{1.0L}{m} \cdot \frac{1.4m}{130W} \cdot \frac{1000W_{NOC}}{kW_{NOC}} = 10.8 \frac{L}{kW_{NOC}}$$

$$V_{NOC}(X_g = 80) = \frac{1.0L}{m} \cdot \frac{1.4m}{260W} \cdot \frac{1000W_{NOC}}{kW_{NOC}} = 5.4 \frac{L}{kW_{NOC}}$$

$$GWP(X_g = 40) = \frac{(0.975 - 0.150) \frac{kg CO_2}{kWh} \cdot 2000 \frac{kWh}{kW_{NOC} \cdot yr} \cdot 20 yr}{10.8 \frac{L}{kW_{NOC}} \cdot 1.6 \frac{kg_{HFC}}{L}} = 1,910 \frac{kg CO_2}{kg HFC}$$

$$GWP(X_g = 80) = \frac{(0.975 - 0.150) \frac{kg CO_2}{kWh} \cdot 2000 \frac{kWh}{kW_{NOC} \cdot yr} \cdot 20 yr}{5.4 \frac{L}{kW_{NOC}} \cdot 1.6 \frac{kg_{HFC}}{L}} = 3,784 \frac{kg CO_2}{kg HFC}$$

B.8 Maximum series connected CPV receiver length

$$\frac{Q}{\dot{m}c} = \Delta T_L = \frac{q \cdot L \cdot d_h}{\rho \cdot Q_{fl} \cdot c} = \frac{G_N X_g \eta_o (1 - \eta_e) L d_h}{\rho (0.25 \pi \cdot d_h^2 \cdot u) c} \quad (\text{B.2})$$

$$L = \frac{\rho \cdot \pi \cdot d_h \cdot c \cdot u \cdot \Delta T_L}{4 G_N X_g \eta_o (1 - \eta_e)} \quad (\text{B.3})$$

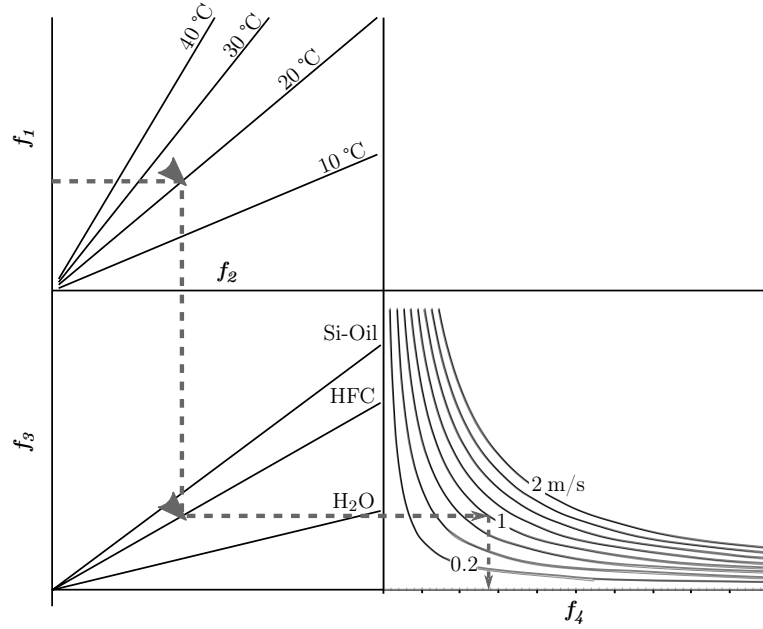


Figure B.1: Four Square Graphs Explained

$$f_1(X_g) = X_g \quad (\text{B.4})$$

$$f_2(f_1) = \frac{f_1}{\Delta T_L} \quad (\text{B.5})$$

$$f_3(f_2) = \frac{4 G_N \eta_o (1 - \eta_e)}{\rho \pi d_h c} f_2 \quad (\text{B.6})$$

$$f_4(f_3) = \frac{u}{f_3} \quad (\text{B.7})$$

$$= L \quad (\text{see Eq. B.3})$$

B. EQUATIONS

B.9 Performance and cost utility functions: Eq. 6.22-6.24

In Section 6.9, the concept of marginal utility is utilized to understand the increase in performance or cost for an increase in cooler cost. Marginal utility is the measure of utility gained from an increase in consumption of a good. This concept is covered in many introductory and intermediate-level economic textbooks. For example, it is covered in Chapter 2 of Ref. [74]. For the purpose of Section 6.9 of this thesis, utility is measured in terms of performance (power output) and total system cost, where “increase in consumption of a good” refers to an increase in the size and cost of the cooling system.

Marginal performance (MP) is defined as a percentage change in power output, where power output is defined using Eq. 5.4, from system “ n ” to system “ $n + 1$.” The term “ n ” serves to denote successive “ n -increases” in the size of the back cooler, where each “ n ” represents a 1% increase in both the size (in terms of h_{bc}) and cost of the back cooler.

$$MP = \frac{G_N X_g \eta_o \eta_e(n+1) - G_N X_g \eta_o \eta_e(n)}{G_N X_g \eta_o \eta_e(n)}$$

MP may be reduced further as it is only dependent on cell operating efficiency “ η_e .”

$$MP = \frac{\eta_e(n+1) - \eta_e(n)}{\eta_e(n)}$$

Substituting “ η_e ” for Eq. 5.5 gives:

$$MP = \frac{\eta_{stc}(1 - \Delta T_{n+1} \gamma_t) - \eta_{stc}(1 - \Delta T_n \gamma_t)}{\eta_{stc}(1 - \Delta T_n \gamma_t)}$$

Further algebraic manipulation leads to:

Equation 6.22

$$MP = \frac{(1 - \Delta T_{n+1} \gamma_t)}{(1 - \Delta T_n \gamma_t)} - 1 \quad \boxed{MP = \left[\frac{1 - \Delta T_o (1 - r)^{(n+1)} \gamma_t}{1 - \Delta T_o (1 - r)^{(n)} \gamma_t} \right] - 1}$$

Each successive increase in cooler size will increase the total system cost of the CPV system. The total system cost can be calculated for any value of “ n ” by,

$$TSC(n) = C_o(1 + r)^{(n)} + E_o$$

B.9 Performance and cost utility functions: Eq. 6.22-6.24

where “ C_o ” represents the initial cost of the cooling system, “ r ” represents the rate of increase (i.e. 1%). Marginal total system cost (MTSC), Eq. 6.23, may be calculated by considering cases “ n ” and “ $n + 1$.”

Equation 6.23

$$\boxed{MTSC} = \frac{TSC(n+1) - TSC(n)}{TSC(n)} = \left[\frac{TSC(n+1)}{TSC(n)} \right] - 1 = \boxed{\left[\frac{E_o + C_o(1+r)^{(n+1)}}{E_o + C_o(1+r)^{(n)}} \right] - 1}$$

With further algebraic manipulation one may arrive at the following expression:

$$MTSC = \left[\frac{\frac{E_o}{E_o} + \frac{C_o}{E_o}(1+r)^{(n+1)}}{\frac{E_o}{E_o} + \frac{C_o}{E_o}(1+r)^{(n)}} \right] - 1 = \left[\frac{1 + \frac{C_o}{E_o}(1+r)^{(n+1)}}{1 + \frac{C_o}{E_o}(1+r)^{(n)}} \right] - 1 \quad (\text{B.8})$$

To reduce the number of variables in Eq. B.8, the parameter C_r is introduced, where $C_r = C_o/(C_o + E_o)$ and represents the initial cost of the back cooler as a percentage of total system cost.

$$\begin{aligned} C_r &= \frac{C_o}{C_o + E_o} = \frac{C_o}{E_o} \cdot \frac{1}{\frac{C_o}{E_o} + 1} \\ C_r \left(\frac{C_o}{E_o} + 1 \right) &= \frac{C_o}{E_o} \\ C_r \frac{C_o}{E_o} + C_r &= \frac{C_o}{E_o} \\ C_r &= \frac{C_o}{E_o} - C_r \frac{C_o}{E_o} \\ C_r &= \frac{C_o}{E_o} (1 - C_r) \\ \frac{C_r}{(1 - C_r)} &= \frac{C_o}{E_o} \end{aligned}$$

By substituting $\frac{C_r}{1-C_r}$ for $\frac{C_o}{E_o}$ in Eq. B.8 one arrives at:

Equation 6.24

$$MTSC = \left[\frac{1 + \frac{C_r}{1-C_r}(1+r)^{(n+1)}}{1 + \frac{C_r}{1-C_r}(1+r)^{(n)}} \right] - 1$$

B. EQUATIONS

Appendix C

Additional Tables and Figures

C. ADDITIONAL TABLES AND FIGURES

Table C.1: World Wide CSP Potential in km² - World wide land surfaces in km² deemed acceptable for CSP development [18]. Totals according to direct normal irradiation (DNI) class and region are shown in the last row and column respectively. The three regions with the greatest square kilometers of solar resource are highlighted for each DNI class.

Land	DNI Class [kWh/(m ² .yr)]				Total [km ²]
	2000-2199	2200-2399	2400-2599	2600-2800+	
Africa	2,477,950	2,657,220	3,606,120	4,215,070	12,956,360
Australia	257,910	1,167,700	3,091,230	1,566,610	6,083,450
Mid. East	161,997	935,953	932,749	557,949	2,588,648
S. America	542,023	424,445	88,475	136,004	1,190,947
China	272,776	678,824	196,364	42,374	1,190,338
USA	322,031	361,998	281,831	19,144	985,004
Asia	99,782	390,731	209,898	3,166	703,577
Mexico	51,122	89,028	200,427	27,531	368,108
Cen. Asia	154,134	5,236	569	0	159,939
India	95,032	12,479	3,890	1,096	112,497
EU27+	14,179	7,879	1,391	527	23,976
Europe	188	23	0	0	211
Japan	0	0	0	0	0
Canada	0	0	0	0	0
Russia	0	0	0	0	0
S. Korea	0	0	0	0	0
Total [km²]	4,449,124	6,731,516	8,612,944	6,569,471	26,363,055

Table C.2: CSP Potential as Percent of Total km² - Of the total 26,363,055 km² identified by [18], the following data provide the relative percent share held within each direct normal irradiation (DNI) class index and country or region. Totals according to DNI class and region are shown in the last row and column respectively. The three regions with the greatest share of the total land deemed suitable for CSP [18] are highlighted for each DNI class.

Land	DNI Class [kWh/(m ² ·yr)]				Total [%]
	2000-2199	2200-2399	2400-2599	2600-2800+	
Africa	9.4	10.1	13.7	16.0	49.1
Australia	1.0	4.4	11.7	5.9	23.1
Mid. East	0.6	3.6	3.5	2.1	9.8
S. America	2.1	1.6	0.3	0.5	4.5
China	1.0	2.6	0.7	0.2	4.5
USA	1.2	1.4	1.1	0.1	3.7
Asia	0.4	1.5	0.8	0.0	2.7
Mexico	0.2	0.3	0.8	0.1	1.4
Cen. Asia	0.6	0.0	0.0	0.0	0.6
India	0.4	0.0	0.0	0.0	0.4
EU27+	0.1	0.0	0.0	0.0	0.1
Europe	0.0	0.0	0.0	0.0	0.0
Japan	0.0	0.0	0.0	0.0	0.0
Canada	0.0	0.0	0.0	0.0	0.0
Russia	0.0	0.0	0.0	0.0	0.0
S. Korea	0.0	0.0	0.0	0.0	0.0
Total [%]	16.9	25.5	32.7	24.9	-

C. ADDITIONAL TABLES AND FIGURES

Table C.3: BOM - Condensed version of the bill of materials (BOM).

Part Name	Quantity		Unit	€/Unit		Total €	
	Part	Unit		Low	High	Low	High
Extrusion	1	3	kg	3.50	5.50	10.50	16.50
Thermal Tape	1	1.32	m	12.00	24.00	15.84	31.68
Solar Cells	26	26	cell	1.26	1.40	32.76	36.40
Copper Tabs	104	104	tab	0.014	0.024	1.43	2.47
Solder - Cell to Tab	1	0.026	kg	40.00	40.00	1.04	1.04
Encapsulant	1	0.439	kg	28.39	33.92	12.46	14.90
Glass	1	1	-	3.41	6.82	3.41	6.82
Female WtrCon	1	1	-	17.00	17.00	17.00	17.00
Male WtrCon	1	1	-	7.90	7.90	7.90	7.90
BPD & Wiring Assy	1	1	-	18.90	21.45	18.90	21.45

Table C.4: BOM Total Cost Summary - Total costs of the CPV receiver and cooling system. ¹1000 W/m², 25°C, <1m/s. ²900 W/m², 65°C, <3m/s, $\eta_o = 0.8$, parasitic losses at 10%. ³ Assy Receiver + Cooler cost divided by the relative percentage costs of 28.4% and 37.9% for the Low and High estimates, from Figures 3.3 and 3.4 respectively. See Chapter 3, Section 3.6.

Absolute Costs € and €/m	Low	High
Material Costs per receiver	106.78	141.85
Material Costs per meter	74.15	98.51

Costs in €/W _p @ STC ¹	Low	High
Receiver Material Costs	0.447	0.594
Receiver Manufacturing Costs	0.105	0.139
Cost of Assembled Receiver	0.552	0.734
Cooler Cost	0.676	1.35
Cost of Assy Receiver + Cooler	1.23	2.09
Estimated Total System Cost ³	4.39	5.49

Costs in €/W _{NOC} ²	Low	High
Receiver Material Costs	0.592	0.786
Receiver Manufacturing Costs	0.139	0.184
Cost of Assembled Receiver	0.731	0.971
Cooler Cost	0.676	1.35
Cost of Assy Receiver + Cooler	1.41	2.32
Estimated Total System Cost ³	5.02	6.11

C. ADDITIONAL TABLES AND FIGURES

References

- [1] **Los Angeles Times: Climate skeptic admits he was wrong to doubt global warming data**, October 20, 2011.
- [2] **New York Daily News: Richard Muller, Koch brothers-funded scientist, declares global warming is real**, October 31, 2011.
- [3] **Renewable Energy World.com: Why the Energy Transition is Longer Than We Admit**, April 22, 2010.
- [4] JOERI ROGELJ, WILLIAM HARE, JASON LOWE, DETLEF P. VAN VUUREN, KEYWAN RIAHI, BEN MATTHEWS, TATSUYA HANAOKA, KEJUN JIANG, AND MALTE MEINSHAUSEN. **Emission pathways consistent with a 2°C global temperature limit**. *Nature Clim. Change*, 1(8):413–418, November 2011.
- [5] RACHEL WARREN. **The role of interactions in a world implementing adaptation and mitigation solutions to climate change**. *Philosophical Transactions of the Royal Society A: Mathematical, Physical and Engineering Sciences*, 369(1934):217–241, 2011.
- [6] NICHOLAS STERN. *The Economics of Climate Change*. The Stern Review, 2007.
- [7] M.R. SWANSON. **The Promise of Concentrators**. *Progress in Photovoltaics: Research and Applications*, 8:93–111, 2000.
- [8] G. SALA, D. PACHON, I. ANTON, E. CAAMANO, W. WARTA, G. SIEFER, R. KENNY, R. KERN, F.P. SPIESS, AND A. LINARES. **C-Rating Project Final Report Book1 Chapter 3 The History of Modern Concentrators**. Technical report, IES of UPM, 2003.
- [9] E. C. BOES AND A. LUQUE. *Photovoltaic Concentrator Technology*, chapter 8, pages 361–401. Island Press, 1993.
- [10] S. KURTZ. **Opportunities and Challenges for Development of a Mature Concentrating Photovoltaic Power Industry**. Technical report, NREL, 2009.
- [11] WORK GROUP 3 OF THE EU PV TECHNOLOGY PLATFORM. **A Strategic Research Agenda for Photovoltaic Solar Energy Technology**. Technical report, EU PV Technology Platform, 2007.
- [12] V. WITTEWER, W. STAHL, AND A. GOETZBERGER. **Fluorescent planar concentrators**. *Solar Energy Materials*, 11(3):187 – 197, 1984.
- [13] **Renewable Energy World.com: Solar Silicon Market a Seller’s Paradise**, February 14, 2005.
- [14] **Bloomberg: Solar Glut Worsens as Supply Surge Cuts Prices 93Commodities**, November 10, 2011.
- [15] **Efficiency Matters: SunPower Sets Efficiency Record With a 20% Module**. <http://www.greentechmedia.com/articles/read/Efficiency-Matters-SunPower-Sets-Efficiency-Record-With-a-20-Module/>, June 2011.
- [16] SOITEC. **Soitec’s Concentrix Technology**. <http://www.soitec.com/en/technologies/concentrix/>, Nov 2011.
- [17] AMONIX. **CPV Technology, Multijunction Solar Cells Pioneers**. <http://amonix.com/content/cpv-technology>, November 2011.
- [18] FRANZ TRIEB, CHRISTOP SCHILLINGS, MARLENE O’SULLIVAN, THOMAS PREGGER, AND HOYER-KLICK CARSTEN. **Global Potential of Concentrating Solar Power**. In *Proceedings of the SolarPaces Conference Berlin*, 2009.
- [19] A. BLAKERS. **Efficient 20-50 Sun Concentrator Cells**. In *Proceedings of the 16th EU PVSEC*, 2000.
- [20] J. SMETLINK, A. BLAKERS, AND S. HIRON. **The 20 kW PV/Trough Concentrator**. In *Proceedings of the 2nd World Conference on Photovoltaic Energy Conversion*, pages 2193–2195, 1998.
- [21] J. SMETLINK, A. BLAKERS, AND S. HIRON. **The ANU 20kW PV/Trough Concentrator**. In *Melbourne Conference*, 1999.
- [22] J. COVENTRY. *A solar concentrating photovoltaic/thermal collector*. PhD thesis, Australian National University, 2004.
- [23] J. SMETLINK AND A. BLAKERS. **40kW PV Thermal Roof Mounted Concentrator System**. In *Proceedings of the IEEE 4th World Conference on Photovoltaic Energy Conversion*, 2006.
- [24] J. SMETLINK AND A. BLAKERS. **A hybrid pv-thermal linear microconcentrator for domestic application**. In *Proceedings of the 22nd European Photovoltaic and Solar Energy Conference and Exhibition*, 2007.
- [25] I. ANTON AND G. SALA. *Concentrator Photovoltaics: The EUCLIDES Concentrator*. Springer, 2007.
- [26] A. LUQUE, G. SALA, J.C. ARBOIRO, T. BRUTON, D. CUNNINGHAM, AND N. MASON. **Some Results of the EUCLIDES Photovoltaic Concentrator**. *Progress in Photovoltaics: Research and Applications*, 5:195–212, 1997.
- [27] G. SALA, A. LUQUE, J.C. ZAMORANO, P. HEUERGO, AND J.C. ARBOIRO. **Lightweight Heat Sinks for the EUCLIDES Concentrator Array**. In *Proceedings of the 13th European Photovoltaic and Solar Energy Conference and Exhibition*, 1995.

REFERENCES

- [28] G. SALA, J. C. ARBOIRO, A. LUQUE, I. ANTÓN, M. P. GASSON, N. B. MASON, K. C. HEASMAN, T. M. BRUNTON, E. MERA, E. CAMBLOR, P. DATTA, M. CENDAGORTA, M. P. FRIEND, P. VALERA, S. GONZÁLEZ, F. DOBÓN, AND F. PÉREZ. **480 kW peak EUCLIDES concentrator power plant using parabolic troughs**. In *Proceedings of the 2nd World Conference on Photovoltaic Solar Energy Conversion*, pages 1963–1968, 1998.
- [29] G. SALA, I. ANTÓN, J. C. ARBOIRO, A. LUQUE, E. CAMBLOR, E. MERA, M. GASSON, M. CENDAGORTA, P. VALERA, M. P. FRIEND, J. MONDERO, S. GONZÁLEZ, F. DOBÓN, AND I. LUQUE. **The 480kWp EUCLIDES Thermie Power Plant Installation Set-Up and First Results**. In *Proceedings of the 16th European Photovoltaic and Solar Energy Conference and Exhibition*, 2000.
- [30] V. EVERETT, J. HARVEY, M. VIVAR, E. THOMSEN, M. FUENTES, M. EBERT, P. LE. LIEVRE, M. GREAVES, A. TANNER, AND A. BLAKERS. **Electrical and Thermal Performance of the ANU-Chromasun Micro-Concentrator System**. In *Proceedings of the 26th European Photovoltaic Solar Energy Conference*, 2011.
- [31] M. O NEIL, A. J. McDANAL, D. SPEARS, C. STEVENSON, AND D. GELBAUM. **Low-Cost 20X Silicon-Cell-Based Linear Fresnel Lens Concentrator Panel**. In *Paper presented at 7th International Conference on Concentrating Photovoltaic Systems*, 2011.
- [32] M. FINOT, A. MAYO, AND B. MACDONALD. **High Volume Silicon Cell Technologies Enabling Low-Cost CPV Systems**. In *Proceedings of the 26th European Photovoltaic Solar Energy Conference*, 2011.
- [33] J. SMETLINK AND A. BLAKERS. **A Hybrid PV-Thermal Linear Concentrator for Domestic Applications**. In *Presentation*, 2007.
- [34] M. VIVAR, R. VAN SCHEPPINGEN, M. CLARKE, V. EVERETT, D. WALTER, J. HARVEY, S. SURVE, J. MURIC- NESIC, AND A. BLAKERS. **Integrating the design and reliability assessment of a hybrid Pv-Thermal microconcentrator system**. In *Photovoltaic Specialists Conference (PVSC), 2010 35th IEEE*, pages 3098 – 3103, 2010.
- [35] M. VIVAR. *Optimization of the EUCLIDES Photovoltaic Concentrator*. PhD thesis, Universidad Politécnica de Madrid, 2009.
- [36] C. BREYER, A. GERLACH, J. MÜLLER, H. BEHACKER, AND A. MILNER. **Grid-Parity Analysis for EU and US Regions and Market Segments - Dynamics of Grid-Parity and Dependence on Solar Irradiance, Local Electricity Prices and PV Progress Ratio**. In *Proceedings of the 24th European Photovoltaic Solar Energy Conference*, pages 4492–4500, September 2009. DOI:10.4229/24th EUPVSEC2009-6DV.2.34.
- [37] K. WILLIGES, J. LILLIESTAM, AND A. PATT. **Making concentrated solar power competitive with coal: The costs of a European feed-in tariff**. *Energy Policy*, **38**:3089–3097, 2010.
- [38] IEC **62108 Concentrator photovoltaic (CPV) modules and assemblies Design qualification and type approval**.
- [39] A. ET AL. KALNAY. **The NCEP/NCAR 40-year re-analysis project**. *American Meteorology Society*, **77**:470, 1996.
- [40] NOAA. **Globe Earth System Poster**. www.globe.gov/wist/earthsystposter.jsp, Jan 2011.
- [41] C. CANIZO, G. COSO, AND W.C. SINKE. **Crystalline silicon solar module technology: Towards the 1 €/per Watt-peak goal**. *Progress in Photovoltaics*, **17**:199–209, 2009.
- [42] **Solar Buzz, Solar Market Research and Analysis: Module Pricing**. <http://www.solarbuzz.com/node/3184>, Jan 2012.
- [43] THERMOKEY. **Thermokey 2009 Price List**. Technical report, Thermokey, 2009.
- [44] D. RHODES. **Fortschrittliche und alternative Energieanlagen**. Technical report, TU Wien, 2010.
- [45] JENNY NELSON. *Physics of Solar Cells*. Imperial College Press, 2003.
- [46] A.W. BETT, F. DIRMROTH, AND G. SIEFER. *Concentrator Photovoltaics: Multijunction Concentrator Solar Cells*. Springer, 2007.
- [47] ANJA ROYNE, CHRISTOPHER J. DEY, AND DAVID R. MILLS. **Cooling of photovoltaic cells under concentrated illumination: a critical review**. *Solar Energy Materials and Solar Cells*, **86**(4):451 – 483, 2005.
- [48] A. BAR-COHEN. **Fin Thickness for an Optimized Natural Convection Array of Rectangular Fins**. *Transactions of the ASME*, **101**:564–566, 1979.
- [49] V.V. ZHIRNOV, III CAVIN, R.K., J.A. HUTCHBY, AND G.I. BOURIANOFF. **Limits to binary logic switch scaling - a gedanken model**. *Proceedings of the IEEE*, **91**:1934–9, 2003.
- [50] A. MALHAMMER. **Thermal Design for Electronics**. Aug-30-2005.
- [51] JOHN H. IV LIENHARD AND JOHN H. V LIENHARD. *A Heat Transfer Textbook Third edition*, chapter 7: Forced convection in a variety of configurations, pages 341–396. Phlogiston Press, 2006.
- [52] RECKNAGEL, SPRENGER, AND SCHRAMEK. *Taschenbuch fuer Heizung und Klima Technik 05 06*, chapter 1.3, pages 149–155. Oldenburg, R and Schramek, 2004.
- [53] D. GORENFLO AND D. KENNING. *VDI Heat Atlas*, chapter 2, pages 757–792. Springer-Verlag, 2010.
- [54] J. COLLIER AND J. THOME. *Convective Boiling and Condensation Third Edition*, chapter 4, pages 155–6. Oxford Science, 1996.
- [55] J.P. HOLMAN. *Heat Transfer*, chapter 9, page 515. McGraw-Hill, 2000.
- [56] R. PRASHER. **Thermal Interface Materials: Historical Perspectives, Status, and Future Directions**. *Proceedings of the IEEE*, **94**:1571–86, 2006.

REFERENCES

- [57] ASM AEROSPACE SPECIFICATION METALS INC. **Aluminum 6063-T5**. <http://asm.matweb.com/search/SpecificMaterial.asp?bassnum=MA6063T5>, Sep 2010.
- [58] EFUNDA. **Thermal Conductivity: Silicon**. http://www.efunda.com/materials/elements/TC_Table.cfm?Element_ID=Si, Oct 2011.
- [59] MEMSNET. **Material: Silicon (Si), Bulk**. <http://www.memsnet.org/material/siliconsibulk/>, Sep 2010.
- [60] YIPING WANG, ZHENLEI FANG, LI ZHU, QUNWU HUANG, YAN ZHANG, AND ZHIYING ZHANG. **The performance of silicon solar cells operated in liquids**. *Applied Energy*, **86**:1037–42, 2009.
- [61] VASILIS FTHENAKIS AND ERIC ALSEMA. **Photovoltaics Energy Payback Times, Greenhouse Gas Emissions and External Costs: 2004-early 2005 Status**. *Progress in Photovoltaics: Research and Applications*, **14**:275–280, 2006.
- [62] VARUN, I.K. BHAT, AND RAVI PRAKASH. **LCA of renewable energy for electricity generation systems-A review**. *Renewable and Sustainable Energy Reviews*, **13**(5):1067 – 1073, 2009.
- [63] P. SCHEIBENER, J. STRAUB, J.M.H. LEVELT SENGERS, AND J.S. GALLAGHER. **Refractive Index of Water and Steam as Function of Wavelength, Temperature and Density**. *Journal of Physical and Chemical Reference Data*, **19**:677–717, 1990.
- [64] GRANT R. FOWLES. *Introduction to Modern Optics Second Edition*, chapter 2: The Vectorial Nature of Light, pages 21–56. 1989.
- [65] V. EZHIL. *Reliability of lead free soldering in concentrator photovoltaic modules*. Master's thesis, Australian National University, 2011.
- [66] DEREK H. ALLEN. *Economic Evaluations of Projects*, chapter 6: Discounting, Time Value of Money and NPV, pages 28–39. Institution of Chemical Engineers, Rugby, Warwickshire, England, 1991.
- [67] JOHN TWIDELL AND TONY WEIR. *Renewable Energy Resources*, chapter 3: Heat Transfer, pages 46–49. Taylor and Francis, 2007.
- [68] ROBERT W. SERTH. *Process Heat Transfer: Principles and Applications*, chapter 9: Boiling Heat Transfer, pages 388–9. 2007.
- [69] LUDWIG BERGMAN AND CLEMENS SCHAEFER. *Optics of Waves and Particles*, chapter 1: Optical Imaging, page 52. 1999.
- [70] JOHN TWIDELL AND TONY WEIR. *Renewable Energy Resources*, chapter 7: Photovoltaic Generation, page 203. Taylor and Francis, 2007.
- [71] JOHN TWIDELL AND TONY WEIR. *Renewable Energy Resources*, chapter 2: Essentials of Fluid Dynamics, pages 35–38. Taylor and Francis, 2007.
- [72] JOHN TWIDELL AND TONY WEIR. *Renewable Energy Resources*, chapter 8: Hydro-power, page 240. Taylor and Francis, 2007.
- [73] SRBRISLAV GENIC, IVAN ARANDJELOVIC, PETAR KOLENDIC, MARKO JARIC, NIKOLA BUDIMIR, AND VOJISLAV GENIC. **A Review of Explicit Approximations of Colebrook's Equation**. *FME Transactions*, **39**:67–71, 2001.
- [74] SASMITA MISHRA. *Engineering Economics and Costing*, chapter 2: Utility analysis, pages 12–33. New Dehli, 2009.



"The happiest excitement in life is to be convinced that one is fighting for all one is worth on behalf of some clearly seen and deeply felt good." –Ruth Benedict

Personal information

Surname / First name **Clarke, Matthew**
Addresses Vienna, Austria
Telephone
E-mail mclarke1@gmail.com
Nationality United States of America
Date of birth 02.03.1983
Gender Male

Desired employment / Occupational field

Renewable Energy, Energy Storage, E-Mobility

Education and training

Dates December 2008 – December 2011 (expected graduation)
Title of qualification awarded PhD in Mechanical Engineering
Principal subjects/occupational skills Concentrator Photovoltaic Receiver Design
Name and type of organisation providing education and training Vienna University of Technology
Institute for Energy Systems and Thermodynamics

Dates October 2007 – December 2008
Title of qualification awarded MSc in Renewable Energy
Principal subjects/occupational skills Renewable Energy Hybrid Systems
Name and type of organisation providing education and training European Union Renewable Energy Centre (EUREC) Brussels, Belgium
Universities attended through the program (1 semester each):
Loughborough University, U.K. and University of Kassel, Germany
Degree Awarded: MSc from Loughborough University with Distinction
Details: <http://www.master.eurec.be/Introduction>

Dates August 2001 – May 2005
Title of qualification awarded BSc in Mechanical Engineering
Principal subjects/occupational skills Mechanical design, renewable energy technology, and energy security.
Name and type of organisation providing education and training University of Illinois at Urbana-Champaign U.S.A
Details: http://www.mechse.uiuc.edu/media/pdfs/for/undergraduates/me/me_curriculum.pdf

Work experience

Dates December 2008 – Currently Employed
Occupation or position held Research Project Assistant
Main activities and responsibilities Design, research and develop concentrator photovoltaic receivers and cooling systems.
Name and address of employer Vienna University of Technology
Institute for Energy Systems and Thermodynamics E302
Getreidemarkt 9, 1060 Wien, Austria
Type of business or sector University

Dates	Feb 2010 – May 2010
Occupation or position held	Internship/Exchange Program
Main activities and responsibilities	Research and development of concentrator photovoltaic receiver designs.
Name and address of employer	The Australian National University, CSES Dept Engineering North Rd. Bld. 32, ACT 0200, Australia
Type of business or sector	University
Dates	June 2008 – December 2008
Occupation or position held	Engineering Subcontractor
Main activities and responsibilities	Integrate vanadium redox flow batteries, photovoltaics, and smart grids (computer simulations).
Name and address of employer	Austrian Institute of Technology, Giefinggasse 2, 1210 Wien
Type of business or sector	Public/Private Funded Research Facility in Energy and Mobility
Dates	July 2005 – July 2007
Occupation or position held	Automotive Design Engineer
Main activities and responsibilities	Generate new designs for diesel engine components, deliver 3-D models and 2-D prints, validate designs using CAE tools and engine testing, and procure prototype parts for testing.
Name and address of employer	International Truck and Engine Corporation, 10400 Melrose Park, IL, 60160, U.S.A.
Type of business or sector	Medium/Heavy Duty Diesel Truck and Engine Manufacturer
Dates	January – May 2005
Occupation or position held	BSc Project: Reliability of a Spill Body in Caterpillar's MEUIC Fuel Injector
Main activities and responsibilities	Project leader in predicting component reliability utilizing FEM simulations and Monte Carlo methods.
Name and address of employer	Caterpillar Corporation, Mossville, IL, 61552, U.S.A.
Type of business or sector	Construction and mining equipment, diesel and natural gas engines, industrial gas turbines.
Dates	June 2001 – August 2004
Occupation or position held	Summer Internships: Engineer (3 months each year)
Main activities and responsibilities	Develop reusable packaging and new manufacturing floor layout, implement new data system
Name and address of employer	International Truck and Engine Corporation, 10400 Melrose Park, IL, 60160, U.S.A.
Type of business or sector	Medium/Heavy Duty Diesel Truck and Engine Manufacturer

Personal skills and competences

Mother tongue(s) **English**

Other language(s) **German** (according to the Common European Framework of Reference for Languages)

Understanding		Speaking		Writing
Listening	Reading	Spoken interaction	Spoken production	Writing
B2	B2	B2	B2	B2

Organisational skills and competences
Applicable Training: Global 8D Problem Solving, DFMEA, Dealing with Difficult People, Life Coaching

Technical skills and competences
Two years experience in both IDEAS 3-D modelling software and GD&T

Computer skills and competences
Competent in Microsoft Office and MatLab, proficient typist in both QWERTY and Dvorak methods

Artistic skills and competences
Musician (guitar and vocals), avid outdoors enthusiast, ultimate frisbee player (Austrian national team)

Other skills and competences
U.S. Patents: [7305976](#), [7789060](#). Awards: 2011 PVSEC Most Outstanding Student Research

References available upon request